

TERRESTRIAL MERCURY BIOGEOCHEMICAL CYCLING WITHIN THE AUSTRALIAN ENVIRONMENT



Katrina Macsween

BEnv

MRes

Department of Earth and Environmental Sciences


Faculty of Science and Engineering

Macquarie University

*Thesis presented for the degree of Doctor of
Philosophy*



Submitted February 2020



Never half-ass two two things. Whole-ass one
thing

- *Ron Swanson*

STATEMENT OF ORIGINALITY

This work has not previously been submitted for a degree or diploma in any university. To the best of my knowledge and belief, the thesis contains no material previously published or written by another person except where due reference is made in the thesis itself

Katrina MacSween 25 February 2020

ABSTRACT

Mercury (Hg) biogeochemical cycling is a complicated and highly variable process, particularly in the terrestrial environment. Despite many decades of research, the mechanisms involved in controlling Hg are still poorly understood. A clear understanding of the controlling mechanisms is vital for accurate representation in the global Hg models, particularly regarding re-emission. Behaviour of Hg in the environment varies considerably across temporal and spatial scales due to variation in environmental conditions such as meteorological drivers, plant production and atmospheric chemistry. Few long-term field experiments exist, and none in Australia, to verify the roll of these parameters on seasonal time scales.

The primary focus of this thesis was to determine key drivers of Hg's natural cycle within an Australian context. This thesis presents research looking at Hg fluxes over a 14-month period (3 April 2017 to 21 June 2018) at a vegetated background site in Australia (Oakdale, New South Wales). This flux study will allow for a clearer understanding of Australia's contribution to global natural sources of mercury and exploration of environmental influences on these emission rates. Experimentation was undertaken using aerodynamic gradient micrometeorological flux method. Meteorological and atmospheric chemistry variables were measured concurrently throughout the duration of the study. Emissions from biomass burning were also measured using a combination of combustion wind-tunnel and field measurements.

Hg emission flux average over the duration of the study were close to zero (average $0.002 \text{ ng m}^{-2} \text{ h}^{-1}$, ± 14.23), however, there was significant seasonal variation. Highest net surface emission occurred during austral summer, while net deposition occurred during winter and early spring. This variation was largely attributed to seasonal changes in net radiation and surface temperatures, which control the volatilisation of Hg from the substrate. Soil moisture

change due to rainfall appeared to have little prolonged influence on Hg surface emissions, beyond an initial interstitial release.

Atmospheric Hg concentrations followed a similar seasonal trend to the Hg fluxes, where highest concentrations occurred in summer (0.88 ng m^{-3} , ± 0.19) and lowest in winter (0.43 ng m^{-3} , ± 0.08). The study average was 0.68 ng m^{-3} ($\pm 0.22 \text{ ng m}^{-3}$), below currently assumed Southern Hemisphere background concentrations (ranging between 0.85 ng m^{-3} and 1.05 ng m^{-3}). Atmospheric concentrations at the study site are thought to be the product of atmospheric transport, with highest concentrations occurring when air masses had first travelled through the Sydney metropolitan region.

Atmospheric Hg release during biomass burning was less than previously assumed, largely due to low Hg concentrations in both vegetation and soils. These values are $\sim 62\%$ lower than the global average used previously to estimate Australian biomass burning mercury release.

Australia's climate has a significant impact on the rate and timing of terrestrial emissions and atmospheric transport to and from the continent. Measurements of Hg concentrations in ambient air support the conclusion that Hg deposited in remote areas may originate from anthropogenic sources far away. This study clearly demonstrated the complexities of understanding the drivers and influencing parameters affecting emission and deposition in the environment and found that Australia is largely influenced by global Hg circulation.

ACKNOWLEDGEMENTS

This thesis is not just an accomplishment of scientific work but a labour of love, lose, heartache.

First and foremost I wish to acknowledge and thank the two people in the world who believed in and were most proud this work, my Mum and original supervisor and mentor Dr Grant Edwards. You were both the reason, inspiration and proudest of my achievements and sadly passed before you could see what belief in a person could create. I am what I am because of the people around me, most especially these two people.

I would like to whole heartily thank Professor Paul Beggs for taking me on in the final hour and helping me achieve my dream even when it felt like the whole universe was telling me to stop. Thank you for your unwavering support, encouragement and ability to listen to my long unintelligible waffle.

Dr Dean Howard, for finally teaching me Matlab and reluctantly reading all my work. Your patience, kindness and supply of long necks were invaluable. Thank you for continuing to help and support my reckless pursuit of poverty and soul selling.

Kellie Cook, you have been the kindest and most supportive friend I could ever ask for. Thank you for your continued belief and exchange of advice. Our late night pizza coding parties, space poop conversations and mutual love of Harry Potter helped sustain me.

Thank you to the bane of my liver, Simon Mould, Marek Rouilon and Zacc Larkin. We all started this quest together and somehow made it out the other side. Our long lunches in the sun, mid-week drinking sessions and late-night debates on the merit of science helped me keep my sanity and grounded me in reality.

And lastly to my family and friends, of whom there are numerous, thank you for your continued support and proudness despite not having a clue what it is exactly that I do. You can stop asking now, it's finally finished!!

TABLE OF CONTENTS

Statement of Originality.....	ii
Abstract.....	iii
Acknowledgments	v
Table of Contents.....	vi
List of Figures	xiv
List of Tables	xvi
Acronyms and abbreviations	xvix
Chapter 1: Introduction	1
1.1 Thesis Aims and Scope.....	2
1.2 Thesis layout	4
Chapter 2: Literature Review	6
2.1 Introduction.....	6
2.2 Sources of Hg in the environment	8
2.3 Mercury in the atmosphere	10
2.4 Mercury air-surface exchange.....	15
2.4.1 Drivers of terrestrial air-surface exchange	18
2.4.1.1 Soil volatilisation	19
2.4.1.2 Soil moisture	21
2.4.1.3 Vegetation.....	23
2.5 Mercury release form biomass burning	24
2.6 Australia's contributions to the global mercury cycle	25
2.7 Summary	27

Chapter 3: Seasonal mercury fluxes at a terrestrial background site in South-Eastern Australia.	28
3.1 Preface.....	28
Seasonal mercury fluxes at a terrestrial background site in South-Eastern Australia	30
Abstract.....	30
1. Introduction.....	31
2. Methods.....	34
2.1 Site description.....	34
2.2 Hg flux gradient method	35
2.3 Substrate analysis	36
2.4 Eddy covariance measurments	37
2.5 Environmental variables.....	37
2.6 Data analysis methods	37
3. Results.....	39
3.1 Site Characteristics.....	39
3.2 Mercury fluxes	39
3.3 Relationship with Environmental variables	44
4. Discussion	49
5. Conclusion	54
6. References.....	55
Chapter 4: The role of precipitation and soil moisture in enhancing mercury fluxes at a background site in South-Eastern Australia.....	60
4.1 Preface.....	60
The role of precipitation and soil moisture in enhancing mercury fluxes at a background site in South-Eastern Australia.	62
Abstract.....	62

1.Introduction.....	63
2. Methods.....	66
2.1 Site description.....	66
2.2 Hg flux gradient method	66
2.3 Environmental variables.....	68
2.4 Hg flux rainfall analysis	68
2.5 Hg flux enhancement factor	69
2.6 Statistical analysis	70
3.Results.....	70
4 Discussion	79
5 Conclusion	82
References.....	83
Chapter 5: Atmospheric mercury variability at a terrestrial background site, South-Eastern Australia.....	86
5.1 Preface.....	86
Atmospheric mercury variability at a terrestrial background site, South-Eastern Australia. ..	88
Abstract.....	88
1.Introduction.....	89
2. Methods.....	92
2.1 Site characteristics.....	92
2.2 Ambient mercury measurements.....	93
2.3 Reactive mercury filter system.....	94
2.4 Environmental Variables.....	94
2.5 HYSPLIT	95
3.Results and discussion	96
3.1 GEM characteristics	96

3.2 Reactive mercury characteristics.....	99
3.3 Meteorological drivers across seasons	102
3.4 Photo-reduction pathways	10210
4.Conclusion	114
5.References.....	115
Chapter 6: Investigation of mercury emissions from burning of Australian eucalypt forest surface fuels using a combustion wind tunnel and field observations	122
6.1 Preface.....	122
Investigation of mercury emissions from burning of Australian eucalypt forest surface fuels using a combustion wind tunnel and field observations	124
Chapter 7: Australia’s contribution to the global mercury biogeochemical cycle	135
7.1 Preface	135
7.2 Introduction.....	136
7.3 Methods.....	141
7.3.1 GEOS-Chem model	141
7.3.2 Observation methods.....	145
7.4 Results and Discussion	146
7.4.1 Australia’s Hg Cycle	146
7.4.2 Surface emissions.....	148
7.4.3 Terrestrial deposition.....	154
7.5 Model verses observation evaluation.....	157
7.6 Limitations and conclusions	159
Chapter 8: Key findings and conclusions	163
References	169
Appendix 1	188
Appendix 2.....	189

Appendix 3.....	190
Appendix 4	191

LIST OF FIGURES

Chapter 2

- Figure 1.** Global biogeochemical cycle for mercury. Natural (preindustrial) fluxes [Mg a^{-1}] and inventories [in Mg] are noted in black. Anthropogenic contributions are in red. Natural fluxes augmented by anthropogenic activities are noted by red-and-black dashed lines (Selin, 2009) 9
- Figure 2.** Atmospheric chemistry pathways of mercury reduction and Oxidation (Si and Ariya, 2018). 12
- Figure 3.** Box-and-whisker plots of gaseous elemental mercury yearly distribution (GEM, ng m^{-3}) at all GMOS stations for (a) 2013 and (b) 2014. The sites are organised according to their latitude from the northern to the southern locations. Each box includes the median (midline) and 25th and 75th percentiles (box edges), 5th and 95th percentiles (whiskers) (Sprovieri et al., 2016). 14
- Figure 4.** Schematic diagram of major processes and factors affecting mercury volatilization from soil. Major processes of reducible mercury formation (Step 1) and production of elemental mercury from this reducible mercury (Step 2) are identified. Within the soil particles and soil solution OM is Organic matter and DOM is Dissolved Organic matter (DOM) (Pannu et al., 2014). 21

Chapter 3

- Figure 1.** All Hg fluxes (blue), ambient Hg (Green) and cumulative Hg flux (magenta) 3 April 2017 to 21 June 2018 in Oakdale, New South Wales. Axis label colour corresponds to line colour. Shading represents changes in season, as labelled. 42

Figure 2. Diel mean composite trends for Hg flux (navy line), shaded area shows inter-quartile range, soil temperature at 5cm, air temperature, net all-wave radiation, and total short-wave radiation across each season at Oakdale, NSW. Dotted vertical lines indicate median sunrise and sunset times for each season. 43

Figure 3. Monthly mean Hg flux and associated environmental variables. Months that were repeated averaged together to confine trends to 12-month period. For Hg flux (a) column the monthly average and bars represents upper and lower inter-quartile range. For the environmental variables (b-e), solid line is mean value and shading is the inter-quartile range. 45

Figure 4. CO₂ diel composite for each season at Oakdale, NSW, 3 April 2017 to 21 June 2018. Solid line represents median value, shaded area inter-quartile range. Grey shaded region indicates night-time measurements. 49

Chapter 4

Figure 1. Hg flux (a), soil volumetric water content, at depths of 5cm, 15cm and 30cm (b), and rain (c) at 30 minute intervals for 3 April 2017 to 21 June 2018 at Oakdale, NSW. Grey boxes indicate rainfall that had a corresponding VWC and Hg flux change. Shading indicates changes in seasons as labelled. 72

Figure 2. Box and whisker plot of rain, no rain and all Hg fluxes for all measured seasons. Red centre line represents median value. Boxes show 25 and 75 quartile range and whiskers standard error. 73

Figure 3. Rain events based on those identified in Figure 1 to influence Hg fluxes and VWC. Roman numerals at the top of individual graphs correspond to the timing or event in Figure 1. Each individual event includes a minimum 12 hours before and after rain occurred. 75

Chapter 5

Figure 1. Site map of Oakdale field site in Australia (left) and within the Sydney geological basin (right). Blue dot indicates location of Oakdale study site; red dot shows Sydney central business district.	93
Figure 2. Monthly composite of the daily mean (bold line) and standard deviation (shaded area) of total gaseous mercury concentration at Oakdale, New South Wales, from 3 April 2017 to 21 June 2018.	98
Figure 3. Diel composite of GEM for each season at Oakdale, New South Wales, from 3 April 2017 to 21 June 2018. Bold line gives median concentrations, shaded area inter-quartile range. Grey shaded areas show night, including sun rise and sun set times.	99
Figure 4. Reactive Mercury measurements made at Oakdale, New South Wales, from 3 April 2017 to 21 June 2018. Columns show 2-weekly mean concentration and bars show standard deviation. Shaded/unshaded background depicts Australia's seasons.	100
Figure 5. Wind rose with GEM concentrations for each season at Oakdale, New South Wales, from 3 April 2017 to 21 June 2018.	107
Figure 6. Hourly GEM-weighted HYSPLIT trajectories for 75% quartile and 25% quartile for each season at Oakdale, New South Wales, from 3 April 2017 to 21 June 2018.	108
Figure 7. Half hourly ozone (on the left y axis), specific humidity (on the right y axis), and elemental gaseous mercury (on the right y axis) for the entire study period (3 April 2017 to 21 June 2018) at Oakdale, NSW. Shaded/unshaded background depicts Australia's seasons. Note that the right hand y axis is a log scale.	110
Figure 8. Diel composite of ozone for each season at Oakdale, New South Wales, from 3 April 2017 to 21 June 2018. Bold line gives median concentrations, shaded	

area inter-quartile range. Grey shaded areas show night, including sun rise and sun set times. 112

Chapter 6

Fig. 1. Map of Australian biomes as defined by Olson and Dinerstein (Olson and Dinerstein, 2002), along with average annual fire frequency as determined by Maier (Maier, 2016). Based on raster data at 1 km² resolution. Due to the sampling algorithm, generally only fires of size 4 km² or larger are counted. Numbers 1 and 2 show locations of fuel sampling sites. 125

Fig. 2. **a.** time series of GEM, CO₂ and CO as observed at CGBAPS during 25th January – 14th February 2016. Vertical lines denote the start and end times of identified plume strike events. **b.** HYSPLIT back trajectories corresponding to identified plume strike events, along with MODIS hot spot data for corresponding days. 128

Fig. 3. Left: time series of GEM enhancements for a. Load 1, c. Load 2, e. Load 3, g. Load 4 and i. backing fires. Right: CO₂ (yellow) and CO (blue) enhancements for the same fires. Black lines denote median values, shading denotes range of values. Vertical lines show median times of EOFs and Fines Out. (For interpretation of the references to colour in this figure legend, the reader is referred to the Web version of this article.) 129

Fig. 4. Above: GEM enhancements against a. CO₂ and b. CO enhancements. Lines show least-squares regressions for FP (dotted), FS (dashed) and SM (solid) stages. Middle: GEM enhancements against c. CO₂ and d. CO enhancements for plume strike events observed at CGBAPS. Lines show linear least-square regressions \pm standard error. Below: e. $\Delta\text{GEM}/\Delta\text{CO}_2$ and f. $\Delta\text{GEM}/\Delta\text{CO}$ ratios for each observation against modified combustion efficiency for experimental burn (circles) and CGBAPS plume strike (diamonds) data. Here FP, FS and SM categories are defined according to MCE ranges and refer to experimental burn data only. 130

Chapter 7

<p>Figure 1. Schematic of the global terrestrial mercury model (GTMM). Boxes represent pools tied to carbon cycling in the model. Numbers in the boxes give the present-day storage of mercury (Mg), and other numbers give mercury fluxes in and out of pools (Mg yr^{-1}). Numbers in parenthesis are preindustrial values. Deposition of Hg^0 and Hg^{2+} are taken from the GEOS-Chem mercury simulation [Selin et al., 2008]. Mercury enters organic soils by either leaf senescence or washoff and wet deposition of Hg^{2+} (green arrows). Soils emit mercury to the atmosphere via revolatilisation, photoreduction, and respiration (red arrows) (Smith-Downey et al., 2010).....</p>	139
<p>Figure 2 Australian atmospheric Hg^0 concentration distribution (Left) and Australian surface fluxes (Right) for latitudes 10° to 45° south and longitudes 110° to 155° east. GEOS-Chem output averaged for 2013-2017.....</p>	147
<p>Figure 3. Daily simulated Terrestrial surface emissions and Hg^0 dry deposition for the $2^\circ \times 2.5^\circ$ grid square surrounding Oakdale field site, along with observation flux measurements made at Oakdale for 2017.</p>	150
<p>Figure 4. Daily simulated Hg^0 dry deposition, along with observed dry deposition and observed dry deposition velocity at Oakdale for 2017 (Top). Reactive Hg wet deposition and rainfall for the $2^\circ \times 2.5^\circ$ grid square surrounding Oakdale field site (Bottom).</p>	155
<p>Figure 5. Linear least square regression for observation Hg flux with simulation NEF (GEOS-Chem) (Top) and Observation atmospheric Hg^0 (ng m^{-3}) with simulation atmospheric Hg^0 GEOS-Chem (bottom).....</p>	159

LIST OF TABLES

Chapter 2

Table 1. Atmospheric ground-based sites that are part of the Global Mercury Observation System network, adapted from Sprovieri et al., (2016)	15
--	----

Chapter 3

Table 1. Seasonal means and standard deviation (SD) for Hg flux measurements and measured environmental variables across the study duration (3 April 2017 to 21 June 2018) at Oakdale, NSW. Averages were separated into day and night to show diel variability for those variables known to exhibit diel variability. Net all-wave radiation (Net Rad) provides day maxima and night negative maxima. Total solar is the total short-wave radiation (incoming – outgoing).	41
--	----

Table 2. Spearman correlations with all Hg fluxes and positive Hg fluxes for each season and across the entire study duration at Oakdale, NSW. T_s is the soil temperature at each measured depth, VWC is the volumetric water content at each measured depth, RH is the relative humidity and Q^* is the net all-wave radiation. Bold values indicate significant correlations (p-value <0.01).	47
---	----

Chapter 4

Table 1. Seasonal averages and standard deviations (SD) for volumetric water content (VWC) at three measurement depths, daily average cumulative rainfall and latent heat measurements made at Oakdale, NSW (3 April 2017 to 21 June 2018)..	71
---	----

Table 2. Correlation between Hg fluxes and VWC at three measurement depths and rainfall, for each season at Oakdale, NSW (3 April 2017 to 21 June 2018). Bold values have p-values <0.05.....	77
--	----

Table 3. Enhancement factor for VWC and Hg flux when VWC at each measurement depth increased one standard deviation above the monthly mean VWC and it was raining. EF was calculated for each measurement month.	78
--	-----------

Chapter 5

Table 1. Seasonal mean and standard deviation (SD) for Gaseous Elemental Mercury (GEM), Reactive Mercury (RM), wind speed (WS), air temperature, relative humidity (RH), specific humidity, ozone (O ₃), nitrogen oxides (NO _x), and total solar radiation (total solar) at Oakdale, New South Wales, from 3 April 2017 to 21 June 2018	97
Table 2. Spearman correlations with two weekly RM at Oakdale, New South Wales, from 3 April 2017 to 21 June 2018. Bold values represent those deemed to be statistically significant, based on a p-value <0.05.....	102
Table 3. Spearman correlations with atmospheric GEM at Oakdale, New South Wales, from 3 April 2017 to 21 June 2018. Bold values represent statistically significant correlation (p-value <0.05).....	104

Chapter 6

Table 1. Overview of burned area derived from AVHRR 1997–2011 data (Maier, 2016) and mean total mercury concentrations (Packham et al., 2009) reproduced for vegetation and soils, categorised by Australian ecoregions (Olson and Dinerstein, 2002). Parentheses denote number of sample locations.....	126
Table 2. Total mercury (THg) concentrations in different fuel types. Values are means ± one standard deviation.....	128
Table 3. Overview of fire behaviour parameters. Median with range in parentheses.....	129
Table 4. Mercury emission ratios for all fire stages. Calculated as the least squares slope of GEM _y with standard error.....	130

Table 5. Mercury emission factors for all fire stages, along with mercury release fractions expressed as mean GEM emission factor as a percentage of mean mercury concentration in dry fuel. Emission factor calculated from mass balance technique ($EF_{\text{THg/fuel}}$) included for reference.....	131
---	------------

Chapter 7

Table 1. Comparisons of Hg Budget of Australia (rates are in Mg a^{-1}) determined using GEOS-Chem here and Hg budgets determined by Page (2017) and Nelson et al., (2012).	148
--	------------

Table 2. Seasonal 2 seasonal Hg source average based on GEOS-Chem output for the $2^\circ \times 2.5^\circ$ grid square surrounding Oakdale field site with observation measurements made at the Oakdale field site	153
--	------------

ACRONYMS AND ABBREVIATIONS

Br	Bromine
CEM	Cation-exchange membrane
CGBAPS	Cape Grim Baseline Air Pollution Station
CO	Carbon monoxide
CO₂	Carbon dioxide
CSIRO	Commonwealth Scientific and Industrial Research Organisation
CTM	Chemical Transport Model
EF	Enhancement factors/ Emission factor
ENSO	El Nino Southern Oscillation
EOFS	End of forward spread
ER	Emission ratios
GEM, Hg⁰	Gaseous elemental mercury
GEOS	Goddard Earth Observation System (NASA)
GEOS-Chem	GEOS-Chem chemical transport model
GMOS	Global Mercury Observation System
GOM, Hg²⁺	Gaseous oxidised mercury
Hg	Mercury
Hg²⁺	Divalent mercury
HYSPLIT	Hybrid Single Particle Lagrangian Integrated Trajectory
ITCZ	Intertropical convergence zone
MC	Moisture content

MCE	Modified combustion efficiency
MD	Mean Difference
MeHg	Methyl-Mercury
MQ	Macquarie University
NEF	Net emission flux
NOAA	National Oceanic and Atmospheric Administration
O₃	Ozone
PBM, Hg_p	Particulate bound mercury
PPHM	Parts per hundred million
SD	Standard deviation
TGM	Total Gaseous Mercury
THg	Total mercury
UNRRMAS	University of Nevada-Reno Reactive Mercury Active System
US-EPA	United States Environmental Protection Agency
VWC	Volumetric Water Content
WHO	World Health Organization

CHAPTER 1

INTRODUCTION

As a naturally occurring element, mercury (Hg) is found ubiquitously across the globe (Driscoll et al., 2013; Obrist et al., 2018; Schroeder and Munthe, 1998). Originating in the earth's crust, mercury has been utilised by human civilisations for centuries. Despite its common use and natural occurrence, mercury is highly toxic to humans and other animals alike. The long history of anthropogenic extraction and utilisation has led to significant increases in atmospheric and environmental loadings (Giang et al., 2015). Mercury's unique chemical properties mean that it is a liquid at room temperature and easily vaporised into a gas. As such, Hg also occurs naturally in the atmosphere, which forms the dominant pathway for the global distribution. Long range transport allows Hg to be redistributed to distant terrestrial and aquatic ecosystems, causing the contamination of pristine ecosystems (Selin, 2009). Thus, Hg has become a global problem not only affecting local areas that are heavily industrialised, but also areas that are remote from emitting sources (Nelson et al., 2012).

Global concerns about Hg toxicity have led to the development of the Minamata Convention on Mercury, a global treaty with the key objective of protecting human health and the environment from anthropogenic emissions and releases of Hg and Hg compounds (UNEP, 2013a). In order to address this objective, focus is given to continuous improvements to measurement, modelling and understanding of the complex biogeochemical cycle. However,

the global nature of Hg makes understanding and limiting its effects difficult. Despite a growing consensus on the global nature of Hg pollution and an increasing concern regarding its impacts, relatively little attention has been paid to levels of Hg in the Australian environment (Jardine and Bunn, 2010).

Australia is home to many unique environments and potentially distinctive oxidative conditions, and therefore plays a significant role in the natural mercury cycle. Relatively low emissions of Hg from both natural and anthropogenic sources make Australia an ideal location for understanding the natural cycling of atmospheric mercury (Edwards and Howard, 2013; Howard and Edwards, 2017). Australia is mostly a dry arid continent, but also host to a range of climate zones that include equatorial, tropical, subtropical, desert, grassland and temperate regions. As Hg fluxes are influenced by precipitation rates, temperature, and vegetation type, it is expected that Hg fluxes will differ between these different climate zones. This climate variability is likely to cause Australian Hg fluxes to behave differently to those observed in other regions of the world (Pirrone et al., 2010).

1.1 Thesis Aims and Scope

Understanding of Hg cycling between the terrestrial-atmospheric interface in the Southern Hemisphere is exceptionally limited. Australia is one of the largest land masses in the Southern Hemisphere and comprised of many unique ecosystems. Despite this, only two air-surface mercury exchange studies have taken place here. In order to address this key knowledge gap the primary aims of this thesis are to:

- Characterise the seasonal Hg emission fluxes and concentrations at a terrestrial background site in South-Eastern Australia.

- Examine the nature of the role of precipitation and soil moisture in enhancing Hg fluxes at a terrestrial background site in South-Eastern Australia.
- Examine the role of other environmental parameters on mercury fluxes and concentrations, such as temperature and solar radiation, at a terrestrial background site in South-Eastern Australia.
- Quantify the release of mercury from the burning of Australian eucalypt forest surface fuels.
- Evaluate how well identified Hg air-surface exchange rates and trends align with the current understanding of Australia's contribution to the global mercury cycle.

By addressing these aims this thesis will provide a better understanding of and quantify the natural biogeochemical cycling of Hg within the Australian terrestrial environment.

The scope of this thesis is primarily restricted to a single field site located in South-Eastern Australia, with a key focus on the natural sources and perturbation of the Hg cycle. The site was chosen to be representative of the environments typically found around South-Eastern Australia. The chosen field site was classified as a background site (substrate Hg concentration <100 ppb) with no primary anthropogenic sources in the region. Measurements were made continuously using a micrometeorological aerodynamic flux gradient method over a 14-month period. This study represents the first long-term mercury air-surface exchange measurements to take place in Australia.

1.2 Thesis layout

The following chapters address the aims outlined here in order to demonstrate the importance of understanding mercury air-surface exchange in the context of the Australian environment. Chapters 3 to 6 are journal manuscripts either published, submitted or prepared for submission and therefore have been structured and formatted to reflect individual journal requirements. Chapter 7 is not intended for publication but has been included to provide both broader Australian and global context for the key findings of the previous chapters.

Chapter 2, the literature review, will outline the properties of mercury in the environment and highlight the current state of knowledge regarding the influence of meteorological parameters and atmospheric conditions on Hg cycling between the surface and the atmosphere and the knowledge gaps that still exist.

Chapter 3 explores the seasonal variability in mercury air-surface exchange at a terrestrial background site in South-Eastern Australia and the potential drivers of this variability. This study investigated the drivers of Hg fluxes across multiple seasons in order to gain understanding of the influence of vegetation and environmental parameters on Hg air-surface exchange across seasonal time scales.

Chapter 4 focuses on investigating Hg flux in response to precipitation and soil moisture changes over extended periods at a background site in South-Eastern Australia. The main purpose of this chapter is to investigate if soil moisture changes in response to rainfall had any prolonged influence on Hg flux magnitude and if this response varied depending on season.

Chapter 5 analyses 14 months of atmospheric gaseous elemental mercury and reactive mercury measurements at a terrestrial background site, South-Eastern Australia, to determine if there

was seasonal variation in atmospheric mercury concentrations and to determine the potential drivers of this variation within the Australian terrestrial context.

Chapter 6 reports on and compares two different studies of mercury release from the burning of Australian native forest surface fuels. The study was developed in response to the general lack of Australian-derived emission ratios or emission factors in Australian mercury emission modelling and aimed to provide a better understanding of Hg release during biomass burning.

The purpose of Chapter 7 is to put the main findings of the thesis into the broader Australian and global context. This chapter compares the natural sources and trends of atmospheric mercury identified in the previous chapters with GEOS-Chem chemical transport model output to assess how well the modelled assumptions capture Australia's variability and natural sources.

The final chapter of this thesis (Chapter 8) provides the overall findings of the thesis, the implications of these findings, and its conclusions. Key limitations of the undertaken studies and still existing knowledge gaps will also be addressed in this chapter.

This chapter has provided a brief introduction to the thesis, including its aims and the thesis structure. As indicated above, the next chapter provides an in-depth literature review of the thesis topic.

CHAPTER 2

SOURCES AND DRIVERS OF THE MERCURY BIOGEOCHEMICAL CYCLE

2.1 Introduction

Mercury (Hg) is a naturally occurring element found within the Earth's crust and is ubiquitous throughout the environment. Hg's unique chemical properties mean that it is a liquid at room temperature and easily vaporised into a gas. As such, Hg also occurs naturally in the atmosphere. Despite Hg being a natural substance, it is highly toxic to humans, other animals and ecosystems (Carpi and Lindberg, 1997). Global concerns about Hg toxicity have led to the development of the Minamata Convention on Mercury, a global treaty aimed at protecting human health and the environment from anthropogenic emissions and releases of Hg and Hg compounds (UNEP, 2013a). The atmosphere forms the dominant pathway for the global distribution of Hg, allowing it to be transported to terrestrial and aquatic ecosystems where it can cause the contamination of pristine environments (Boening, 2000; Gustin et al., 2002; Laurier and Mason, 2007; Schroeder and Munthe, 1998).

The World Health Organization (WHO) classifies Hg exposure as one of the most hazardous and substantial global public health concerns (WHO, 2019). However, the global nature of Hg makes understanding and limiting its effects difficult. Exposure to Hg occurs through inhalation, skin contact and ingestion. Exposure rates and impacts are largely dependent on the form of Hg found within the environment. Up to 80% of elemental Hg inhaled can be absorbed into the body, however atmospheric concentrations are generally not significant enough to be of concern, except when in close proximity to major sources (Gaffney and Marley, 2014). The highly toxic form, Methyl-Mercury (MeHg), can be introduced into the environment by the conversion of inorganic Hg to organic forms of Hg. MeHg bioaccumulates within an ecosystem, enhancing its mobilisation and potential for exposure. This is of particular concern within aquatic ecosystems where inorganic Hg is more readily converted to MeHg. MeHg is particularly hazardous to human health as it is able to cross the blood-brain divide, forming a potent neurotoxin, and penetrate the placenta exposing the foetus to the neurotoxin (Schroeder and Munthe, 1998).

Increased understanding of Hg's health impacts and emission implications has led to the development of numerous national and international policies, including the development of the Minamata Convention on Mercury (UNEP, 2013a). The Minamata Convention on Mercury was developed with the explicit aim to “protect human health and the environment from anthropogenic emissions and releases of mercury”. With 128 signatories, the Minamata Convention on Mercury was fully ratified and became legally binding in 2017 (UNEP, 2017). Continuing to advance our understanding of the sources, pathways and behaviour of Hg is vital for limiting the impacts to human health and reaching the goals outlined by the Minamata Convention.

2.2 Sources of Hg in the environment

Mercury enters the environment from both natural and anthropogenic sources. Natural geogenic sources are dominantly comprised of volcanic activity, crustal degassing, weathering and biological particles and account for approximately 5-13% of total emissions (Agnan et al., 2016; Amos et al., 2013; Driscoll et al., 2013). These sources are usually located along plate tectonic boundaries and volcanic hotspots where degassing takes place, contributing approximately 60 Mg Hg a⁻¹ to the atmosphere. However, volcanic activity alone is estimated to release between 30 and 800 Mg Hg a⁻¹ (Nriagu and Becker, 2003). Natural emission also occurs from enriched mineral sites where mineralised forms of mercury such as cinnabar, corderoite and livingstonite are found in large quantities (Gustin, 2003; Gustin et al., 2008). Reservoirs of Hg also exist in surface soils, water bodies and vegetation surfaces, although primarily derived from previously deposited atmosphere mercury of natural and anthropogenic origin (Figure 1) (Gustin et al., 2008). These reservoirs account for a far greater source of Hg than geogenic sources, contributing 5207 Mg Hg a⁻¹ (Pirrone et al., 2010).

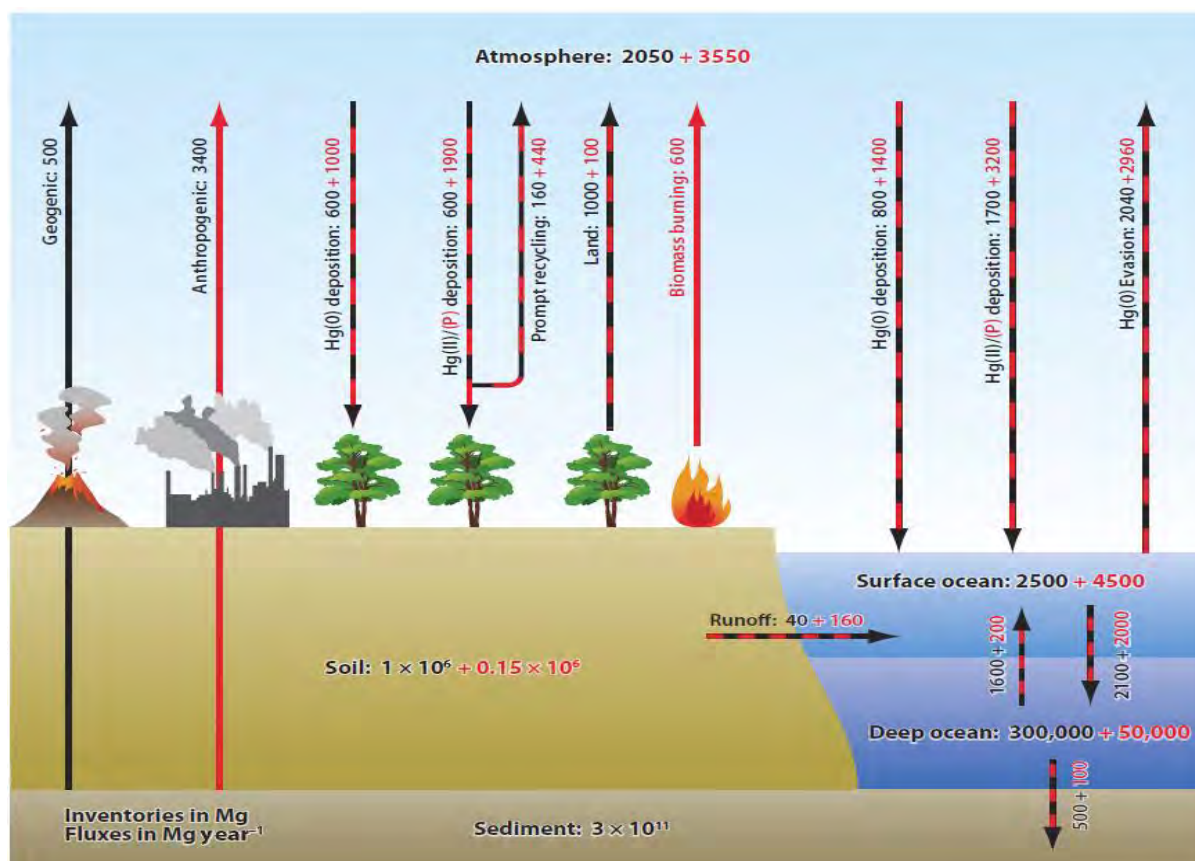


Figure 1. Global biogeochemical cycle for mercury. Natural (preindustrial) fluxes [Mg a^{-1}] and inventories [in Mg] are noted in black. Anthropogenic contributions are in red. Natural fluxes augmented by anthropogenic activities are noted by red-and-black dashed lines (Selin, 2009).

Anthropogenic sources account for approximately 30% of annual Hg emissions (Pirrone et al., 2010; Streets et al., 2017; UNEP, 2013b). Major sources include fossil fuel combustion, metal smelting, waste treatment, and artisanal and small-scale gold mining (AMAP/UNEP, 2013; Driscoll et al., 2013). Current anthropogenic loading to the atmosphere is approximately between 1875 and 2900 Mg a^{-1} (Agnan et al., 2016; Streets et al., 2017; UNEP, 2013b). These contributions have plateaued over recent decades due to decreased emissions from North America and Europe, offsetting increased emissions across Asia (Sundseth et al., 2015). Asia's global contributions currently account for 65% of total global anthropogenic emissions (Amos et al., 2013). By comparison, Australia's anthropogenic sources only account for 2% of global loadings (22 Mg a^{-1}) (UNEP, 2013b). Coal combustion and artisanal and small-scale gold

mining account for the largest global source of anthropogenic Hg (35% and 24%, respectively) (UNEP, 2013b). Increases to anthropogenic sources across the globe have seen atmospheric deposition increase between 3 and 5 fold above pre-industrial levels (Amos et al., 2013). The recent ratification of the Minamata Convention on Mercury and a combination of climate change and rapid land-use change is likely to see significant changes to these regional and point sources in the future (Giang et al., 2015; Obrist et al., 2018).

Legacy Hg comprises of Hg previously deposited from both natural and anthropogenic sources and accounts for 60% of total atmospheric Hg (Amos et al., 2015). The re-emission of this previously deposited Hg allows it to be redistributed on regional and global scales to terrestrial and ocean surfaces (Driscoll et al., 2013). Eventually, Hg is deposited into deep-sea sediments or slow response armoured terrestrial soil pools to form long-term reservoirs (Amos et al., 2013). However, continuous re-emission and lack of global inventories means there are considerable uncertainties with the estimates of re-emission to the atmosphere (Wang et al., 2006). Understanding how long these sources of Hg remain active in the environment is vital for sound decision making aimed at reducing anthropogenic impacts of Hg emissions.

2.3 Mercury in the atmosphere

Mercury exists in the atmosphere in three operationally defined forms: gaseous elemental mercury (GEM, Hg^0); gaseous oxidised mercury (GOM, Hg^{2+}); and particulate bound mercury (PBM, Hg_p). The complex physicochemical properties of GOM and PBM make it difficult to define the species in the atmosphere, and are therefore referred to collectively as reactive mercury (RM) (Gustin et al., 2015; Huang et al., 2013; Weiss-Penzias et al., 2015). GEM is the dominant form of Hg found in the atmosphere, accounting for 90% of all Total Gaseous Mercury (TGM, RM + GEM) present. Its low water solubility and reactivity allow it to remain

in the atmosphere between 5 – 12 months (Horowitz et al., 2014; Horowitz et al., 2017; Streets et al., 2017). The high reactivity of RM means that it is quickly removed from the atmosphere once formed, usually anywhere from hours to weeks (Poissant et al., 2005). The chemical and physical state of Hg determines the fate and distribution within the environment, forming the global Hg cycle (Blackwell et al., 2014; Choi and Holsen, 2009; Gabriel et al., 2006). Understanding the processes and drivers of atmospheric Hg is vital for understanding how Hg is transported on global, regional and local scales.

Conversion of Hg from one form to another (i.e., oxidation/reduction reactions) will determine the atmospheric residence time and hence transportation distance before deposition (De Simone et al., 2016). Once Hg undergoes the deposition processes it is returned to sinks on the Earth's surface (Gustin et al., 2015). Background TGM concentrations range between 1.3 and 1.7 ng m⁻³ in the Northern Hemisphere and 0.85 and 1.2 ng m⁻³ in the Southern Hemisphere (Dommergue et al., 2010; Driscoll et al., 2013; Lindberg et al., 2007; Slemr et al., 2015; Sprovieri et al., 2010; Sprovieri et al., 2016).

Understanding of the mercury oxidation and reduction processes that take place in the atmosphere is still incomplete but is critical for determining global patterns of atmospheric Hg deposition (Horowitz et al., 2017). Oxidation and reduction processes primarily occur via gas phase, aqueous phase or particulate phase pathways, although the exact mechanisms are not yet clearly understood (Figure 2). GEM in the atmosphere is oxidised by these pathways before it is deposited into the environment as RM (Ariya et al., 2015; Horowitz et al., 2017; Lin and Pehkonen, 1999). Photochemical oxidation in the upper troposphere and lower stratosphere is thought to deplete GEM concentrations and enrich RM concentrations (Jones et al., 2016). Current proposed oxidation pathways of GEM in the gas phase are bromine (Br), ozone (O₃), OH radical, nitrate (NO₃), chloride (Cl) and various halogen species (Holmes et al., 2010; Holmes et al., 2009; Holmes et al., 2006; Horowitz et al., 2017; Lynam and Keeler, 2005;

Mastromonaco et al., 2016; Rutter et al., 2012; Sommar et al., 1997; Weiss-Penzias et al., 2009). These oxidants of GEM are thought to vary spatially, such that oxidants occurring in urban environments are different to those in marine and polar environments (Holmes et al., 2006; Lynam and Keeler, 2005; Soerensen et al., 2010).

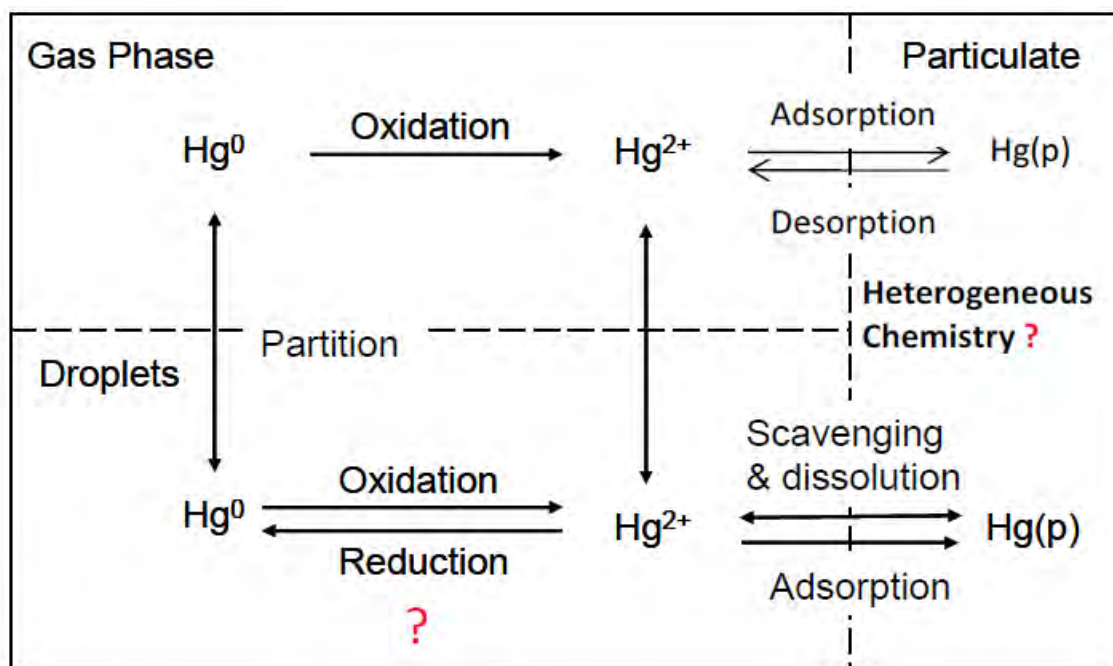


Figure 2. Atmospheric chemistry pathways of mercury reduction and Oxidation (Si and Ariya, 2018).

The oxidation of GEM to RM by Br and Cl is considered a two-step process. For example, GEM first reacts with the Br radical to form HgBr. HgBr then reacts with multiple potential oxidants (Br, I, OH, BrO, IO, NO_2) to generate different RM species (Dibble et al., 2012; Goodsite et al., 2004; Horowitz et al., 2017; Jiao and Dibble, 2017; Wang et al., 2014; Ye et al., 2016). Secondary oxidation of HgCl occurs via reactions with NO_2 , HO_2 , ClO or BrO (Ariya et al., 2015; Si and Ariya, 2018; Sun et al., 2016). Secondary reactants have been shown throughout the literature to vary latitudinally. Aircraft measurements undertaken in the subtropics found GEM oxidation due to BrO present in subtropical anti-cyclones (Gratz et al., 2015; Shah et al., 2016). Arctic and Antarctic GEM oxidation is driven by the photolytic formation of halogen radicals present in the atmosphere (Obrist et al., 2018).

In contrast to GEM, both GOM and PBM are highly soluble in water and readily deposit to surfaces (Driscoll et al., 2013). The low vapour pressure of GOM and PBM cause a short atmospheric life time of hours to weeks (Ariya et al., 2015; Landis et al., 2002). These forms of Hg are easily scavenged from the atmosphere due to high deposition velocities and precipitation (Landis et al., 2002; Lyman et al., 2007). Wet deposition is the result of aqueous oxidation of Hg into cloud droplets which can then be removed by precipitation to the Earth's surface (Lin et al., 2006). RM accounts for the remaining 1-5% of TGM present, with concentrations ranging between 0-50 pg m⁻³ (Gustin, 2012). The short atmospheric lifetime of GOM and PBM typically means deposition occurs close to anthropogenic emission sources. However, they can also be deposited to remote locations due to photochemical oxidation of GEM (Ariya et al., 2015; Mao et al., 2008; Schroeder and Munthe, 1998). Additionally, RM is introduced into the boundary layer through entrainment and convective mixing from the free troposphere, allowing it to be transported greater distances (Huang et al., 2013; Weiss-Penzias et al., 2009).

Gaseous Elemental Mercury is transported and deposited efficiently within its hemisphere of origin. Atmospheric transport of Hg across the equator is limited by the intertropical convergence zone (ITCZ) and the role of Hadley circulation that reduces the hemispheric exchange of air masses (Hamilton et al., 2008). As a result, cross hemisphere transport is less efficient resulting in Southern Hemisphere concentrations approximately 30% lower than those observed in the Northern Hemisphere (Driscoll et al., 2013; Horowitz et al., 2017; Howard et al., 2017; Song et al., 2016). Atmospheric Hg measurement and monitoring is undertaken globally with extensive networks covering much of the Northern Hemisphere as part of the Global Mercury Observation System (GMOS), which is comprised of 27 sites, 6 of which are located in the Southern Hemisphere (Table 1) (Sprovieri et al., 2016). Figure 3 shows the distribution of GEM concentrations for all GMOS sites operating between 2013 and 2014. The

limited number of monitoring sites in the Southern Hemisphere has resulted in the primary understanding of Southern Hemisphere trends being derived from aircraft and ship measurements. The large ratio of ocean to land masses in the Southern Hemisphere is believed to cause significantly different drivers than those observed in the Northern Hemisphere. However, the lack of long-term monitoring also means that understanding of these influences is also significantly less.

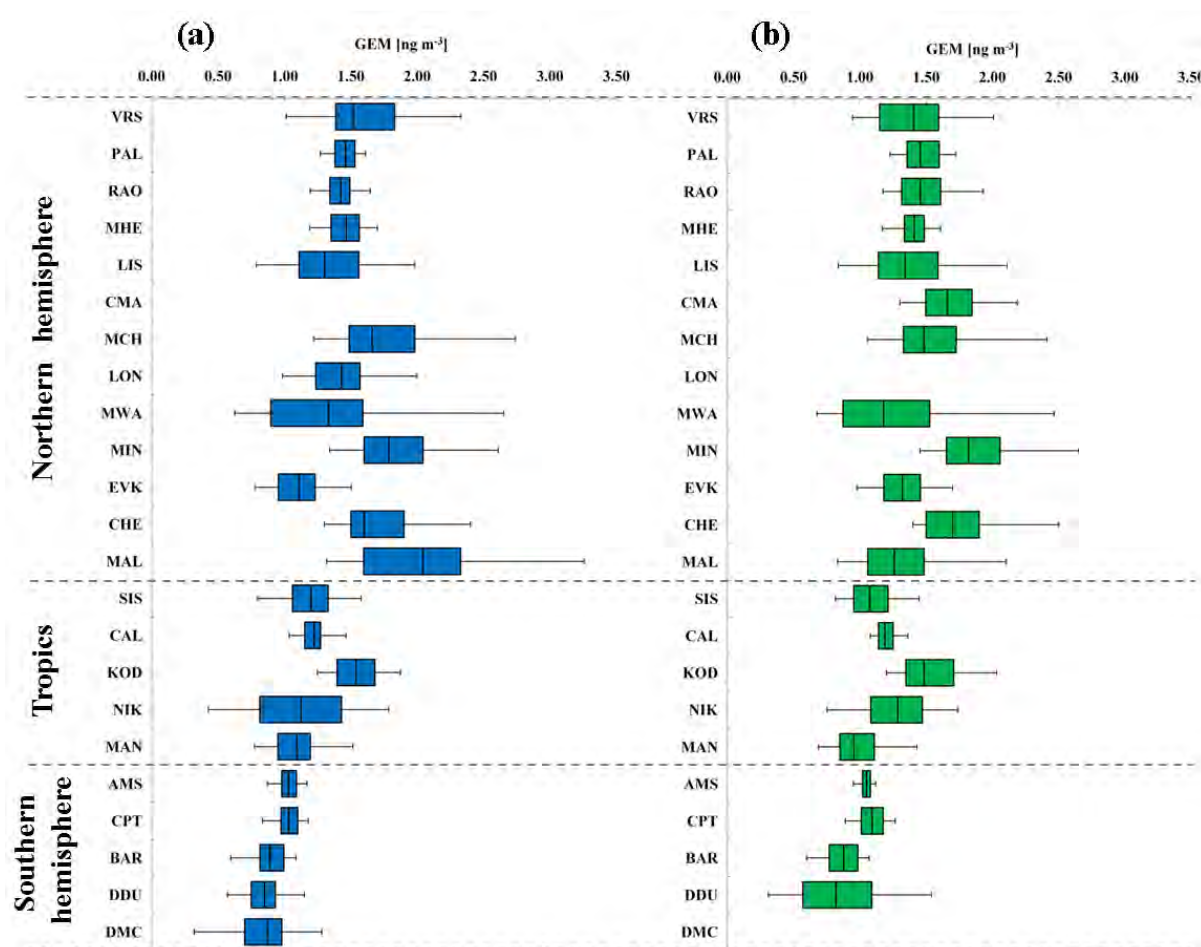


Figure 3. Box-and-whisker plots of gaseous elemental mercury yearly distribution (GEM, ng m^{-3}) at all GMOS stations for (a) 2013 and (b) 2014. The sites are organised according to their latitude from the northern to the southern locations. Each box includes the median (midline) and 25th and 75th percentiles (box edges), 5th and 95th percentiles (whiskers) (Sprovieri et al., 2016). List of full station names, locations and codes are supplied in Table 1.

Table 1. Atmospheric ground-based sites that are part of the Global Mercury Observation System network, adapted from Sprovieri et al., (2016)

Code	Site	Country	Elevation (m asl)	Lat (°)	Long (°)
AMS	Amsterdam Island	Terres Australes et Antarctiques Françaises	70	-37.79604	77.55095
BAR	Bariloche	Argentina	801	-41.128728	-71.420100
CAL	Calhau	Cabo Verde	10	16.86402	-24.86730
CHE	Cape Hedo	Japan	60	26.86430	128.25141
CMA	Col Margherita	Italy	2545	46.36711	11.79341
CPT	Cape Point	South Africa	230	-34.353479	18.489830
CST	Celestún	Mexico	3	20.85838	-90.38309
DDU	Dumont d'Urville	Antarctica	40	-66.66281	140.00929
DMC	Concordia Station	Antarctica	3220	- 75.10170	123.34895
EVK	Ev-K2	Nepal	5050	27.95861	86.8133
ISK	Iskrba	Slovenia	520	45.56122	14.85805
KOD	Kodaicanal	India	2333	10.23170	77.46524
LIS	Listvyanka	Russia	670	51.84670	104.89300
LON	Longobucco	Italy	1379	39.39408	16.61348
LSM	La Seyne-sur-Mer	France	10	43.106119	5.885250
MAL	Mt. Ailao	China	2503	24.53791	101.03024
MAN	Manaus	Brazil	110	- 2.89056	-59.96975
MBA	Mt. Bachelor	WA, USA	2743	43.977516	-121.685968
MCH	Mt. Changbai	China	741	42.40028	128.11250
MHD	Mace Head	Ireland	8	53.32661	-9.90442
MIN	Minamata	Japan	20	32.23056	130.40389
MWA	Mt. Walinguan	China	3816	36.28667	100.89797
NIK	Nieuw Nickerie	Suriname	1	5.95679	-57.03923
PAL	Pallas	Finland	340	68.00000	24.23972
RAO	Rao	Sweden	5	57.39384	11.91407
SIS	Sisal	Mexico	7	21.16356	-90.04679
VRS	Villum Research Station	Greenland	30	81.58033	-16.60961

2.4 Mercury air-surface exchange

Once Hg has been released into the atmosphere, it continually undergoes deposition and re-emission, creating a dynamic global cycle (Schroeder and Munthe, 1998). The continual re-emission of Hg and lack of global inventories has led to considerable uncertainties associated

with estimates of re-emission loadings to the atmosphere (Wang et al., 2006). It is generally not possible to differentiate between primary natural emissions and re-emission when performing air-surface exchange measurements (Gustin et al., 2006). RM is quickly scavenged from the atmosphere by wet and dry deposition processes (Lyman et al., 2007). Once deposited, Hg is easily volatilised and re-emitted back to the atmosphere as GEM (Hintelmann et al., 2002). The historical legacy of anthropogenic Hg emissions has led to an estimated global enhancement factor of 1.5 for terrestrial surfaces, 2.1 in deep ocean sediment, 5.4 for surface oceans and 7.5 in the atmosphere, relative to 2000 BC (Amos et al., 2013). Increases to atmospheric loadings have also led to an estimated threefold increase to atmospheric deposition (Lamborg et al., 2002).

Natural sinks of atmospheric Hg include soils, plant foliage, the marine boundary layer and polar regions, which are continually experiencing re-emission and deposition processes (Gustin et al., 2008). The re-emission of Hg from land surfaces is thought to contribute between 14% and 24% to the global Hg budget (Baya and Van Heyst, 2010). The ocean-atmosphere exchange of Hg accounts for 90% of outputs from the ocean, while wet and dry deposition accounts for 70% of Hg inputs to the ocean (Mason et al., 2017). Recent global reviews of terrestrial Hg⁰ flux measurements (Agnan et al., 2016; Zhu et al., 2016) indicate that in most of the world, elemental mercury (Hg⁰) evasion from background soils is generally low, particularly when soils are covered by leaf litter or plants. Many background soils also experience periods of net Hg⁰ deposition (Choi and Holsen, 2009; Gustin et al., 2006) with recent work finding that 20% of measurements over bare soils and 45% of measurements over covered soils showed net deposition (Agnan et al., 2016).

Hg air-ocean exchange is primarily dominated by emission, making the global oceans a net source of Hg⁰ to the atmosphere, although the magnitude is uncertain (Mason et al., 2017; Song et al., 2016). This exchange helps to mitigate increases in MeHg concentrations in the upper

ocean, thereby limiting fish and human contamination (Mason et al., 2017). Hg evasion varies between oceans and across ocean basins (Mason et al., 2017), with evasion fluxes largely driven by sea-surface temperature (De Simone et al., 2016), although other factors including wind speed, primary productivity, solar radiation levels and air temperature in the surface boundary layer also have an impact (Kwon and Selin, 2016; Soerensen et al., 2010). The upwelling of colder and nutrient-rich waters (particularly in the tropics) is also associated with increased Hg evasion as it increases phytoplankton concentrations in these regions and their ability to reduce divalent mercury (Hg^{2+}) to Hg^0 and enhance the photochemical reduction of Hg^{2+} to the volatile Hg^0 (Semeniuk and Dastoor, 2017; Wang et al., 2013).

Mercury emissions from natural terrestrial sources are highly variable temporally and spatially making them difficult to quantify and characterise. Mercury emissions from terrestrial environments are controlled by various and interacting factors, such as substrate mercury content (Eckley et al., 2010; Liu et al., 2014), soil physical–chemical factors (soil type, soil porosity, soil moisture and soil chemistry) (Choi and Holsen, 2009; Wang et al., 2006) and meteorological parameters (temperature, solar radiation, and wind speed and turbulence) (Gabriel et al., 2011). Studies analysing the influence of these factors on mercury emissions are often inconsistent and even contradictory (Park et al., 2014). Thus regional field and simulation studies of air-surface exchange are particularly important for our understanding of the global Hg cycle (Zhang et al., 2017). In the terrestrial environment, the largest Hg pools are located in soils (Obrist et al., 2011). Smith-Downey et al. (2010), estimated soil Hg storage pools to be 240 Gg, which has increased 20% above pre-industrial levels. More recent model simulations utilising new observational constraints (Horowitz et al., 2017; Streets et al., 2011; Streets et al., 2017) estimate higher present-day organic soil Hg pools (250–1000 Gg with a best estimate of 500 Gg) and propose that anthropogenic activities have doubled the Hg stored in organic soils (Amos et al., 2015; Amos et al., 2013). Atmospheric GEM emissions from

land surfaces were previously estimated to range between 1600 and 2900 Mg a⁻¹ (Lindberg et al., 2007; Selin et al., 2008; Smith-Downey et al., 2010), but more recent estimates are considerably lower, averaging 607 Mg a⁻¹ (ranging between 513 and 1353 Mg a⁻¹) (Agnan et al., 2016).

Terrestrial surfaces are classified as either enriched or background sites. Naturally enriched sites occur due to mineralisation initiated by ancient geological processes. Soils are classified as enriched if Hg concentrations are greater than 100 ppb. Background sites or uncontaminated sites contain substrate Hg concentrations less than 100 ppb (Agnan et al., 2016; Gustin et al., 2008). The dominant source of Hg to background sites is deposition of atmospheric Hg. Highest Hg concentrations are found in the surface layer, decreasing with depth and are bound to carbon and organic matter (Hararuk et al., 2013). There is a large bias toward Hg⁰ flux measurements over Hg-enriched sites, accounting for 63% of all flux measurements, while only 37% of all flux measurements are carried out at background sites (Agnan et al., 2016). Air-surface Hg exchange at enriched sites is heavily skewed towards emission, with increases in the magnitude taking place on diurnal time scales due to the volatilising influences of solar radiation and air temperature (Agnan et al., 2016; Edwards and Howard, 2013). The magnitude of Hg emission from these sites is spatially dependent on the concentration of Hg-containing minerals (Agnan et al., 2016; Gustin, 2003). Large uncertainties regarding terrestrial Hg⁰ sink and source strengths, particularly over background areas and vegetated areas, make atmosphere–terrestrial interactions one of the least understood processes in the global Hg cycle (Obrist et al., 2018).

2.4.1 Drivers of terrestrial air-surface exchange

The short-term balance between Hg flux drivers and deposition processes governs diel and seasonal variation (Jiskra et al., 2018). The flux is defined as the net exchange between Hg entering and exiting a surface. Herein, net flux is positive if the surface is emitting Hg, and when net flux is negative Hg is being deposited on the surface (Carpi and Lindberg, 1997). Most studies suggest that the soil-air interface provides a net source of Hg emissions, with Hg⁰ emission dominating during the daytime and deposition limited to night periods due to variation in temperature and solar radiation (Zhu et al., 2016). Emissions are generally higher during the summer, when solar radiation and temperature levels are also highest. Fluxes in winter tend to be dominated by near zero exchange, while spring trends are influenced by new foliage uptake (Wright and Zhang, 2015).

Soils that contain higher concentrations of Hg are also found to have higher levels of Hg⁰ evasion (Wright and Zhang, 2015). Soils with smaller grain sizes and that contain higher amounts of clay and silt particles tend to have both a higher Hg content and level of Hg⁰ flux (Zhu et al., 2016). Atmospheric Hg⁰ concentrations can both positively and negatively influence the level of Hg⁰ fluxes (Agnan et al., 2016; Wright and Zhang, 2015). Increased evasion tends to occur with lower atmospheric Hg⁰ concentrations, while deposition occurs with higher atmospheric Hg⁰ concentrations (Zhu et al., 2016). In general, higher levels of atmospheric turbulence (e.g., wind and surface friction speeds) promote Hg⁰ evasion as this enhances the mass transfer of Hg⁰ within soil and promotes its evasion from the soil surface (Zhu et al., 2016).

2.4.1.1 Soil volatilisation

Ambient air temperature, soil surface temperature and solar radiation are all positively correlated with Hg⁰ emissions, forming the dominant drivers of diel and seasonal flux patterns

(Choi and Holsen, 2009). Solar radiation enhances Hg fluxes through enhanced photo-reduction occurring within the substrate (Carpi and Lindberg, 1997; Moore and Carpi, 2005). Higher temperature leads to increased rates of volatilisation of Hg from the substrate due to a reduction in the activation energy required to release Hg from the substrate (Kim et al., 2012). The sensitivity to temperature creates diel Hg trends, with the effects of temperature reducing with soil depth (Carpi and Lindberg, 1997). Hg emissions have been shown to sharply increase from early morning until noon where they reach their peak. Emissions then start to decrease at a slowed rate from noon to early evening. These patterns of flux follow closely the diel soil and air temperature trends (Gabriel et al., 2006). The temperature-solar radiation relationship also heavily influences seasonal cycling, where highest Hg flux rate coincides with the warm months and lowest or near zero exchange occurs during the cooler months (Corbett-Hains et al., 2012; Wang et al., 2006).

Solar radiation influences soil Hg evasion in two ways. The first is that increased solar radiation in the surface layer reduces the activation energy required to induce the emission of Hg from the substrate (Lin et al., 2010). The second is solar radiation acting as a catalyst for the transformation of deposited Hg^{2+} to Hg^0 , which can then be emitted to the atmosphere (Carpi and Lindberg, 1997; Gustin et al., 2002; Moore and Carpi, 2005). Solar radiation is thought to cause photoreduction of atmospherically deposited Hg^{2+} to Hg^0 within the substrate that can be emitted to the atmosphere, while increasing soil temperature opens up the soil pore space allowing the photo-reduced Hg^0 to be emitted into the atmosphere (Figure 4) (Zhang et al., 2001). Background sites have been shown to experience increased reduction of Hg^{2+} to Hg^0 during light periods, causing them to become net sources of Hg. When there is no longer any solar radiation to initiate Hg reduction, background soils become a net sink (Xin and Gustin, 2007). Over longer periods, solar radiation is able to influence Hg flux by increasing the soil

temperature through the conversion of solar energy to thermal energy (Zhang et al., 2001).

High soil temperatures drive abiotic and biotic processes within the substrate.

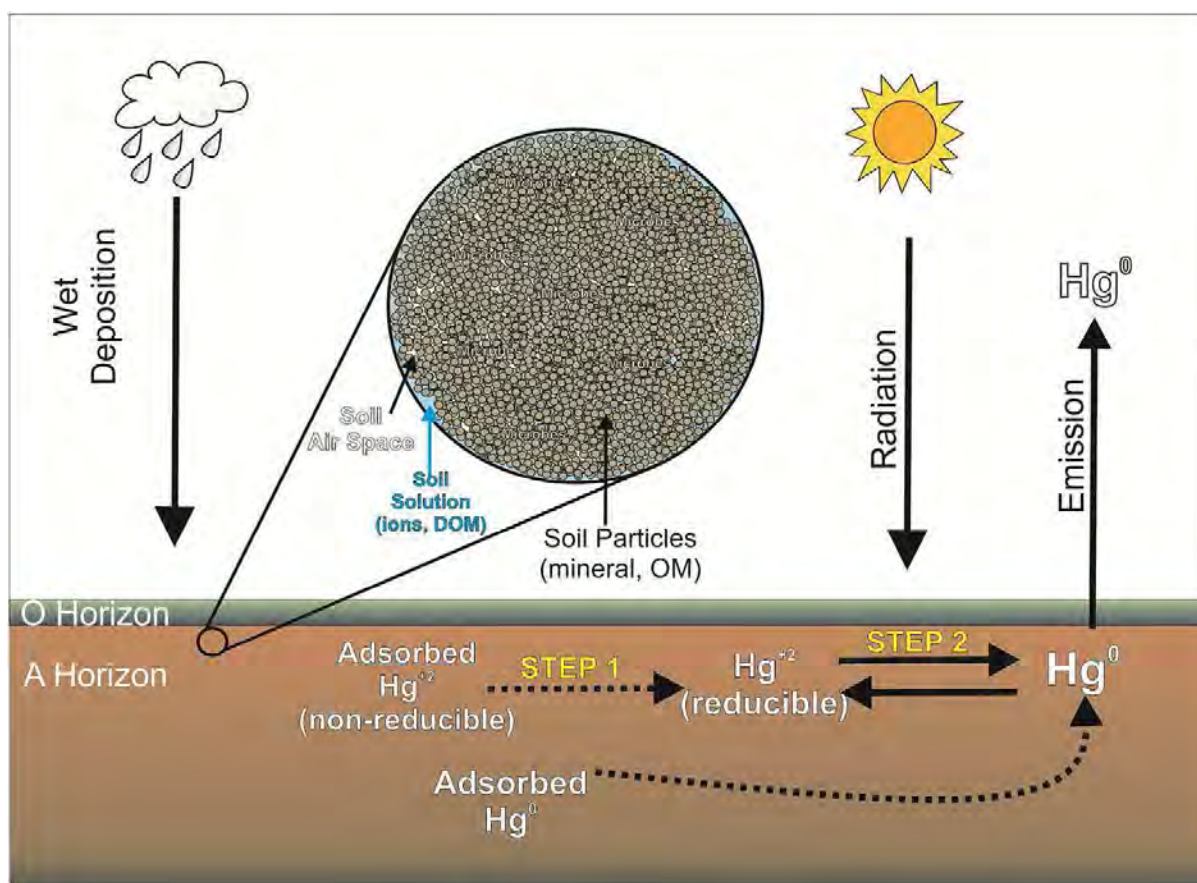


Figure 4. Schematic diagram of major processes and factors affecting mercury volatilization from soil. Major processes of reducible mercury formation (Step 1) and production of elemental mercury from this reducible mercury (Step 2) are identified. Within the soil particles and soil solution OM is Organic matter and DOM is Dissolved Organic matter (DOM) (Pannu et al., 2014).

2.4.1.2 Soil moisture

Precipitation and soil moisture play a significant role in the emissions of Hg from soils (Gustin et al., 2006). The addition of water results in an immediate release of Hg from soils. Hg emissions are hypothesised to be caused by the displacement of air within the soil pores containing Hg^0 by the infiltrating rain water, as well as enhancing the mobility of Hg^{2+} due to

an increase in the soil pore water content and enabling redox reactions associated with the incoming water and soil exchange effects (Song and Van Heyst, 2005). Wetting of dry soils has been shown to induce a greater flux than additional moisture added to already wet soils. The wetting of dry soils has been shown to result in a 2-17 fold increase depending on precipitation type, amount, intensity and timing (Eckley et al., 2011). The magnitude of flux is correlated with Hg concentrations found in the soil substrates. Repeated water additions have been shown to decrease the amount of Hg released from soils, indicating that the effects of precipitation events are dependent on the amount of Hg in the soils available for emission (Song and Van Heyst, 2005). Controlled studies have also shown that the duration of exacerbated flux after watering is a function of the amount of water added and the rate at which soil dries (Gustin et al., 2006).

It is proposed that soil moisture promotes the reduction of Hg^{2+} and desorption of Hg^0 from soil particles into the soil pore space. In general, Hg fluxes increase with an increase in soil moisture as this helps to facilitate the movement of Hg^0 towards the soil surface and its subsequent evasion into the atmosphere. Gustin and Stamenkovic (2005), found that at a soil moisture content of 13%, mean diel Hg fluxes are higher than those observed for dry soils over a 24 hour emission period. Night-time fluxes at 13% soil moisture in the same experiment were greater than those measured from dry soil over the same period. Further to this, Gustin et al. (2006) found that when the soil moisture was increased to 23%, Hg fluxes became similar to those from dry soil with no diel pattern. Once soil moisture was increased above 30%, Hg flux was suppressed (Gustin et al., 2006). Briggs and Gustin (2013) recorded Hg emissions 1 to 2 times higher following the wetting of dry soils. These increases were attributed to the displacement of Hg^0 present in the soil gas, aqueous facilitation of reduction of Hg^{2+} compounds, the movement of Hg compounds toward the surface associated with soil moisture

evaporation and the desorption of loosely bound Hg^0 as the more polar water molecules outcompete it for binding sites.

2.4.1.3 Vegetation

The presence of vegetation within a terrestrial ecosystem significantly influences mercury air-surface exchange. Vegetated ecosystems have been shown to be both a net sink and a net source of atmospheric Hg, with debate still continuing as to which is dominant (Amos et al., 2013; Lindberg et al., 2007; Obrist et al., 2016; Smith-Downey et al., 2010; Zhu et al., 2016). It is estimated that vegetation in forest ecosystems deposits 1232 Mg a^{-1} of atmospheric Hg to terrestrial surfaces through global litterfall, while 1338 Mg a^{-1} of atmospheric Hg is deposited directly onto the soil surface as throughfall. Of this, 381 Mg a^{-1} of Hg is re-emitted back into the atmosphere from the forest floor (Zhu et al., 2016). Throughout the literature it is primarily suggested that grasslands and forested ecosystems are a large net sink of Hg from the atmosphere, with grasslands experiencing an atmospheric deposition of 89 Mg a^{-1} (Agnan et al., 2016). Recent findings by Jiskra et al. (2018) indicate that vegetation acts as a global atmospheric Hg pump. Increasing vegetation production, typically observed during Northern Hemisphere spring, increases the rate of uptake by the plants and contributes to seasonal variation. Current Hg flux data does not provide reliable estimates for the role of foliage in air-vegetation exchanges due to the large uncertainties in quantifying Hg budgets when using bulk methods (e.g., correlation analyses between atmospheric Hg^0 and other trace gases such as CO , CO_2 and CH_4) (Zhang et al., 2016).

Vegetation uptake of Hg^0 is primarily hypothesised to be caused by the direct gaseous exchange of atmospheric Hg^0 that is then sequestered into the leaf tissue (Laacouri et al., 2013; St. Louis et al., 2001). Uptake appears to be greatest during the growing season and is believed to be

driven by atmospheric concentrations, position within the canopy, leaf age, meteorological conditions and CO₂ concentrations (Gustin, 2012). Atmospheric Hg structurally incorporated into leaf tissue has a reduced potential for re-emission due to lack of photo-reduction (Laacouri et al., 2013; Obrist et al., 2016), while Hg²⁺ deposited onto external leaf surfaces is more readily available for re-emission (Graydon et al., 2006). Hg concentrations have been found to be higher in leaves lowest in the canopy and older leaves, although uptake by older leaves occurs at a lower rate than younger leaves (Gustin, 2012).

2.5 Mercury release form biomass burning

Mercury released during biomass burning is the largest natural source within the global Hg budget (Friedli et al., 2009). Biomass burning releases Hg from terrestrial environments back into the atmosphere through volatilisation of Hg within biomass during combustion and through thermal desorption of Hg bound within the soil matrix (Melendez-Perez et al., 2014). Estimates of global Hg emissions from wildfires range from 100 to over 1000 Mg a⁻¹ (Brunke et al., 2001; Friedli et al., 2001; Weiss-Penzias et al., 2007). However, the most recent estimates of 675 ± 240 Mg a⁻¹ from global biomass burning for the years 1997-2006 (Friedli et al., 2009). Hg stored in vegetation, leaf litter and soil are associated with organic rich matter and is mobilised into the atmosphere during a fire, predominantly in the form of Hg⁰. The total amount of Hg released during a wildfire is also limited by the amount of Hg stored in the ecosystem, particularly in the soil, prior to burning (Campos et al., 2015). Therefore, the severity of a fire is an important control on Hg combustion and emission to the atmosphere. Fire severity is furthermore related to the temperature and duration of heating through the soil column and can be influenced by variations in fuel availability, soil moisture, topography, weather, and fire dynamics (Friedli et al., 2003). PBM has also been found to be released during

biomass burning with concentrations increasing with increased fuel moisture, low fire intensity and fuel type (Friedli et al., 2001; Obrist et al., 2008). Spikes in Hg emissions from bushfires have the potential to influence local concentrations, through wet and dry deposition, and regional to global scale Hg concentrations, through long range transport.

The release of mercury from biomass burning is an important, yet complex and poorly understood component of the global mercury cycle as it can lead to re-distribution of mercury to sensitive ecosystems where methylation may occur, or it can result in direct human exposure to mercury through inhalation of biomass burning plumes (Biswas et al., 2008; De Simone et al., 2015). The frequency of both prescribed and wildfires in Australia results in it contributing 3% of total global emissions of Hg from biomass burning. By comparison central Asia, northern hemisphere South America, Europe, and Middle East combined contribute less than 2% of global biomass burning emissions (Friedli et al., 2009). Little focus has been given to understanding Hg emissions and dispersion from Australian bushfires and no published work has been undertaken to measure real time Hg concentrations from fires, prescribed or otherwise.

2.6 Australia's contributions to the global mercury cycle

Australia is one of the largest landmasses in the Southern Hemisphere (area $7.69 \times 10^6 \text{ km}^2$) and a key signatory of the Minamata Convention on Mercury. However, despite globally-growing action and concern regarding the impacts and sources of mercury pollution, little is known about Australia's global contribution (Jardine and Bunn, 2010). Extensive efforts have been made across the Northern Hemisphere to measure, model and estimate the quantities of atmospheric Hg exchange (Zhu et al., 2016). However, there is a lack of reliable estimates for the Australian region regarding the cycling of both natural and anthropogenic emissions

between the atmosphere and terrestrial surface (Edwards and Howard, 2013). A recent emissions inventory found that about 93% of Australia's total Hg emissions are from natural and legacy sources (with emissions from soil and vegetation contributing 66% and 4% of total Hg emissions respectively) and 7% of Hg emissions derive from anthropogenic sources (Nelson et al., 2009; Nelson et al., 2012; Nelson et al., 2004). However, these estimates are uncertain due to a lack of Australia-specific data and uncertainties inherent in estimating emissions factors.

Current attempts to determine Australia's natural Hg cycle have been undertaken as part of global scale modelling studies, which do not consider Australia's unique climate, flora, fauna and soil types. Studies by Nelson et al., (2004, 2009, 2012) are the only efforts to date to treat Australia as a distinct entity. Nelson et al. (2012) estimated annual emissions of 4 to 12 Mg Hg a⁻¹ from vegetation; 27 to 81 Mg Hg a⁻¹ and 43 to 129 Mg Hg a⁻¹ from shaded and bare soil, respectively; and 21 to 63 Mg Hg a⁻¹ from biomass burning. These total between 90 and 93% of estimated emissions from all primary and secondary sources within Australia. Estimates of anthropogenic emissions from these authors range between 10.2 and 15.5 Mg Hg a⁻¹, representing about 0.5% of the estimated global total (Nelson et al., 2004). Approximately 50% of the total anthropogenic emission was reported to originate from a single gold smelter operation in Western Australia which has since altered its operation, in favour of a less environmentally hazardous process which captures rather than releases Hg to the atmosphere (Nelson et al., 2012). Nelson et al. (2009) state that there are considerable uncertainties to these loadings due to the heavy reliance on Northern Hemisphere emission factors and assumptions when modelling natural Hg cycling over the Australia continent.

Australia is home to many unique environments and potentially distinctive oxidative conditions, and therefore plays a significant role in the natural Hg cycle. Despite this, only two air-surface mercury exchange studies have taken place here (Edwards and Howard, 2013;

Howard and Edwards, 2017). Australia is host to a range of climate zones that include equatorial, tropical, subtropical, desert, grassland and temperate regions. As Hg fluxes are influenced by precipitation rates, temperature, and vegetation type, it is expected that Hg fluxes will differ between these different climate zones. The Australian climate is also influenced by interannual climate variables such as El Niño-Southern Oscillation (ENSO), Southern Annular Mode and Indian Ocean Dipole. El Niño brings higher temperatures and reduced rainfall to Australia, while La Niña is accompanied by cooler temperatures and heavy rainfall (Slemr et al., 2016). Southern annular mode and Indian Ocean Dipole can further intensify rainfall and drought conditions which influences the intensity of Australia's fire and vegetation growing seasons (BOM, 2019). This climate variability is likely to cause Australian natural Hg emissions to behave differently to those observed in other regions of the world (Pirrone et al., 2010).

2.7 Summary

This Chapter has provided a detailed overview of the sources, sinks and drivers of the global mercury biogeochemical cycle. Hg cycling is heavily influenced by the surrounding environment and thus concentrations, speciation and behaviour varies over spatial and temporal scales. Meteorology and chemistry (in the surface and the atmosphere) are the biggest drivers of the natural Hg cycle, although the exact mechanisms are still debated. Key uncertainties still exist within the current understanding of the global Hg cycle. These include drivers of atmospheric deposition over both ocean and terrestrial surfaces and the mechanisms driving terrestrial Hg air-surface exchange on diel and seasonal timeframes. The following chapters will focus on developing a better understanding of terrestrial Hg air-surface exchange within an Australian context.

CHAPTER 3

Seasonal mercury fluxes at a terrestrial background site in South-Eastern Australia

3.1 Preface

This chapter explores mercury air-surface exchange at a background site in South-Eastern Australia, with the express purpose of identifying seasonal trends and drivers of variability. Few studies have taken place over extended timeframes, and none have taken place in the Southern Hemisphere. This study investigated the drivers of Hg fluxes across multiple seasons in order to gain an understanding of the influence of vegetation and environmental parameters on Hg air-surface exchange across seasonal time scales, providing a better understanding of Australia's role in the global mercury cycles. This chapter contributes to the thesis by identifying the primary drivers and trends of background mercury air-surface exchange and atmospheric mercury within an Australian landscape.

Author contributions

At time of thesis submission, the paper presented in this chapter had been submitted for publication in *Elementa: Science of the Anthropocene*. The paper has thus been formatted and structured according to journal submission requirements.

The field sites established in this study was maintained and monitored by me. All data collection, analysis and the majority of manuscript preparation was undertaken by me, with intellectual contributions from Co-authors, Dr Grant Edwards and Dr Paul Beggs.

Katrina MacSween: 80%, Grant Edwards: 10%, Paul Beggs: 10%

Seasonal mercury fluxes at a terrestrial background site in South-Eastern Australia

Katrina MacSween*, Grant C. Edwards, Paul J. Beggs

Department of Environmental Sciences, Faculty of Science and Engineering, Macquarie University, Sydney, New South Wales, Australia

* Corresponding author: katrina.macsween@mq.edu.au

Abstract

Terrestrial air-surface exchange of mercury (Hg) forms an important component of the global Hg cycle, with drivers varying across spatial and temporal scales. These drivers primarily include substrate properties, atmospheric chemistry and meteorological factors. However, their influence is still poorly quantified. Few studies have taken place over extended timeframes, and none have taken place in the Southern Hemisphere. This study presents the first long-term mercury air-surface exchange measurements to take place in Australia, investigating the drivers of Hg fluxes across multiple seasons. Measurements were made continuously using a micrometeorological aerodynamic flux gradient method at a low vegetated background site in South-Eastern Australia, over 14 months. Average net Hg fluxes across the entire study period were near zero, $0.002 \text{ ng m}^{-2} \text{ h}^{-1}$ (± 14.23). Variability was observed across seasons, with the highest average net emissions occurring in austral summer (December, January, February) ($0.34 \text{ ng m}^{-2} \text{ h}^{-1}$) and highest net deposition observed in autumn (March, April, May) ($-0.32 \text{ ng m}^{-2} \text{ h}^{-1}$). Vegetation uptake of Hg was most important during winter and spring, when the influence of meteorological variables is reduced. Summer Hg fluxes were mostly dominated by surface emissions. This is largely attributed to the higher net all-wave radiation and soil and air temperatures, which were also highest at this time. For grasslands/low vegetated sites to see

significant vegetation uptake of Hg, the parameters that most influence Hg evasion, i.e., net all-wave radiation, and air and soil temperature, need to be simultaneously reduced.

1. Introduction

Mercury (Hg) is a globally transported atmospheric pollutant that can have adverse environmental and human health effects (Carpi and Lindberg, 1997; Schroeder and Munthe, 1998). Its long atmospheric lifetime and unique chemical properties allow it to be transported over large distances before being deposited, making it ubiquitous in the environment (Corbitt et al., 2011; Gustin, 2012). Mercury is released into the atmosphere naturally, anthropogenically, or through re-emission of natural and anthropogenically-derived Hg (Amos et al., 2013; Gustin et al., 2008). This re-emission of Hg from surfaces is an important component of the global Hg cycle as it is what allows Hg to remain in the environment for long periods of time and to be globally distributed (Hintelmann et al., 2002; Schroeder and Munthe, 1998). Terrestrial air-surface exchange of Hg is heavily influenced by substrate properties, atmospheric chemistry and meteorological factors. These drivers are highly variable between sites and across time, which has made it difficult to adequately assess the key controls (Agnan et al., 2016; Gabriel et al., 2011; Lin et al., 2010; Wang et al., 2006; Zhang et al., 2001).

Studies exploring these processes are usually skewed towards enriched sites (substrate concentration >100 ppb, atmospheric concentrations >3 ng m⁻³) and the Northern Hemisphere, and usually only occur over a period of days to weeks (Agnan et al., 2016). Currently there is a limited number of studies that look at elemental Hg (Hg⁰) exchange on an annual or longer time-scale (Baya and Van Heyst, 2010; Converse et al., 2010; Obrist et al., 2005; Sommar et al., 2016). The variability in Hg fluxes means that short-term studies can create bias in our

understanding of Hg flux trends (Gustin et al., 2006). Long-term studies allow for a broader understanding of the driving processes, enabling a holistic picture of the Hg biogeochemical cycle (Baya and Van Heyst, 2010; Lee et al., 2000). Few studies have taken place on these time scales, and none have taken place in the Southern Hemisphere where season variability is very different to that observed in the Northern Hemisphere (Edwards and Howard, 2013; Nelson et al., 2012). The difference in land to sea ratio between the two hemispheres, means that the Southern Hemisphere is subject to more significant long-term climate variability. This has led to an incomplete understanding in the global seasonal variability of Hg fluxes.

The short-term balance between Hg emission, deposition and re-emission processes at terrestrial sites governs diel and seasonal Hg^0 variations (Jiskra et al., 2018; Zhou et al., 2016). Solar radiation, temperature, soil moisture and substrate Hg concentrations are widely believed to be the main parameters driving Hg air-surface exchange (Choi and Holsen, 2009; Gustin et al., 2006; Gustin et al., 1997; Kim et al., 2012; Kim et al., 1995). The presence of vegetation can also cause net deposition to occur during the growing season (Obrist et al., 2005). Surface emissions tend to be highest around midday when solar radiation and air and soil temperatures are at their highest. On seasonal scales, warmer months often result in higher emission, and near zero or negative fluxes occur during cooler months and overnight (Bahlmann et al., 2006; Fritsche et al., 2008; Wang et al., 2006).

The positive relationship observed between solar radiation, air temperature, soil temperature and Hg emission is believed to be a result of the relationship between the physiochemical properties of Hg^0 and the abiotic processes occurring in the substrate (Bahlmann et al., 2006; Choi and Holsen, 2009). Solar radiation enhances emissions through the reduction of divalent mercury (Hg^{+2}) to Hg^0 within the substrate which is then available for re-emission (Carpi and Lindberg, 1997; Moore and Carpi, 2005). Higher temperature leads to increased rates of volatilisation of Hg from the substrate due to a reduction in the activation energy required to

release Hg from the substrate (Kim et al., 2012). Increasing soil temperatures due to solar irradiation also promote Hg⁰ emissions (Wang et al., 2006). The vapour pressure of volatile Hg species is increased with rising soil temperatures which also decreases Hg sorption to the soil and allows greater emission from the substrate (Liang et al., 2014).

The presence of vegetation in the ecosystem adds an extra layer of complexity to the drivers of Hg air-surface exchange. Vegetated ecosystems can represent both a source and a sink for Hg⁰ over shorter or longer periods, depending on the atmospheric concentration, meteorology, substrates, climate conditions and plant community composition (Agnan et al., 2016; Bash and Miller, 2008; Converse et al., 2010; Lee et al., 2000). In a review of global Hg flux studies Agnan et al. (2016) found 20% of measurements over bare soil within forests and grasslands/shrub lands show net deposition. This increased to 48% of measurements in these ecosystems when the presence of vegetation was taken into consideration (Agnan et al., 2016). The presence of plants and litter may also impact the soil–air Hg flux by altering air mixing, shading the soil, and influencing soil moisture and temperature (Stamenkovic et al., 2008) and therefore must be accounted for when considering whole ecosystem-level Hg exchange.

Australia is host to unique climates, vegetation and soil types, all of which may cause Hg air-surface exchange to behave differently to that elsewhere. Despite Australia having a highly variable climate and being one of the largest landmasses in the Southern Hemisphere, few attempts have been made to quantify Hg exchange rates and drivers (Edwards and Howard, 2013; Howard and Edwards, 2017). South-Eastern Australia's climate is primarily classified as temperate or subtropical, experiencing warm to hot summers and cool winters, with an annual average maximum temperature of 25°C and annual average minimum temperature of 13°C. Annual average regional rainfall typically ranges between 600 and 1000mm. Rainfall variability in the region is typically driven by El Niño-Southern Oscillation, where El Niño causes higher temperatures and decreased rainfall and La Niña causes lower temperatures and

increased rainfall (Bureau of Meteorology, 2019). Further, UV radiation in the Southern Hemisphere is approximately 50% greater than the Northern Hemisphere due to earth's elliptical orbit, more efficient ozone transportation from the equator to higher latitudes and overall less aerosols present in the atmosphere (McKenzie et al., 1996). Higher radiation could increase the potential for photo-chemical reduction to take place within terrestrial substrates.

This study represents the first long-term mercury air-surface exchange measurements to take place in Australia. This study investigated the drivers of Hg fluxes across multiple seasons in order to gain an understanding of the influence of vegetation and environmental parameters on Hg air-surface exchange across seasonal time scales. Measurements were made continuously using a micrometeorological aerodynamic flux gradient method at a low vegetated background site in South-Eastern Australia, over a 14 month period.

2. Methods

2.1 Site description

This study took place at Oakdale, New South Wales, Australia a rural area on the far south-west edge of the Sydney basin (lat. 34° 03' 11"S, long. 150° 29' 50"E, altitude 457m). Measurements were undertaken from 3 April 2017 to 21 June 2018 (445 days), within an agricultural grazing paddock. Soils for the region were classified as sandy clay loam. No known major point sources of Hg were identified within the region. Vegetation cover consisted of low grass, edged by tall eucalyptus trees, however these were out of the measurement fetch. At the start of the study the vegetation coverage was patchy, and the greatest coverage occurred during spring. The paddock was also regularly grazed, keeping canopy height to less than 0.02 m over the duration of the field campaign.

2.2 Hg flux gradient method

Hg⁰ fluxes were determined using a micrometeorological aerodynamic flux gradient method and assumptions outlined in Edwards et al. (2005). Hg⁰ flux was calculated according to Equation 1:

$$F = -K \frac{\Delta C}{\Delta z} = \frac{u^* k (C_2 - C_1)}{\ln\left(\frac{z_2 - d}{z_1 - d}\right) - \Psi_{z_2} + \Psi_{z_1}} \quad (\text{Equation 1})$$

where F is the Hg flux (ng m⁻² s⁻¹), K is the eddy diffusivity (m² s⁻¹), C is the Hg⁰ concentration at height z (z₁ = 0.44 m and z₂ = 1.24 m), u* is the friction velocity (m s⁻¹), k is the von Kármán constant (0.40), d is the zero-plane displacement height (m), and Ψ is the integrated universal similarity functions as given by Businger et al. (1971) for the two measurement heights (z₁ and z₂). By convention, a positive flux is upward (emission) and a negative flux is downward (deposition).

Hg⁰ gradients were calculated using air samples collected alternating between two heights (z₁ = 0.44 m and z₂ = 1.24 m) and quantified using a Tekran 2537B (Tekran Instruments, Knoxville, TN, USA), with detection limit of 0.1 ng m⁻³. Sample air was drawn from the sample inlets through a 0.2 μm polytetrafluoroethylene (PTFE) filter by a PTFE pump at 10 L min⁻¹. The 2537B sub-sampled from this flow through an additional 0.2 μm PTFE filter. Switching of sampling between the intakes took place every 10 minutes (2 × 2537B samples) and was achieved using a PTFE solenoid valve controlled by LabVIEW software. Internal calibration of the 2537B occurred every 23 hours throughout the study using the internal mercury permeation source. Permeation sources were verified at the beginning and end of the study, as well as part-way through when the Tekran was removed for routine maintenance using manual

mercury vapour injection to 2% resolution of the permeation source. Thirty-minute running means of the Tekran measurements were used to calculate flux gradient.

The average flux gradient was first constructed using a 90 min averaging period (five 10 min samples at one height and four 10 min samples at the other height). After the first gradient was constructed, a running 90 min mean gradient was then updated every half hour. Density corrections due to water vapour and heat outlined by Webb et al. (1980) were applied to each averaging period. Quality assurance methods were applied to the micrometeorological data based on the constraints of Monin-Obukov similarity theory. This included filtering for low wind speeds (<0.5 m/s) and wind direction, to allow for sufficient fetch. Highly stable and unstable conditions (stability parameter, z/L (Monin-Obukhov length) less than -5 or greater than 5), were also removed so that turbulence theory hold true (Wagner-Riddle et al., 1997). 77% of the data obtained over the study period remained after these quality assurance measures were applied to the dataset.

2.3 Substrate analysis

Soil substrate samples were collected 3 times over the duration of the study, at the beginning, mid-way point (September) and end of the study. Samples were collected at 5 locations within the main fetch of the flux tower. Surface vegetation, along with soils at depths of 0 to 2 cm and 5 to 10 cm were sampled using clean equipment and stored in double sealed plastic bags. Vegetation and soil samples were dried at 105 °C for 24 h before analysis (Mudroch and Bourbonniere, 1994). Hojdova et al. (2015) estimated that between 5 and 8% of Hg was lost from the sample when dried in an oven over 3 days. Samples were only dried for 24 hours to limit the potential amount of Hg lost in the drying process. Soil samples were then sieved into >250 μm , 63 μm to 250 μm (sand), and < 63 μm (silt/clay) size fractions. Total mercury (THg)

contents of soil and vegetation samples were determined in triplicate using a DMA-80 direct mercury analyser (Milestone Inc., Shelton, CT, USA) and US EPA Method 7473. Instrument precision was verified to within 5 % using 5 repetitions of 100 µl of a 100 ppb Hg standard. Calibrations were checked using National Institute of Standards and Technology (NIST) traceable Standard Reference Material (SRM, NIST 1575a and 2709a). Soil organic carbon (SOC) was determined according to the loss on ignition method described by Nelson and Sommers (1996).

2.4 Eddy covariance measurements

Eddy covariance flux measurements of sensible and latent heat, carbon dioxide (CO₂), water vapour and momentum (required for Hg flux gradient) were taken at a height of 3.12 m using a CSAT-3 sonic anemometer (Campbell Scientific, Logan, UT, USA) and LI-7200 closed-path, infrared gas analyser (Li-Cor Biosciences, Lincoln, NE, USA). CO₂ flux measurements were also conducted using LI-7200 closed-path, infrared gas analyser to look at the relationship between Hg flux and vegetation uptake. CO₂ net exchange provides an estimation of ecosystem respiration rates over time (Sommar et al., 2016). Li-Cor Samples were collected at 10 Hz using a SmartFlux System (version 1.10). Li-cor 7200 was replaced part way through the study period with an open-path 7500 Analyzer due to hardware malfunction. Post-processing and quality control of eddy covariance fluxes was undertaken using Li-cor EddyPro[®] software (version 6.2.0).

2.5 Environmental variables

The four components of net radiation, long-wave incoming (LW↓) and outgoing (LW↑), and short-wave incoming (SW↓) and outgoing (SW↑), were measured at 3.12 m using a Net

Radiometer (apogee SN-500). Air temperature was obtained using a CSAT-3 sonic anemometer and relative humidity were measured using LI-7200. Soil temperature was measured using five t-type thermocouples at depths of 2cm, 5cm, 10cm, 20cm and 30cm. Soil Volumetric Water Content (VWC) was measured at three depths (5cm, 15cm, and 30cm), using a CS616 water content reflectometer (Campbell Scientific Inc.) for 5cm measurements and MP306 Moisture Probes at 15cm and 30cm. Soil heat flux was measured at two depths (5cm and 15cm) using HFP01SC Self-Calibrating Heat Flux Sensors (Campbell Scientific Inc.). All radiation and substrate variables were logged using a CR3000 Campbell Scientific data logger, averaged over 30 minutes at 60 Hz.

2.6 Data analysis methods

Statistical analysis was undertaken in numerous forms to assess the potential relationships between Hg fluxes and environmental parameters and to determine significance of variance between Hg fluxes across multiple time scales. All statistical analysis and correlations were undertaken using MATLAB® software. Variables were chosen based on those previously shown to influence Hg fluxes in the literature. Analysis was performed across the entire study period and then for each season (autumn 2017 and 2018 were grouped together). Fluxes were also filtered for positive fluxes (emission) to identify if environmental variables influenced Hg emission.

Two-way *t*-tests were used to determine if seasonal and diel Hg flux trends were statistically different from each other. Null hypothesis was rejected if the difference between means was found to have a significance less than 5% ($p\text{-value} < 0.05$), unless stated otherwise. Spearman correlations were performed to determine relationships between Hg fluxes and individual

environmental variables. Correlations were deemed to be statistically significant if p-values were <0.01.

Diel composites were calculated by first binning each measurement made in the same half-hour period over 24 hours within each season. Basic statistical values (mean, maximum, minimum, median, 25% quartile (lower) and 75% quartile (upper)) were then calculated for each half-hour binned period to provide a 24hr time series. Cumulative Hg fluxes were calculated by continuously adding the previous half-hour value to current value over the entire study duration. Gaps within the data were forced to zero to preserve the cumulative calculations.

3. Results

3.1 Site Characteristics

Soil substrate Hg concentrations at this site averaged 68.83 ppb (standard deviation (SD) 22.10 ppb) over the duration of the study, classifying it as a background site. Substrate Hg concentration at a depth of 0-2cm and 5-10 cm was 67.44ppb (SD 19.86) and 73.13 ppb (SD 23.38), respectively. Surface vegetation mercury concentration averaged 82.25 ppb (SD 4.46). Concentrations were found to vary little both within the measurement area and over the duration of the study.

3.2 Mercury fluxes

Mercury emission fluxes averaged across the entire study period were near zero, $0.002 \text{ ng m}^{-2} \text{ h}^{-1}$ (SD 14.23). However, fluxes were highly variable, demonstrating diel bidirectional exchange. Daytime fluxes averaged $0.31 \text{ ng m}^{-2} \text{ h}^{-1}$ (SD 11.94), while night-time fluxes

averaged $-0.22 \text{ ng m}^{-2} \text{ h}^{-1}$ (SD 11.34) (Table 1). 19.80% of Hg flux values fell below the theoretical gradient resolution as defined by equation 8 of Edwards et al., (2005). These values were not removed from the data analysis to avoid any artificial increase in observed means. Variability was also observed across seasons with the highest average net emissions occurring in austral summer (December, January, February) ($0.69 \text{ ng m}^{-2} \text{ h}^{-1}$) and highest average net deposition observed in winter 2017 (June, July, August) ($-0.50 \text{ ng m}^{-2} \text{ h}^{-1}$). Winter 2018 presented with a higher average deposition rate of $-0.95 \text{ ng m}^{-2} \text{ h}^{-1}$, however, only 21 days were recorded before measurement period ended. Spring and autumn 2017 exhibited diel bidirectional exchange with spring having a daytime average of $0.81 \text{ ng m}^{-2} \text{ h}^{-1}$ and night time average of $-0.19 \text{ ng m}^{-2} \text{ h}^{-1}$. Autumn 2017 observed the opposite trend with deposition occurring during the day ($-0.65 \text{ ng m}^{-2} \text{ h}^{-1}$) and emission occurring at night ($0.79 \text{ ng m}^{-2} \text{ h}^{-1}$). Atmospheric Hg concentrations echoed observed flux trends with highest concentrations occurring during summer (0.88 ng m^{-3}) and lowest in winter (0.43 ng m^{-3}). Overall, ambient Hg average was 0.68 ng m^{-3} (SD 0.22), below both global and Southern Hemisphere background levels.

Table 1. Seasonal means and standard deviation (SD) for Hg flux measurements and measured environmental variables across the study duration (3 April 2017 to 21 June 2018) at Oakdale, NSW. Averages were separated into day and night to show diel variability for those variables known to exhibit diel variability. Net all-wave radiation (Net Rad) provides day maxima and night negative maxima. Total solar is the total short-wave radiation (incoming – outgoing).

		Hg Flux ng m ⁻² h ⁻¹		Air Temperature °C		Soil Temperature (5cm) °C		Net Rad W m ⁻²	Total Solar W m ⁻²		VWC (5cm) %		Sensible heat flux W m ⁻²		CO ₂ flux μmol m ⁻² s ⁻¹		Ambient Hg ng m ⁻³	
		mean	SD	mean	SD	mean	SD	max	mean	SD	mean	SD	mean	SD	mean	SD	mean	SD
Autumn 2017	Day	-0.65	7.79	14.45	0.64	15.78	2.07	569.90	117.96	181.75			120.62	87.41	-6.46	7.46		
	Night	0.79	10.96	14.36	0.78	15.78	1.88	-98.18					47.17	73.02	4.22	7.24		
	All	0.11	9.61	14.40	0.73	15.8	1.95				21.65	2.80	76.03	86.70	0.04	7.74	0.46	0.10
Winter 2017	Day	-0.99	11.60	13.17	2.35	11.49	1.38	547.40	109.63	171.23			128.61	120.01	-0.80	2.00		
	Night	-0.07	11.85	11.91	3.38	11.64	1.24	-100.05					58.49	109.52	1.27	1.79		
	All	-0.50	11.74	12.37	3.09	11.59	1.29				22.46	3.14	85.41	118.65	0.47	3.03	0.43	0.08
Spring 2017	Day	0.81	10.51	14.22	1.13	18.64	3.72	776.13	183.77	257.38			184.46	136.70	-1.54	3.70		
	Night	-0.19	7.73	13.86	1.45	17.99	3.25	-105.27					82.92	122.22	1.53	2.78		
	All	0.32	9.28	14.03	1.38	18.31	3.49				15.95	1.16	130.74	138.58	-0.01	5.13	0.71	0.19
Summer 2017/2018	Day	0.94	7.41	20.45	5.70	25.03	3.25	818.12	202.31	257.38			122.14	100.47	0.38	14.39		
	Night	0.37	8.20	17.58	3.78	24.49	2.59	-120.57					23.96	57.22	3.36	26.16		
	All	0.69	7.76	19.03	5.05	24.76	2.95				14.04	1.28	74.99	96.02	1.85	21.10	0.88	0.19
Autumn 2018	Day	-0.40	16.22	17.63	4.58	19.32	3.58	788.95	138.11	208.40			108.67	106.83	-0.66	8.94		
	Night	-0.22	13.85	15.56	3.22	19.10	3.37	-115.31					46.25	107.62	2.01	7.24		
	All	-0.31	15.02	16.43	3.98	19.19	3.46				14.43	1.29	73.24	111.63	0.89	8.10	0.64	0.17
Winter 2018	Day	2.20	17.08	13.49	1.64	11.60	1.38	392.93	81.83	123.87			151.91	136.97	0.77	1.55		
	Night	-1.59	17.08	12.24	2.65	11.85	1.31	-100.38					81.38	113.18	1.32	1.91		
	All	-0.95	16.45	12.68	2.42	11.76	1.34				15.62	1.33	106.17	126.56	1.12	1.81	0.52	0.08
All	Day	0.31	11.94	15.98	4.47	18.29	5.67	818.12	147.36	255.46			135.63	117.96	-0.78	5.42		
	Night	-0.22	11.34	14.29	3.42	17.16	5.17	-120.57					54.92	102.65	1.39	7.82		
	All	0.00	14.23	15.01	3.99	17.65	5.40				17.15	3.97	90.20	116.69	0.65	10.05	0.68	0.22

Cumulative mercury flux shown in Figure 1 indicates that the site was dominated by net deposition until early spring. The site then switched to net emission which continued through summer to mid-autumn 2018, where cumulative fluxes began to decline again. The net cumulative emission stage was greater than the net cumulative deposition stage, with cumulative flux maximum reaching 2683.20 ng m^{-2} (on 30 April 2018) while cumulative flux minimum was -1028.10 ng m^{-2} (13 September 2017).

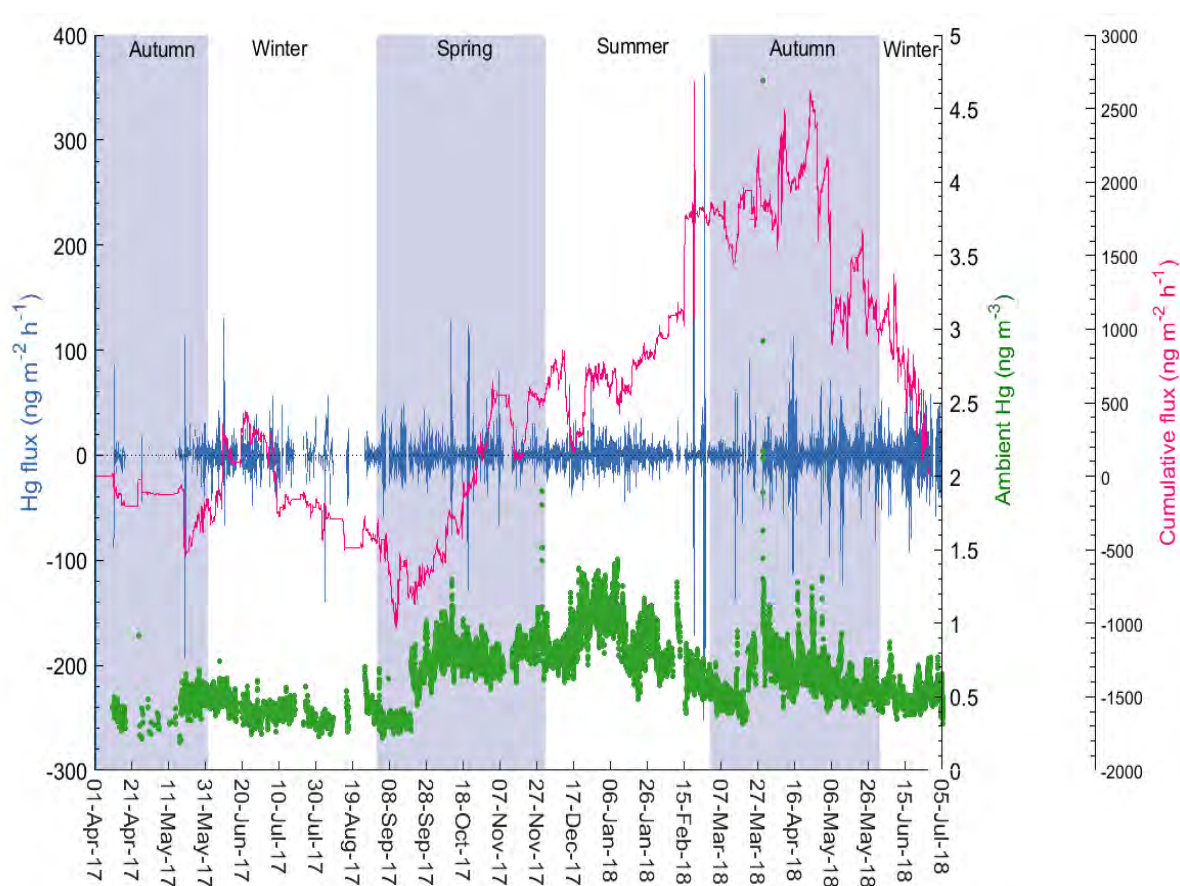


Figure 1. All Hg fluxes (blue), ambient Hg (Green) and cumulative Hg flux (magenta) 3 April 2017 to 21 June 2018 in Oakdale, New South Wales. Axis label colour corresponds to line colour. Shading represents changes in season, as labelled.

Diel composite trend for mean Hg fluxes and meteorological trends were clearest during summer and winter, although opposite (Figure 2). Autumn and winter diel composites include both autumn 2017 and 2018 measurements. Winter was the only season to have a statistically

significant (p -value < 0.01) difference between day and night time measurements (Appendix 1, Table 1). Summer predominantly experienced emission during the day and deposition overnight. This trend follows the soil temperature trend, although Hg flux peak coincides with radiation maxima. Winter diel Hg fluxes show net deposition occurring during the day and emission overnight. Diel trends for both spring and autumn are less clear, with both seasons shifting continually between emission and deposition over the 24 hour period. Springs diel trends indicated higher variability during the day than overnight, as indicated by the inter-quartile range. However, the mean 24 hour values did not reflect this to the same extent.

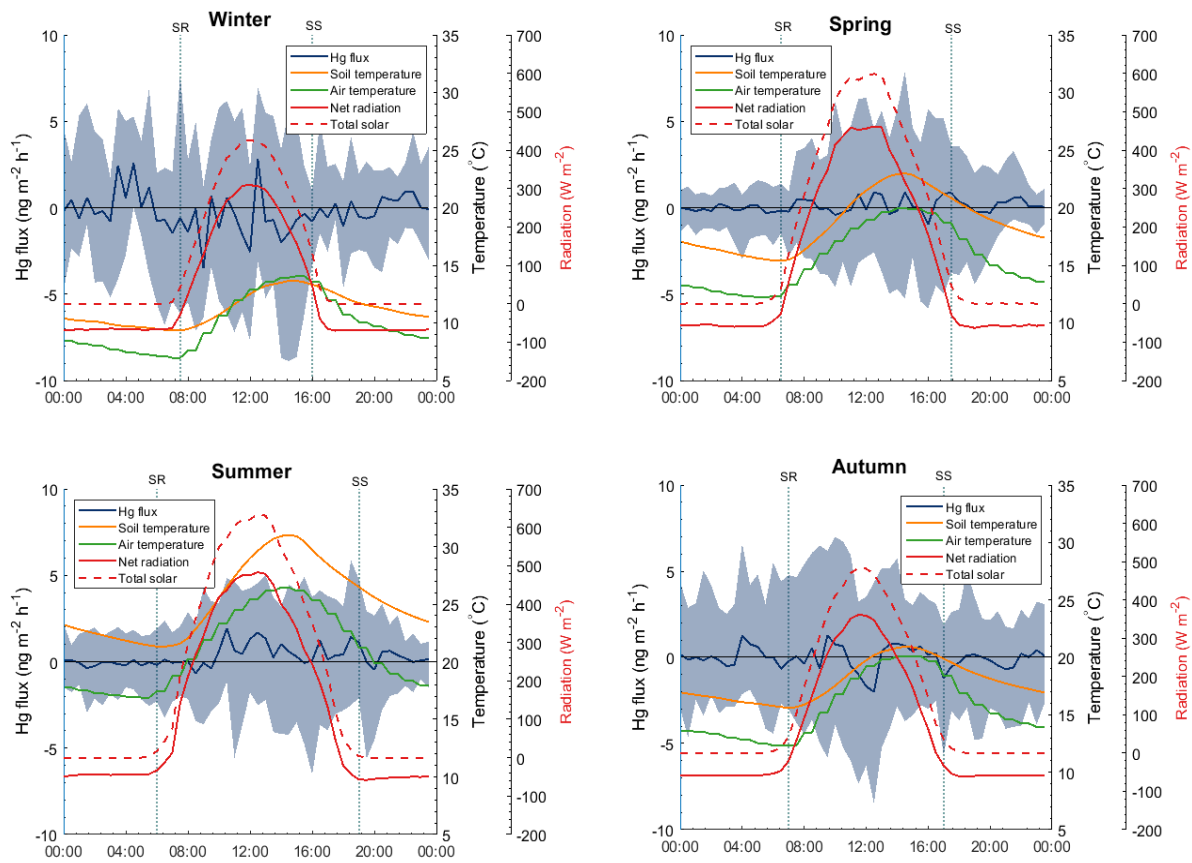


Figure 2. Diel mean composite trends for Hg flux (navy line), shaded area shows inter-quartile range, soil temperature at 5cm, air temperature, net all-wave radiation, and total short-wave radiation across each season at Oakdale, NSW. Dotted vertical lines indicate median sunrise and sunset times for each season.

3.3 Relationship with Environmental variables

Monthly average Hg fluxes follow a trend similar to those seen for net all-wave radiation and air temperature (Figure 3). Highest Average air temperature, soil temperature and maximum daytime net radiation occurred during summer (19.03 °C, 24.76°C and 818.12 W m⁻², respectively (Table 1)). Fluxes are lowest in July, during the middle of winter, and peak in the summer month of February. The winter Hg flux minima closely aligns with the minima observed for net all-wave radiation, air temperature and soil temperature, all of which occur around July. Winter (2017) had the lowest average air temperature (12.37 °C), soil temperature (11.59 °C) and maximum daytime net all-wave radiation (547.40 W m⁻²). The maximum February Hg flux is slightly offset from the peaks in temperature and net all-wave radiation that were observed in November. VWC trends were opposite to these trends, peaking in June (30%), when Hg fluxes averaged net zero emissions.

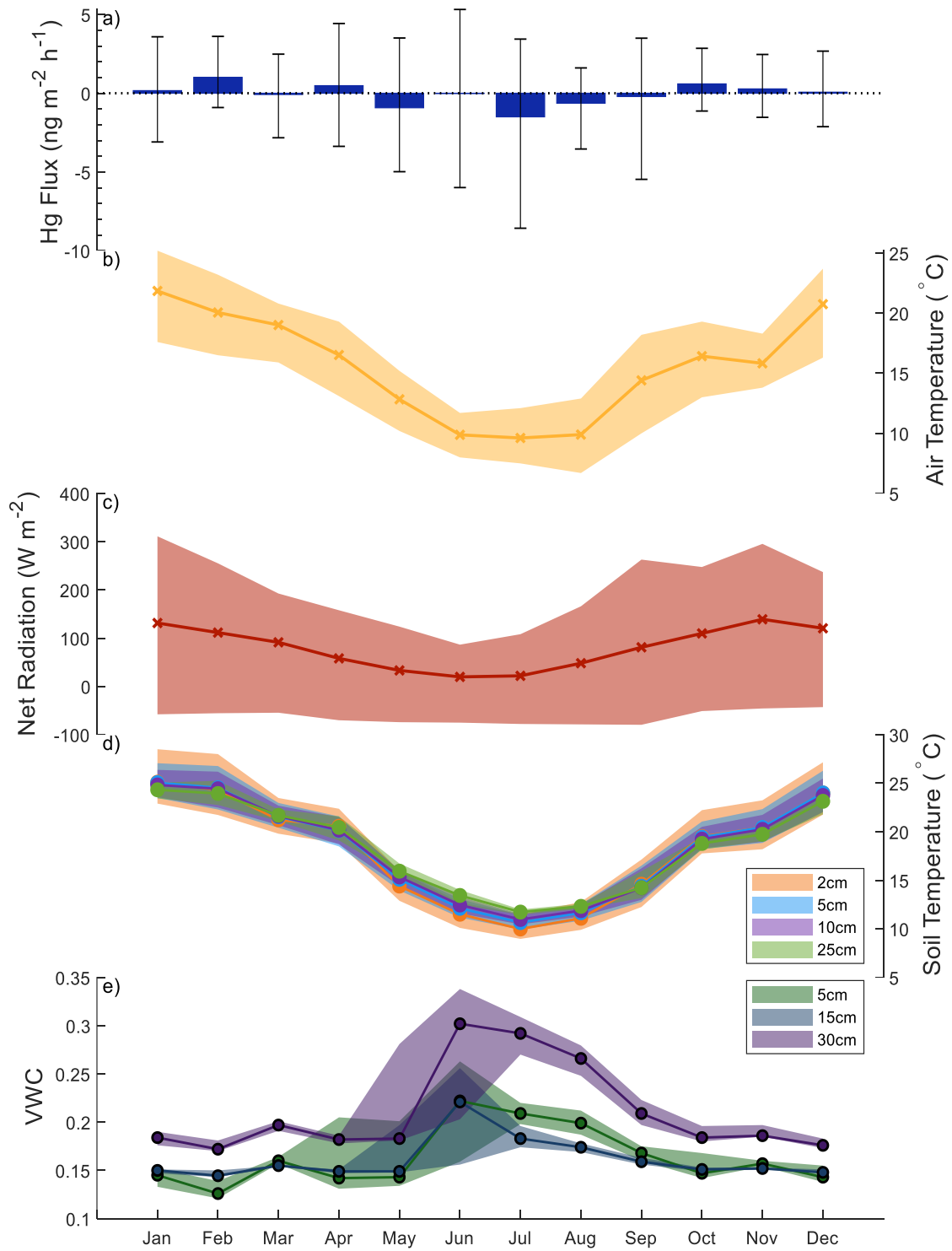


Figure 3. Monthly mean Hg flux and associated environmental variables. Months that were repeated averaged together to confine trends to 12-month period. For Hg flux (a) column the monthly average and bars represents upper and lower inter-quartile range. For the environmental variables (b-e), solid line is mean value and shading is the inter-quartile range.

Across the entire study period, Hg fluxes were found to have a significant relationship (p-value <0.01) with net radiation, air temperature, relative humidity and soil temperature at all depths, however correlations were low (Table 2). When Hg fluxes were isolated to just positive fluxes the only variable not to have a significant relationship was air temperature. Sensible heat had the strongest relationship with positive Hg fluxes, $r = 0.26$. Soil temperatures at all depths presented with a negative correlation with positive Hg fluxes across the entire study period, contrary to what has been observed in the literature. These relationships do however vary between seasons.

Table 2. Spearman correlations with all Hg fluxes and positive Hg fluxes for each season and across the entire study duration at Oakdale, NSW. T_s is the soil temperature at each measured depth, VWC is the volumetric water content at each measured depth, RH is the relative humidity and Q^* is the net all-wave radiation. Bold values indicate significant correlations (p-value <0.01).

	Spring		Summer		Autumn		Winter		All	
	Positive flux	All flux	Positive flux	All flux	Positive flux	All flux	Positive flux	All flux	Positive flux	All flux
T_s 2cm	0.10	0.08	0.19	0.00	-0.11	-0.03	-0.01	-0.00	-0.11	0.03
T_s 5cm	-0.04	0.07	-0.04	-0.04	-0.13	-0.03	-0.08	0.03	-0.15	0.02
T_s 10cm	-0.11	0.06	0.03	-0.06	-0.13	-0.02	-0.09	0.04	-0.17	0.02
T_s 25cm	-0.19	0.05	-0.04	-0.06	-0.11	-0.01	-0.05	0.04	-0.17	0.02
VWC 5cm	0.21	0.00	0.10	0.01	-0.11	0.01	0.12	0.02	0.06	-0.01
VWC 15cm	0.21	-0.03	0.11	0.02	-0.09	0.00	0.10	0.02	0.09	-0.02
VWC 30cm	0.19	-0.02	0.11	0.01	-0.08	0.00	0.14	0.01	0.11	-0.01
Sensible Heat	0.51	-0.01	0.28	0.13	0.19	-0.03	0.06	-0.05	0.26	0.01
Latent Heat	0.44	0.04	0.31	0.04	0.11	-0.06	0.16	-0.06	0.23	0.02
CO ₂ flux	-0.32	-0.03	-0.15	-0.02	-0.07	0.04	-0.04	0.04	-0.17	0.00
Air temperature	0.21	0.08	0.19	0.01	-0.02	0.02	0.11	-0.03	0.03	0.03
RH	-0.17	0.06	-0.22	-0.04	-0.25	0.02	0.06	0.00	-0.21	0.02
Total Solar	0.36	0.05	0.23	0.05	0.14	0.01	0.13	-0.06	0.19	0.03
Q^*	0.28	0.06	0.22	0.07	0.03	-0.02	0.11	-0.06	0.13	0.04
ambient Hg	-0.28	0.05	-0.06	-0.03	-0.10	-0.01	-0.13	0.04	-0.20	0.02

Between seasons when considering bidirectional fluxes together correlations were considerably low, and a large proportion were not deemed significant. However, positive Hg fluxes presented with a much larger proportion of significant correlations. The strongest correlation with Hg flux across all seasons was found to be sensible heat during summer ($r = 0.13$). Spring presented with the most significant values although correlations were still low. Spring correlations were also the strongest when just the positive fluxes were considered. Autumn all flux was found to only have significant correlations with CO₂ flux ($r = 0.04$), Latent Heat ($r = -0.06$) and total solar ($r = 0.01$). Like the other seasons, autumn positive fluxes presented with stronger and more statistically significant relationships.

Diel CO₂ flux composite measurements show that there is a clear diel trend across all seasons where deposition (or uptake) occurs mostly during the day and CO₂ emission occurs overnight (Figure 4). Relationships between Hg emission (positive fluxes) and CO₂ fluxes were found to be significant, $r = -0.17$, across the entire study duration. The strongest relationship between positive Hg flux and CO₂ flux was observed during spring ($r = -0.32$) and summer ($r = -0.15$), which suggest that Hg emissions are less during times of high CO₂ uptake.

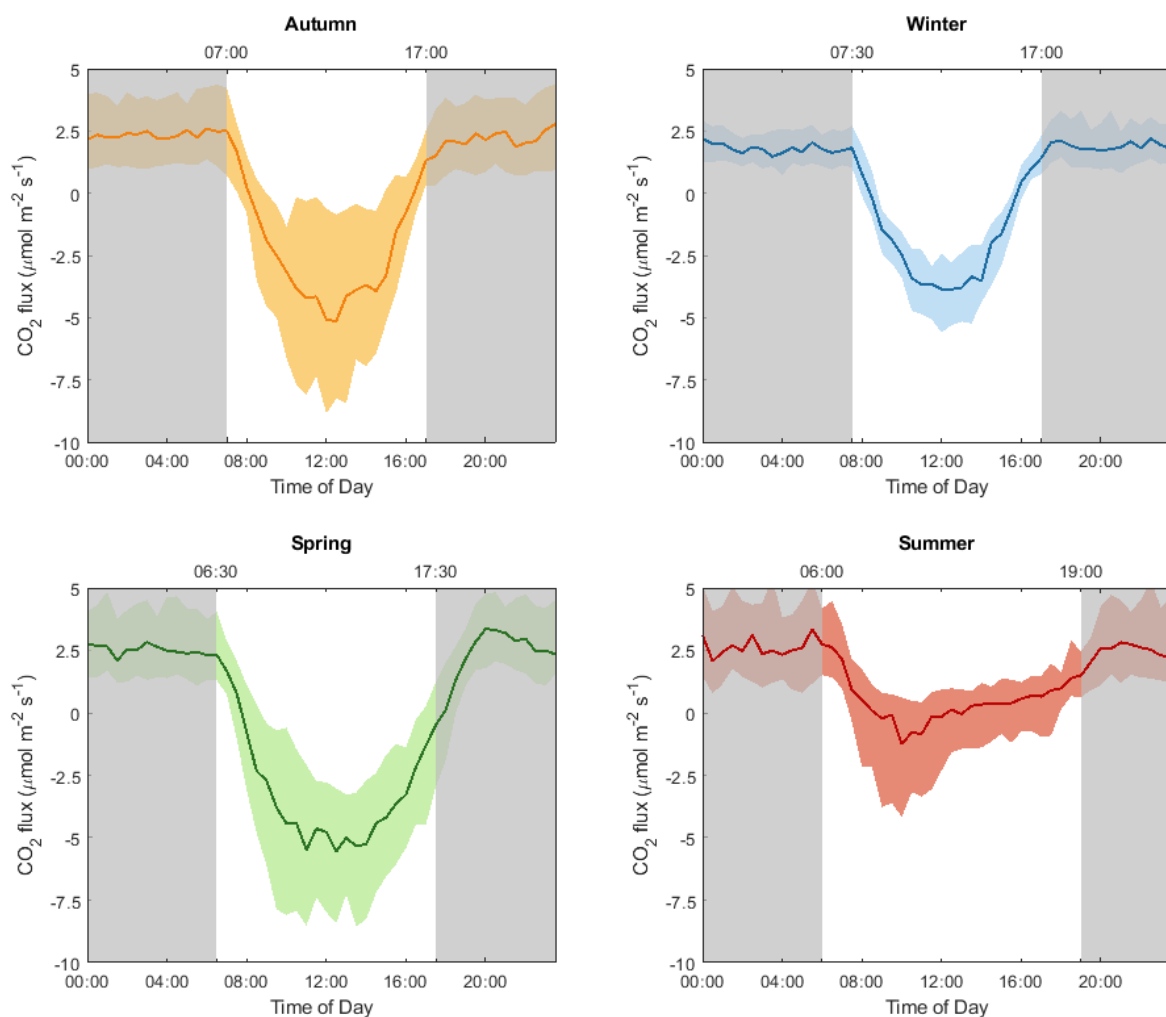


Figure 4. CO₂ diel composite for each season at Oakdale, NSW, 3 April 2017 to 21 June 2018. Solid line represents median value, shaded area inter-quartile range. Grey shaded region indicates night-time measurements.

4. Discussion

Mercury air-surface exchange measurements in Australia and the Southern Hemisphere in general are limited. To date, the study undertaken here is the longest continuously running Hg flux measurements in the Southern Hemisphere. Howard and Edwards (2017) undertook a micrometeorological Hg flux measurement study in sub-alpine South-Eastern Australia (Nimmo Plains) during austral summer with an average Hg flux of $0.2 \text{ ng m}^{-2} \text{ h}^{-1}$ ($\pm 14.5 \text{ ng m}^{-2} \text{ h}^{-1}$), comparable to the summer fluxes observed at this site of $0.34 \text{ ng m}^{-2} \text{ h}^{-1}$ ($\pm 16.6 \text{ ng m}^{-2} \text{ h}^{-1}$).

¹). Flux chamber measurements at a background site (Pulganbar, north-eastern New South Wales) observed average fluxes of $0.17 \text{ ng m}^{-2} \text{ h}^{-1}$ in both April and June (Edwards and Howard, 2013), whereas Oakdale experienced negative fluxes during this time (Table 1). Differences between these sites may be driven by the differences in site characteristics. Both Nimmo Plains and Oakdale were dominated by similar surface vegetation, whereas, Pulganbar measurements were conducted over bare soil and dominated by Hg emissions.

Average ambient Hg values at Oakdale (0.68 ng m^{-3} over the study duration) are well below the global background concentration of 1.2 ng m^{-3} (Sprovieri et al., 2016) and below values reported for the Southern Hemisphere or Australia (Howard et al., 2017; Slemr et al., 2015). Howard and Edwards (2017) did observe similar concentrations at an alpine site in South-Eastern Australia, with an atmospheric Hg concentration of 0.6 ng m^{-3} . Atmospheric Hg concentrations and trends are discussed in detail in Chapter 5 (Paper 3).

The majority of observed relationships between environmental variables and Hg fluxes were not statistically significant and had low correlations, most likely due to high variability in Hg flux measurements and concentrations close to detection limits. Vegetation at this site was dominated by low-lying grasses, with surface coverage varying over the study duration. It was therefore assumed that trends in Hg fluxes would follow those typically seen at vegetated background sites. Winter vegetation coverage was sparse, exposing more bare soil, and greatest during spring when increased rainfall allowed for greater growth. Observed seasonal variation appears to be contradictory to what is typically observed at vegetated sites. Seasonal Hg flux measurements made over a cornfield were highest in spring ($19.5 \text{ ng m}^{-2} \text{ h}^{-1}$) while corn was growing, and lowest in autumn ($-0.1 \text{ ng m}^{-2} \text{ h}^{-1}$) when the field was bare and snow covered (Baya and Van Heyst, 2010). Converse et al. (2010), at a high elevation meadow, observed deposition during spring ($-4.8 \text{ ng m}^{-2} \text{ h}^{-1}$), emission during summer and winter ($2.5 \text{ ng m}^{-2} \text{ h}^{-1}$ and $4.1 \text{ ng m}^{-2} \text{ h}^{-1}$, respectively) and near zero flux in autumn. Oakdale, on the other hand,

experienced average deposition in winter and autumn, and emission in summer and spring. The discrepancies between these seasonal trends may be a combination of changing vegetation coverage and Australia's climate resulting in Hg fluxes seasonally offset from those typically observed.

Vegetated sites have been found to exhibit deposition occurring during the day and emission at night during the growing season (Jiskra et al., 2018). Hg is taken up by vegetation through stomatal respiration, leading to accumulation within the leaves. Higher Hg concentrations found in the surface vegetation (82.25 ppb) than in the substrate (68.83 ppb) indicates that more Hg is being stored in the vegetation than is being released to the atmosphere. Greater Hg uptake by vegetation has been observed to occur during the growing season, following a negative relationship with CO₂ and leading to net deposition (Fritsche et al., 2008; Gustin, 2012). Only spring presented with a statistically significant relationship with CO₂ fluxes. Spring diel Hg fluxes showed emissions during the day and near zero exchange overnight.

The presence of vegetation has been shown to cause ambient Hg and fluxes to behave according to variation in compensation point, whereby when ambient Hg concentrations are above the compensation point deposition will occur and when ambient Hg is below the compensation point emission will occur. The compensation point is defined as the ambient Hg concentration when Hg fluxes are zero (Bash, 2010; Hanson et al., 1995). As ambient Hg was highest during summer when Hg fluxes were also highest suggests that Hg fluxes at this site do not conform to this theory. This is most likely because vegetation coverage is not enough to be the dominant source or sink of Hg to the atmosphere. Hg fluxes in forested ecosystems have been found to be dependent on ambient Hg concentration (Ericksen and Gustin, 2004; Hanson et al., 1995). However, soils have not been found to exhibit this same behaviour (Sommar et al., 2016). Correlations between ambient Hg and Hg fluxes were low across the entire study duration and only spring was found to be statistically significant ($r = 0.05$). Spring positive Hg fluxes had

the strongest relationship with both ambient Hg and CO₂ fluxes ($r = -0.28$ and -0.32 , respectively) indicating that this was the only season where vegetation coverage may have been enough for Hg fluxes to be controlled by ambient Hg concentrations.

Summer Hg fluxes at Oakdale were mostly dominated by surface emissions. This is largely attributed to the higher net all-wave radiation and soil and air temperatures, which were also highest at this time. High net all-wave radiation and soil temperatures enhance photoreduction and volatilisation occurring in the substrate allowing emissions to dominate (Carpi and Lindberg, 1997; Choi and Holsen, 2009). This is further confirmed by the Spearman correlations, which showed these parameters had the strongest relationship with positive Hg fluxes. Baya and Van Heyst (2010) saw similar diel trends during both summer and spring where Hg fluxes experienced net emissions during high net all-wave radiation and increased surface temperatures. Further, diel CO₂ fluxes during summer are comparatively flat (Figure 4), indicating little influence from vegetation during this time, allowing soil emissions to be the key sources of Hg to the atmosphere. Converse et al. (2010), observed that despite summer being the dominant growing period, solar radiation and temperature relationships allowed more Hg to be released from the substrate than was being taken up by the surrounding vegetation. Strong springtime relationships are also seen between net radiation, both soil and air temperature and Hg flux, suggesting that the influence of these parameters on the evasion of Hg from the substrate is greater than the rate of uptake by vegetation at this site.

Australia's winters are commonly milder than those reported throughout the literature. Unlike North America and Asia, where 56.6% and 25.1% of Hg flux studies have taken place, respectively (Agnan et al., 2016), most of South-Eastern Australia does not experience freeze-thaw cycles or snowfall, and rarely sees temperatures below 0 °C. Additionally, winter was observed to be the driest part of the year (Chapter 4, paper 2). As such, Hg air-surface exchanges during this period behave differently to those typically observed. Winter diel trends

saw near zero emissions overnight, which follows the trends commonly observed in the literature (Baya and Van Heyst, 2010; Converse et al., 2010; Osterwalder et al., 2017). Lack of exchange is thought to be caused by the cooler soil temperatures limiting the substrate ability to uptake and release Hg (Bahlmann et al., 2006; Baya and Van Heyst, 2010). Winter soil temperatures averaged 11.6°C and was the only season to experience daytime diel temperature trends lower than air temperature. This indicates that incoming radiation was not sufficient enough to cause substantial surface heating. The daytime trend of deposition somewhat contradicts what has commonly been seen in the literature, where emission still occurs during the day. This deposition trend is even more surprising, as soil moisture levels were highest during this time, which is thought to enhance evasion of Hg from the substrate (Gustin and Stamenkovic, 2005), discussed in Chapter 4.

The deposition trend seen in winter at the site may be due to the increased influence of vegetation on the uptake of Hg compared to other variables during winter. Diel CO₂ fluxes during winter are still strong, suggesting that plant uptake is still occurring during this time, unlike in other regions of the world where low temperatures mean plant growth is dormant (Sommar et al., 2016). However, the correlation between CO₂ fluxes and Hg were low and not significant. Uptake of Hg by vegetation has been shown to increase during the growing season, concentrations then remain constant or reduced once plants reach maturity (Ericksen et al., 2003; Poissant et al., 2008; Rea et al., 2002). This plateauing of vegetation uptake allows other environmental variables to take over control of the Hg fluxes (Converse et al., 2010). Lower net all-wave radiation and temperatures observed during winter reduce the ability for volatilisation and reduction reactions to occur in the substrate which may be allowing vegetation uptake to drive Hg flux trends.

Autumn Hg fluxes indicated little influence from environmental variables, with diel composite trends showing little diel variation. This is largely attributed to a reduction in solar radiation

and temperature (Yu et al., 2018). Correlations with measured environmental variables were the lowest and has the least number of significant relationships. These trends were similar to those observed by Converse et al. (2010) at a high alpine site, who noted weak correlations with the majority of environmental variables. The lack of relationship was likely caused by decreases in photoreduction occurring in the substrate, reducing evasion, and senescence causing a reduction in deposition. This leads to an overall balance between emission and deposition in the Hg fluxes.

Hg fluxes in autumn had the strongest relationship with relative humidity ($r = -0.25$). This relationship may explain why average fluxes indicated more deposition. Relative humidity is theorised to be an indicator of Hg deposition occurring because of condensation of water onto the surface vegetation (Fritsche et al., 2008). Howard and Edwards (2017) suggested that nocturnal Hg depletion events were caused by dew formation and fog creating potential sink of Hg. Autumn diel trends and to a lesser extent spring, exhibit deposition leading up to sunrise which then shift to emission shortly after sunrise. This could be an indication that Hg deposition with dew formation is occurring which is then volatilising back into the atmosphere as the dew is evaporated at Oakdale (Converse et al., 2010). Reduced air temperatures and overnight temperature conditions and atmospheric stability during autumn is favourable for frequent fog and dew formation, allowing for greater Hg deposition to occur.

5. Conclusion

Mercury fluxes and drivers observed at this background site are in line with those observed for similar sites in the Northern Hemisphere. However, low Hg fluxes and high variability made it difficult to definitely determine the strength of these relationships. Average net Hg flux over the duration of the study was near zero. Fluxes were dominated by net emission during summer

and net deposition in winter. Hg fluxes during the warm season is dominantly influenced by photoreduction occurring in the substrate and increased volatilisation promoting increased surface evasion, due to higher temperatures and radiation.

The lack of vegetation influence at this site (with the possible exception of winter, where net deposition was clearest during the day) indicates that the soil is the cause of Hg air-surface exchange at this site. Vegetation uptake of Hg is most important during winter when the influence of meteorological variables is reduced. Vegetation seems to be acting as a store of Hg, with little influence over the net emissions, as indicated by the higher Hg concentrations found in the surface vegetation. In order for grasslands/low vegetated sites to see significant vegetation uptake of Hg, the parameters that most influence Hg evasion, i.e., net radiation, and air and soil temperature, need to be simultaneously reduced. The dominance of Hg emission observed during summer indicates that Hg fluxes are driven by releases from the substrate, rather than controlled by the presence of vegetation. More research is needed at sites with similar characteristics to better quantify if photoreduction always dominates over vegetation uptake within the Australian environment or if the dominant drivers identified here are site specific.

6. References

- Agnan, Y., Le Dantec, T., Moore, C. W., Edwards, G. C. & Obrist, D. 2016. New Constraints on Terrestrial Surface-Atmosphere Fluxes of Gaseous Elemental Mercury Using a Global Database. *Environ Sci Technol*, 50, 507-24.10.1021/acs.est.5b04013
- Amos, Helen M., Jacob, Daniel J., Streets, David G. & Sunderland, Elsie M. 2013. Legacy impacts of all-time anthropogenic emissions on the global mercury cycle. *Global Biogeochemical Cycles*, 27, 410-421.10.1002/gbc.20040
- Bahlmann, E., Ebinghaus, R. & Ruck, W. 2006. Development and application of a laboratory flux measurement system (LFMS) for the investigation of the kinetics of mercury emissions from soils. *J Environ Manage*, 81, 114-25.10.1016/j.jenvman.2005.09.022

- Bash, Jesse O. 2010. Description and initial simulation of a dynamic bidirectional air-surface exchange model for mercury in Community Multiscale Air Quality (CMAQ) model. *Journal of Geophysical Research*, 115.10.1029/2009jd012834
- Bash, Jesse O. & Miller, David R. 2008. A Relaxed Eddy Accumulation System for Measuring Surface Fluxes of Total Gaseous Mercury. *Journal of Atmospheric and Oceanic Technology*, 25, 244-257.10.1175/2007jtecha908.1
- Baya, A. P. & Van Heyst, B. 2010. Assessing the trends and effects of environmental parameters on the behaviour of mercury in the lower atmosphere over cropped land over four seasons. *Atmospheric Chemistry and Physics*, 10, 8617-8628.10.5194/acp-10-8617-2010
- Bureau of Meteorology. 2019. *Long-range weather and climate* [Online]. <http://www.bom.gov.au/climate/>. [Accessed 2/8/2019 2019].
- Businger, J.A., Wyngaard, J.C., Izumi, Y. & Bradley, E.F 1971. Flux-Profile Relationships in the Atmospheric Surface Layer. *Journal of Atmospheric Sciences*, 28, 181-189
- Carpi, Anthony & Lindberg, S. 1997. Sunlight-Mediated Emission of Elemental Mercury from Soil Amended with Municipal Sewage Sludge. *Environmental Science & Technology*, 31, 2085-2091
- Choi, H. D. & Holsen, T. M. 2009. Gaseous mercury emissions from unsterilized and sterilized soils: the effect of temperature and UV radiation. *Environ Pollut*, 157, 1673-8.10.1016/j.envpol.2008.12.014
- Converse, A. D., Riscassi, A. L. & Scanlon, T. M. 2010. Seasonal variability in gaseous mercury fluxes measured in a high-elevation meadow. *Atmospheric Environment*, 44, 2176-2185.10.1016/j.atmosenv.2010.03.024
- Corbitt, E. S., Jacob, D. J., Holmes, C. D., Streets, D. G. & Sunderland, E. M. 2011. Global source-receptor relationships for mercury deposition under present-day and 2050 emissions scenarios. *Environ Sci Technol*, 45, 10477-84.10.1021/es202496y
- Edwards, G. C. & Howard, D. A. 2013. Air-surface exchange measurements of gaseous elemental mercury over naturally enriched and background terrestrial landscapes in Australia. *Atmospheric Chemistry and Physics*, 13, 5325-5336.10.5194/acp-13-5325-2013
- Edwards, G. C., Rasmussen, P. E. , Schroeder, W. H. , Wallace, D. M. , Halfpenny-Mitchell, L. , Dias, G. M. , Kemp, R. J. & Ausma, S. 2005. Development and evaluation of a sampling system to determine gaseous Mercury fluxes using an aerodynamic micrometeorological gradient method. *Journal of Geophysical Research*, 110.10.1029/2004jd005187
- Ericksen, J. A. & Gustin, M. S. 2004. Foliar exchange of mercury as a function of soil and air mercury concentrations. *Sci Total Environ*, 324, 271-9.10.1016/j.scitotenv.2003.10.034
- Ericksen, J. A., Gustin, M. S., Schorran, D. E., Johnson, D. W., Lindberg, S. E. & Coleman, J. S. 2003. Accumulation of atmospheric mercury in forest foliage. *Atmospheric Environment*, 37, 1613-1622.10.1016/s1352-2310(03)00008-6
- Fritsche, J., Obrist, D., Zeeman, M., Conen, F., Eugster, W. & Alewell, C. 2008. Elemental mercury fluxes over a sub-alpine grassland determined with two micrometeorological methods. *Atmospheric Environment*, 42, 2922-2933.10.1016/j.atmosenv.2007.12.055
- Gabriel, Mark C., Williamson, Derek G. & Brooks, Steve 2011. Potential impact of rainfall on the air-surface exchange of total gaseous mercury from two common urban ground surfaces. *Atmospheric Environment*, 45, 1766-1774.10.1016/j.atmosenv.2010.11.035

- Gustin, Mae Sexauer 2012. Exchange of mercury between the atmosphere and terrestrial ecosystems. *Environmental chemistry and toxicology of mercury*, 423-451
- Gustin, Mae Sexauer, Engle, Mark, Ericksen, Jody, Lyman, Seth, Stamenkovic, Jelena & Xin, Mei 2006. Mercury exchange between the atmosphere and low mercury containing substrates. *Applied Geochemistry*, 21, 1913-1923.10.1016/j.apgeochem.2006.08.007
- Gustin, Mae Sexauer, Lindberg, Steven E. & Weisberg, Peter J. 2008. An update on the natural sources and sinks of atmospheric mercury. *Applied Geochemistry*, 23, 482-493.10.1016/j.apgeochem.2007.12.010
- Gustin, Mae Sexauer & Stamenkovic, Jelena 2005. Effect of Watering and Soil Moisture on Mercury Emissions from Soils. *Biogeochemistry*, 76, 215-232.10.1007/s10533-005-4566-8
- Gustin, Mae Sexauer, Taylor, George E. & Maxey, Rachel A. 1997. Effect of temperature and air movement on the flux of elemental mercury from substrate to the atmosphere. *Journal of Geophysical Research: Atmospheres*, 102, 3891-3898.10.1029/96jd02742
- Hanson, P. J., Lindberg, S.E., Tabberer, T.A., Owens, J.G. & Kim, K.-H. 1995. Foliar exchange of mercury vapor: Evidence for a compensation point. *Water Air Soil Pollution*, 80, 373-382
- Hintelmann, Holger, Harris, Reed, Heyes, Andrew, Hurley, James P, Kelly, Carol A, Krabbenhoft, David P, Lindberg, Steve, Rudd, John WM, Scott, Karen J & St. Louis, Vincent L 2002. Reactivity and mobility of new and old mercury deposition in a boreal forest ecosystem during the first year of the METAALICUS study. *Environmental Science & Technology*, 36, 5034-5040
- Howard, Dean & Edwards, Grant C. 2017. Mercury fluxes over an Australian alpine grassland and observation of nocturnal atmospheric mercury depletion events. *Atmospheric Chemistry and Physics Discussions*, 1-24.10.5194/acp-2017-580
- Howard, Dean, Nelson, Peter F., Edwards, Grant C., Morrison, Anthony L., Fisher, Jenny A., Ward, Jason, Harnwell, James, van der Schoot, Marcel, Atkinson, Brad, Chambers, Scott D., Griffiths, Alan D., Werczynski, Sylvester & Williams, Alastair G. 2017. Atmospheric mercury in the southern hemisphere tropics: seasonal and diurnal variations and influence of inter-hemispheric transport. *Atmospheric Chemistry and Physics Discussions*, 1-20.10.5194/acp-2017-307
- Jiskra, Martin, Sonke, Jeroen E., Obrist, Daniel, Bieser, Johannes, Ebinghaus, Ralf, Myhre, Cathrine Lund, Pfaffhuber, Katrine Aspmo, Wängberg, Ingvar, Kyllönen, Katriina, Worthly, Doug, Martin, Lynwill G., Labuschagne, Casper, Mkololo, Thumeka, Ramonet, Michel, Magand, Olivier & Dommergue, Aurélien 2018. A vegetation control on seasonal variations in global atmospheric mercury concentrations. *Nature Geoscience*, 11, 244-250.10.1038/s41561-018-0078-8
- Kim, K. H., Yoon, H. O., Jung, M. C., Oh, J. M. & Brown, R. J. 2012. A simple approach for measuring emission patterns of vapor phase mercury under temperature-controlled conditions from soil. *ScientificWorldJournal*, 2012, 940413.10.1100/2012/940413
- Kim, Ki-Hyun, Lindberg, Steven E. & Meyer, C. P. 1995. Micrometeorological Measurements Of Mercury Vapor Fluxes Over Background Forest Soils In Eastern Tennessee. *Atmospheric Environment*, 29, 267-282
- Lee, Xuhui, Benoit, Gaboury & Hu, Xinzhang 2000. Total gaseous mercury concentration and flux over a coastal saltmarsh vegetation in Connecticut, USA. *Atmospheric Environment*, 34, 4205-4213

- Liang, P., Zhang, C., Yang, Y. & Wang, D. 2014. A simulation study of mercury release fluxes from soils in wet-dry rotation environment. *J Environ Sci (China)*, 26, 1445-52.10.1016/j.jes.2014.05.010
- Lin, Che-Jen, Gustin, Mae S, Singhasuk, Pattaraporn, Eckley, Chris & Miller, Matthieu 2010. Empirical models for estimating mercury flux from soils. *Environmental Science & Technology*, 44, 8522-8528
- Moore, Chad & Carpi, Anthony 2005. Mechanisms of the emission of mercury from soil: Role of UV radiation. *Journal of Geophysical Research*, 110.10.1029/2004jd005567
- Nelson, Darrell W & Sommers, Lee E 1996. Total carbon, organic carbon, and organic matter. *Methods of soil analysis part 3—chemical methods*, 961-1010
- Nelson, Peter F., Morrison, Anthony L., Malfroy, Hugh J., Cope, Martin, Lee, Sunhee, Hibberd, Mark L., Meyer, C. P. & McGregor, John 2012. Atmospheric mercury emissions in Australia from anthropogenic, natural and recycled sources. *Atmospheric Environment*, 62, 291-302.10.1016/j.atmosenv.2012.07.067
- Obrist, Daniel, Gustin, Mae S., Arnone, John A., Johnson, Dale W., Schorran, David E. & Verburg, Paul S. J. 2005. Measurements of gaseous elemental mercury fluxes over intact tallgrass prairie monoliths during one full year. *Atmospheric Environment*, 39, 957-965.10.1016/j.atmosenv.2004.09.081
- Osterwalder, S., Bishop, K., Alewell, C., Fritsche, J., Laudon, H., Akerblom, S. & Nilsson, M. B. 2017. Mercury evasion from a boreal peatland shortens the timeline for recovery from legacy pollution. *Sci Rep*, 7, 16022.10.1038/s41598-017-16141-7
- Poissant, Laurier, Pilote, Martin, Yumvihoze, Emmanuel & Lean, David 2008. Mercury concentrations and foliage/atmosphere fluxes in a maple forest ecosystem in Québec, Canada. *Journal of Geophysical Research*, 113.10.1029/2007jd009510
- Rea, A. W. , Lindberg, S. E., Scherbatskoy, T. & Keeler, G. J. 2002. Mercury accumulation in foliage over time in two northern mixed-hardwood forests. *Water, Air, and Soil Pollution*, 133, 49–67
- Schroeder, W. & Munthe, J. 1998. Atmospheric Mercury - An Overview. *Atmospheric Environment*, 32, 809-822
- Slemr, F., Angot, H., Dommergue, A., Magand, O., Barret, M., Weigelt, A., Ebinghaus, R., Brunke, E. G., Pfaffhuber, K. A., Edwards, G., Howard, D., Powell, J., Keywood, M. & Wang, F. 2015. Comparison of mercury concentrations measured at several sites in the Southern Hemisphere. *Atmospheric Chemistry and Physics*, 15, 3125-3133.10.5194/acp-15-3125-2015
- Sommar, Jonas, Zhu, Wei, Shang, Lihai, Lin, Che-Jen & Feng, Xinbin 2016. Seasonal variations in metallic mercury (Hg⁰) vapor exchange over biannual wheat–corn rotation cropland in the North China Plain. *Biogeosciences*, 13, 2029-2049.10.5194/bg-13-2029-2016
- Sprovieri, Francesca, Pirrone, Nicola, Bencardino, Mariantonia, amp, apos, Amore, Francesco, Carbone, Francesco, Cinnirella, Sergio, Mannarino, Valentino, Landis, Matthew, Ebinghaus, Ralf, Weigelt, Andreas, Brunke, Ernst-Günther, Labuschagne, Casper, Martin, Lynwill, Munthe, John, Wängberg, Ingvar, Artaxo, Paulo, Morais, Fernando, Barbosa, Henrique de Melo Jorge, Brito, Joel, Cairns, Warren, Barbante, Carlo, Diéguez, María del Carmen, Garcia, Patricia Elizabeth, Dommergue, Aurélien, Angot, Helene, Magand, Olivier, Skov, Henrik, Horvat, Milena, Kotnik, Jože, Read, Katie Alana, Neves, Luis Mendes, Gawlik, Bernd Manfred, Sena, Fabrizio, Mashyanov, Nikolay, Obolkin, Vladimir, Wip,

- Dennis, Feng, Xin Bin, Zhang, Hui, Fu, Xuewu, Ramachandran, Ramesh, Cossa, Daniel, Knoery, Joël, Maruszczak, Nicolas, Nerentorp, Michelle & Norstrom, Claus 2016. Atmospheric mercury concentrations observed at ground-based monitoring sites globally distributed in the framework of the GMOS network. *Atmospheric Chemistry and Physics*, 16, 11915-11935.10.5194/acp-16-11915-2016
- Stamenkovic, J., Gustin, M. S., Arnone, J. A., 3rd, Johnson, D. W., Larsen, J. D. & Verburg, P. S. 2008. Atmospheric mercury exchange with a tallgrass prairie ecosystem housed in mesocosms. *Sci Total Environ*, 406, 227-38.10.1016/j.scitotenv.2008.07.047
- Wagner-Riddle, C. , Thurtell, G. W. , Kidd, G. K. , Beauchamp, E. G. & Sweetman, R. 1997. Estimates of nitrous oxide emissions from agricultural fields over 28 months. *Canadian Journal Of Soil Science*, 77, 135–144
- Wang, D., He, L., Shi, X., Wei, S. & Feng, X. 2006. Release flux of mercury from different environmental surfaces in Chongqing, China. *Chemosphere*, 64, 1845-54.10.1016/j.chemosphere.2006.01.054
- Webb, E. K., Pearman, G. I. & Leuning, R. 1980. Correction of flux measurements for density effects due to heat and water vapour transfer. *Jornal of the Royal Meterological Society*, 106, 85-100
- Yu, Qian, Luo, Yao, Wang, Shuxiao, Wang, Zhiqi, Hao, Jiming & Duan, Lei 2018. Gaseous elemental mercury (GEM) fluxes over canopy of two typical subtropical forests in south China. *Atmospheric Chemistry and Physics*, 18, 495-509.10.5194/acp-18-495-2018
- Zhang, H., Lindberg, S., Marsik, F. & Keeler, G. J. 2001. Mercury air/surface exchange kinetics of background soils of the tahquamenon river watershed in the michigan upper peninsula. *Water, Air, & Soil Pollution*, 126, 151–169
- Zhou, J., Wang, Z., Sun, T., Zhang, H. & Zhang, X. 2016. Mercury in terrestrial forested systems with highly elevated mercury deposition in southwestern China: The risk to insects and potential release from wildfires. *Environ Pollut*, 212, 188-196.10.1016/j.envpol.2016.01.003

CHAPTER 4

The role of precipitation and soil moisture in enhancing mercury fluxes at a background site in South-Eastern Australia

4.1 Preface

This chapter further explores the drivers of mercury air-surface exchange at Oakdale background site. As stated in Chapter 3, soil moisture has been found to have a significant influence on mercury air-surface exchange. Increased soil moisture is thought to enhance Hg surface emissions through interstitial release from the substrate and accelerating the redox reactions taking place within the substrate. This understanding has primarily been derived from laboratory and short-term studies. How these responses manifest over extended periods in the field is largely unknown. The main purpose of this chapter is to investigate if soil moisture changes in response to rainfall had any prolonged influence on Hg flux magnitude and if this response varied depending on season. This chapter contributes to the thesis by identifying the influence of one of the key parameters believed to enhance Hg emissions to the atmosphere and its overall influences on Australia's natural mercury cycle.

Author contributions:

The paper presented in this chapter is intended for submission to *Atmospheric Environment*. The paper has thus been formatted and structured according to this journal's submission requirements.

The field site and design were established by Dr Grant Edwards and me. Beyond the initial set up the field site was maintained and monitored by me. All data collection, analysis and most manuscript preparation was undertaken by me, with intellectual contributions from co-author, Dr Grant Edwards.

Katrina MacSween: 85%, Grant Edwards: 15%.

The role of precipitation and soil moisture in enhancing mercury fluxes at a background site in South-Eastern Australia.

Katrina MacSween, Grant C. Edwards

Department of Earth and Environmental Sciences, Faculty of Science and Engineering,
Macquarie University, Sydney, Australia

Corresponding author: katrina.macsween@mq.edu.au

Abstract

Exchange of mercury (Hg) between terrestrial surfaces and the atmosphere is an important component of the global atmospheric Hg cycle that influences its distribution in the environment. Soil moisture content is thought to be one of the most important parameters controlling Hg fluxes, particularly at background sites. Rainfall across the temperate regions of Australia is highly variable on both annual and inter-annual scales. As such, it is plausible that Australian terrestrial fluxes do not respond to precipitation and soil moisture changes in the same way as observed in the Northern Hemisphere. This study focused on investigating Hg flux in response to precipitation and soil moisture changes at a background site in South-Eastern Australia over a 14 month measurement period. The 2017/2018 austral summer experienced the greatest rainfall, with a cumulative average of 3.21 mm d^{-1} and rainfall occurring during 5.95% of the half-hourly measurements during this period. Autumn 2018 had the lowest daily rainfall (1.20 mm d^{-1}). Hg fluxes during rainfall averaged $1.03 \text{ ng m}^{-2} \text{ h}^{-1}$ (standard deviation (SD), 20.78), compared to the overall study average of $0.002 \text{ ng m}^{-2} \text{ h}^{-1}$ (SD 14.23), signifying influence from the occurrence of rain. Mercury fluxes at this site show substantial spikes that often coincide with the occurrence of rainfall. Mercury released from

the substrate during rainfall is primarily due to the interstitial release of Hg as the water infiltrates the soil pore space. There was little evidence of enhanced Hg fluxes occurring because of increased soil volumetric water content. Lack of enhancement suggests that Hg stores within the substrate are depleted during the initial release.

1. Introduction

Mercury (Hg) is found ubiquitously across the globe due to its low vapour pressure and long atmospheric lifetime (Pirrone et al., 2010). Hg is continuously recycled between the atmosphere and the Earth's surface, where it can enter waterways and bioaccumulate up the food chain, exposing humans and other animals to potentially hazardous levels of Hg (Driscoll et al., 2013; Gabriel et al., 2006; Schroeder and Munthe, 1998). Exchange of Hg between terrestrial surfaces and the atmosphere is an important component of the global atmospheric Hg cycle that influences its distribution in the environment (Gustin et al., 2006; Schroeder and Munthe, 1998; Wang et al., 2006). Behaviour within the terrestrial environment is strongly influenced by soil properties, biotic and abiotic processes, meteorology, and atmospheric physics and chemistry. Solar radiation, air and soil temperature, soil moisture, and substrate Hg concentrations are widely considered the dominant factors controlling Hg evasion from terrestrial surfaces (Choi and Holsen, 2009; Feng et al., 2005; Gustin et al., 2006; Gustin et al., 1997; Kim et al., 2012; Kim et al., 1995). Soil moisture content is thought to be one of the most important parameters controlling Hg fluxes, particularly at background sites (substrate Hg concentrations <100ppb) (Briggs and Gustin, 2013).

Soil moisture content and precipitation are hypothesised to influence Hg evasion from substrates in two ways. The first is the interstitial release of soil air containing Hg as rainwater

infiltrates into the soil pore space (Gillis and Miller, 2000). As water infiltrates the soil pore, Hg that occupies the space is forced to the active surface layer where it is released directly to the atmosphere as elemental mercury (Hg^0). Wetting of dry soils has been shown to induce a greater flux than additional moisture added to already wet soils. Repeated water additions have been shown to decrease the amount of Hg released from soils, indicating that the effects of precipitation events are dependent on the amount of Hg in the soils available for emission (Song and Van Heyst, 2005). Controlled studies have also shown that the duration of exacerbated flux after watering is a function of the amount of water added and the rate at which soil dries (Gustin et al., 2006).

It is also hypothesised that an increasing soil moisture content within the substrate will enhance the magnitude of Hg flux. The increased soil pore water increases redox reactions occurring within the soil column, converting divalent mercury (Hg^{+2}) to Hg^0 . As the water evaporates from the soil column, Hg is transported by capillary action to the surface where it undergoes volatilisation and then released to the atmosphere (Liang et al., 2014; Song and Van Heyst, 2005). Studies have shown that Hg emissions from soils are highly dependent on soil moisture content. Briggs and Gustin (2013) found, at a soil moisture content of 13%, the mean diurnal Hg fluxes are higher than those observed for dry soils over a 24 hour emission period. Night-time fluxes at 13% soil moisture in the same experiment were greater than those measured from dry soil over the same period. When the soil moisture was increased to 23%, fluxes became similar to those from dry soil with no diel pattern. Once soil moisture was increased above 30%, Hg flux was suppressed (Briggs and Gustin, 2013; Gustin et al., 2006). These two processes often work in conjunction with each other. The interstitial release creates an initial pulse in Hg emissions. Fluxes then decrease but remain elevated, gradually decreasing as Volumetric Water Content (VWC) returns to levels prior to the rain event.

Evaporation from the substrate is enhanced at higher temperatures, promoting additional Hg evasion from soil surfaces (Lin et al., 2010). Higher temperatures also increase the rate of soil respiration leading to a subsequent increase in Hg emissions (Raich and Schlesinger, 1992). Liang et al. (2014) found, over the course of two wetting periods, that the first wetting period had higher Hg emissions because it took place during summer when air temperature and solar radiation were higher. Gustin et al. (2006) suggested that the Hg emissions recorded from the soil samples with 13% soil moisture would have been higher if light intensity was higher than the 150 W m^{-2} the samples were exposed to under laboratory conditions. It is therefore plausible that the influence of soil moisture on Hg evasion would be highly seasonal due to both variations in temperatures and changes to soil moisture throughout any given year.

Australia represents an understudied and unique climate region regarding Hg flux research. Australia is a relatively dry continent with much of the region not experiencing snowfall or snowmelt as is common across much of the Northern Hemisphere. Rainfall across the temperate regions of South-Eastern Australia is highly variable on both annual and inter-annual scales. Autumn and winter rainfall are influenced by the occurrence of blocking highs, which create dry conditions on the scale of weeks to months, and cut-off lows that can bring sustained heavy rainfall and high winds over several days. June also tends to experience more frequent east coast lows, which create intense storm systems. Summer and spring rainfall are dominated by easterly troughs, which cause early evening rainfall due to land surface heating. In conjunction with these annual drivers of rainfall variability, large-scale inter-annual climate drivers such as El Niño Southern Oscillation influence the strength and timing of these rainfall trends (Bureau of Meteorology, 2019). The variability of rainfall in this region means that soil moisture content is also likely to be more variable than that observed throughout the Northern Hemisphere. As such, it is plausible that Australian terrestrial Hg fluxes do not respond to

precipitation and soil moisture changes in the same way as observed in the Northern Hemisphere.

This study aimed to investigate Hg fluxes responses to changes in soil moisture and precipitation events at background site over 14 months in South-Eastern Australia. Our hypothesis was that since Hg release is facilitated by precipitation interaction with dry soil, we should see pulses of Hg to the air and increased flux with rain events. Further, this study aims to investigate if soil moisture and Hg flux changes in response to rainfall varied between seasons or over extended timeframes.

2. Methods

2.1 Site description

This study took place at Oakdale, New South Wales, Australia, a rural area on the far south-west edge of the Sydney basin (lat. 34° 03' 11" S, long. 150° 29' 50" E, altitude 457 m above sea level). Measurements were undertaken from 3 April 2017 to 21 June 2018 (445 days), within an agricultural grazing paddock. The site predominantly consisted of surface grasses with a canopy height less than 2 cm. Soils for the region were classified as sandy clay loam and a Hg substrate concentration of 68.83 ppb (see Chapter 3, Paper 1), with no known major point sources of Hg within the region. Total organic carbon content was 7.34% (\pm 3.18).

2.2 Hg flux gradient method

Hg⁰ fluxes were determined using a micrometeorological aerodynamic flux gradient method and assumptions outlined in Edwards et al. (2005). Hg⁰ flux was calculated according to Equation 1:

$$F = -K \frac{\Delta C}{\Delta z} = \frac{u^* k (C_2 - C_1)}{\ln\left(\frac{z_2 - d}{z_1 - d}\right) - \Psi_{z_2} + \Psi_{z_1}} \quad (\text{Equation 1})$$

where F is the Hg flux ($\text{ng m}^{-2} \text{s}^{-1}$), K is the eddy diffusivity ($\text{m}^2 \text{s}^{-1}$), C is the Hg^0 concentration at height z ($z_1 = 0.44 \text{ m}$ and $z_2 = 1.24 \text{ m}$), u^* is the friction velocity (m s^{-1}), k is the von Kármán constant (0.40), d is the zero-plane displacement height (m), and Ψ is the integrated universal similarity functions as given by Businger et al. (1971) for the two measurement heights (z_1 and z_2). By convention, a positive flux is upward (emission) and a negative flux is downward (deposition).

Hg^0 gradients were calculated using air samples collected alternating between two heights ($z_1 = 0.44 \text{ m}$ and $z_2 = 1.24 \text{ m}$) and quantified using a Tekran 2537B (Tekran Instruments, Knoxville, TN, USA), with detection limit of 0.01 ng m^{-3} . Sample air was drawn from the sample inlets through a $0.2 \mu\text{m}$ polytetrafluoroethylene (PTFE) filter by a PTFE pump at 10 L min^{-1} . The 2537B sub-sampled from this flow through an additional $0.2 \mu\text{m}$ PTFE filter. Switching of sampling between the intakes took place every 10 minutes ($2 \times 2537\text{B}$ samples) using a PTFE solenoid valve controlled by LabVIEW software. Internal calibration of the 2537B occurred every 23 hours throughout the study using the internal mercury permeation source. Permeation sources were verified at the beginning and end of the study, as well as part-way through (September) when the Tekran was removed for routine maintenance, using manual mercury vapour injections ($\pm 2\%$).

Thirty-minute running means of the Tekran measurements were used to calculate flux gradient. The average flux gradient was first constructed using a 90 min averaging period (five 10 min samples at one height and four 10 min samples at the other height). After the first gradient was constructed, a running 90 min mean gradient was then updated every half hour. Density corrections due to water vapour and heat outlined by Webb et al. (1980) were applied to each averaging period. Quality assurance methods were applied to the micrometeorological data

based on the constraints of Monin-Obukov similarity theory. This included filtering for low wind speeds (<0.5 m/s) and wind direction, to allow for sufficient fetch. Highly stable and unstable conditions (stability parameter, z/L , less than -5 or greater than 5), were also removed since micrometeorological methods are most suitable for slightly stable to slightly unstable conditions (Wagner-Riddle et al., 1997).

Latent heat and momentum required for gradient calculations were measured using a CSAT-3 sonic anemometer (Campbell Scientific, Logan, UT, USA) and LI-7200 closed-path, infrared gas analyser (Li-Cor Biosciences, Lincoln, NE, USA). Samples were collected at 10 Hz using the SmartFlux System (version 1.10). The LI-7200 was replaced part way through the study period with an open-path 7500 Analyzer due to hardware malfunction. Post-processing and quality control of eddy covariance fluxes was undertaken using Li-Cor EddyPro[®] software (version 6.2.0).

2.3 Environmental variables

Volumetric Water Content (VWC) was measured at three depths (5cm, 15cm, and 30cm), using MP306 Moisture Probes at 15cm and 30cm and a CS616 water content reflectometer (Campbell Scientific Inc.) at 5cm. Measurements were logged at $\frac{1}{2}$ hour intervals at 60 Hz using a CR3000 Campbell Scientific data logger. Rainfall measurements were made using tipping bucket gauges (RIMCO 7499-020) that were maintained, calibrated and quality controlled by NSW Office of Environment and Heritage air quality monitoring network (OEHL, 2018).

2.4 Hg flux rainfall analysis

To determine how rainfall and soil VWC influenced Hg fluxes, the flux data were separated into rain fluxes and no rain fluxes. Two different conditions were used to distinguish between

the two flux categories. The first was to simply separate fluxes for when rainfall was recorded and when no rain was recorded, i.e., when rain was greater than zero, Hg fluxes were flagged as rain fluxes, and when rain was recorded as zero, Hg fluxes were flagged as no rain fluxes. The second condition for Hg flux filtering was based on notable changes to VWC. Under this condition Hg fluxes were flagged as rain fluxes if VWC increased a minimum of one standard deviation above the monthly mean VWC. Hg fluxes below this VWC value were flagged as non-rain Hg fluxes regardless of whether rainfall was recorded at the time. This was done to account for the offset between rainfall and the water infiltrating the soil column and to account for VWC remaining elevated after rainfall occurs. As VWC was recorded at 3 measurement depths, Hg rain fluxes were also separated based on the depth that the change in VWC was recorded at. For example, if VWC measured at 30cm increased one standard deviation above the mean, Hg fluxes were flagged as rain flux at 30cm, and so on.

2.5 Hg flux enhancement factor

In order to explore the relationship between VWC and initial Hg flux change, enhancement factors (EF) were calculated for both VWC and Hg flux (Briggs and Gustin, 2013). Enhancement factors were calculated for when soil moisture increased one standard deviation above the mean VWC for each calendar month, using equation 2:

$$EF = \frac{VWC_{\text{before}}(\text{Flux}_{\text{before}}) - VWC_{\text{after}}(\text{Flux}_{\text{after}})}{VWC_{\text{before}}(\text{Flux}_{\text{before}})} \quad (\text{Equation 2})$$

Where $VWC_{\text{before}}(\text{Flux}_{\text{before}})$ is the monthly average VWC or Hg flux. $VWC_{\text{after}}(\text{Flux}_{\text{after}})$ was the average VWC and Hg flux when VWC was elevated, as outlined above.

2.6 Statistical analysis

Two-way *t*-tests using MATLAB® software were used to determine if rain Hg fluxes were statistically different from no rain fluxes. T-tests were performed using the same conditions outlined in section 2.5 to determine if there was a statistical difference between mean Hg fluxes during no rainfall and Hg fluxes when rainfall occurred. Null hypothesis was rejected if the difference between means was found to have a significance less than 5% (p-value <0.05), unless stated otherwise. Spearman correlations were also performed MATLAB® software to identify potential relationships between Hg fluxes and rainfall and changes in VWC at the three measured depths. Correlations were deemed to be statistically significant if p-values were <0.05.

3. Results

Total cumulative rainfall over the 445 day study period was 972.4 mm. Rainfall occurred on 4.22% of the 30 minute measurements during the study period (Table 1). The majority of rainfall that occurred throughout the study duration occurred as short events, lasting for less than an hour to several hours. Austral summer (December, January, February) experienced the greatest rainfall, with a daily cumulative average of 3.21 mm d⁻¹ and 5.95% of measurements occurring during rainfall (winter 2018 was higher but this was only the first 21 days of the season, at which point the data collection ceased). Autumn 2018 (March, April, May) had the lowest daily rainfall (1.21 mm d⁻¹). Winter 2017 (June, July, August) experienced the lowest percent of rainfall measurements (2.49%) but a slightly higher daily cumulative average than autumn (2018), indicating that when rainfall occurred during winter it was often in the form of larger rain events than those in autumn.

Table 1. Seasonal averages and standard deviations (SD) for volumetric water content (VWC) at three measurement depths, daily average cumulative rainfall and latent heat measurements made at Oakdale, NSW (3 April 2017 to 21 June 2018).

Year	Season	VWC (%)						Daily rain (mm)	% Rain	Latent Heat (W m ⁻²)	
		5cm		15cm		30cm				Mean	SD
		Mean	SD	Mean	SD	Mean	SD				
2017	Autumn	21.65	2.80	22.23	3.85	30.23	4.09	2.16	3.75	26.25	42.00
	Winter	22.46	3.14	20.80	4.22	30.05	3.79	1.50	2.49	19.06	27.58
	Spring	15.95	1.16	15.43	0.45	19.78	1.78	1.90	4.07	41.76	61.08
2017/2018	Summer	14.04	1.28	14.83	0.04	18.09	1.29	3.21	5.95	38.29	58.60
2018	Autumn	14.43	1.29	15.09	0.03	18.68	0.88	1.21	4.04	23.52	34.25
	Winter	15.62	1.33	15.59	0.04	21.24	3.52	4.32	7.64	10.37	17.50
All		17.15	3.97	16.86	3.51	22.22	5.60	2.19	4.22	28.72	46.42

Volumetric water content (VWC) over the duration of the study demonstrated an overall drying trend (Figure 1). Average VWC across the entire study was 17.15% at 5 cm, 16.86% at 15 cm and 22.22% at 30 cm. Winter and autumn 2017 had the highest VWC, while summer, and autumn 2018, presented with the lowest VWC (Table 1). Despite the general drying trend, Figure 1 demonstrates large short-lived VWC spikes corresponding to rain events. VWC at 30cm appears to be the most acutely sensitive to rainfall. These spikes are often short-lived, returning to similar VWC values in a matter of hours, suggesting that additional water was quickly drained to lower in the soil column.

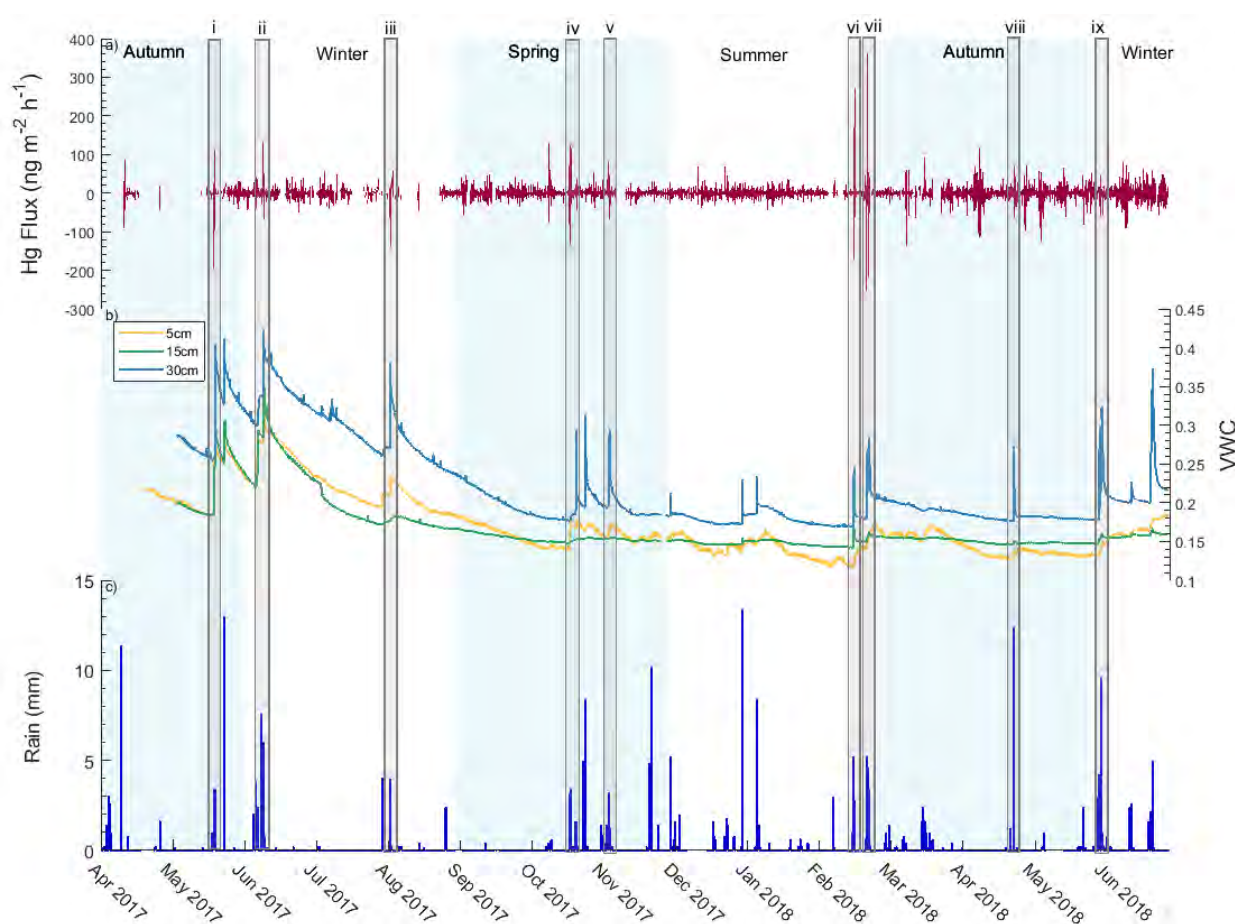


Figure 1. Hg flux (a), soil volumetric water content, at depths of 5cm, 15cm and 30cm (b), and rain (c) at 30 minute intervals for 3 April 2017 to 21 June 2018 at Oakdale, NSW. Grey boxes indicate rainfall that had a corresponding VWC and Hg flux change. Shading indicates changes in seasons as labelled.

Hg fluxes during rainfall averaged $1.03 \text{ ng m}^{-2} \text{ h}^{-1}$ (standard deviation (SD), 20.78), compared to the overall study average of $0.002 \text{ ng m}^{-2} \text{ h}^{-1}$ (SD 14.23) (Appendix 2, Table 1). All seasons, except for spring 2017 and autumn (2018), saw increased variability in Hg fluxes during rainfall (Figure 2). Autumn (2017) experienced the greatest variation during rainfall, with both the average Hg flux and lower quartile range indicating deposition was more likely to occur. Winter Hg fluxes during rainfall saw increased emission from the surface. Spring was the only season to see a statistically significant difference (p-value <0.01) between Hg no rain flux and Hg rain fluxes (Appendix 2, Table 2).

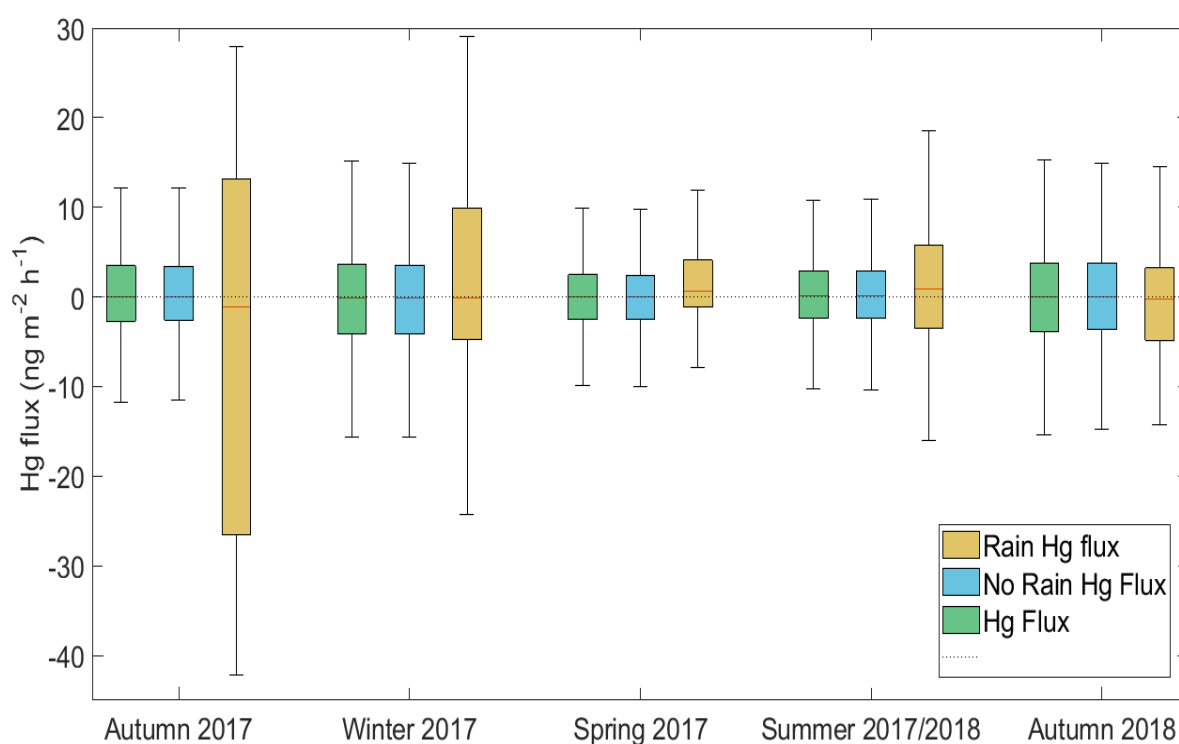


Figure 2. Box and whisker plot of rain, no rain and all Hg fluxes for all measured seasons. Red centre line represents median value. Boxes show 25 and 75 quartile range and whiskers standard error.

Spikes in Hg fluxes tend to coincide more often with spikes in VWC than the occurrence of rainfall. Figure 1 shows Hg fluxes, VWC at three depths and rainfall over the duration of the study. Grey boxes indicate rainfall events that coincide with a change in VWC and Hg flux patterns. Water infiltrating the substrate appears to result in an almost instantaneous release of

Hg from the substrate. These flux trends do not indicate any prolonged increase to Hg emissions beyond these initial trends, despite VWC remaining elevated after rainfall. Given that not every rainfall event resulted in a change in VWC or Hg flux, rain Hg fluxes were also determined for when VWC increased one standard deviation above the monthly mean. Student T-tests between VWC increase at 5cm and corresponding Hg flux change further confirmed lack of relationship. The only season to have a statistically significant difference when VWC was elevated was winter (P-value <0.01, $t = -2.64$). Winter also presented with the highest average VWC.

Rain events that were identified in Figure 1 to influence Hg fluxes and VWC were separated and presented as individual graphs in Figure 3 to determine timing of VWC and Hg response to rainfall. Events i and ix were not included, due to gaps in the measurements either just prior to rainfall or at the start of recorded rainfall. No two rain events presented with the same response to rain, but all did show clear increases in the magnitude of Hg flux around the same time as rainfall. Rain events at the end of February were split into two events (vi and vii). Both events show Hg flux response to increased VWC to be offset several hours from the initial change in VWC. Fluxes remain elevated for a limited time and then experience a period of deposition before returning to normal. Several events also experienced increased deposition during periods of increased VWC. The clearest example was seen during rain event iii (3-5 August) where increased deposition coincided with increasing VWC at 30cm and rainfall.

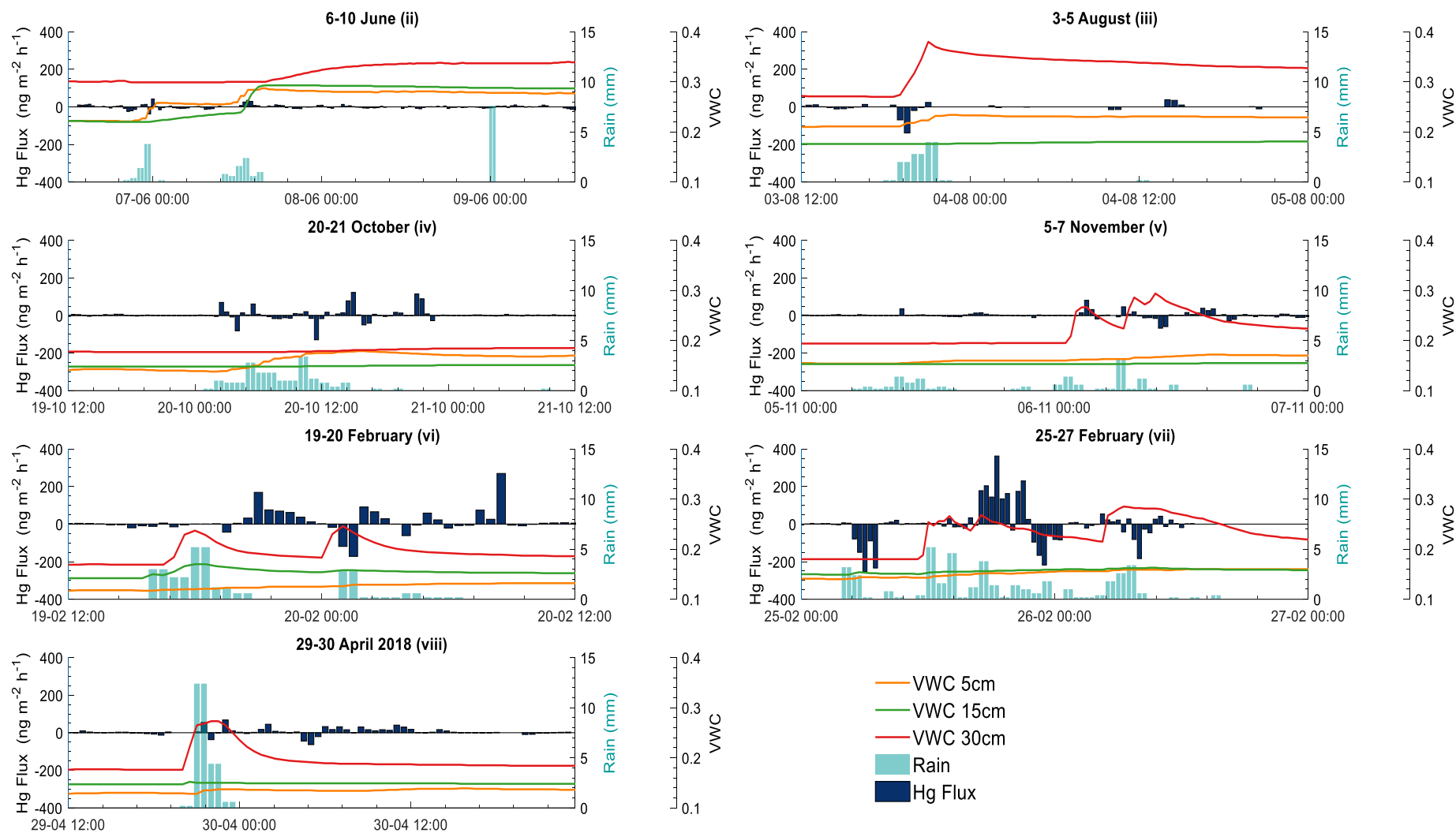


Figure 3. Rain events based on those identified in Figure 1 to influence Hg fluxes and VWC. Roman numerals at the top of individual graphs correspond to the timing or event in Figure 1. Each individual event includes a minimum 12 hours before and after rain occurred.

Spearman correlations were calculated to determine the relationship between Hg fluxes and rainfall and changes in VWC at the three measured depths (Table 2). Fluxes were also separated when the VWC conditions were met for each measured depth. Correlations for the full study period were presented in Chapter 3, paper 1. Correlations for all conditions across the study period were weak and for the most part deemed not to be statistically significant. Hg flux and rainfall in winter had the strongest correlation ($r = 0.17$, $p\text{-value} < 0.05$). Spring was the only season to have any significant correlation between VWC and Hg fluxes. This further suggests that changes to soil moisture at this site have little influence on the observed Hg flux trends.

Table 2. Correlation between Hg fluxes and VWC at three measurement depths and rainfall, for each season at Oakdale, NSW (3 April 2017 to 21 June 2018). Bold values have p-values <0.05.

	Winter			Spring			Summer			Autumn		
	Flux 5cm	Flux 15cm	Flux 30cm	Flux 5cm	Flux 15cm	Flux 30cm	Flux 5cm	Flux 15cm	Flux 30cm	Flux 5cm	Flux 15cm	Flux 30cm
VWC 5cm	0.04	0.01	0.03	0.00	0.11	0.03	-0.04	-0.07	-0.02	0.04	0.04	-0.07
VWC 15cm	0.00	0.00	0.03	0.12	0.00	0.12	-0.08	-0.02	-0.02	-0.04	-0.06	-0.05
VWC 30cm	0.05	0.05	0.06	0.04	0.10	0.02	0.04	0.07	0.04	0.04	0.03	0.05
Rain	0.17	0.17	0.16	0.01	-	0.02	0.02	0.01	-0.05	0.09	0.06	-0.04

Soil moisture EF at 15 cm showed little change during rainfall, except at the start of the study when soil moisture was at its highest (Table 3). In general, soil moisture EF at 30 cm showed the greatest enhancement during rainfall and high variability between months, ranging between 2% and 53%. Soil moisture EF at 5cm was often less than that observed at 30cm, ranging between 6% and 35%. Hg flux EFs did not correspond to higher soil moisture EF and mostly indicated a negative enhancement, with the clear exception of June, July, and August. This suggests that overall Hg scavenging and deposition from the atmosphere is dominating over Hg evasion from the terrestrial substrate. This may also in part explain why there is little relationship between soil moisture EF and Hg flux EF.

Table 3. Enhancement factor for VWC and Hg flux when VWC at each measurement depth increased one standard deviation above the monthly mean VWC and it was raining. EF was calculated for each measurement month.

Month	VWC EF			Flux EF		
	5cm (%)	15cm (%)	30cm (%)	5cm	15cm	30cm
April 2017	-	-	-	-	-	-
May 2017	35	43	34	-19.68	-25.58	-3.55
June 2017	9	31	19	112.81	84.83	43.96
July 2017	12	22	9	3.91	6.87	9.78
August 2017	15	5	27	70.66	-	57.17
September 2017	-	-	-	-	-	-
October 2017	18	3	43	-17.02	-31.90	-8.23
November 2017	8	2	32	-5.22	-4.06	12.76
December 2017	13	3	8	-24.40	44.09	-10.78
January 2018	11	3	12	-12.75	4.46	-3.00
February 2018	22	9	41	16.66	21.87	10.22
March 2018	6	1	5	-6.36	-5.89	3.15
April 2018	12	3	42	-4.94	-4.64	39.92

May 2018	-	-	2	-	-	-178.61
June 2018	16	5	53	39.78	461.10	24.46
All	65	75	68	11.23	179.34	-89.50

4 Discussion

Rainfall and VWC appear to have very little lasting influence on Hg fluxes at this field site. Changes in Hg fluxes are short-lived and require a change to the VWC rather than the sole occurrence of rainfall. Simultaneous spikes in both VWC and Hg emissions suggest that Hg was being forced from the substrate by the infiltrating water. There is also little evidence to suggest that Hg fluxes are influenced by the change in VWC beyond this initial spike. Spikes in Hg fluxes are largely driven by the interstitial release of Hg from the substrate. As the rainwater infiltrates the soil column, soil Hg gas contained within the soil pore space is displaced towards the surface (Lindberg et al., 1999). Additional Hg may be displaced from deeper in the soil as water continues to infiltrate lower in the column, increasing the magnitude of the Hg flux pulse (Gustin and Stamenkovic, 2005).

Eckley et al. (2011) found that the wetting of dry soils resulted in a 2-17 fold increase in Hg evasion depending on precipitation type, amount, intensity and timing. Lin et al. (2010) also found that Hg emissions increased from 6 to 390 ng m⁻² h⁻¹ after the initial wetting of background soils. However, a second wetting did not produce the same response with Hg emissions only recording an increase to 42 ng m⁻² h⁻¹. The magnitude changes in Hg flux during rainfall at Oakdale was not consistent between different rain events. Largest increase was seen in February 2018 (398 ng m⁻² h⁻¹), while other times during the study observed values were similar to those seen by Lin et al., (2010) during second wettings.

Oakdale Hg Fluxes following rainfall quickly return to pre-rainfall values with little evidence of elevated Hg fluxes due to higher soil moisture or due to increased evaporation. Hg fluxes from dry soils can increase between 2 to 5 times the average flux when soil moisture is increased but soils are not yet saturated (Erickson et al., 2006; Gustin and Stamenkovic, 2005). However, VWC at this site did not drop below 10% during the study, which has typically been used in the literature to classify soils as dry. Song and Van Heyst (2005) noted that during laboratory experiments when soil moisture was greater than 15%, no enhancement in fluxes following precipitation was observed. Soil moisture levels observed at this site were lowest during summer and autumn 2018 at 14% at 5 cm and flux enhancements were not observed. Autumn 2017 at 30cm had an average soil moisture content of 30% primarily driven by May rainfall. However, suppression of Hg fluxes was also not observed during periods of elevated VWC.

The magnitude of Hg flux pulse in relation to rainfall is related to how readily the soil Hg pool is available. Substrate Hg concentration at this site was 68.83 ppb, classifying it as a background site. The low substrate concentration and lack of nearby sources suggest that the site is largely driven by atmospheric deposition (see Chapter 5, Paper 3). As the site is reliant on deposition processes to replenish the substrate Hg pool, it is possible the pool is easily depleted and not quickly replenished. If the soil pool has recently been depleted or atmospheric deposition has not replenished the Hg pool, the magnitude of the pulse will be reduced (Engle et al., 2001; Song and Van Heyst, 2005; Zhou et al., 2017). This is most clearly seen in Figure 1 where consecutive rainfall events do not necessarily see a pulse in Hg fluxes, or a reduction in the second pulse's magnitude occurs. The observed initial pulse in Hg emissions appears to be sufficient to deplete Hg stores within the substrate (Song and Van Heyst, 2005), while atmospheric deposition and Hg^{2+} reduction reactions in the substrate are insufficient to see any prolonged flux enhancement (Lin et al., 2010). The limited flux enhancements during

consecutive rain events may also indicate that the redox reaction rates are slow within the substrate, so that Hg stores take a while to replenish. This suggests the depth of water penetration within the soil column most strongly influences Hg flux enhancement.

The lack of enhancement while VWC was high could also suggest that increased water in the substrate is not accelerating redox reactions either. Increases in soil moisture will often cause decreased soil redox potential, thereby increasing the reduction of Hg^{2+} to Hg^0 (Moore and Castro, 2012; Zárate-Valdez et al., 2006). Infiltrating water changes the availability of electrons for oxidation–reduction reactions increasing the rate of Hg^{2+} reduction in the substrate (Obrist et al., 2009; Schlüter, 2000; Schultz et al., 1999; Zhang and Lindberg, 1999). Soil moisture may be high enough at this site to reduce redox potential in the substrate. However, this has previously only been observed when soil moisture is above 30% (Zhou et al., 2017). The time scale and dynamics of the flux from wetted soils and its subsequent replenishment under realistic environmental conditions are currently not well-understood (Lin et al., 2010).

Hg fluxes during rainfall commonly saw a sharp deposition flux either immediately after or before the spike in Hg emissions. However, similar to the emission spikes, deposition only occurred on short time scales with little evidence of prolonged deposition occurring. Lindberg and Stratton (1998) noted that at sites with low atmospheric Hg concentrations, that during times of increased soil moisture dry deposition was significantly enhanced. This deposition may be a response to water infiltrating deeper in the soil column and drawing in air to fill the empty pore spaces. As air fills the pore space it is also bringing with it atmospheric Hg, increasing the rate of dry deposition and replenishing some of the lost Hg from the substrate.

While the Hg flux method applied here is only able to determine dry deposition, it is plausible that wet deposition is also occurring alongside these increases in dry deposition. Most significant deposition was seen in February (Figure 3) when convective storms are most common for this region. Previous studies have shown that wet deposition is a major sink for

atmospheric mercury (Keeler et al., 2005; Miller et al., 2005). Wet deposition of mercury results from mercury oxidation followed by the scavenging of oxidised mercury into atmospheric water droplets, and the removal by precipitation to the Earth's surface (i.e., rainout) (Lin et al., 2006). Atmospheric scavenging during rainfall is supplying RM to the surface. However, it is not being made available for re-emission while VWC is elevated. Rate of deposition is primarily driven by precipitation amount and type, such as convective storms, which are able to scavenge RM from higher in the atmosphere (Gratz et al., 2009; Sprovieri et al., 2017).

5 Conclusion

Mercury fluxes at this site show substantial spikes that often coincide with the occurrence of rainfall. Mercury released from the substrate during rainfall is primarily due to the interstitial release of Hg as the water infiltrates the soil pore space. Not every rain event had a corresponding change in VWC and Hg flux. Similar spikes in negative Hg fluxes demonstrate scavenging of Hg from the atmosphere occurring alongside the spikes in emissions. This deposition is introducing Hg back to the substrate likely in the form of Hg^{2+} . There was little evidence of enhanced Hg fluxes occurring as a result of increased VWC. Lack of enhancement suggests that Hg stores within the substrate are depleted during the initial release. Redox reaction rates are not substantial enough to replace the stores while VWC is elevated despite Hg^{2+} being made available from deposition. Soil moisture has been identified as a key parameter influencing Hg fluxes, however that does not seem to be the case for this site. More research is needed looking into how soil type and characteristic may influence the ability of soil moisture to influence Hg release from the substrate.

References

- Bahlmann, E., Ebinghaus, R. & Ruck, W. 2006. Development and application of a laboratory flux measurement system (LFMS) for the investigation of the kinetics of mercury emissions from soils. *J Environ Manage*, 81, 114-25.10.1016/j.jenvman.2005.09.022
- Briggs, Christian & Gustin, Mae Sexauer 2013. Building upon the Conceptual Model for Soil Mercury Flux: Evidence of a Link Between Moisture Evaporation and Hg Evasion. *Water, Air, & Soil Pollution*, 224.10.1007/s11270-013-1744-5
- Bureau of Meteorology. 2019. *Long-range weather and climate* [Online]. <http://www.bom.gov.au/climate/>. [Accessed 2/8/2019 2019].
- Businger, J.A., Wyngaard, J.C., Izumi, Y. & Bradley, E.F 1971. Flux-Profile Relationships in the Atmospheric Surface Layer. *Journal of Atmospheric Sciences*, 28, 181-189
- Choi, H. D. & Holsen, T. M. 2009. Gaseous mercury emissions from unsterilized and sterilized soils: the effect of temperature and UV radiation. *Environ Pollut*, 157, 1673-8.10.1016/j.envpol.2008.12.014
- Driscoll, C. T., Mason, R. P., Chan, H. M., Jacob, D. J. & Pirrone, N. 2013. Mercury as a global pollutant: sources, pathways, and effects. *Environ Sci Technol*, 47, 4967-83.10.1021/es305071v
- Edwards, G. C., Rasmussen, P. E. , Schroeder, W. H. , Wallace, D. M. , Halfpenny-Mitchell, L. , Dias, G. M. , Kemp, R. J. & Ausma, S. 2005. Development and evaluation of a sampling system to determine gaseous Mercury fluxes using an aerodynamic micrometeorological gradient method. *Journal of Geophysical Research*, 110.10.1029/2004jd005187
- Engle, Mark A, Gustin, Mae Sexauer & Zhang, Hong 2001. Quantifying natural source mercury emissions from the Ivanhoe Mining District, north-central Nevada, USA. *Atmospheric Environment*, 35, 3987-3997
- Ericksen, J. A., Gustin, M. S., Xin, M., Weisberg, P. J. & Fernandez, G. C. 2006. Air-soil exchange of mercury from background soils in the United States. *Sci Total Environ*, 366, 851-63.10.1016/j.scitotenv.2005.08.019
- Feng, Xinbin, Wang, Shaofeng, Qiu, Guangle, Hou, Yamin & Tang, Shunlin 2005. Total gaseous mercury emissions from soil in Guiyang, Guizhou, China. *Journal of Geophysical Research: Atmospheres*, 110, n/a-n/a.10.1029/2004jd005643
- Gabriel, Mark C., Williamson, Derek G., Zhang, Hong, Brooks, Steve & Lindberg, Steve 2006. Diurnal and seasonal trends in total gaseous mercury flux from three urban ground surfaces. *Atmospheric Environment*, 40, 4269-4284.10.1016/j.atmosenv.2006.04.004
- Gillis, Alison A. & Miller, David R. 2000. Some local environmental effects on mercury emission and absorption at a soil surface. *The Science of the Total Environment*, 260, 191-200
- Gratz, Lynne E, Keeler, Gerald J & Miller, Eric K 2009. Long-term relationships between mercury wet deposition and meteorology. *Atmospheric Environment*, 43, 6218-6229
- Gustin, Mae Sexauer, Engle, Mark, Ericksen, Jody, Lyman, Seth, Stamenkovic, Jelena & Xin, Mei 2006. Mercury exchange between the atmosphere and low mercury containing substrates. *Applied Geochemistry*, 21, 1913-1923.10.1016/j.apgeochem.2006.08.007

- Gustin, Mae Sexauer & Stamenkovic, Jelena 2005. Effect of Watering and Soil Moisture on Mercury Emissions from Soils. *Biogeochemistry*, 76, 215-232.10.1007/s10533-005-4566-8
- Gustin, Mae Sexauer, Taylor, George E. & Maxey, Rachel A. 1997. Effect of temperature and air movement on the flux of elemental mercury from substrate to the atmosphere. *Journal of Geophysical Research: Atmospheres*, 102, 3891-3898.10.1029/96jd02742
- Keeler, Gerald J, Gratz, Lynne E & Al-Wali, Khalid 2005. Long-term atmospheric mercury wet deposition at Underhill, Vermont. *Ecotoxicology*, 14, 71-83
- Kim, K. H., Yoon, H. O., Jung, M. C., Oh, J. M. & Brown, R. J. 2012. A simple approach for measuring emission patterns of vapor phase mercury under temperature-controlled conditions from soil. *ScientificWorldJournal*, 2012, 940413.10.1100/2012/940413
- Kim, Ki-Hyun , Lindberg, Steven E. & Meyer, C. P. 1995. Micrometeorological Measurements Of Mercury Vapor Fluxes Over Background Forest Soils In Eastern Tennessee. *Atmospheric Environment*, 29, 267-282
- Liang, P., Zhang, C., Yang, Y. & Wang, D. 2014. A simulation study of mercury release fluxes from soils in wet-dry rotation environment. *J Environ Sci (China)*, 26, 1445-52.10.1016/j.jes.2014.05.010
- Lin, Che-Jen, Gustin, Mae S, Singhasuk, Pattaraporn, Eckley, Chris & Miller, Matthieu 2010. Empirical models for estimating mercury flux from soils. *Environmental Science & Technology*, 44, 8522-8528
- Lin, Che-Jen, Pongprueksa, Pruek, Lindberg, Steve E, Pehkonen, Simo O, Byun, Daewon & Jang, Carey 2006. Scientific uncertainties in atmospheric mercury models I: Model science evaluation. *Atmospheric Environment*, 40, 2911-2928
- Lindberg, S. E., Zhang, H., Gustin, M., Vette, A., Marsik, F., Owens, J., Casimir, A., Ebinghaus, R., Edwards, G., Fitzgerald, C., Kemp, J., Kock, H. H., London, J., Majewski, M., Poissant, L., Pilote, M., Rasmussen, P., Schaedlich, F., Schneeberger, D., Sommar, J., Turner, R., Wallschläger, D. & Xiao, Z. 1999. Increases in mercury emissions from desert soils in response to rainfall and irrigation. *Journal of Geophysical Research: Atmospheres*, 104, 21879-21888.10.1029/1999jd900202
- Lindberg, SE and & Stratton, WJ 1998. Atmospheric mercury speciation: concentrations and behavior of reactive gaseous mercury in ambient air. *Environmental Science & Technology*, 32, 49-57
- Miller, Eric K, Vanarsdale, Alan, Keeler, Gerald J, Chalmers, Ann, Poissant, Laurier, Kamman, Neil C & Brulotte, Raynald 2005. Estimation and mapping of wet and dry mercury deposition across northeastern North America. *Ecotoxicology*, 14, 53-70
- Moore, Christopher W & Castro, Mark S 2012. Investigation of factors affecting gaseous mercury concentrations in soils. *Science of The Total Environment*, 419, 136-143
- Obrist, D, Johnson, DW & Lindberg, SE 2009. Mercury concentrations and pools in four Sierra Nevada forest sites, and relationships to organic carbon and nitrogen. *Biogeosciences*, 6, 765-777
- Pirrone, N., Cinnirella, S., Feng, X., Finkelman, R. B., Friedli, H. R., Leaner, J., Mason, R., Mukherjee, A. B., Stracher, G. B., Streets, D. G. & Telmer, K. 2010. Global mercury emissions to the atmosphere from anthropogenic and natural sources. *Atmospheric Chemistry and Physics*, 10, 5951-5964.10.5194/acp-10-5951-2010

- Raich, James W & Schlesinger, William H 1992. The global carbon dioxide flux in soil respiration and its relationship to vegetation and climate. *Tellus B*, 44, 81-99
- Schlüter, K 2000. evaporation of mercury from soils. An integration and synthesis of current knowledge. *Environmental Geology*, 39, 249-271
- Schroeder, W. & Munthe, J. 1998. Atmospheric Mercury - An Overview. *Atmospheric Environment*, 32, 809-822
- Schultz, Martin G., Jacob, Daniel J., Wang, Yuhang, Logan, Jennifer A., Atlas, Elliot L., Blake, Donald R., Blake, Nicola J., Bradshaw, John D., Browell, Edward V., Fenn, Marta A., Flocke, Frank, Gregory, Gerald L., Heikes, Brian G., Sachse, Glen W., Sandholm, Scott T., Shetter, Richard E., Singh, Hanwant B. & Talbot, Robert W. 1999. On the origin of tropospheric ozone and NO_x over the tropical South Pacific. *J. Geophys. Res.*, 104, 5829-5843.10.1029/98jd02309
- Song, X. & Van Heyst, B. 2005. Volatilization of mercury from soils in response to simulated precipitation. *Atmospheric Environment*, 39, 7494-7505.10.1016/j.atmosenv.2005.07.064
- Sprovieri, Francesca, Pirrone, Nicola, Bencardino, Mariantonia, amp, apos, Amore, Francesco, Angot, Helene, Barbante, Carlo, Brunke, Ernst-Günther, Arcega-Cabrera, Flor, Cairns, Warren, Comero, Sara, Diéguez, María del Carmen, Dommergue, Aurélien, Ebinghaus, Ralf, Feng, Xin Bin, Fu, Xuewu, Garcia, Patricia Elizabeth, Gawlik, Bernd Manfred, Hageström, Ulla, Hansson, Katarina, Horvat, Milena, Kotnik, Jože, Labuschagne, Casper, Magand, Olivier, Martin, Lynwill, Mashyanov, Nikolay, Mkololo, Thumeka, Munthe, John, Obolkin, Vladimir, Ramirez Islas, Martha, Sena, Fabrizio, Somerset, Vernon, Spandow, Pia, Vardè, Massimiliano, Walters, Chavon, Wängberg, Ingvar, Weigelt, Andreas, Yang, Xu & Zhang, Hui 2017. Five-year records of mercury wet deposition flux at GMOS sites in the Northern and Southern hemispheres. *Atmospheric Chemistry and Physics*, 17, 2689-2708.10.5194/acp-17-2689-2017
- Wagner-Riddle, C. , Thurtell, G. W. , Kidd, G. K. , Beauchamp, E. G. & Sweetman, R. 1997. Estimates of nitrous oxide emissions from agricultural fields over 28 months. *Canadian Journal Of Soil Science*, 77, 135–144
- Wang, D., He, L., Shi, X., Wei, S. & Feng, X. 2006. Release flux of mercury from different environmental surfaces in Chongqing, China. *Chemosphere*, 64, 1845-54.10.1016/j.chemosphere.2006.01.054
- Webb, E. K., Pearman, G. I. & Leuning, R. 1980. Correction of flux measurements for density effects due to heat and water vapour transfer. *Jornal of the Royal Meterological Society*, 106, 85-100
- Zárate-Valdez, José L, Zasoski, Robert J & Läuchli, André E 2006. Short-term effects of moisture content on soil solution pH and soil Eh. *Soil Science*, 171, 423-431
- Zhang, H. & Lindberg, S. E. 1999. Processes influencing the emission of mercury from soils: A conceptual model. *Journal of Geophysical Research: Atmospheres*, 104, 21889-21896.10.1029/1999jd900194
- Zhou, Jun, Wang, Zhangwei, Zhang, Xiaoshan & Sun, Ting 2017. Investigation of factors affecting mercury emission from subtropical forest soil: A field controlled study in southwestern China. *Journal of Geochemical Exploration*, 176, 128-135.10.1016/j.gexplo.2015.10.007

CHAPTER 5

ATMOSPHERIC MERCURY VARIABILITY AT A TERRESTRIAL BACKGROUND SITE, SOUTH EASTERN AUSTRALIA.

5.1 Preface

Chapter 5 explores drivers of mercury in the atmosphere over the terrestrial background site. Background sites are largely driven by deposition processes, which are then able to drive re-emission from terrestrial surfaces. Chapters 3 and 4 primarily focused on seasonal drivers of surface emissions. This chapter will explore the seasonal drivers of atmospheric mercury concentration before it is deposited to the surface and made available for re-emission. The atmosphere plays a crucial role in the chemical and physical transformations of Hg, governing its resident time and global cycling. Atmospheric deposition, both wet and dry, represents the major pathway for Hg input to terrestrial and aquatic environments. Understanding of the long-term atmospheric mercury trends over terrestrial environments has largely been unexplored in the Southern Hemisphere. Terrestrial air masses are influenced by regional sources of Hg, such as pollution hotspots and biomass burning. The large ratio of ocean to terrestrial surfaces and the overall limited number of studies in the Southern Hemisphere means that long-term terrestrial measurements of atmospheric mercury are rare. As such, variations and drivers of

atmospheric mercury deposition over terrestrial surfaces in the Southern Hemisphere are largely unknown. This chapter contributes to the overall thesis aims by characterising the atmospheric component of the mercury terrestrial cycle.

Author contributions:

The manuscript presented in this chapter is intended for publication in *Atmospheric Chemistry and Physics* and thus has been formatted according to the journal's publication requirements.

The field site established in this study was maintained and monitored by me. All data collection, analysis and the majority of manuscript preparation was undertaken by me, with intellectual contributions from Co-authors, Dr Grant Edwards. Dr Dean Howard contributed HYSPLIT back trajectory analysis as well as intellectual contribution to the manuscript.

Katrina MacSween: 80%, Grant Edwards: 10%, Dean Howard: 10%

Atmospheric mercury variability at a terrestrial background site, South-Eastern Australia.

Katrina MacSween*, Grant C. Edwards, Dean A. Howard

Department of Earth and Environmental Sciences, Faculty of Science and Engineering, Macquarie University, Sydney, Australia

*Corresponding author: katrina.macsween@mq.edu.au

Abstract

Understanding of Southern Hemisphere atmospheric mercury (Hg) is vastly underrepresented in the current global understanding of seasonal variation and drivers of Hg, particularly over terrestrial environments. Relationships have been observed between atmospheric Hg and air temperature, solar radiation, relative humidity, wind speed and direction and meso and macro scale atmospheric circulation, but these have largely been unexplored in the Southern Hemisphere. This study provides 14 months of ambient Gaseous Elemental Mercury (GEM) and Reactive Mercury (RM) measurements undertaken at an Australian terrestrial background site to determine seasonal variation and its potential drivers. GEM concentrations were quantified using a Tekran 2537B. Measurements of RM were undertaken concurrently using the University of Nevada-Reno Reactive Mercury Active System. Study average GEM concentrations were 0.68 ng m^{-3} (standard deviation $\pm 0.22 \text{ ng m}^{-3}$). Highest concentrations occurred during austral summer and lowest in austral winter (0.88 and 0.43 ng m^{-3} , respectively). RM 2-weekly concentrations over the study average 2.41 pg m^{-3} (standard deviation 1.68 pg m^{-3}). These concentrations also peaked in summer (3.43 pg m^{-3}) and were lowest in winter (1.93 pg m^{-3}). Summer and spring are influenced by air masses transporting higher Hg concentrations from the Sydney urban region, which is to the north-east of the site.

Gaseous oxidation was also found to be more efficient during this time. Winter concentrations were primarily driven by ocean evasion being transported inland. Overall, atmospheric mercury trends at this site appear to be driven by seasonal shifts in the prevailing air mass transport, creating seasonal variation in the observed Hg concentrations.

1. Introduction

Atmospheric mercury (Hg) has a complex chemistry and unique speciation that allows it to be transported and deposited across vast temporal and spatial scales (Lan et al., 2012). The atmosphere plays a crucial role in the chemical and physical transformations of Hg, governing its resident time and global cycling (Ariya et al., 2015). Atmospheric deposition, both wet and dry, represents the major pathway for Hg input to terrestrial and aquatic environments (Gustin et al., 2015). Within the atmosphere, Hg exists in both vapour and particulate phase, creating three operationally defined forms (Schroeder and Munthe, 1998). Gaseous Elemental Mercury (GEM) is the most dominant form, accounting for 90-99% of all Hg present. GEM has a low atmospheric reactivity and low solubility, allowing it to reside in the atmosphere between 5 and 17 months (Horowitz et al., 2014; Horowitz et al., 2017; Lindberg et al., 2007). The other two forms are Gaseous Oxidised Mercury (GOM) and Particulate Bound Mercury (PBM), collectively referred to as Reactive Mercury (RM) (Gustin et al., 2015; Weiss-Penzias et al., 2015). RM is thought to represent between 1 and 3% of Total Gaseous Mercury (TGM) in the atmosphere, however, this can vary significantly on regional and local scales (Lindberg and Stratton, 1998). The reactivity of RM means that it is readily scavenged from the atmosphere, usually deposited on a scale of days to weeks after formation, resulting in atmospheric concentrations being highly variable and highly regional (Poissant et al., 2005; Valente et al., 2007).

Global mean concentrations of TGM range between 0.8 and 1.6 ng m⁻³ (Sprovieri et al., 2016). Total global atmospheric loading is estimated to be between 4400 and 5300 Mg, approximately three times greater than preindustrial times (Amos et al., 2013; Horowitz et al., 2017; Streets et al., 2017). A hemispheric gradient exists between the Northern and Southern Hemispheres, with Northern Hemisphere concentrations ranging between 1.3 and 1.6 ng m⁻³, while Southern Hemisphere concentrations range between 0.8 and 1.1 ng m⁻³ (Slemr et al., 2015; Sprovieri et al., 2016). Seasonal and annual variations in atmospheric concentrations have been observed at the majority of long-term monitoring sites. Peak concentrations are generally observed during winter and minima's occur during summer, although this does appear to be highly regional (Jiskra et al., 2018).

The atmosphere is an important pathway for the distribution and deposition of Hg to terrestrial and aquatic ecosystems (Gustin et al., 2015). Temporal and spatial variability in atmospheric Hg is a function of chemical and physical processes. Numerous factors can influence these processes including proximity to anthropogenic point sources, meteorology and oxidation/reduction reactions (Han et al., 2004; Karthik et al., 2017; Mao et al., 2008; Ren et al., 2016). Relationships have been observed between atmospheric Hg and air temperature, solar radiation, relative humidity, wind speed and direction, and meso and macro scale atmospheric circulation (Lynam and Keeler, 2005). Wind speed and direction and atmospheric circulation predominately influence Hg concentration by transporting Hg-containing air masses from anthropogenic point sources or high Hg production regions, such as polar regions, to sampling locations (Engle et al., 2010; Jaffe and Strode, 2008). Higher air temperature, solar radiation and relative humidity all work to enhance Hg photo-oxidation/reduction occurring in the atmosphere or increase surface evasion (Han et al., 2004; Obrist et al., 2018).

Seasonal variation is also considered to be driven by oxidation chemistry, although the exact mechanisms for oxidation are not clearly understood (Horowitz et al., 2017). Drivers of oxidation can be highly regional, making it difficult to determine rates and concentrations of Hg species. Gas phase oxidation of GEM is thought to be influenced by O_3 , H_2O_2 , OH radicals, NO_3 radicals and by various halogen species (Ariya et al., 2002). Aqueous phase oxidation in atmospheric water droplets is considered to be influenced by O_3 , OH, chlorine ($HOCl/OCl^-$) and bromine ($Br_2/HOBr/BrO^-$) (Si and Ariya, 2018). Gas-phase oxidation pathways are highly spatially variable, with marine boundary layer oxidation pathways dominated by Br, BrO and O_3 (Holmes et al., 2006; Horowitz et al., 2017). Coastal and inland sites have been shown to primarily be influenced by O_3 and OH oxidation pathways and can account for up to 80-99% of GEM production in the atmosphere (Travnikov et al., 2017). The high solubility of RM in water can enhance aqueous phase oxidation, leading to immediate deposition of Hg through enhanced oxidation or photo-oxidation rates of GEM to RM (Subir et al., 2012). During periods of high oxidation, TGM concentrations are low as GEM is transformed to GOM and is rapidly deposited (Holmes et al., 2010).

Minimal seasonal variability has been observed in the Southern Hemisphere which is largely driven by the higher proportion of ocean evasion compared with the Northern Hemisphere (Horowitz et al., 2017; Jiskra et al., 2018). However, Southern Hemisphere measurements are limited, primarily relying on ship measurements and 6 long-term station records (compared with 46 sites in the Northern Hemisphere) the longest of which has been operating since 2007 (Angot et al., 2014; Howard et al., 2017; Slemr et al., 2015; Soerensen et al., 2012; Sprovieri et al., 2016). The location of these long-term monitoring sites also means that they are all heavily influenced by the marine boundary layer. Some seasonal variation has been observed at Cape Point (South Africa), Amsterdam Island, and Cape Grim (Australia) (Angot et al., 2016; Slemr et al., 2015). This variation is attributed to climatically-driven changes in the air

masses, switching from low TGM ocean air masses to terrestrial-derived air masses containing higher TGM concentrations (Angot et al., 2016). The terrestrial air masses are influenced by regional sources of Hg, such as pollution hotspots and biomass burning (Angot et al., 2014; Angot et al., 2016; Slemr et al., 2015).

The large ratio of ocean to terrestrial surfaces and the overall limited number of studies in the Southern Hemisphere means that long-term terrestrial measurements of atmospheric mercury are rare. As such, variations and drivers of atmospheric mercury deposition over terrestrial surfaces in the Southern Hemisphere are largely unknown. This study provides 14 months of ambient GEM and RM measurements undertaken at a terrestrial background site south-west of Sydney, Australia. The aim of the study was to determine if there was seasonal variation in ambient mercury concentrations and to determine the potential drivers of this variation within the Australian terrestrial context.

2. Methods

2.1 Site characteristics

This study took place at Oakdale, New South Wales, Australia, a rural area on the far south-west edge of the Sydney basin (lat. 34° 03' 11" S, long. 150° 29' 50" E, altitude 457 m) (Figure 1). Measurements were undertaken from 3rd April 2017 to 21st June 2018 (445 days), within an agricultural grazing paddock (vegetation height <0.02 m). The site is located within a rural farming region with no known anthropogenic Hg sources. However, its location within the Sydney geological basin (68.38 km from the central business district) means that air masses arriving at the site may have been transported through the metropolitan regions. Atmospheric drainage patterns within the basin are influenced by elevated terrain to the north, west and south, and the Pacific Ocean to the east (Jiang et al., 2016).

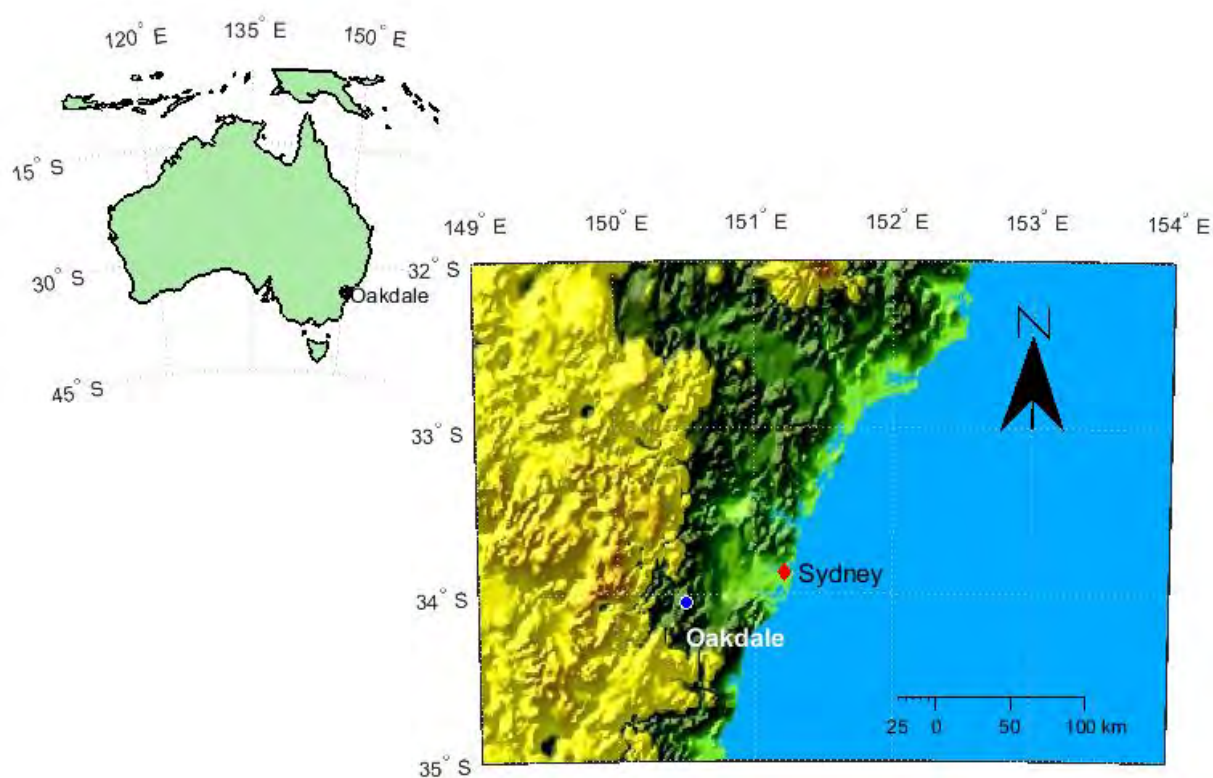


Figure 1. Site map of Oakdale field site in Australia (left) and within the Sydney geological basin (right). Blue dot indicates location of Oakdale study site; red dot shows Sydney central business district.

2.2 Ambient mercury measurements

Ambient Gaseous Elemental Mercury (GEM) concentrations were quantified using a Tekran 2537B (Tekran Instruments, Knoxville, TN, USA), with detection limit of 0.1 ng m^{-3} . Sample air was drawn from the sample inlets through a $0.2 \text{ }\mu\text{m}$ polytetrafluoroethylene (PTFE) filter by a PTFE pump drawing at 10 lpm. The 2537B sub-sampled from this flow through an additional $0.2 \text{ }\mu\text{m}$ PTFE filter. Continuous 5-minute samples were obtained at a height of 1.24m. Automated calibration of the 2537B was obtained every 23 hours throughout the study using the internal mercury permeation source. Permeation sources were verified using manual

mercury vapour injections within $\pm 2\%$, at the beginning and end of the study, as well as at the approximate half-way point of the study (September, 2017).

2.3 Reactive mercury filter system

Measurements of ambient Reactive Mercury were undertaken concurrently with Hg measurements, using the University of Nevada-Reno Reactive Mercury Active System (UNRRMAS). Three dual in-line 47 mm Teflon filter holders were mounted under an aluminium frame attached to a steel mast located on the roof of a New South Wales Office of Environment and Heritage air quality monitoring instrument container (3.6 m above the ground). Each port contained a polyethersulone cation-exchange membrane (CEM), for selective uptake of RM. The dual in-line set up allowed for collection of RM on a primary filter with a secondary filter to capture and quantify potential breakthrough. Air was pulled through the filter packs along Teflon tubes (6.35mm) at a flow rate of 1 l min^{-1} by vacuum pumps (Huang et al., 2013). The system was run at a 2-week collection resolution. CEM filters were analysed using the Tekran 2600-ivs System according to United States Environmental Protection Agency (US-EPA) method 1631 (Rev. E modified) (Miller, 2018). Blank CEM filters were analysed alongside collected filters. Instrument resolution for the Tekran 2600-ivs system is 1 ppt Hg while in aqueous solution. The method detection limit for RM collected on the CEM filters was 0.35 pg m^{-3} , based on average blank filter concentrations.

2.4 Environmental Variables

The four components of net all-wave radiation [long-wave incoming ($\text{LW}\downarrow$) and outgoing ($\text{LW}\uparrow$), plus short-wave incoming ($\text{SW}\downarrow$) and outgoing ($\text{SW}\uparrow$)] were measured using a Net

Radiometer (Apogee SN-500). Ozone and NO_x measurements were collected, maintained, calibrated and quality controlled by New South Wales Office of Environment and Heritage air quality network and conform to Australian and International Standards (OEH, 2018). Air temperature, wind speed and wind direction were obtained using a CSAT-3 sonic anemometer (Campbell Scientific, Logan, UT, USA). Specific humidity and relative humidity were measured using LI-7200 closed-path, infrared gas analyser (Li-Cor Biosciences, Lincoln, NE, USA). Both instruments were at a height of 3.12 m. All samples were collected at 10 Hz using the SmartFlux System (version 1.10). The Li-Cor 7200 was replaced part-way through the study period with an open-path 7500 analyser due to hardware malfunction. Post-processing and quality control of Li-Cor and CSAT-3 was undertaken using Li-Cor EddyPro[®] software (version 6.2.0).

2.5 HYSPLIT

The US National Oceanic and Atmospheric Administration (NOAA) Hybrid Single Particle Lagrangian Integrated Trajectory (HYSPLIT) Model was used to characterise air mass movement to gain an understanding of how air circulation may influence Hg concentrations. Back trajectories were compiled over 120-hour (<http://www.arl.noaa.gov/ready/hysplit4.html>). Global Data Assimilation System 0.5° meteorological reanalysis data were used to drive the model, and trajectories were initialised at 0.5 times the mixed layer height as determined by HYSPLIT. Back trajectories were calculated for each hour of the day to account for the influence of local daily variation in GEM. For each trajectory, air parcel coordinates were calculated every two hours.

3. Results and discussion

3.1 GEM characteristics

Gaseous Elemental Mercury concentrations at Oakdale were below previously reported global background concentrations for the duration of the study, averaging 0.68 ng m^{-3} (standard deviation $\pm 0.22 \text{ ng m}^{-3}$, Table 1). The site exhibited significant seasonal variation, with highest concentrations occurring during austral summer (December, January, February) and lowest in winter (June, July, August) (0.88 and 0.43 ng m^{-3} , respectively). Two-way t-tests between seasonal values demonstrated variance to be statistically significant ($p\text{-value} < 0.01$, Appendix 3, Table 1). Monthly averages showed GEM concentrations peaked in January and were lowest in August (Figure 2). Concentrations were lower than those currently recorded in Australia and elsewhere in the Southern Hemisphere. Southern Hemisphere concentrations have been found to range between 0.85 ng m^{-3} and 1.05 ng m^{-3} (Song et al., 2015; Sprovieri et al., 2016). Cape Grim, Tasmania, Australia's long-term baseline monitoring station, had an annual average concentration of 0.88 ng m^{-3} (Howard, 2017). GEM concentrations were within range of those recorded for rural and remote sites in the Northern Hemisphere, which have been shown to range between 0.2 and 18 ng m^{-3} , although lower than the median concentration (1.6 ng m^{-3}) (Mao et al., 2016).

Table 1. Seasonal mean and standard deviation (SD) for Gaseous Elemental Mercury (GEM), Reactive Mercury (RM), wind speed (WS), air temperature, relative humidity (RH), specific humidity, ozone (O₃), nitrogen oxides (NO_x), and total solar radiation (total solar) at Oakdale, New South Wales, from 3 April 2017 to 21 June 2018.

	WS m s ⁻¹		Air Temperature °C		RH %		Specific Humidity g/kg		O ₃ pphm		NO _x ppm		Total solar W m ⁻²		RM pg m ⁻³		GEM ng m ⁻³	
	Mean	SD	Mean	SD	Mean	SD	Mean	SD	Mean	SD	Mean	SD	Mean	SD	Mean	SD	Mean	SD
Autumn 2017	0.85	0.45	14.25	0.73	65.42	16.22	7.00	2.00	2.23	0.60	0.12	0.20	117.96	181.75	--	--	0.46	0.10
Winter 2017	0.75	0.37	12.25	3.10	51.46	14.78	5.00	1.00	2.57	0.56	0.06	0.12	109.63	171.23	1.93	1.52	0.43	0.08
Spring 2017	1.00	0.63	13.88	1.32	66.89	21.69	7.00	2.00	2.86	0.88	0.13	0.19	183.77	257.38	2.80	0.79	0.71	0.19
Summer 2017/2018	1.60	1.12	18.88	5.05	71.45	21.28	10.00	3.00	2.69	1.45	0.20	0.21	202.31	283.56	3.43	1.86	0.88	0.19
Autumn 2018	1.35	0.78	16.30	4.00	68.13	18.40	8.00	2.00	2.60	0.88	0.17	0.22	138.11	208.40	2.05	2.12	0.64	0.17
All	1.10	0.77	14.93	5.96	64.20	19.95	7.10	2.70	2.61	0.93	0.13	0.20	147.36	255.46	2.41	1.68	0.68	0.22

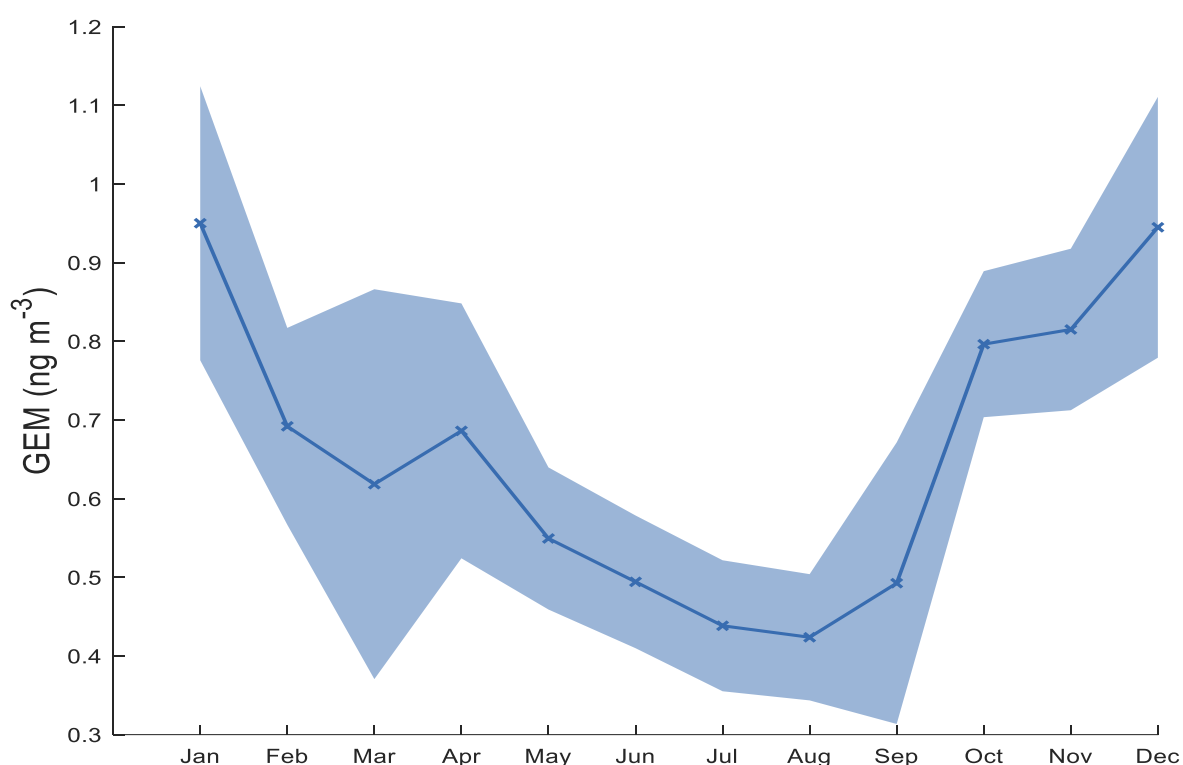


Figure 2. Monthly composite of the daily mean (bold line) and standard deviation (shaded area) of total gaseous mercury concentration at Oakdale, New South Wales, from 3 April 2017 to 21 June 2018.

Diel concentrations and trends varied between seasons. Variation was relatively small across most seasons with the exception of summer (Figure 3). Spring showed a minor diel trend with decreased atmospheric GEM concentrations occurring after midday and slightly higher concentrations overnight (p-value <0.01, t-score -3.18, Appendix 3, Table 2). Autumn also showed slightly higher concentrations in the late afternoon to early evening. Winter diel trends did not show any significant variation between day and night concentrations. Lack of variation suggest that there is likely no potential Hg point sources within the region. Rural and elevated site GEM has been shown to exhibit weak if any diel trend (Choi et al., 2008; Engle et al., 2010; Han et al., 2004; Mao et al., 2008; Sigler et al., 2009; Zhang et al., 2009; Zhang et al., 2013). The summer diel trend observed here, with higher GEM concentrations overnight, has been observed to be more typical of polluted urban regions, indicating that Hg-containing air

is being transported from heavily urbanised regions to this site (Cole et al., 2014; Fu et al., 2015; Gratz et al., 2013; Li et al., 2011; Lyman and Gustin, 2008; Nguyen et al., 2011; Zhang et al., 2013).

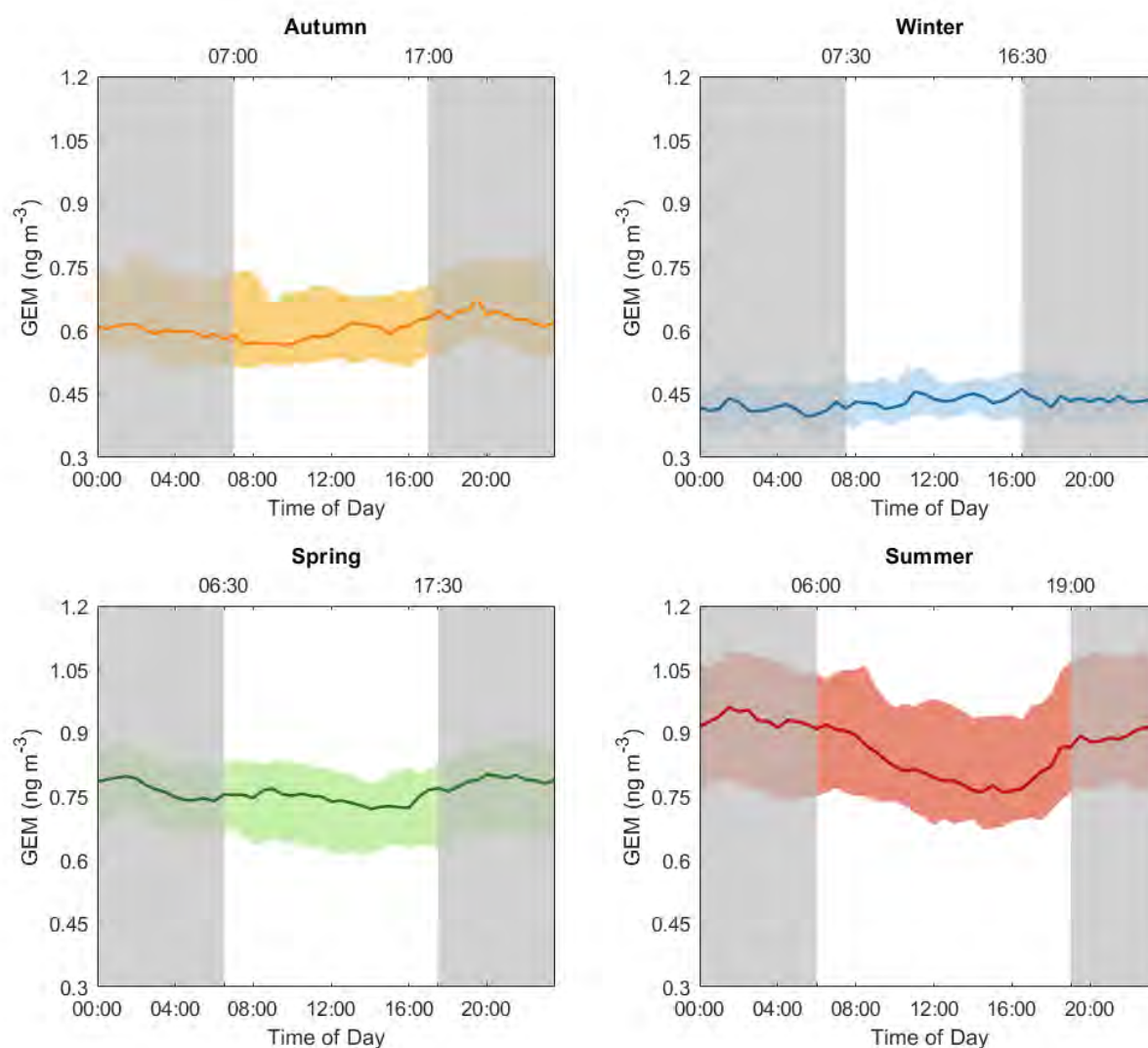


Figure 3. Diel composite of GEM for each season at Oakdale, New South Wales, from 3 April 2017 to 21 June 2018. Bold line gives median concentrations, shaded area inter-quartile range. Grey shaded areas show night, including sun rise and sun set times.

3.2 Reactive mercury characteristics

Reactive mercury 2-week concentrations over the entire study period average 2.41 pg m^{-3} ($\pm 1.68 \text{ pg m}^{-3}$) (Figure 4). Concentrations peaked in summer (3.43 pg m^{-3}) and were lowest in

winter 2017 (1.93 pg m^{-3}) (Table 1). Two-way t-tests indicated seasonal variability was not statistically significant, apart from winter to spring (t-score= -4.56, p-value < 0.01). Malcolm et al. (2003), at a background site in Florida, recorded RM concentrations of 1.7 pg m^{-3} when the site was only being influenced by marine air flows and 4.5 pg m^{-3} when the site was influenced by mixed marine and urban air flows. Similar trends were observed at Oakdale and could indicate air mass transportation significantly influences RM concentrations.

The short atmospheric life time of RM means that it is deposited close to the source of emission and as such highly regionally variable (Schroeder and Munthe, 1998). The low concentrations observed over the duration of this study further indicates that there was no significant source of RM within the region. Therefore, it is likely that RM arriving at the Oakdale field site is the product of oceanic sources rather than nearby point sources. Prevailing wind direction over the duration of the study period varied between NE and SE, suggesting air masses arriving at the site are influenced by urban and oceanic sources.

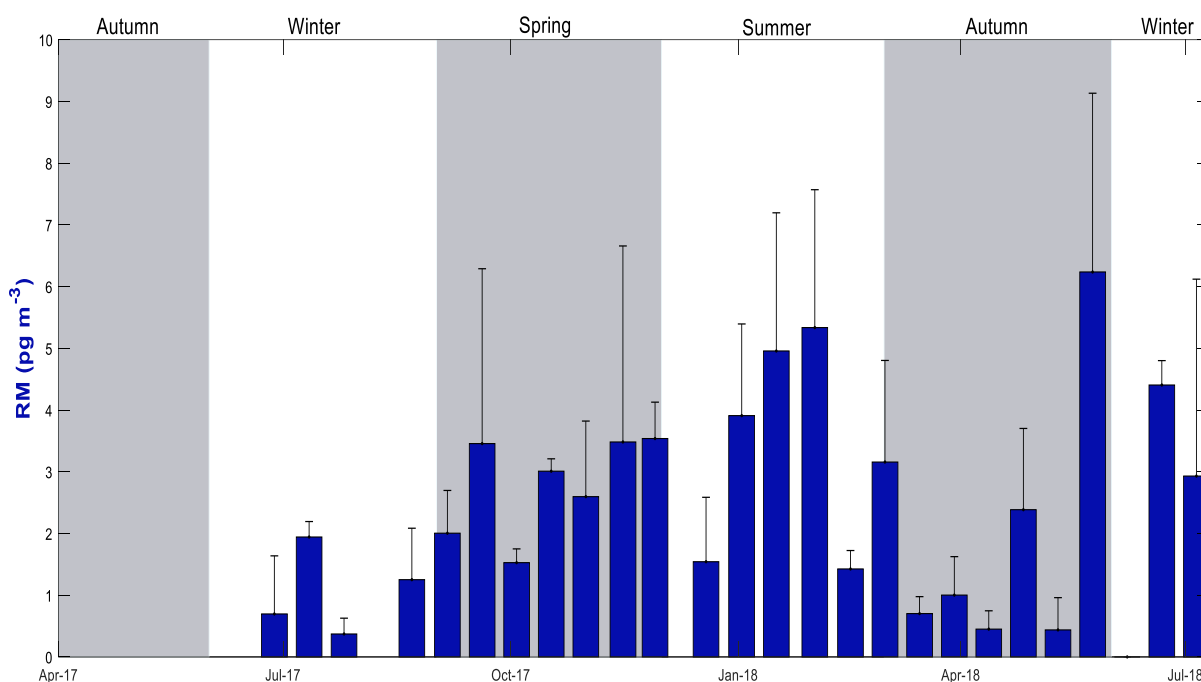


Figure 4. Reactive Mercury measurements made at Oakdale, New South Wales, from 3 April 2017 to 21 June 2018. Columns show 2-weekly mean concentration and bars show standard deviation. Shaded/unshaded background depicts Australia's seasons.

RM measured using the same sampling techniques at Macquarie University (MQ), located in Sydney's urban region, and at Cape Grim, north-western Tasmania, recorded average concentrations substantially higher than Oakdale: 17.8 pg m^{-3} and 15.9 pg m^{-3} , respectively (Cook, 2017; Miller, 2018). MQ experienced significant seasonal variation, peaking in winter. This seasonality was largely attributed to variation in local and regional sources. Cape Grim did not show any significant seasonal variation. RM measurements undertaken at Amsterdam Island in the Southern Ocean, using Tekran speciation system, observed similarly low concentrations to those recorded at Oakdale. Amsterdam Island measured highest concentrations in summer (1.58 pg m^{-3}) and lowest in winter (1.34 pg m^{-3}), however, KCl denuder based measurements are assumed to bias low compared to other methods (Lynam and Keeler, 2005). This seasonal variation was attributed to enhanced photo-chemistry occurring during summer (Angot et al., 2014).

RM is influenced by local sources and local chemistry to a much greater extent than GEM. RM is removed quickly from ambient air due to significant dry and wet deposition, so its residence time is very short (up to several days), causing large concentration differences between sites near sources and background sites (Han et al., 2004). The coarse time resolution of the RM sampling method deployed at Oakdale makes it difficult to accurately identify potential drivers of RM concentrations at these shortened time scales. In order to look at the relationship between potential environmental drivers of RM and RM concentrations, Spearman correlations were performed using 2-weekly averaged measurements to match the 2-weekly RM concentrations (Table 2). For all included variables listed in Table 2, only total solar radiation across the entire data set was deemed to be statistically significant ($p\text{-value} < 0.05$) despite several strong

correlations. Lack of significant seasonal relationships may be attributed to a combination of a limited number of RM measurements available for each season ($n \approx 6$) and not being able to capture the shorter data variation.

Table 2. Spearman correlations with two weekly RM at Oakdale, New South Wales, from 3 April 2017 to 21 June 2018. Bold values represent those deemed to be statistically significant, based on a p-value <0.05.

	Total solar	Air temp	Specific humidity	Relative humidity	Wind direction	WS	Ozone	NOx	GEM
All	0.38	0.18	0.12	0.09	-0.12	0.18	0.18	-0.02	0.34
Winter	0.00	-0.40	-0.40	0.40	0.40	-0.20	0.00	0.00	-0.8
Spring	0.64	0.14	0.54	0.54	-0.43	0.71	-0.75	-0.14	0.43
Summer	0.09	0.26	0.80	0.10	-0.60	0.09	0.77	0.43	0.60
Autumn	0.03	-0.66	-0.43	-0.26	0.14	-0.43	-0.14	-0.71	-0.14

3.3 Meteorological drivers across seasons

Oakdale's location on the south-west edge of the Sydney basin results in it being influenced by air masses transported from or through metropolitan and marine regions. Mountainous topography to the west creates early morning drainage flows into the basin, usually mixing and transporting air trapped in the basin overnight (Jiang et al., 2017). The presence of the Pacific Ocean to the east generates onshore sea breezes during the day, particularly during the warmer months, transporting air masses inland through the heavily urbanised region and trapping the air masses on the western edges of the basin (Jiang et al., 2016; Jiang et al., 2017). Large urbanised areas within the Sydney basin can result in the mixing of polluted urban air with

cleaner, marine air. As a consequence, this mixing has been found to bring pollutants, such as elevated ozone, that have been transported offshore back onshore during a sea breeze (Malcolm et al., 2003). South to south-west of the Oakdale field is dominated by rural and remote land surfaces. Apart from an immediately adjacent National Park, south-west of the field site, most vegetation is sparse grasslands. The lack of significant sources likely means that GEM arriving at the site from this direction is the product of long-range atmospheric transport. Seasonality in the wind patterns at Oakdale may cause considerable dilution or enrichment of atmospheric GEM through atmospheric transport (Karthik et al., 2017).

Strongest correlations between GEM, meteorological variables and photo-pollutants were all seen during spring (Table 3). Correlations between GEM and air temperature, relative humidity, specific humidity, and total solar radiation are in general weakest during summer and autumn at this site, with some exceptions. The weak correlation between these variables and GEM could indicate that the higher observed GEM concentrations during summer are likely a combination of Hg being transported over and through the Sydney Basin and enhance surface evasion at the field site. Higher total solar radiation and air temperature (Table 1) promotes the release of Hg from terrestrial substrates due to increased photo-reduction occurring at the soil surface. Solar radiation stimulates the reduction of deposited RM within the substrate. Higher solar radiation also leads to increased thermal energy and soil temperatures within the substrate. Higher temperatures enhance the rate of GEM volatilisation in terrestrial surfaces, thereby increasing GEM concentrations within the substrate (Choi et al., 2013; Wang et al., 2016). The photo-reduction of RM within the substrate is one of the most important factors regulating GEM surface emission (Ci et al., 2016). Both air temperature and solar radiation peaked during summer (18.88 °C and 202.31 W m⁻², respectively) increasing the likelihood of photo-reduction occurring during this time. Discrepancies between 2017 and 2018 autumn concentrations are largely driven by differences in meteorological parameters

during this time. 2018 experienced higher average air temperatures and wind speeds, likely causing the higher concentrations than observed in 2017.

Table 3. Spearman correlations with atmospheric GEM at Oakdale, New South Wales, from 3 April 2017 to 21 June 2018. Bold values represent statistically significant correlation (p-value <0.05).

	Total solar	Air temp	Specific humidity	Relative humidity	Ozone	NOx
All	0.03	0.54	0.66	0.54	-0.02	0.40
Winter	-0.04	0.16	0.38	0.09	-0.15	0.17
Spring	-0.13	0.18	0.82	0.79	-0.31	0.55
Summer	-0.22	0.10	0.35	0.47	0.03	0.27
Autumn	-0.09	0.20	0.36	0.36	0.11	0.22

Spring GEM concentrations also appear to be influenced by enhanced photochemical reduction occurring at this time. A strong negative correlation was observed between GEM and O₃ ($r = -0.31$) and RM and O₃ ($r = -0.75$) and a weak but significant negative relationship between GEM and total solar radiation ($r = -0.13$), indicating photo-chemical oxidation has a significant role in the spring trends. Higher RM in the warm seasons is primarily driven by photochemical production due to increased solar radiation, O₃, and other atmospheric oxidants (Choi et al., 2013; Liu et al., 2010; Xu et al., 2015).

RM at Oakdale showed the strongest positive correlations with air temperature, solar radiation, and ozone concentrations, suggesting the role of photochemistry in its production, although these relationships were not statistically significant (Table 2). Pollutant-containing air transported from metropolitan regions to Oakdale enhances the reduction of GEM to RM,

which can then be deposited. High urban emissions from the Sydney metropolitan region can be transported across the basin by prevailing mesoscale airflows such as sea breezes during warmer months. Poor air quality is associated with anticyclone conditions and good air quality often occurs under unstable/cyclonic conditions (Jiang et al., 2016). Higher O₃ levels are also typically found in the afternoon during times of higher solar radiation, which can result in higher Hg photo-chemical oxidation (Holland et al., 2003). Changes to air circulation at Oakdale during warmer months may bring higher Hg concentrations from the urbanised regions of Sydney, making the atmospheric concentrations more susceptible to these driving processes.

RM measurements at Oakdale were lowest in winter, averaging 1.93 pg m⁻³ and ranging between 0.70 and 4.41 pg m⁻³. The low concentrations suggest there are no nearby sources and limited potential for reduction of GEM to RM within the vicinity of the field site. Prevailing wind direction during winter indicates RM is being transported from marine sources to the south-east and long-range transport from rural/remote to the south-west. Winter also had the weakest correlations between RM, ozone, and NO_x ($r = 0.00$), further indicating limited influence from local and regional pollution sources. A strong negative relationship between GEM and RM ($r = -0.8$) suggests RM is being deposited before reaching Oakdale, allowing GEM to be the dominant Hg species. Within marine air masses, Br and OH are the dominant reactants initiating the reduction of GEM to RM, which is then rapidly deposited deposition back to the ocean through wet and dry deposition before it is able to be transported (Ariya et al., 2015; Holmes et al., 2006; Horowitz et al., 2017). Halogens emitted from the ocean also destroy ozone that may otherwise have been transported inland to facilitate the production of RM (Mao et al., 2008).

Modelling studies suggest that re-emission from oceans is a major contributor to atmospheric concentrations of GEM, particularly in the Southern Hemisphere where oceans were shown to contribute more than half of the surface atmospheric concentration (Strode et al., 2007). Cape Grim GEM measurements were found to be higher when measurement fetch was over the Southern Ocean, indicating it was a net source of GEM (Howard, 2017). Overall, ocean evasion in the Southern Hemisphere is considered to be relatively consistent across seasons (Angot et al., 2014). Ocean transport is able to drive Hg concentrations at Oakdale during winter as temperature and solar radiation are lowest at this time, reducing the potential for terrestrial surface evasion to occur and the dominant wind sector is such that air masses transported from the ocean are not influenced by urban sources of Hg.

Prevailing wind direction during summer was ENE and corresponded to highest GEM (Figure 5). GEM concentrations were lowest in winter when prevailing wind direction was to the SE and SW. Higher concentrations in winter were seen when wind direction was from the SE and lowest when wind direction was from the SW when air masses spent the most time over rural landscapes. South-east of the site is sparsely populated and the shortest distance to the coastline. Air masses travelling from ENE circulate through the heavily urbanised Sydney basin where they are exposed to numerous potential Hg pollution sources and photo-chemical pollutants that can cause the oxidation of GEM to RM. Jiang et al. (2017) found that prevailing air flow patterns during the warmer months transported higher urban emissions from the central business district to the SW quadrant of the Sydney Basin.

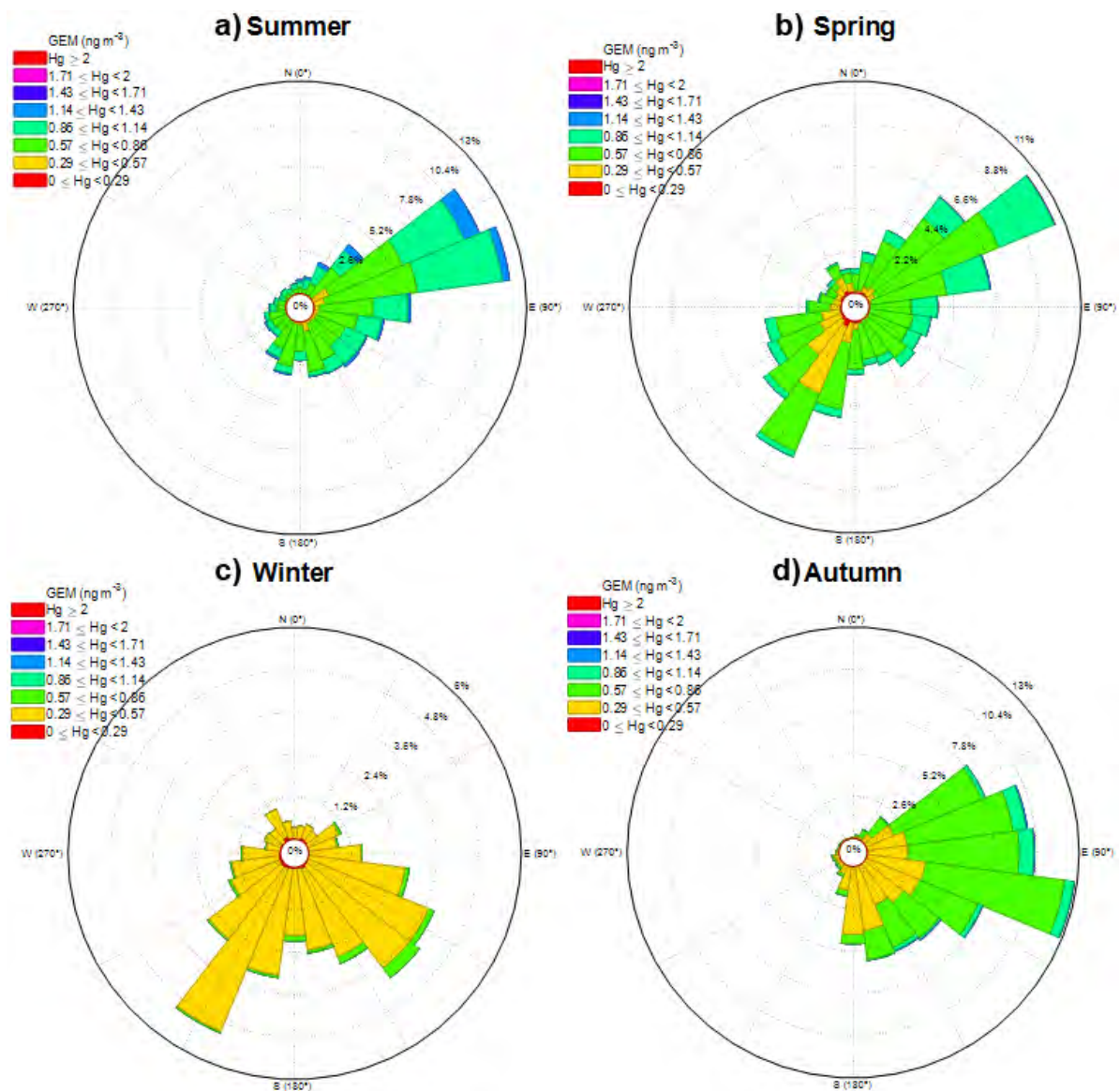


Figure 5. Wind rose with GEM concentrations for each season at Oakdale, New South Wales, from 3 April 2017 to 21 June 2018.

Spring and autumn trends appear to be driven by several contributing factors. Prevailing wind direction during autumn was from the ESE, indicating the potential for ocean evasion influences. Spring prevailing wind was SE and SSW where trends are largely driven by variations in air mass transport from urban and rural air sources. Lowest GEM concentrations for both spring and autumn occur when wind direction is SSW, HYSPLIT back trajectories also echo this trend. Trajectories run for GEM concentration in the upper 75% quartile indicate that highest concentrations occur when air masses are transported from the east (Figure 6),

while lower 25% quartile concentrations are seen when the air masses spend a greater time over terrestrial surfaces and away from potential Hg point sources (SW direction).

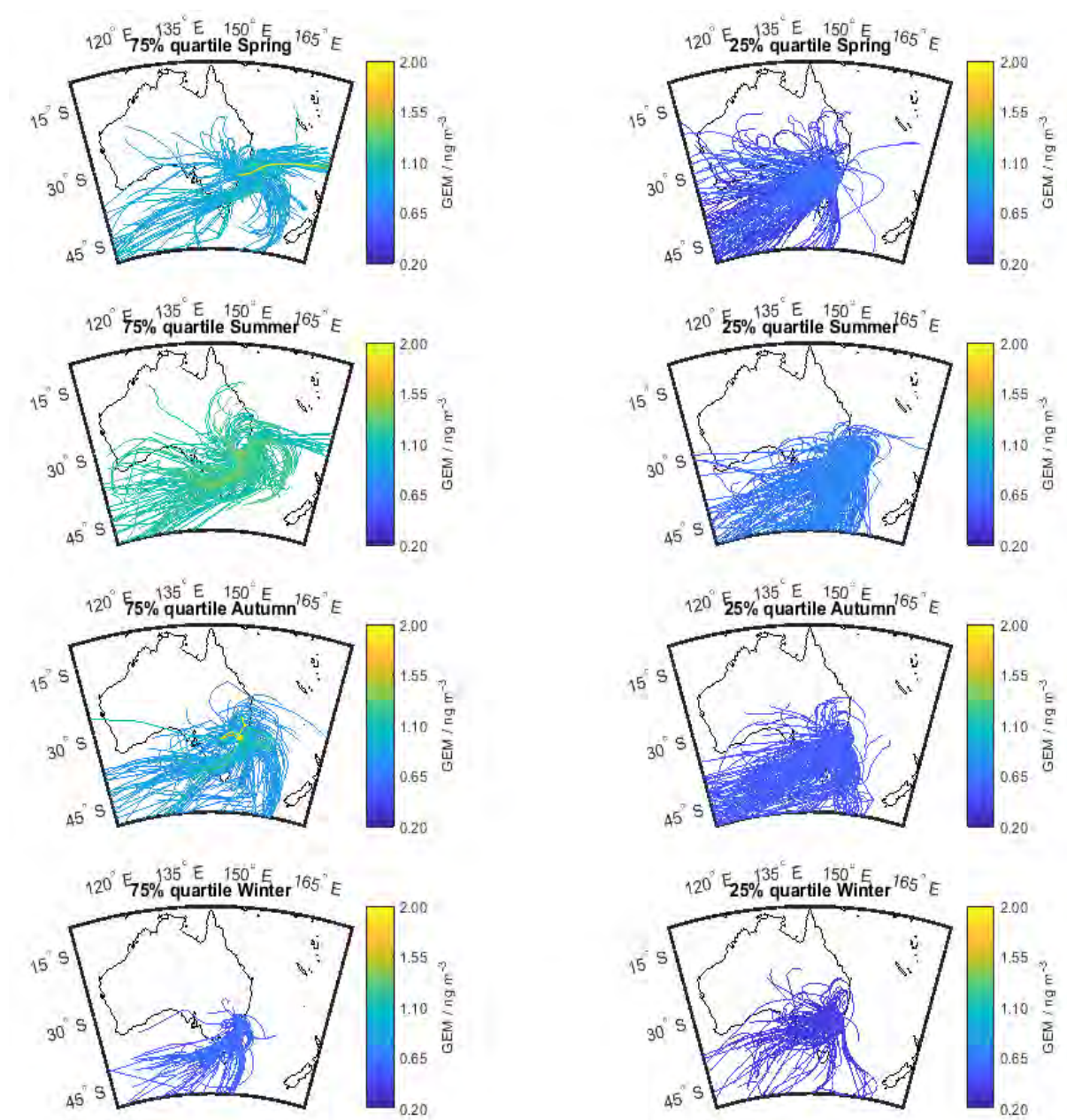


Figure 6. Hourly GEM-weighted HYSPLIT trajectories for 75% quartile and 25% quartile for each season at Oakdale, New South Wales, from 3 April 2017 to 21 June 2018.

HYSPLIT trajectories for autumn indicate higher GEM concentrations when air masses are transported from the Tasman Sea in the south to the Pacific Ocean before reaching the site.

Lower 25% quartile air masses spend a greater time tracking over land, limiting the potential for oxidation to occur and resulting in lower GEM and RM concentrations. During winter and autumn highest GEM concentrations occurred when air masses travelled along the east coast before being transported inland (Figure 6). Higher GEM concentration when air masses are transported from this sector could indicate greater coastal and ocean influences. Globally the ocean is the largest natural emission source of GEM and therefore ocean evasion can have a significant impact on ambient GEM concentrations as both a direct source of GEM and by enhanced production of oxidants and halogens (Mason and Sheu, 2002).

Autumn 2018 experienced numerous high spikes in GEM consistent with increased local hazard reduction burns (Figure 7). Combustion of vegetation and heating of soil during fires has been found to volatilise large amounts of Hg previously stored within vegetation and soils, predominantly in the form of GEM (Friedli et al., 2003). Hazard reduction burns occur frequently during autumn and spring, while temperatures are cooler and soils contain more moisture, to limit the potential of wildfires occurring during the dry and hot summer (Paton-Walsh et al., 2014). These burns also tend to occur when atmospheric conditions are such to limit the potential of smoke dispersion (limited wind gusts and wind speeds) to reduce the likelihood of the fire getting out of control (Haikerwal et al., 2015). This often leads to high amounts of atmospheric pollutants accumulating within the immediate vicinity and likely responsible for the higher concentrations of GEM observed during April and May 2018. Hazard reduction burning varies in frequency and timing from year to year as conditions need to be precise for them to occur. This is highlighted by the fact that autumn 2017 did not experience the same excursions in Hg concentrations as 2018, largely due to the high rainfall that occurred at the start of 2017 leaving the soil and vegetation too moist to adequately burn (BOM, 2018).

3.4 Photo-reduction pathways

Temporal variation in atmospheric GEM is considered an indication of chemical and physical sources and sink influences (Mao et al., 2008). Removal from the atmosphere is facilitated by photo-chemical transformation of GEM to RM and subsequent wet and dry deposition. These photochemical transformations can be accelerated by increased water present in the atmosphere (Ariya et al., 2015). Figure 7 illustrates half hour averaged temporal variation in GEM concentrations, O₃, and specific humidity over the entire field study duration. Specific humidity follows a similar trend as GEM over the whole study, with peaks and troughs occurring at similar timing to GEM. O₃ appears to only follow a similar temporal pattern during the warmer months (October to February), with the cooler months showing different variability. The relationship during the warmer months is likely caused by higher solar radiation increasing the rate of photo-chemistry.

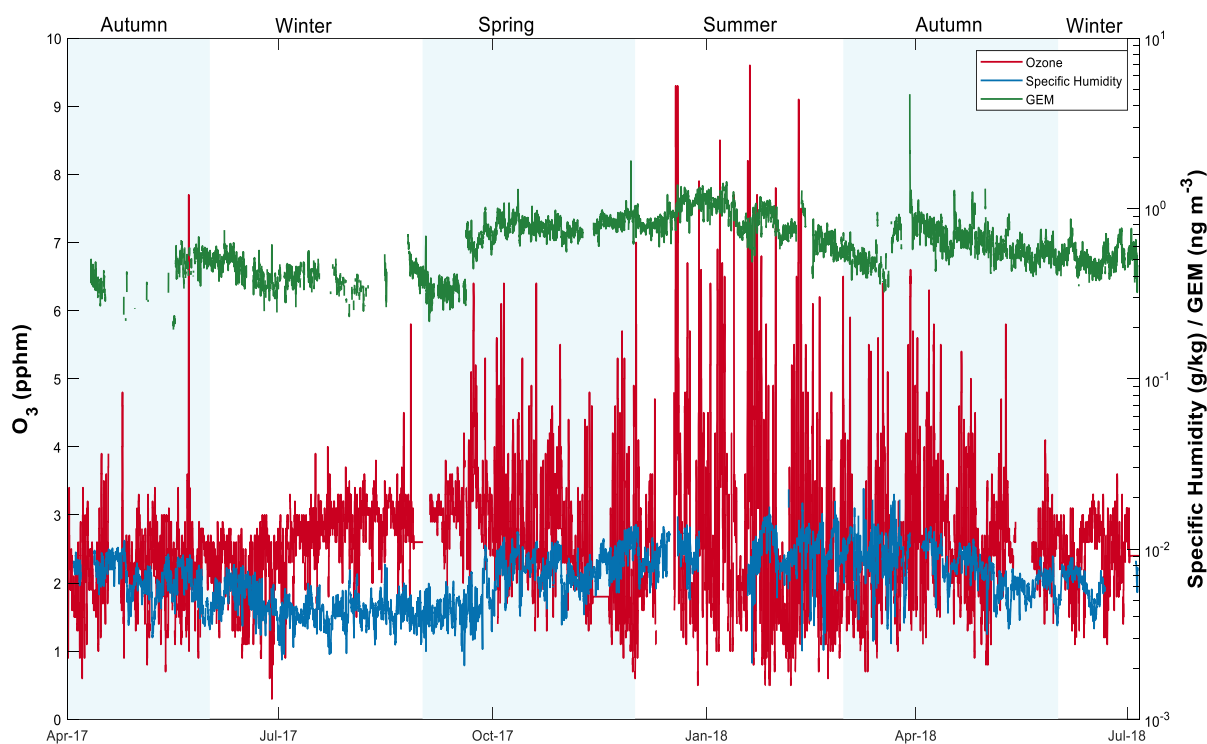


Figure 7. Half hourly ozone (on the left y axis), specific humidity (on the right y axis), and elemental gaseous mercury (on the right y axis) for the entire study period (3 April 2017

to 21 June 2018) at Oakdale, NSW. Shaded/unshaded background depicts Australia's seasons. Note that the right hand y axis is a log scale.

Strongest negative correlation between GEM and O₃ was observed during spring ($r = -0.31$). RM also had a strong negative r of -0.75 during spring and a positive relationship during summer ($r = 0.64$). These relationships suggest gaseous phase photochemical oxidation influences GEM trends during Australia's spring and summer. During these warmer months when solar radiation is highest, O₃ follows a similar diel trend with concentrations peaking in the late afternoon (Choi et al., 2013; Holland et al., 2003). This diel O₃ trend was present across all seasons but most pronounced during spring and summer (Figure 8), gaps in the data at 2am is due to a 24 hour ozone calibration cycle. Summer GEM diel composite trends show similar pattern to O₃, with GEM minimums occurring at similar timing to maximum O₃ concentrations. Elevated O₃ concentrations increase the rate of oxidation of GEM to RM, leading to a positive relationship between RM and O₃ and a negative relationship with GEM as the reactions reduce the availability of GEM and increases RM concentrations (Lynam and Keeler, 2005). Air pollution production in the Sydney basin is greatest during warm months and accumulates to the north-west and south-west of the basin close to Oakdale due to prevailing air circulation during this time (Jiang et al., 2017). Production and accumulation is largely driven by the presence of a high-pressure cell in the region (Jiang et al., 2016). Mesoscale meteorology during the cooler months did not favour the production of O₃, and therefore relationships with GEM and RM were not observed.

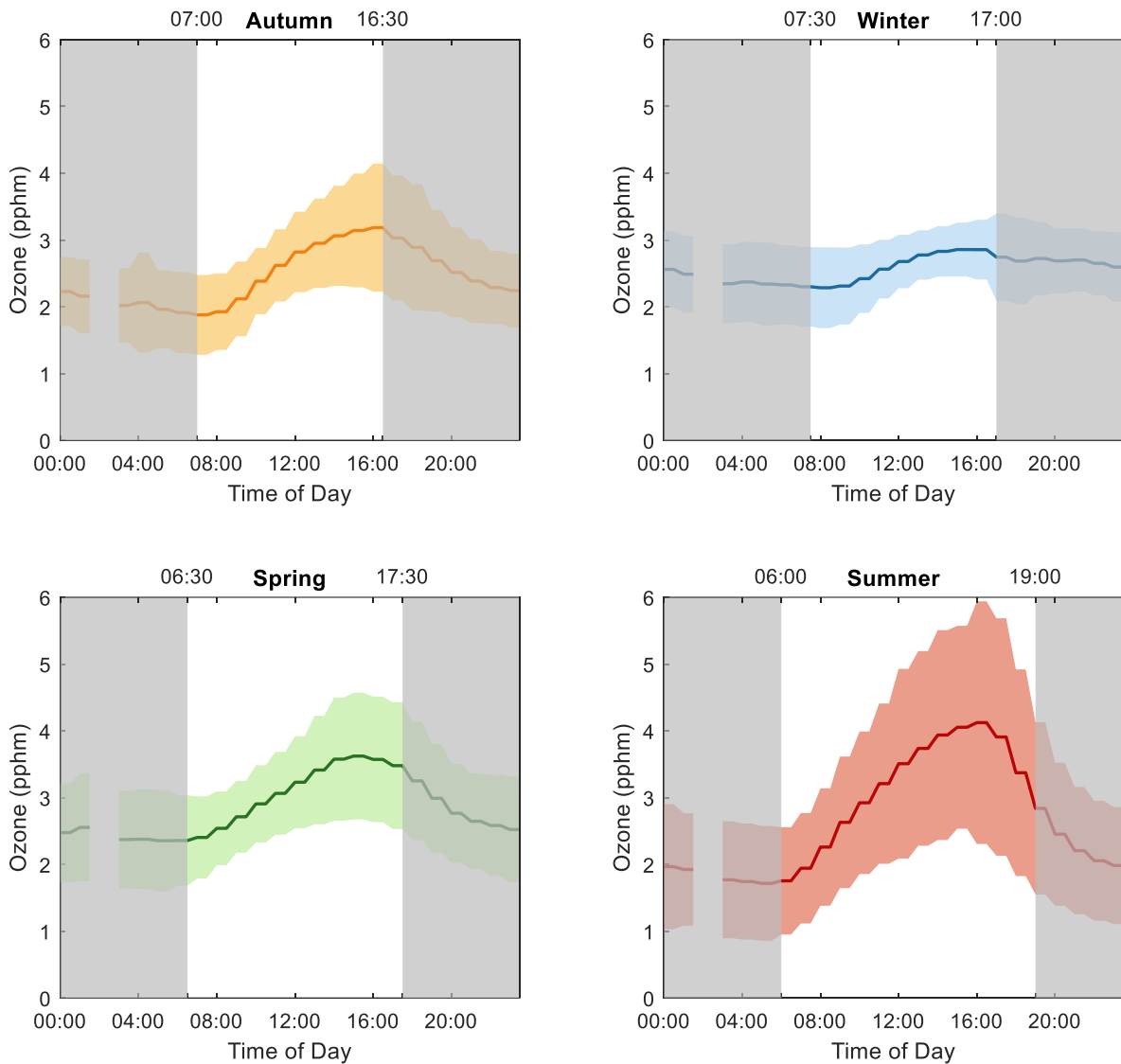


Figure 8. Diel composite of ozone for each season at Oakdale, New South Wales, from 3 April 2017 to 21 June 2018. Bold line gives median concentrations, shaded area inter-quartile range. Grey shaded areas show night, including sun rise and sun set times.

Relationships between GEM and major pollutants, such as NO_x , CO and SO_2 , have commonly been observed and are indicators of anthropogenic pollution sources (Friedli et al., 2001; Lynam and Keeler, 2005; Mao et al., 2008). NO_x , the major pollutant measured (with the exception of O_3), showed an overall strong relationship with GEM ($r = 0.4$), with the strongest relationship occurring in spring ($r = 0.55$). This relationship is most likely a reflection of GEM and NO_x being co-emitted from combustion sources, such a vehicle emissions from nearby traffic corridors, which are then transported from the urban region to Oakdale (Carpi, 1997;

Sigler et al., 2009). The strong positive correlation between NO_x and RM during summer ($r = 0.49$, Table 3) may also be indicating that nitrate radicals are contributing to the oxidation of GEM to RM. Nitrogen compounds present in the atmosphere produce O_3 and NO_2 through photochemical reactions. This increased O_3 is then available to oxidise TGM also present in the atmosphere (Han et al., 2004).

Water in the atmosphere helps to enhance and accelerate the rate of Hg oxidation through aqueous phase reactions. GEM correlations with specific humidity were the strongest of all measured meteorological parameters across all seasons (Table 2). Figure 7 shows that variations in specific humidity closely follow the variation observed in GEM concentrations. Water in the form of clouds, fog and rain is sufficient enough to initiate aqueous phase reduction of Hg in the atmosphere (Ariya et al., 2015). Higher specific humidity is an indicator of increased liquid water present in the atmosphere and on surface particles, increasing the availability of aqueous phase reduction to occur (Choi et al., 2013). Specific humidity was highest in summer (10.00 g/kg) and lowest in winter (5.00 g/kg), following the same trend as GEM concentrations. The major pathway for the reduction of RM in the aqueous phase in the atmosphere involves reduction with sulphite (SO_3^{2-}) and reductions by hydroperoxyl radical (HO_2) and iron (III) (Zhang and Lindberg, 2001).

Solar radiation can accelerate Hg reduction by aqueous phase radicals by iron(III)-induced photo-reduction (Zhang and Lindberg, 2001). Photo-reduction of RM in the presence of iron(III) in atmospheric waters results in a dramatic increase in GEM (Dedik et al., 1992; Lin and Pehkonen, 1997). As specific humidity is a measure of water vapour content, it is plausible that higher specific humidity could indicate an increased likelihood of iron(III) presence in the atmosphere. The stronger relationship between specific humidity and RH and GEM than

between O₃ and GEM could indicate that these aqueous phase radicals are the primary reduction pathways rather than gas phase reactions.

4. Conclusion

Atmospheric concentrations of both GEM and RM were below global average background concentrations, averaging 0.68 ng m⁻³ (±0.22). Concentrations peaked in summer and were at minimum in winter. Variations in air mass transport across seasons is the most significant driver in GEM and RM concentration recorded at the Oakdale field site. Summer and spring are influenced by air masses transported through the Sydney urban region to the north-east of the site. These air masses bring both higher Hg concentrations from urban point sources and potential Hg oxidants. Summer is also influenced by increased surface evasion due to higher temperatures and solar radiation.

Winter concentration were primarily driven by ocean evasion being transported inland. Autumn trends suggest the possibility of inter-annual variability due to changing fire seasons. Autumn 2018 higher fire occurrences resulted in increased GEM emissions in the region, while autumn 2017 appears to have not experienced the same fire regime. Relationships observed between ozone, specific humidity and Hg suggest both aqueous and gaseous phase oxidation appear to be playing a role in the reduction of GEM to RM. Gaseous oxidation is most efficient during spring and summer, aqueous phase oxidation active all year round as indicated by the year round consistent relationship with specific humidity. Measurements over multiple years would help to better quantify how all identified drivers vary from year to year, along with further research into aqueous phase reactions over terrestrial environments.

5. References

- Agnan, Y., Le Dantec, T., Moore, C. W., Edwards, G. C. & Obrist, D. 2016. New Constraints on Terrestrial Surface-Atmosphere Fluxes of Gaseous Elemental Mercury Using a Global Database. *Environ Sci Technol*, 50, 507-24.10.1021/acs.est.5b04013
- Amos, Helen M., Jacob, Daniel J., Streets, David G. & Sunderland, Elsie M. 2013. Legacy impacts of all-time anthropogenic emissions on the global mercury cycle. *Global Biogeochemical Cycles*, 27, 410-421.10.1002/gbc.20040
- Angot, H., Barret, M., Magand, O., Ramonet, M. & Dommergue, A. 2014. A 2-year record of atmospheric mercury species at a background Southern Hemisphere station on Amsterdam Island. *Atmospheric Chemistry and Physics*, 14, 11461-11473.10.5194/acp-14-11461-2014
- Angot, Hélène, Magand, Olivier, Helmig, Detlev, Ricaud, Philippe, Quennehen, Boris, Gallée, Hubert, Del Guasta, Massimo, Sprovieri, Francesca, Pirrone, Nicola, Savarino, Joël & Dommergue, Aurélien 2016. New insights into the atmospheric mercury cycling in central Antarctica and implications on a continental scale. *Atmospheric Chemistry and Physics*, 16, 8249-8264.10.5194/acp-16-8249-2016
- Ariya, P. A., Amyot, M., Dastoor, A., Deeds, D., Feinberg, A., Kos, G., Poulain, A., Ryjkov, A., Semeniuk, K., Subir, M. & Toyota, K. 2015. Mercury physicochemical and biogeochemical transformation in the atmosphere and at atmospheric interfaces: a review and future directions. *Chem Rev*, 115, 3760-802.10.1021/cr500667e
- Ariya, Parisa A. , Khalizov, Alexei & Gidas, Alexios 2002. Reactions of Gaseous Mercury with Atomic and Molecular Halogens: Kinetics, Product Studies, and Atmospheric Implications. *The Journal of Physical Chemistry A*, 106
- Carpi, Anthony 1997. Mercury from combustion sources: a review of the chemical species emitted and their transport in the atmosphere. *Water, Air, and Soil Pollution*, 98, 241-254
- Choi, H. D., Huang, J., Mondal, S. & Holsen, T. M. 2013. Variation in concentrations of three mercury (Hg) forms at a rural and a suburban site in New York State. *Sci Total Environ*, 448, 96-106.10.1016/j.scitotenv.2012.08.052
- Choi, Hyun-Deok, Holsen, Thomas M & Hopke, Philip K 2008. Atmospheric mercury (Hg) in the Adirondacks: Concentrations and sources. *Environmental science & technology*, 42, 5644-5653
- Ci, Zhijia, Zhang, Xiaoshan, Yin, Yongguang, Chen, Jinsheng & Wang, Shiwei 2016. Mercury redox chemistry in waters of the eastern Asian seas: from polluted coast to clean open ocean. *Environmental Science & Technology*, 50, 2371-2380
- Cole, Amanda, Steffen, Alexandra, Eckley, Chris, Narayan, Julie, Pilote, Martin, Tordon, Rob, Graydon, Jennifer, St. Louis, Vincent, Xu, Xiaohong & Branfireun, Brian 2014. A Survey of Mercury in Air and Precipitation across Canada: Patterns and Trends. *Atmosphere*, 5, 635-668.10.3390/atmos5030635

- Cook, Kellie. 2017. *Comparative Analysis of Reactive Mercury Measurement Methodology and Environmental Correlates in Australia*. Masters of Research Thesis, Macquarie University.
- Corbitt, E. S., Jacob, D. J., Holmes, C. D., Streets, D. G. & Sunderland, E. M. 2011. Global source-receptor relationships for mercury deposition under present-day and 2050 emissions scenarios. *Environ Sci Technol*, 45, 10477-84.10.1021/es202496y
- Dedik, AN, Hoffmann, P & Ensling, J 1992. Chemical characterization of iron in atmospheric aerosols. *Atmospheric Environment. Part A. General Topics*, 26, 2545-2548
- Engle, Mark A, Tate, Michael T, Krabbenhoft, David P, Schauer, James J, Kolker, Allan, Shanley, James B & Bothner, Michael H 2010a. Comparison of atmospheric mercury speciation and deposition at nine sites across central and eastern North America. *Journal of Geophysical Research: Atmospheres*, 115
- Engle, Mark A., Tate, Michael T., Krabbenhoft, David P., Schauer, James J., Kolker, Allan, Shanley, James B. & Bothner, Michael H. 2010b. Comparison of atmospheric mercury speciation and deposition at nine sites across central and eastern North America. *Journal of Geophysical Research*, 115.10.1029/2010jd014064
- Friedli, H. R., Radke, L. F., Prescott, R., Hobbs, P. V. & Sinha, P. 2003. Mercury emissions from the August 2001 wildfires in Washington State and an agricultural waste fire in Oregon and atmospheric mercury budget estimates. *Global Biogeochemical Cycles*, 17, n/a-n/a.10.1029/2002gb001972
- Friedli, Hans R, Radke, Lawrence F & Lu, Julia Y 2001. Mercury in smoke from biomass fires. *Geophysical Research Letters*, 28, 3223-3226
- Fu, X. W., Zhang, H., Lin, C. J., Feng, X. B., Zhou, L. X. & Fang, S. X. 2015. Correlation slopes of GEM / CO, GEM / CO₂, and GEM / CH₄ and estimated mercury emissions in China, South Asia, the Indochinese Peninsula, and Central Asia derived from observations in northwestern and southwestern China. *Atmospheric Chemistry and Physics*, 15, 1013-1028.10.5194/acp-15-1013-2015
- Gratz, Lynne E, Keeler, Gerald J, Morishita, Masako, Barres, James A & Dvonch, J Timothy 2013. Assessing the emission sources of atmospheric mercury in wet deposition across Illinois. *Science of The Total Environment*, 448, 120-131
- Gustin, M. S., Amos, H. M., Huang, J., Miller, M. B. & Heidecorn, K. 2015. Measuring and modeling mercury in the atmosphere: a critical review. *Atmospheric Chemistry and Physics*, 15, 5697-5713.10.5194/acp-15-5697-2015
- Haikerwal, A., Reisen, F., Sim, M. R., Abramson, M. J., Meyer, C. P., Johnston, F. H. & Dennekamp, M. 2015. Impact of smoke from prescribed burning: Is it a public health concern? *J Air Waste Manag Assoc*, 65, 592-8.10.1080/10962247.2015.1032445
- Han, Young-Ji, Holsen, Thomas M., Lai, Soon-Onn, Hopke, Philip K., Yi, Seung-Muk, Liu, Wei, Pagano, James, Falanga, Lauren, Milligan, Michael & Andolina, Chris 2004. Atmospheric gaseous mercury concentrations in New York State: relationships with meteorological data and other pollutants. *Atmospheric Environment*, 38, 6431-6446.10.1016/j.atmosenv.2004.07.031
- Holland, Frank, Hofzumahaus, Andreas, Schäfer, Jürgen, Kraus, Alexander & Pätz, Hans-Werner 2003. Measurements of OH and HO₂ radical concentrations and photolysis frequencies during BERLIOZ. *Journal of Geophysical Research: Atmospheres*, 108, PHO 2-1-PHO 2-23

- Holmes, C. D., Jacob, D. J., Corbitt, E. S., Mao, J., Yang, X., Talbot, R. & Slemr, F. 2010. Global atmospheric model for mercury including oxidation by bromine atoms. *Atmospheric Chemistry and Physics*, 10, 12037-12057.10.5194/acp-10-12037-2010
- Holmes, Christopher D, Jacob, Daniel J & Yang, Xin 2006. Global lifetime of elemental mercury against oxidation by atomic bromine in the free troposphere. *Geophysical Research Letters*, 33
- Horowitz, H. M., Jacob, D. J., Amos, H. M., Streets, D. G. & Sunderland, E. M. 2014. Historical Mercury releases from commercial products: global environmental implications. *Environ Sci Technol*, 48, 10242-50.10.1021/es501337j
- Horowitz, Hannah M., Jacob, Daniel J., Zhang, Yanxu, Dibble, Theodore S., Slemr, Franz, Amos, Helen M., Schmidt, Johan A., Corbitt, Elizabeth S., Marais, Eloïse A. & Sunderland, Elsie M. 2017. A new mechanism for atmospheric mercury redox chemistry: implications for the global mercury budget. *Atmospheric Chemistry and Physics*, 17, 6353-6371.10.5194/acp-17-6353-2017
- Howard, D. 2017. *Aspects of the Biogeochemical Cycling of Mercury in Australia and the Southern Hemisphere*. PhD, Macquarie University.
- Howard, Dean, Nelson, Peter F., Edwards, Grant C., Morrison, Anthony L., Fisher, Jenny A., Ward, Jason, Harnwell, James, van der Schoot, Marcel, Atkinson, Brad, Chambers, Scott D., Griffiths, Alan D., Werczynski, Sylvester & Williams, Alastair G. 2017. Atmospheric mercury in the southern hemisphere tropics: seasonal and diurnal variations and influence of inter-hemispheric transport. *Atmospheric Chemistry and Physics Discussions*, 1-20.10.5194/acp-2017-307
- Jaffe, Dan & Strode, Sarah 2008. Sources, fate and transport of atmospheric mercury from Asia. *Environmental Chemistry*, 5, 121.10.1071/en08010
- Jiang, N., Betts, A. & Riley, M. 2016. Summarising climate and air quality (ozone) data on self-organising maps: a Sydney case study. *Environ Monit Assess*, 188, 103.10.1007/s10661-016-5113-x
- Jiang, Ningbo, Dirks, Kim N & Luo, Kehui 2014. Effects of local, synoptic and large-scale climate conditions on daily nitrogen dioxide concentrations in Auckland, New Zealand. *International Journal of Climatology*, 34, 1883-1897
- Jiang, Ningbo, Scorgie, Yvonne, Hart, Melissa, Riley, Matthew L., Crawford, Jagoda, Beggs, Paul J., Edwards, Grant C., Chang, Lisa, Salter, David & Virgilio, Giovanni Di 2017. Visualising the relationships between synoptic circulation type and air quality in Sydney, a subtropical coastal-basin environment. *International Journal of Climatology*, 37, 1211-1228.10.1002/joc.4770
- Jiskra, Martin, Sonke, Jeroen E., Obrist, Daniel, Bieser, Johannes, Ebinghaus, Ralf, Myhre, Cathrine Lund, Pfaffhuber, Katrine Aspmo, Wängberg, Ingvar, Kyllönen, Katriina, Worthy, Doug, Martin, Lynwill G., Labuschagne, Casper, Mkololo, Thumeka, Ramonet, Michel, Magand, Olivier & Dommergue, Aurélien 2018. A vegetation control on seasonal variations in global atmospheric mercury concentrations. *Nature Geoscience*, 11, 244-250.10.1038/s41561-018-0078-8
- Karthik, R., Paneerselvam, A., Ganguly, D., Hariharan, G., Srinivasalu, S., Purvaja, R. & Ramesh, R. 2017. Temporal variability of atmospheric Total Gaseous Mercury and its correlation with meteorological parameters at a high-altitude station of the South India. *Atmospheric Pollution Research*, 8, 164-173.10.1016/j.apr.2016.08.010

- Lan, X., Talbot, R., Castro, M., Perry, K. & Luke, W. 2012. Seasonal and diurnal variations of atmospheric mercury across the US determined from AMNet monitoring data. *Atmospheric Chemistry and Physics*, 12, 10569-10582.10.5194/acp-12-10569-2012
- Li, Zheng, Xia, Chonghuan, Wang, Xinming, Xiang, Yunrong & Xie, Zhouqing 2011. Total gaseous mercury in Pearl River Delta region, China during 2008 winter period. *Atmospheric Environment*, 45, 834-838
- Lin, Che-jen & Pehkonen, Simo O 1997. Aqueous free radical chemistry of mercury in the presence of iron oxides and ambient aerosol. *Atmospheric Environment*, 31, 4125-4137
- Lindberg, SE and & Stratton, WJ 1998. Atmospheric mercury speciation: concentrations and behavior of reactive gaseous mercury in ambient air. *Environmental Science & Technology*, 32, 49-57
- Lindberg, Steve, Bullock, Russell, Ebinghaus, Ralf, Engstrom, Daniel, Feng, Xinbin, Fitzgerald, William, Pirrone, Nicola, Prestbo, Eric & Seigneur, Christian 2007. A synthesis of progress and uncertainties in attributing the sources of mercury in deposition. *AMBIO: a Journal of the Human Environment*, 36, 19-34
- Liu, Yan, Xu, Zhenghe & Kuznicki, Steven M. 2010. Development of a Novel Mercury Cartridge for Mercury Analysis†. *Energy & Fuels*, 24, 10-17.10.1021/ef900501p
- Lyman, Seth N. & Gustin, Mae Sexauer 2008. Speciation of atmospheric mercury at two sites in northern Nevada, USA. *Atmospheric Environment*, 42, 927-939.10.1016/j.atmosenv.2007.10.012
- Lynam, Mary M & Keeler, Gerald J 2005. Artifacts associated with the measurement of particulate mercury in an urban environment: The influence of elevated ozone concentrations. *Atmospheric Environment*, 39, 3081-3088
- Malcolm, Elizabeth G., Keeler, Gerald J. & Landis, Matthew S. 2003. The effects of the coastal environment on the atmospheric mercury cycle. *Journal of Geophysical Research*, 108.10.1029/2002jd003084
- Mao, H. , Talbot, R. W. , Sigler, J. M. , Sive, B. C. & Hegarty, J. D. 2008. Seasonal and diurnal variations of Hg over New England. *Atmospheric Chemistry and Physics*, 8, 1403-1421.<hal-00296482>
- Mao, H. & Talbot, R. 2012. Speciated mercury at marine, coastal, and inland sites in New England – Part 1: Temporal variability. *Atmospheric Chemistry and Physics*, 12, 5099-5112.10.5194/acp-12-5099-2012
- Mao, H., Talbot, R., Hegarty, J. & Koerner, J. 2012. Speciated mercury at marine, coastal, and inland sites in New England – Part 2: Relationships with atmospheric physical parameters. *Atmospheric Chemistry and Physics*, 12, 4181-4206.10.5194/acp-12-4181-2012
- Mao, Huiting, Cheng, Irene & Zhang, Leiming 2016a. Current understanding of the driving mechanisms for spatiotemporal variations of atmospheric speciated mercury: a review. *Atmospheric Chemistry and Physics*, 16, 12897-12924.10.5194/acp-16-12897-2016
- Mao, Huiting, Cheng, Irene & Zhang, Leiming 2016b. Current understanding of the driving mechanisms for spatiotemporal variations of atmospheric speciated mercury: a review. *Atmospheric Chemistry and Physics*, 16, 12897-12924.10.5194/acp-16-12897-2016

- Mason, Robert P & Sheu, G-R 2002. Role of the ocean in the global mercury cycle. *Global Biogeochemical Cycles*, 16, 40-1-40-14
- Miller, Matthieu B 2018. *Concentrations of atmospheric reactive mercury in Australia and emissions of reactive mercury from contaminated mine materials using cation exchange membranes*. PhD Thesis, Macquarie University.
- Nguyen, Duc Luong, Kim, Jin Young, Shim, Shang-Gyoo & Zhang, Xiao-Shan 2011. Ground and shipboard measurements of atmospheric gaseous elemental mercury over the Yellow Sea region during 2007–2008. *Atmospheric Environment*, 45, 253-260
- Obrist, D., Kirk, J. L., Zhang, Lei, Sunderland, E. M., Jiskra, Martin & Selin, N. 2018. A review of global environmental mercury processes in response to human and natural perturbations: Changes of emissions, climate, and land use. *Ambio*.10.1007/s13280-017-1004-9
- Paton-Walsh, C., Smith, T. E. L., Young, E. L., Griffith, D. W. T. & Guérette, É A. 2014. New emission factors for Australian vegetation fires measured using open-path Fourier transform infrared spectroscopy – Part 1: Methods and Australian temperate forest fires. *Atmospheric Chemistry and Physics*, 14, 11313-11333.10.5194/acp-14-11313-2014
- Poissant, Laurier, Pilote, Martin, Beauvais, Conrad, Constant, Philippe & Zhang, Hong H 2005. A year of continuous measurements of three atmospheric mercury species (GEM, RGM and Hgp) in southern Quebec, Canada. *Atmospheric Environment*, 39, 1275-1287
- Ren, Xinrong, Luke, Winston T., Kelley, Paul, Cohen, Mark D., Artz, Richard, Olson, Mark L., Schmeltz, David, Puchalski, Melissa, Goldberg, Daniel L., Ring, Allison, Mazzuca, Gina M., Cummings, Kristin A., Wojdan, Lisa, Preaux, Sandra & Stehr, Jeff W. 2016. Atmospheric mercury measurements at a suburban site in the Mid-Atlantic United States: Inter-annual, seasonal and diurnal variations and source-receptor relationships. *Atmospheric Environment*, 146, 141-152.10.1016/j.atmosenv.2016.08.028
- Schroeder, W. & Munthe, J. 1998. Atmospheric Mercury - An Overview. *Atmospheric Environment*, 32, 809-822
- Shahgedanova, M, Burt, TP & Davies, TD 1998. Synoptic climatology of air pollution in Moscow. *Theoretical and Applied Climatology*, 61, 85-102
- Si, Lin & Ariya, Parisa 2018. Recent Advances in Atmospheric Chemistry of Mercury. *Atmosphere*, 9, 76.10.3390/atmos9020076
- Sigler, JM, Mao, H & Talbot, R 2009. Gaseous elemental and reactive mercury in Southern New Hampshire. *Atmospheric Chemistry and Physics*, 9, 1929-1942
- Slemr, F., Angot, H., Dommergue, A., Magand, O., Barret, M., Weigelt, A., Ebinghaus, R., Brunke, E. G., Pfaffhuber, K. A., Edwards, G., Howard, D., Powell, J., Keywood, M. & Wang, F. 2015. Comparison of mercury concentrations measured at several sites in the Southern Hemisphere. *Atmospheric Chemistry and Physics*, 15, 3125-3133.10.5194/acp-15-3125-2015
- Soerensen, Anne L., Jacob, Daniel J., Streets, David G., Witt, Melanie L. I., Ebinghaus, Ralf, Mason, Robert P., Andersson, Maria & Sunderland, Elsie M. 2012. Multi-decadal decline of mercury in the North Atlantic atmosphere explained by changing subsurface seawater concentrations. *Geophysical Research Letters*, 39, n/a-n/a.10.1029/2012gl053736

- Song, S., Selin, N. E., Soerensen, A. L., Angot, H., Artz, R., Brooks, S., Brunke, E. G., Conley, G., Dommergue, A., Ebinghaus, R., Holsen, T. M., Jaffe, D. A., Kang, S., Kelley, P., Luke, W. T., Magand, O., Marumoto, K., Pfaffhuber, K. A., Ren, X., Sheu, G. R., Slemr, F., Warneke, T., Weigelt, A., Weiss-Penzias, P., Wip, D. C. & Zhang, Q. 2015. Top-down constraints on atmospheric mercury emissions and implications for global biogeochemical cycling. *Atmospheric Chemistry and Physics*, 15, 7103-7125.10.5194/acp-15-7103-2015
- Sprovieri, Francesca, Pirrone, Nicola, Bencardino, Mariantonia, amp, apos, Amore, Francesco, Carbone, Francesco, Cinnirella, Sergio, Mannarino, Valentino, Landis, Matthew, Ebinghaus, Ralf, Weigelt, Andreas, Brunke, Ernst-Günther, Labuschagne, Casper, Martin, Lynwill, Munthe, John, Wängberg, Ingvar, Artaxo, Paulo, Morais, Fernando, Barbosa, Henrique de Melo Jorge, Brito, Joel, Cairns, Warren, Barbante, Carlo, Diéguez, María del Carmen, Garcia, Patricia Elizabeth, Dommergue, Aurélien, Angot, Helene, Magand, Olivier, Skov, Henrik, Horvat, Milena, Kotnik, Jože, Read, Katie Alana, Neves, Luis Mendes, Gawlik, Bernd Manfred, Sena, Fabrizio, Mashyanov, Nikolay, Obolkin, Vladimir, Wip, Dennis, Feng, Xin Bin, Zhang, Hui, Fu, Xuewu, Ramachandran, Ramesh, Cossa, Daniel, Knoery, Joël, Maruszczak, Nicolas, Nerentorp, Michelle & Norstrom, Claus 2016. Atmospheric mercury concentrations observed at ground-based monitoring sites globally distributed in the framework of the GMOS network. *Atmospheric Chemistry and Physics*, 16, 11915-11935.10.5194/acp-16-11915-2016
- Streets, D. G., Horowitz, H. M., Jacob, D. J., Lu, Z., Levin, L., Ter Schure, A. F. H. & Sunderland, E. M. 2017. Total Mercury Released to the Environment by Human Activities. *Environ Sci Technol*, 51, 5969-5977.10.1021/acs.est.7b00451
- Strode, Sarah A., Jaeglé, Lyatt, Selin, Noelle E., Jacob, Daniel J., Park, Rokjin J., Yantosca, Robert M., Mason, Robert P. & Slemr, Franz 2007. Air-sea exchange in the global mercury cycle. *Global Biogeochemical Cycles*, 21, n/a-n/a.10.1029/2006gb002766
- Subir, Mahamud, Ariya, Parisa A & Dastoor, Ashu P 2012. A review of the sources of uncertainties in atmospheric mercury modeling II. Mercury surface and heterogeneous chemistry—A missing link. *Atmospheric Environment*, 46, 1-10
- Travnikov, Oleg, Angot, Hélène, Artaxo, Paulo, Bencardino, Mariantonia, Bieser, Johannes, amp, apos, Amore, Francesco, Dastoor, Ashu, De Simone, Francesco, Diéguez, María del Carmen, Dommergue, Aurélien, Ebinghaus, Ralf, Feng, Xin Bin, Gencarelli, Christian N., Hedgecock, Ian M., Magand, Olivier, Martin, Lynwill, Matthias, Volker, Mashyanov, Nikolay, Pirrone, Nicola, Ramachandran, Ramesh, Read, Katie Alana, Ryjkov, Andrei, Selin, Noelle E., Sena, Fabrizio, Song, Shaojie, Sprovieri, Francesca, Wip, Dennis, Wängberg, Ingvar & Yang, Xin 2017. Multi-model study of mercury dispersion in the atmosphere: atmospheric processes and model evaluation. *Atmospheric Chemistry and Physics*, 17, 5271-5295.10.5194/acp-17-5271-2017
- Valente, Ralph J, Shea, Catherine, Humes, K Lynn & Tanner, Roger L 2007. Atmospheric mercury in the Great Smoky Mountains compared to regional and global levels. *Atmospheric Environment*, 41, 1861-1873
- Weiss-Penzias, P., Amos, H. M., Selin, N. E., Gustin, M. S., Jaffe, D. A., Obrist, D., Sheu, G. R. & Giang, A. 2015. Use of a global model to understand speciated atmospheric mercury observations at five high-elevation sites. *Atmospheric Chemistry and Physics*, 15, 1161-1173.10.5194/acp-15-1161-2015

- Xu, L., Chen, J., Yang, L., Niu, Z., Tong, L., Yin, L. & Chen, Y. 2015. Characteristics and sources of atmospheric mercury speciation in a coastal city, Xiamen, China. *Chemosphere*, 119, 530-539.10.1016/j.chemosphere.2014.07.024
- Zhang, Hong & Lindberg, Steve E 2001. Sunlight and iron (III)-induced photochemical production of dissolved gaseous mercury in freshwater. *Environmental Science & Technology*, 35, 928-935
- Zhang, Wei, Wei, Wen, Hu, Dan, Zhu, Yan & Wang, Xuejun 2013. Emission of Speciated Mercury from Residential Biomass Fuel Combustion in China. *Energy & Fuels*, 27, 6792-6800.10.1021/ef401564r

Chapter 6

Investigation of mercury emissions from burning of Australian eucalypt forest surface fuels using a combustion wind tunnel and field observations

6.1 Preface

Chapter 6 explores Hg release from biomass burning, which has been found by previous studies to be the second largest natural source of Hg in Australia. Volatilisation and emission of mercury from vegetation, litter and soil during burning represents a significant return pathway for previously-deposited atmospheric mercury. No modelling efforts to date have utilised local mercury emission factors (mass of emitted mercury per mass of dry fuel) or local mercury emission ratios (ratio of emitted mercury to another emitted species, typically carbon monoxide), which are dependent on plant species-specific uptake of atmospheric mercury as well as fire characteristics. In response to the general lack of Australian-derived emission ratios or emission factors this paper reports on and compares two different studies of mercury release from the burning of Australian native forest surface fuels. Experimental burns of dry sclerophyll surface fuels took place in a combustion wind tunnel designed for the study of combustion of vegetation fuels. Results from this laboratory-scale study are then compared with observations of biomass burning plumes from the Cape Grim Baseline Air Pollution

Station in Tasmania. The analysis undertaken in this chapter adds to the growing knowledge surrounding mercury in vegetation and its release during biomass burning, and contributes to the thesis by constraining uncertainty regarding natural mercury cycling over the Australian continent.

Author contributions:

The paper presented in this chapter has been published in the journal: *Atmospheric Environment*. Published formatting had been preserved for inclusion in this thesis.

Study design was by the co-authors from CSIRO, University of Wollongong and Dr Grant Edwards as part of a larger project. Wind tunnel measurements and Cape Grim field measurements were performed by Dr Dean Howard and Dr Grant Edwards. Particulate bound mercury, soil and vegetation analysis was undertaken by me. I also performed the initial emission ratio and emission factor calculations. The majority of data analysis was undertaken by Dr Dean Howard who also did the majority of the manuscript preparation with some contributions by me. Intellectual contributions were made by myself and all other contributions throughout the publication process.

Dean Howard: 70%, Katrina MacSween 15%, Grant C. Edwards 10%, Maximilien Desservettaz 0.5%, Elise-Andrée Guérette 0.5%, Clare Paton-Walsh 0.5%, Nicholas C. Surawski 0.5%, Andrew L. Sullivan 0.5%, Christopher Weston 0.5%, Liubov Volkova 0.5%, Jennifer Powell 0.5%, Melita D. Keywood 0.5%, Fabienne Reisen 0.5%, C.P. (Mick) Meyer 0.5%



Contents lists available at ScienceDirect

Atmospheric Environment

journal homepage: www.elsevier.com/locate/atmosenv

Investigation of mercury emissions from burning of Australian eucalypt forest surface fuels using a combustion wind tunnel and field observations

Dean Howard^{a,b,*}, Katrina Macsween^a, Grant C. Edwards^a, Maximilien Desservettaz^c,
Elise-Andrée Guérette^c, Clare Paton-Walsh^c, Nicholas C. Surawski^{d,e}, Andrew L. Sullivan^c,
Christopher Weston^f, Liubov Volkova^f, Jennifer Powell^g, Melita D. Keywood^g, Fabienne Reisen^g,
C.P. (Mick) Meyer^g

^a Department of Environmental Sciences, Macquarie University, North Ryde, NSW, Australia

^b Environmental, Earth and Atmospheric Sciences, University of Massachusetts Lowell, Lowell, MA, USA

^c Centre for Atmospheric Chemistry, University of Wollongong, Wollongong, NSW, Australia

^d School of Civil and Environmental Engineering, University of Technology Sydney, Ultimo, NSW, Australia

^e CSIRO Land and Water, Canberra, ACT, Australia

^f School of Ecosystem and Forest Sciences, The University of Melbourne, Creswick, VIC, Australia

^g CSIRO Oceans and Atmosphere, Aspendale, VIC, Australia

ARTICLE INFO

Keywords:

gaseous elemental mercury
Biogeochemical cycling
Emissions
Biomass burning
Australia

ABSTRACT

Environmental cycling of the toxic metal mercury (Hg) is ubiquitous, and still not completely understood. Volatilisation and emission of mercury from vegetation, litter and soil during burning represents a significant return pathway for previously-deposited atmospheric mercury. Rates of such emission vary widely across ecosystems as they are dependent on species-specific uptake of atmospheric mercury as well as fire return frequencies. Wildfire burning in Australia is currently thought to contribute between 1 and 5% of the global total of mercury emissions, yet no modelling efforts to date have utilised local mercury emission factors (mass of emitted mercury per mass of dry fuel) or local mercury emission ratios (ratio of emitted mercury to another emitted species, typically carbon monoxide). Here we present laboratory and field investigations into mercury emission from burning of surface fuels in dry sclerophyll forests, native to the temperate south-eastern region of Australia. From laboratory data we found that fire behaviour — in particular combustion phase — has a large influence on mercury emission and hence emission ratios. Further, emission of mercury was predominantly in gaseous form with particulate-bound mercury representing < 1% of total mercury emission. Importantly, emission factors and emission ratios with respect to carbon monoxide and carbon dioxide, from both laboratory and field data all show that gaseous mercury emission from biomass burning in Australian dry sclerophyll forests is currently overestimated by around 60%. Based on these results, we recommend a mercury emission factor of $28.7 \pm 8.1 \mu\text{g Hg kg}^{-1}$ dry fuel, and emission ratio of gaseous elemental mercury relative to carbon monoxide of $0.58 \pm 0.01 \times 10^{-7}$, for estimation of mercury release from the combustion of Australian dry sclerophyll litter.

1. Introduction

The global nature of mercury (Hg) pollution has long been recognised (Driscoll et al., 2013). With natural sinks, sources and cycles, the unique physicochemical properties of this toxic metal allow for constant transfer between biological, terrestrial, aquatic and atmospheric reservoirs, making it ubiquitous throughout the environment (Fitzgerald et al., 1998; Selin, 2009; Mason et al., 2012; Krabbenhoft and Sunderland, 2013). Increases in mercury emission sources due to

human activities have perturbed this natural cycle in a manner that has become a threat to human and ecosystem health (Streets et al., 2011, 2017; Amos et al., 2013). This threat is globally recognised in the Minamata Convention on Mercury (Kessler, 2013), aimed at reducing anthropogenic emissions of mercury to the environment. Article 19 of the convention addresses the need to understand mercury's complex natural cycling by calling for parties to the convention to, where possible, increase research and extend current monitoring efforts.

In the atmosphere, mercury exists largely in the form of gaseous

* Corresponding author. Department of Environmental Sciences, Macquarie University, North Ryde, NSW, Australia.
E-mail address: dean.howard@colorado.edu (D. Howard).

<https://doi.org/10.1016/j.atmosenv.2018.12.015>

Received 13 June 2018; Received in revised form 21 November 2018; Accepted 3 December 2018

Available online 22 December 2018

1352-2310/ © 2018 Published by Elsevier Ltd.

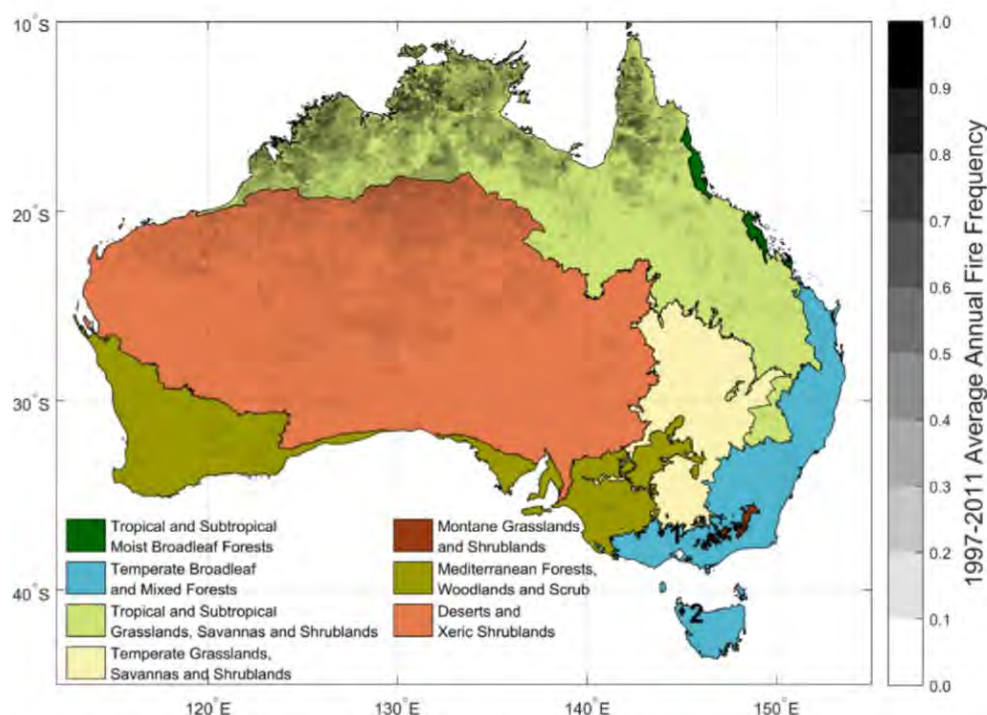


Fig. 1. Map of Australian biomes as defined by Olson and Dinerstein (Olson and Dinerstein, 2002), along with average annual fire frequency as determined by Maier (Maier, 2016). Based on raster data at 1 km² resolution. Due to the sampling algorithm, generally only fires of size 4 km² or larger are counted. Numbers 1 and 2 show locations of fuel sampling sites.

elemental mercury (GEM), with the operationally-defined gaseous oxidised mercury (GOM) and particulate bound mercury (PBM) forms generally thought to comprise less than 10% of tropospheric atmospheric concentrations (Pirrone et al., 2010). The long atmospheric lifetime of GEM [estimated at between 5 and 12 months (Holmes et al., 2010; Horowitz et al., 2017; Lindberg et al., 2007)] means transport of mercury can take place through the atmosphere — but also in water-courses and the ocean — to regions far-removed from their sources. From the atmosphere, mercury is deposited to terrestrial surfaces and waterways, taken up by vegetation, and re-emitted in a complex natural cycle that is still not completely understood (Smith-Downey et al., 2010; Amos et al., 2013; Agnan et al., 2016). Atmospheric mercury may be taken into vegetation during photosynthesis (Rea et al., 2001) or deposited via dry or wet deposition processes onto vegetated surfaces, whereby it can be incorporated into the cell membrane through foliar uptake (Mason et al., 1995; Stamenkovic and Gustin, 2009; Hintelmann et al., 2002). Throughfall, litterfall and surface dry/wet deposition processes deliver atmospheric mercury to the underlying surface litter, whereby leaf decomposition and further atmospheric deposition enhance soil mercury levels due to binding of mercury to organic matter within the soil (Wright et al., 2016; Hartman et al., 2009). Vegetation type, coverage and growth rates, and atmospheric mercury concentrations all affect the rate at which mercury is stored within these components (Johnson and Lindberg, 1995; Erickson and Gustin, 2004; Cobbett and Van Heyst, 2007).

Biomass burning releases mercury from these stores back into the atmosphere through volatilisation of mercury within biomass during combustion and through thermal desorption of mercury bound within the soil matrix (Melendez-Perez et al., 2014). Herein we limit the definition of biomass burning to free-burning vegetation fires (both intentionally and accidentally ignited) and exclude burning of biomass for industrial/cultural purposes (e.g. wood burners and stoves). The release of mercury from biomass burning is an important yet complex and poorly understood component of the global mercury cycle as it can

lead to redistribution of mercury to sensitive ecosystems where methylation may occur, or it can result in direct human exposure to mercury through inhalation of biomass burning plumes (Simone et al., 2015). Mercury is often completely volatilised from combusted biomass (Friedli et al., 2003) and this emitted mercury is largely in the form of GEM (Friedli et al., 2001, 2003), however Obrist et al. (2007) showed that increasing PBM levels are associated with increasing fuel moisture and decreasing fire intensity. The lower atmospheric lifetime of PBM leads to changing mercury deposition patterns in response to emission partitioning (Simone et al., 2016). The extent to which thermal desorption takes place in the soil is related to the intensity of the fire, as low intensity, slow-moving fires may heat the soil to higher temperatures than faster moving, higher-intensity fires (Webster et al., 2016). As such, release of mercury is not only dependent on the loading of mercury within the fuels but also on fire behaviour.

Ecosystem-scale estimates of mercury release from biomass burning are typically achieved by applying a mixture of empirical and remotely-sensed data. Burned areas are often derived from satellite data products, from which emission of mercury (or other chemical species) can be estimated by applying an empirically-derived emission factor (ratio of emitted species per mass of dry fuel), or an emission ratio with reference to another chemical species along with its emission factor. These approaches are outlined generally below (Aalde et al., 2006):

$$E_x = A \cdot L \cdot BE \cdot EF_x \quad (1)$$

$$E_x = A \cdot L \cdot BE \cdot EF_y \cdot ER_{x/y} \quad (2)$$

where E_x is the emitted mass of species x , A the area burned, L the fuel loading in mass per area, BE the burning efficiency and EF_x the emission factor for species x . Where emission factors for species x are poorly constrained or not known, these can be determined by using an emission ratio $ER_{x/y}$ and applying this to the known emission factor for species y . Emission ratios for mercury are generally derived from ground- or aerial-based measurements of smoke plumes and are

typically reported with respect to carbon monoxide (CO), although ratios with carbon dioxide (CO₂) have been presented by Brunke et al. (2001). The use of emission ratios is advantageous as, due to turbulent mixing in the plume, it provides an average enhancement across the horizontal and vertical extent of the fire. Emission factors are instead based on fuel mercury concentrations and empirically-derived estimates of release during combustion. These provide the most direct estimate of mercury release from specific vegetation types and from soils when the amount of biomass burned is known, yet require significant sampling to obtain data suitable at an ecosystem scale (Andreae and Merlet, 2001).

Australia is a particularly fire-prone continent, and global-scale models of mercury emission from biomass burning estimate that emissions over Australia represent between 1 and 5% of the global total (Friedli et al., 2009; Simone et al., 2015). Based on the National Oceanic and Atmospheric Administration's Advanced Very High Resolution Radiometer (NOAA-AVHRR) satellite data, an average of 41 million ha (5% total land mass) burned annually in the years 1997–2011 [Fig. 1 (Maier, 2016)]. Home to 32 major vegetation groups (Australian Government Department of the Environment and Energy (DEE), 2016) and spanning a broad range of climates, Australia's ecosystems are subject to varying degrees of fire frequency and intensity. Tropical savannah in northern Australia may undergo burning every 1–2 years (Meyer et al., 2012), whilst temperate forests in south-eastern Australia typically experience burning every 15 + years (Gill et al., 1981), which can result in greater uptake of mercury over a longer growing period. Simplification of vegetation types across continental scales is necessary in modelling biomass burning mercury emissions, a global example of which is the terrestrial ecoregion [(Olson and Dinerstein, 2002), (Bailey, 1995), see Fig. 1]. To date, the most extensive investigation into vegetation mercury content across Australia was performed by Packham et al. (2009) (see Table 1), yet these have not been used in any subsequent mercury modelling efforts. Modelling estimates of mercury emissions from biomass burning in Australia have instead so far only been obtained using empirically-derived emission factors or emission ratios from studies undertaken in the Northern Hemisphere (Friedli et al., 2003, 2009). The resulting estimates of annual release over Australia are currently poorly constrained, spanning a range between 7 Mg Hg a⁻¹ and 129 Mg Hg a⁻¹ (Friedli et al., 2009; Nelson et al., 2009, 2012; Packham et al., 2009; Cope et al., 2009; Simone et al., 2015).

In response to the general lack of knowledge surrounding mercury in Australian vegetation — and the complete lack of Australian-derived emission ratios or emission factors in Australian mercury emission modelling — this paper reports on and compares two different studies of mercury release from the burning of Australian native forest surface fuels. In this paper we limit our analysis to the eucalypt-dominated dry sclerophyll forests, the most widespread forest type in south-eastern

Australia (Montreal Process Implementation Group for Australia and National Forest Inventory Steering Committee, 2013). Native to Australia, eucalypts have been cultivated globally and can now be found on all inhabited continents. Experimental burns of dry sclerophyll surface fuels took place in a combustion wind tunnel designed for the study of combustion of vegetation fuels (Sullivan et al., 2013), which provided the unique advantage that the influence of fire propagation on emissions could be investigated. Results from this laboratory-scale study are then compared with observations of biomass burning plumes from the Cape Grim Baseline Air Pollution Station (CGBAPS) in Tasmania. These data add to the growing knowledge surrounding mercury in vegetation and its release during biomass burning, and will contribute to constraining uncertainty regarding natural mercury cycling over the Australian continent and the Southern Hemisphere in general.

2. Methods

2.1. Fuel collection and analysis

Surface fuels used in the experimental burns were collected from a dry sclerophyll forest in Pumphouse, Central Victoria (Site 1, Fig. 1). This forest is classified as Shrubby Foothill, dominated by Broad-leaved Peppermint (*Eucalyptus dives*), Australian Oak (*Eucalyptus obliqua*) and Narrow-leaved Peppermint (*Eucalyptus radiata*). Fine fuels (herein leaves, bark and twigs with diameter < 6 mm) and coarse fuels (woody debris with diameter between 6 and 50 mm) were collected separately in late January 2014 and immediately transported to the CSIRO laboratory in Canberra where sorting and sieving took place. Fine fuels were sieved to remove any remaining components > 6 mm and to remove inorganic material (such as stones and rocks) and decomposed fuel elements. Representative subsamples were collected, sorted and weighed after oven drying at 105 °C for 24 h to determine relative fractions of leaves, bark and twigs on a gravimetric basis. Coarse fuels were sorted into components with diameters 6–25 mm and 25–50 mm. Prior to each experimental burn, between two and four subsamples (~50–100 g) of fine fuel were collected and weighed to determine experimental fuel moisture content (MC). Subsamples were oven-dried at 105 °C for 24 h and then reweighed, from which fuel moisture content was calculated (Matthews, 2010). For further detail regarding fuel collection see Sullivan et al. (2018).

An additional subsample of each fuel type, along with a sample of ash, was collected from each experimental burn for total mercury (THg) content analysis. These were dried and homogenised, then mercury contents were analysed using a Milestone direct mercury analyser (DMA-80) and US EPA method 7473. The sampling protocol involved triplicate sampling to determine precision, the introduction of blanks to reduce memory effects and liquid standards to determine analytical accuracy. Calibrations were checked using National Institute of

Table 1

Overview of burned area derived from AVHRR 1997–2011 data (Maier, 2016) and mean total mercury concentrations (Packham et al., 2009) reproduced for vegetation and soils, categorised by Australian ecoregions (Olson and Dinerstein, 2002). Parentheses denote number of sample locations.

	Total Area	Area Burned	Vegetation [THg]	Soil [THg]
	Gha	Gha a ⁻¹	µg kg ⁻¹	µg kg ⁻¹
Tropical and Subtropical Moist Broadleaf Forests	2.77	0.03	–	–
Temperate Broadleaf and Mixed Forests	53.48	0.28	80 (3)	47 ^a (1)
Tropical and Subtropical Grasslands and Savannas	188.41	27.37	212 (1)	105 (1)
			9 ^b (1)	9 ^b (1)
Temperate Grasslands, Savannas and Shrublands	48.96	0.06	52 (1)	145 (1)
Montane Grasslands and Shrublands	0.99	0.05	18 ^c (1)	48 ^c (1)
Mediterranean Forests, Woodlands and Scrub	74.08	0.43	213 (2)	90 (1)
Deserts and Xeric Scrubs	321.69	12.74	290 (1)	–

^a Value of 125 µg kg⁻¹ removed, due to possible geogenic source contamination.

^b Values obtained from Howard et al. (2017).

^c Values obtained from Howard and Edwards (2018).

Standards and Technology (NIST) traceable Standard Reference Material (SRM, NIST 1575a and 2709a).

2.2. Experimental burns

Experimental burns were performed at the CSIRO Pyrotron facility, a 25.6 m long stainless-steel wind tunnel with a 2.0×2.0 m cross-sectional area and a 2.0×4.8 m working section designed for investigations into fire behaviour and emissions. Within the working section, fuel beds up to 1.5×4.8 m can be prepared and combusted for details see (Sullivan et al., 2013, 2018; Surawski et al., 2015). An array of 62 thermocouples within the working section record gas temperatures 1–3 cm above the fuel during the experimental burns. Wind speed within the tunnel was set at 1.0 m s^{-1} for all experimental burns. Prior to each experimental burn, fine fuel moisture contents were measured using an A&D MF-50 moisture meter (Chatto and Tolhurst, 1997) and a mass equivalent to a dry fine fuel weight of $1.00 \pm 0.02 \text{ kg m}^{-2}$ was gathered and spread evenly across the working section. Four treatments were applied in this experiment, each with a different load of coarse fuels. These required the addition of 0.0 kg m^{-2} (i.e. control), 0.2 kg m^{-2} , 0.6 kg m^{-2} and 1.2 kg m^{-2} coarse fuels to the 1.0 kg m^{-2} fine fuels. Coarse fuel loads were split evenly between the two size fractions (6–25 mm and 25–50 mm) and distributed evenly across the working section.

The fuel bed was ignited against one edge of the working section using a 1.5 m channel filled with ethanol that was lit with a butane lighter. In addition to investigating changes in coarse fuel load, differing fire behaviour was also investigated by lighting the fuel such that the fire propagated with the wind (heading) or against it (backing). Fuel bed sizes for heading fires were 6.0 m^2 ($1.5 \times 4.0 \text{ m}$). Due to the slower propagation of backing fires, fuel bed sizes were set at 3.0 m^2 ($1.5 \times 2.0 \text{ m}$). In total, 22 experimental burns took place during the experiment. Working section blanks were determined by igniting ethanol spread across the working section, with no appreciable enhancement of mercury recorded.

2.3. Emissions sampling

Emissions from the experimental burns were measured 3.6 m downwind of the working section through $1/4''$ polytetrafluoroethylene (PTFE) tubes supported within stainless steel tubes to a 0.84 m sampling height. Two sampling methods were employed in determining mercury emission concentrations. The first, termed “continuous” sampling, consisted of direct sampling of downwind air by instruments. Sample air was drawn through a $2 \mu\text{m}$ PTFE filter located at the sample inlet. This filter was retained and analysed using a Tekran 2600 and US EPA method 1631 to quantify PBM release. Flow rates through this filter were measured before and after each burn and averaged 4.21 min^{-1} (gas volumes herein are referenced at 1 atm and 0°C). From this sampling stream, CO_2 was measured using a Los Gatos GGA-24r-EP analyser, whilst CO was measured with a Los Gatos 907-0015. GEM was quantified using a Tekran 2537A, drawing at 1 l min^{-1} and sampling continuously every 2.5 min. Previous investigations have shown that the portion of GOM emitted from biomass burning is generally small (Friedli et al., 2003), which is further assumed here. The 2537A was calibrated prior to each burn using an internal mercury permeation source maintained at 50°C . The stability of this permeation source was verified before and after the experiment using manual injections of mercury vapour to within 2%.

The second sampling method, “bag” sampling, employed US EPA method 18 lung sampling, whereby 5 or 101 Tedlar bags were subjected to differential pressure in order to sample air from within the downstream section. Using differential pressure avoids the problem of contamination from the air pump and the advantage of this sampling method over continuous sampling is that the sampling period was able to be shortened to 1 min. After completion of each experimental burn,

air samples were analysed for mercury concentration using the same 2537A used for continuous sampling. CO_2 and CO concentrations were quantified using a Fourier Transform Infrared Spectrometer coupled to a multi-pass optical cell (White cell FTIR). Mole fractions were retrieved from the FTIR spectra using the Multiple Atmospheric Layer Transmission (MALT) model (Griffith, 1996; Griffith et al., 2012). Accuracies of these retrievals were checked using a calibration mixture and were found to be better than 10% for CO and better than 5% for CO_2 over the range of observed values. Tedlar bags were then flushed with N_2 and evacuated by pump in preparation for the next experimental burn.

An open-path FTIR system was deployed at the exhaust outlet of the wind tunnel, approximately 0.5 m downwind of the other sampling locations. This FTIR system is described in detail in Paton-Walsh et al. (2014). Briefly, it consists of a Bomem MB-100 Series FTIR spectrometer (1 cm^{-1} resolution) equipped with a built-in infrared source and fitted with a liquid nitrogen cooled Mercury Cadmium Telluride (MCT) detector and a Meade 12" (305 mm) LX200 telescope. The built-in infrared source modulates the infrared radiation within the spectrometer before it is sent out through the telescope to retro-reflectors that were positioned opposite the cross-section area of the wind tunnel. The radiation is returned through the telescope and the fraction of the radiation that is reflected by the external beam splitter is focused onto the detector. This set-up gave average mole fractions of selected species across the width of the plume with sampling frequency of 20 s.

Emission ratios of GEM to CO_2 and CO ($ER_{\text{GEM}/y}$, where $y = \text{CO}_2$ or CO) were calculated using linear least squares regressions for enhanced GEM concentrations against measured enhancements of CO_2/CO . Uncertainties were quantified as the standard error of the slope. Emission factors for CO_2 and CO were calculated from open-path measurements using Eq. (3) (Ward et al., 1993) and emission factors for GEM ($EF_{\text{GEM}/y}$) were obtained from these by multiplying by observed emission ratios (Eq. (4)). These emission factors for GEM were compared to an emission factor calculated from the loss of mercury mass from the fuel ($EF_{\text{THg}/\text{fuel}}$), using Eq. (5). The modified combustion efficiency (MCE) was calculated using Eq. (6) (Hao and Ward, 1993; Yokelson et al., 1996) to quantitatively describe the relative influence of flaming and smouldering combustion on atmospheric emissions (Desservettaz et al., 2017). The Byram fire line intensity was calculated for each burn by multiplying the lower heating value of the fuel by the fuel consumed and the rate of spread (Byram and Davis, 1959).

$$EF_y = FC \cdot FV \cdot 1000 \cdot \frac{MW_y}{12} \cdot C_y \quad (3)$$

$$EF_{\text{GEM}/y} = ER_{\text{GEM}/y} \cdot \frac{MW_{\text{GEM}}}{MW_y} \cdot EF_y \quad (4)$$

$$EF_{\text{THg}/\text{fuel}} = \sum_f [\text{THg}_f] \cdot F_f - \frac{\sum_r [\text{THg}_r] \cdot L_r}{L} \quad (5)$$

$$\text{MCE} = \frac{\Delta \text{CO}_2}{\Delta \text{CO}_2 + \Delta \text{CO}} \quad (6)$$

Here FC is the fractional carbon content of dry fuel, FV is the fraction of fuel carbon volatilised, MW_{GEM} is the molecular weight of GEM, MW_y the molecular weight of species y , C_y is the percentage of observed emitted carbon species that were in the form species y , $[\text{THg}]_{f,r}$ is the total mercury content of each fuel type $f = \text{leaves/bark/twigs/coarse material}$ or $r = \text{fine/coarse combustion residue}$ and F_f is the fractional mass of fuel type f .

2.4. Biomass burning plumes at CGBAPS

In January and February of 2016, the north-west of Tasmania experienced extensive bushfire burning, with over 140 fires covering > 97,000 ha reported (Gramenz, 2016; Abey, 2016). Throughout this

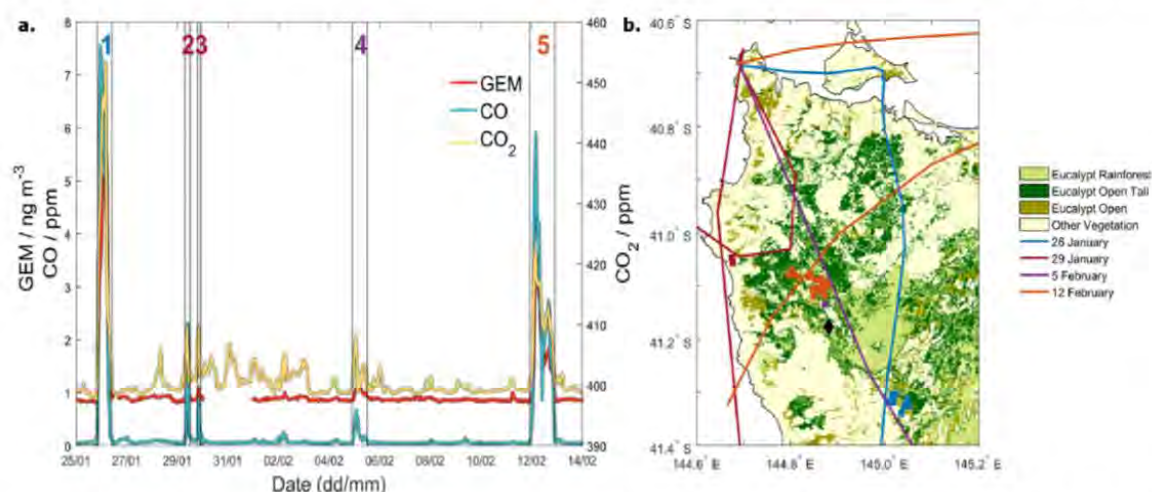


Fig. 2. a. time series of GEM, CO₂ and CO as observed at CGBAPS during 25th January – 14th February 2016. Vertical lines denote the start and end times of identified plume strike events. b. HYSPLIT back trajectories corresponding to identified plume strike events, along with MODIS hot spot data for corresponding days.

Table 2

Total mercury (THg) concentrations in different fuel types. Values are means \pm one standard deviation.

	Site 1	Site 2 (unburned)	Site 2 (burned)
	$\mu\text{g kg}^{-1}$	$\mu\text{g kg}^{-1}$	$\mu\text{g kg}^{-1}$
Leaves	72.9 \pm 10.9	47.8 \pm 3.5	–
Bark	25.0 \pm 11.1	24.5 \pm 4.0	–
Twigs	10.1 \pm 5.4	11.2 \pm 4.1	–
Coarse (6–25 mm)	4.3 \pm 3.8	–	–
Coarse (25–50 mm)	6.1 \pm 8.1	–	–
Fine fuel residue	1.6 \pm 1.6	–	–
Coarse fuel residue	0.3 \pm 0.2	–	–
Soil (0–2 cm)	–	29.4 \pm 17.7	49.3 \pm 29.0
Soil (5–10 cm)	–	25.3 \pm 11.8	45.4 \pm 4.8

period CGBAPS, located on the north-west cape of Tasmania's main island, was intermittently exposed to air masses affected by these fires. Instrumental setups at CGBAPS have been described in detail earlier (Slemr et al., 2015; Lawson et al., 2015); briefly GEM was sampled at this site from a 10 m mast using a Tekran 2537B and CO/CO₂ were sampled from a 70 m mast and quantified using a Picarro G2301.

Fig. 2a shows the time series of these three species during this period. Concentrations for all species were resampled to match the lowest frequency data (1 h⁻¹). Identification of biomass burning plume strike events was achieved using the selection process described by Desservettaz et al. (2017), whereby burning events underwent a first round of selection by identifying enhancements in CO. A second round of selection was employed, ensuring concomitant enhancement of both CO₂ and GEM. The third round of selection described by Desservettaz et al. (2017) (identification of mixed plumes) was not employed. As such, these events may be indicative of emissions from multiple fires. Background concentrations of the three species were calculated as the average taken 2 h before and after the identified event. Emission ratios and MCE were then calculated in the same manner as for the experimental burns.

Air mass back trajectories were computed for plume strike periods using the NOAA Hybrid Single Particle Lagrangian Integrated Trajectory (HYSPLIT) Model (Draxler, 1999; Draxler and Hess, 1998a, 1998b; Stein et al., 2015). Actively burning regions on corresponding days were identified using National Aeronautics and Space Administration (NASA) Moderate Resolution Imaging Spectroradiometer (MODIS) hotspot data. Fig. 2b shows trajectory and hot spot data, along

with selected vegetation community data (Australian Government Department of the Environment and Energy (DEE), 2016). Two vegetation and soil sampling sites within a *Eucalyptus obliqua* rainforest were selected based on these data and accessibility (Site 2, Figs. 1 and 2b). These sites were both within ~ 300 m proximity to a road that served as a fire break during the burning event, with vegetation on one side visibly burned whilst the other side remained intact. Fine surface fuels (fallen leaves, twigs, bark) as well as soils at depths of 0–2 and 5–10 cm were collected. Sample collection took place in May 2017 using trace metal sampling techniques and samples were analysed for total mercury content using the technique described in Section 2.1.

3. Results

3.1. Total mercury in fuels and mercury emission factors

Total mercury concentrations measured in Site 1 fine fuels ranged from 0.38 $\mu\text{g kg}^{-1}$ to 100.14 $\mu\text{g kg}^{-1}$. Split according to fuel type (Table 2), leaves contained the highest concentrations, followed by bark and twigs. Relative mass loading for fine materials was 40.5% (leaves), 7.3% (bark) and 51.7% (twigs), resulting in mean total mercury loads of 32.5 μg , 2.0 μg and 6.0 μg respectively, per kilogram of total fine fuel. Total mercury loads from coarse fuels were significantly smaller ($p < 0.002$, Student's two sample *t*-test) and ranged from 0.8 $\mu\text{g kg}^{-1}$ to 5.0 $\mu\text{g kg}^{-1}$.

Total mercury concentrations in leaves from Site 2 were lower than from Site 1, whilst bark and twigs showed comparable concentrations. Soil total mercury concentrations showed relatively large variability between the unburned and burned sites (mean values at 0–2 cm were 29.4 $\mu\text{g kg}^{-1}$ and 49.3 $\mu\text{g kg}^{-1}$ respectively). Relative concentrations between the upper and lower soils sampled were similar for both sites ($\sim 5 \mu\text{g kg}^{-1}$ higher for soils 0–2 cm from the surface than 5–10 cm).

Mean mercury loss from combustion was considerable, with 95% and 97% of mercury lost from fine and coarse fuels, respectively. There was a very minor difference in mean total mercury loss between heading and backing flaming modes for fine fuels (96% loss for heading and 92% for backing), though no such difference was observed for coarse fuels. Due to the low mercury concentrations in coarse fuels, emission factors based on fuel mass balance ($EF_{\text{THg/fuel}}$) effectively decreased with increasing coarse fuel loads. These values were 28.7 \pm 8.1 $\mu\text{g kg}^{-1}$, 24.9 \pm 7.4 $\mu\text{g kg}^{-1}$, 20.0 \pm 6.6 $\mu\text{g kg}^{-1}$ and 15.9 \pm 5.9 $\mu\text{g kg}^{-1}$ for fuel loads with 0.0 kg m^{-2} , 0.2 kg m^{-2} , 0.6 kg m^{-2} and 1.2 kg m^{-2} coarse fuels, respectively.

Table 3

Overview of fire behaviour parameters. Median with range in parentheses.

	Fuel MC	EOFS	Flaming	Max. point	Rate of	Byram
	%	min:sec	duration	temperature	spread	intensity
			min:sec	°C	m h ⁻¹	kW m ⁻¹
Heading	11.5 (10.0–12.7)	4:55 (2:19–6:55)	9:06 (6:20–11:20)	726 (107–958)	47.7 (36.7–112.6)	211.5 (115.7–478.4)
Backing	11.9 (10.2–12.7)	22:41 (19:46–26:54)	28:37 (27:44–29:30)	621 (127–886)	5.0 (4.6–6.2)	20.1 (13.1–25.6)

3.2. Overview of experimental burns

An overview of the fire behaviour measurements is presented in Table 3. Moisture contents at the beginning of each burn ranged between 10.0 and 12.7%. Maximum temperatures (given for each thermocouple in the working section, not aggregated across burns as a whole) were generally higher for heading fires than for backing, though were not statistically different. End of forward spread (EOFS) was defined as the point in time when the apex of the head fire reached the end of the fuel bed and was used to determine the rate of spread (equal to the length of the fuel bed divided by EOFS). Due to the parabolic head fire shape (Cheney et al., 1993), areas of unburned material along the flanks of the fire remained at EOFS. Heading fires progressed along the fuel bed at a much faster (~9 times) rate than backing fires, consequently showing considerably higher Byram fire line intensities. Based on the Byram fireline intensities, these burns are best described as low-moderate intensity, typical for prescribed burning (Tolhurst and Cheney, 1999). Flaming combustion durations for heading fires increased slightly with higher coarse loading (Fig. 3), partly due to longer flaming periods of coarse fuels and partly due to a slowed rate of

spread. Three distinct periods of the experimental burns were defined: flaming progression (FP) from ignition to EOFS, flaming stationary (FS) from EOFS to the cessation of all flaming combustion (note that “stationary” here refers to the apex of the fire and not the still-progressing flanks) and smouldering (SM) from the end of flaming combustion until the end of the experimental burn.

Carbon release during combustion from all experimental burns was largely in the form of CO₂ and CO, with CO₂ representing the majority of this release (92–97% C) and CO representing 3–7%. Fig. 3 shows that, for heading fires, peak CO₂ occurred before peak CO. The timing of these peaks did not consistently coincide with either EOFS or flame duration, however the period between the peaks did increase with increasing coarse fuel loads. Patterns for CO₂ and CO concentrations during backing fires showed an initial peak following ignition preceding a steady decline for the duration of the burn. Distinct ranges of MCE were observed by the open-path instrument during each combustion stage, with FP showing an MCE range of 0.96–1, FS a range of 0.88–0.96 and SM a range of 0.80–0.88.

Fig. 3 shows that release of GEM during heading fires occurred predominantly during the flaming progression stage, with a peak in

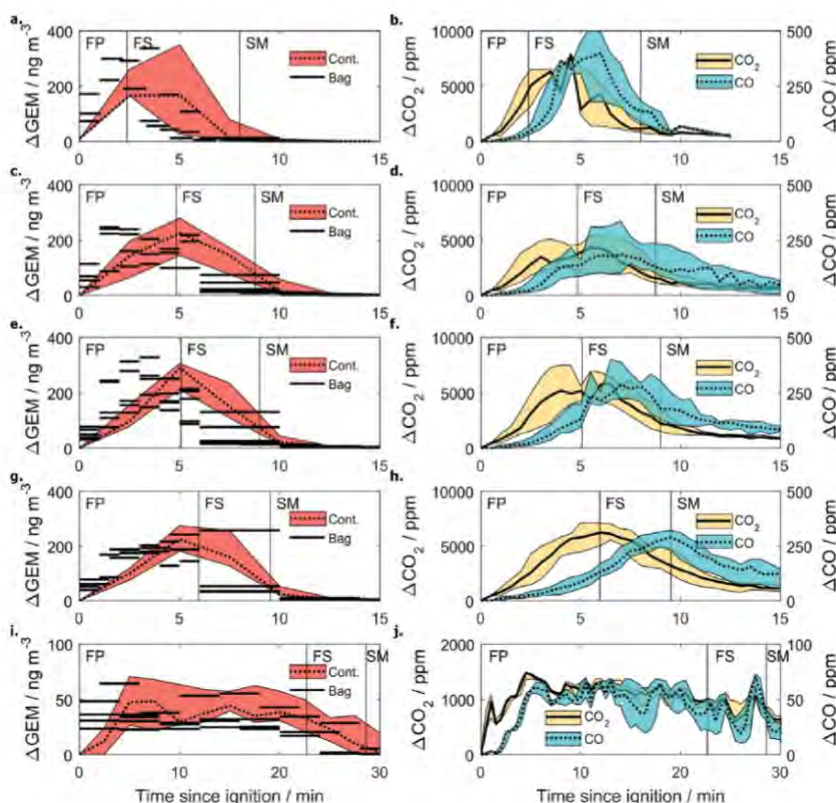


Fig. 3. Left: time series of GEM enhancements for a. Load 1, c. Load 2, e. Load 3, g. Load 4 and i. backing fires. Right: CO₂ (yellow) and CO (blue) enhancements for the same fires. Black lines denote median values, shading denotes range of values. Vertical lines show median times of EOFS and Fines Out. (For interpretation of the references to colour in this figure legend, the reader is referred to the Web version of this article.)

Table 4

Mercury emission ratios for all fire stages. Calculated as the least squares slope of GEM/y with standard error.

	All Data	Flaming Progression	Flaming Stationary	Smouldering	Cape Grim
GEM _{CO₂} ($\times 10^{-9}$)	5.95 ± 0.02	6.55 ± 0.05	4.70 ± 0.07	1.46 ± 0.10	9.77 ± 0.08
GEM _{CO} ($\times 10^{-7}$)	0.82 ± 0.01	2.51 ± 0.03	0.56 ± 0.01	0.08 ± 0.01	0.58 ± 0.01
MCE range	0.80–1.00	0.96–1.00	0.88–0.96	0.80–0.88	0.79–0.97

GEM observed prior to EOFs and very low concentrations following the end of all flaming combustion. The timing in peak GEM was earlier for bag data than for continuous data — this was attributed to the long sampling period of the 2537A (2.5 min) relative to the changes in GEM release from flaming combustion. Bag sampling frequency was kept at 1 min^{-1} during flaming combustion and so finer detail during this stage could be resolved. GEM enhancements during backing fires exhibited a minor peak during the first 5–10 min of combustion and a slow, continual decrease during the extended flaming combustion phase. This pattern did not change considerably across coarse fuel loads and so data for all backing fires are shown here as an aggregate. GEM represented the majority of liberated mercury for all experimental burns, with PBM accounting for < 1% of mercury emission. Emission of PBM showed no relationship with fire spread or fuel loading.

3.3. GEM emission ratios

For experimental burns the mean GEM emission ratio with respect to CO_2 ($ER_{\text{GEM}/\text{CO}_2}$) was $5.95 \pm 0.02 \times 10^{-9}$ and with respect to CO ($ER_{\text{GEM}/\text{CO}}$) was $0.82 \pm 0.01 \times 10^{-7}$ (Table 4). Emission ratios obtained with both bag and continuous sampling methods showed good agreement and are reported here as an aggregate total. Distinct differences in both $ER_{\text{GEM}/\text{CO}_2}$ and $ER_{\text{GEM}/\text{CO}}$ were observed for each of the

experimental burn stages with larger values observed during the initial stages of the burns (Table 4, Fig. 4a and b). This is consistent with the GEM enhancement time series showing that most GEM was released during the flaming progression stage of the experimental burns.

No such distinction between combustion stages was able to be resolved in the CGBAPS plume strike data, with GEM enhancements showing more linear relationships with both CO_2 and CO enhancements across all plume events (Fig. 4c and d). $ER_{\text{GEM}/\text{CO}_2}$ from the CGBAPS plume strike data was significantly higher than that observed during the experimental burns ($9.77 \pm 0.08 \times 10^{-9}$). The value for $ER_{\text{GEM}/\text{CO}}$ from CGBAPS, at $0.58 \pm 0.01 \times 10^{-7}$, was slightly lower than that from all experimental burn data but comparable with that calculated from flaming stationary observations. We note that only data from plume strike events 1 and 5 can reasonably be believed to have originated from eucalypt forest biomass burning (see Fig. 2b). Removing data from events 2–4 (likely from heathland and grassland burning) did not significantly alter the resulting ER values.

Mercury emission factors based on emission ratios were calculated from the experimental burn data only and showed similarly large variability with burn stage, with values for both $EF_{\text{GEM}/\text{CO}_2}$ and $EF_{\text{GEM}/\text{CO}}$ decreasing with burn stage progression (Table 5). GEM release fractions, expressed as the mean GEM loss calculated from these emission factors as a percentage of available fuel mercury, are included

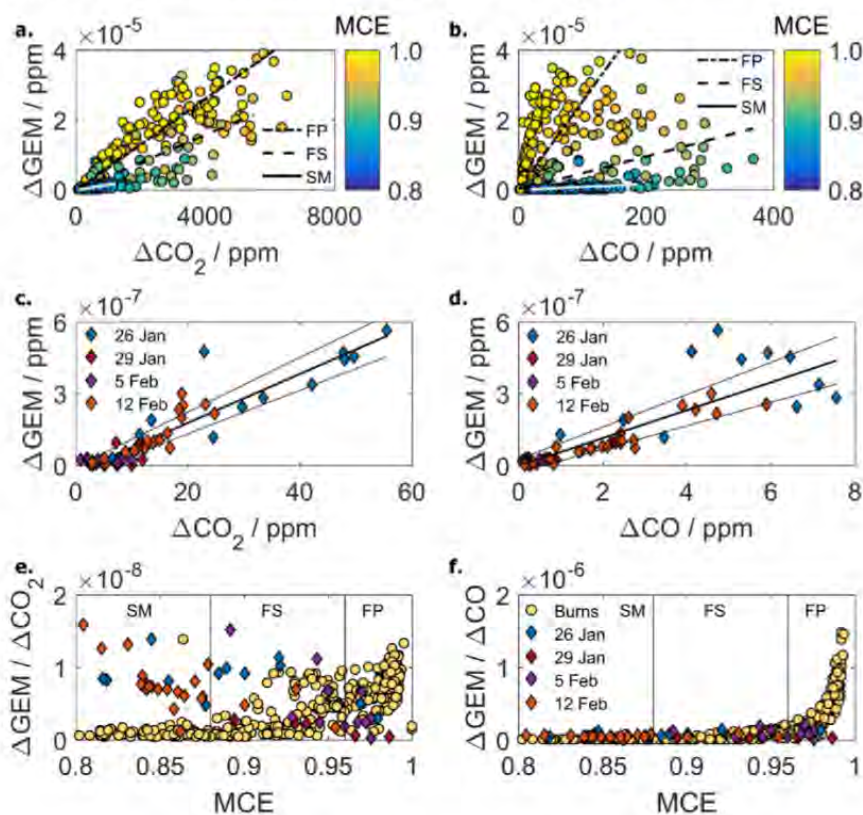


Fig. 4. Above: GEM enhancements against a. CO_2 and b. CO enhancements. Lines show least-squares regressions for FP (dotted), FS (dashed) and SM (solid) stages. Middle: GEM enhancements against c. CO_2 and d. CO enhancements for plume strike events observed at CGBAPS. Lines show linear least-square regressions \pm standard error. Below: e. $\Delta\text{GEM}/\Delta\text{CO}_2$ and f. $\Delta\text{GEM}/\Delta\text{CO}$ ratios for each observation against modified combustion efficiency for experimental burn (circles) and CGBAPS plume strike (diamonds) data. Here FP, FS and SM categories are defined according to MCE ranges and refer to experimental burn data only.

Table 5

Mercury emission factors for all fire stages, along with mercury release fractions expressed as mean GEM emission factor as a percentage of mean mercury concentration in dry fuel. Emission factor calculated from mass balance technique ($EF_{THg/fuel}$) included for reference.

	$EF_{THg/fuel}$	All Data	Flaming Progression	Flaming Stationary	Smouldering
$GEM_{CO_2}/\mu g\ kg^{-1}$	28.7 ± 8.1 96%	37.4 ± 0.7 125%	42.8 ± 0.8 143%	29.0 ± 1.3 97%	7.8 ± 1.0 26%
$GEM_{CO}/\mu g\ kg^{-1}$	28.7 ± 8.1 96%	31.5 ± 7.0 105%	28.8 ± 14.7 96%	25.7 ± 10.1 86%	8.7 ± 10.5 29%

here. Mean overall emission factors were higher for EF_{GEM/CO_2} , though both were within the range of uncertainty of $EF_{THg/fuel}$. EF_{GEM/CO_2} significantly overpredicted GEM release during the flaming progression stage (143% release fraction), though showed good agreement during the flaming stationary stage (97%). $EF_{GEM/CO}$ showed good agreement with $EF_{THg/fuel}$ during the flaming progression (96%) and flaming stationary stages (86%), though with uncertainties an order of magnitude higher than for EF_{GEM/CO_2} . Both emission factors significantly underpredicted GEM release against mass balance techniques during the smouldering stage (26% and 29% for CO_2 and CO, respectively).

4. Discussion

4.1. Mercury in dry sclerophyll fuels and emission factors

Observations of total mercury concentrations within eucalypt vegetation in the literature are rare but are in good agreement with those reported here (Table 2). Hellings et al. (2013) observed concentrations of $78.5 \pm 2.1\ \mu g\ kg^{-1}$ in Australian Eucalyptus leaves, similar to that seen in leaves from Site 1. Total mercury concentrations in eucalypt bark reported by these authors, at $50.1 \pm 2.5\ \mu g\ kg^{-1}$, were slightly higher than those observed here. Packham et al. (2009) similarly measured total mercury concentrations in surface litter biomass of 78, 80 and $83\ \mu g\ kg^{-1}$ within three Walker fire regions (Walker et al., 1981) corresponding to native temperate broadleaf forest. Higher total mercury values within plant leaves have been observed elsewhere and are attributed to uptake of atmospheric mercury via stomatal and foliar exchange (Erickson et al., 2003; Blackwell and Driscoll, 2015). Preferential storage of mercury within the leaves of eucalypts leads to emission factors across the entire fuel bed that are significantly lower than the maximum observed mercury concentrations. Clearly, the very low mercury content within the coarse fuels lead to an effective decrease in the mercury emission factor with increasing coarse fuel loading. The contribution to atmospheric emissions of coarse woody debris in Australian eucalypt forests is poorly known (Volkova and Weston, 2013), due to the focus on fine fuels as the driver of fire propagation (Keeley, 2009). Field observations have further shown high variability in both fuel loading from coarse material and volatilisation of coarse material during biomass burning events (Possell et al., 2015). Due to the low total mercury concentrations in coarse woody debris, the large disparity in burning efficiency of this material, and the large uncertainties in coarse fuel loading within Australian dry sclerophyll forests, we refrain from including coarse fuels in our estimate of mercury emission factors. As such, we conservatively offer an emission factor value of $28.7 \pm 8.1\ \mu g\ kg^{-1}$ as the upper estimate of mercury emission from Australian dry sclerophyll surface fuels based on our observations.

Volatilisation of mercury from soils is another significant emission contribution during biomass burning. THg concentrations in Site 2 soils (Table 2) were comparable to those reported by Hellings et al. (2013), who observed concentrations of $30.1 \pm 1.5\ \mu g\ kg^{-1}$ in soil with particle diameter above $212\ \mu m$ and $61.7 \pm 3.6\ \mu g\ kg^{-1}$ below this diameter. Packham et al. (2009) observed a soil total mercury concentration of $47\ \mu g\ kg^{-1}$ at one Australian native temperate broadleaf

sites and a concentration of $125\ \mu g\ kg^{-1}$ at a second site, although stating that proximity to an old gold mine likely skewed this latter result. The similar differences in concentrations between upper (0–2 cm) and lower (5–10 cm) soil depths at the burned and unburned sampling sites suggests that volatilisation of mercury from the soil was low during this particular fire. The general validity of this result is difficult to quantify without more extensive spatial sampling, however Biswas et al. (2007) suggested that between 15 and 66% of soil mercury may be released during biomass burning events. Using the higher of the two soil concentrations from Site 2, this would equate to an estimated soil mercury emission factor between 4.4 and $32.5\ \mu g\ kg^{-1}$.

In the absence of locally-derived emission factors, the work of Friedli et al., 2003, 2009 is commonly referred to in modelling of mercury release from biomass burning in Australia. These emission factors include a “global average” of $112\ \mu g\ kg^{-1}$ (Friedli et al., 2003) and diversified emission factors for tropical ($19\ \mu g\ kg^{-1}$), extratropical ($242\ \mu g\ kg^{-1}$) and non-forest ($41\ \mu g\ kg^{-1}$) regions (Friedli et al., 2009). For dry sclerophyll forests, we have shown through our own sampling and comparison with other values in the literature that mercury emission factors are considerably lower than both the global average and that for extratropical forests of $242\ \mu g\ kg^{-1}$. Applying a mercury emission factor of $28.7\ \mu g\ kg^{-1}$ would result in estimates of mercury release from eucalypt forest biomass burning between 74 and 88% lower than previously reported.

4.2. GEM and PBM emission ratios

In the emission time series (Fig. 3) it is apparent that the majority of GEM release occurs under flaming combustion, a stage characterised by the most efficient combustion (higher MCE) and the highest proportion of fuel carbon loss. As CO_2 emission represents the largest proportion of fuel carbon loss throughout all burn stages, a stronger linearity between ΔGEM and ΔCO_2 is observed, relative to $\Delta GEM/\Delta CO$ (Fig. 4a and b). Applying ER_{GEM/CO_2} values from all burn stages or during the flaming progression stage however significantly overestimates GEM release against mass balance techniques (Table 5). Values for ER_{GEM/CO_2} in the literature are rare, with only one other study publishing a value of 1.19×10^{-9} (Brunke et al., 2001). All ER_{GEM/CO_2} values observed here are significantly higher than this value (and with consequently higher release fractions), with the exception of smouldering-stage combustion, which was found to not be an accurate predictor of mercury release (Table 5). CGBAPS plume strike data similarly gave a mean ER_{GEM/CO_2} value close to an order of magnitude higher than that reported by (Brunke et al., 2001). The separation of burn stages was not able to be resolved in the CGBAPS field data, with neither $\Delta GEM/\Delta CO_2$ nor $\Delta GEM/\Delta CO$ values showing relationships with MCE similar to those seen in the experimental burns (Fig. 4e and f).

Brunke et al. (2001) also reported an $ER_{GEM/CO}$ value of 2.10×10^{-7} , within the range of 0.79×10^{-7} to 2.39×10^{-7} from other reported values in the literature (Friedli et al., 2003; Sigler et al., 2003; Weiss-Penzias et al., 2007; Ebingerhaus et al., 2007). Our own measurements of $ER_{GEM/CO}$ span a range greater than this within a single experimental burn ensemble ($0.08 \pm 0.01 \times 10^{-7}$ for smouldering combustion to $2.51 \pm 0.03 \times 10^{-7}$ for flaming propagation).

This result highlights the need for careful consideration of plume strike observations and we suggest reporting where possible both ER_{GEM/CO_2} as well as $ER_{GEM/CO}$ values, along with MCE. Within our experimental burn data, $ER_{GEM/CO}$ values during the flaming stationary stage accurately predict GEM release against mass balance techniques (albeit with large uncertainty) and both $ER_{GEM/CO}$ values — and relationships between the $\Delta GEM/\Delta CO$ ratio and MCE — are similar to the CGBAPS field data. For this reason, we speculate that the $ER_{GEM/CO}$ obtained from CGBAPS plume strike data (0.58×10^{-7}) is a more appropriate value to adopt than the global average of Friedli et al. (2009) (1.54×10^{-7}). Again, this is 62% lower than currently accepted values in the literature, highlighting that biomass burning emission of GEM in dry sclerophyll forests is currently overestimated.

With release of PBM below detection limits for many of the experimental burns, we are unable to provide an emission ratio for particulate mercury release. Obrist et al. (2007) observed changes in the relative emission of gaseous and particulate mercury with combustion phase, highlighting increased PBM emission from smouldering-dominated fires in a laboratory-scale experiment. They explored emissions from fuels with initial moisture contents ranging between 9 and 95%. For fuels with moisture content below 30% they saw very little release of PBM, at times below detection limits. As starting fuel moisture here was kept consistent and relatively low, the very small PBM releases observed are consistent with this result.

Fire intensities during wild burning events are strongly related to fuel moistures (Gill et al., 2002), and fuel moistures in this experiment were chosen such that the Byram fireline intensities of the experimental burns are similar to those observed during prescribed burning. Conditions during prescribed burns are chosen such that the resulting burn intensity is low and therefore controllable. Many wildfire burning events in Australia can also be considered low intensity, with an estimated ~50% showing Byram fire line intensities around 300 kW m^{-1} (Gill et al., 2002), within the range of intensities seen during heading experimental burns. Larger, more intense fires generally take place under drier conditions. For this reason we speculate that the very low release of PBM during dry sclerophyll forest biomass burning is broadly applicable; as such we would expect PBM to generally represent a very small proportion of mercury emission from wildfire burning in Australian dry sclerophyll forests. Estimating the moisture content of fuels is still an important step in resolving relative partitioning during mercury biomass burning emissions modelling.

4.3. Directions for future Australian research

There has been a considerable range of biomass burning mercury emission estimates for the Australian continent produced in the literature. Using three biomass burning inventories, Simone et al. (2015) provided estimates of 7, 30.0 and $30.2 \text{ Mg Hg a}^{-1}$, based on the $ER_{GEM/CO}$ value of 1.54×10^{-7} reported by Friedli et al. (2009). Estimates of total mercury release from the Australian continent using emission factors include those by Nelson et al. (2009) (42 Mg Hg a^{-1} using an average emission factor of $112 \mu\text{g kg}^{-1}$) and Friedli et al. (2009) (19 Mg Hg a^{-1} using diversified emission factors for tropical, extratropical and non-forest regions). We have shown here, through both experimental and field observation data, that these emission factors and emission ratios significantly overpredict mercury release for dry sclerophyll forests.

This significant downward adjustment is an important result for predicting mercury emissions from burning of dry sclerophyll forests. However according to AVHRR satellite data, biomass burning of temperate broadleaf forests accounted for only 0.7% of the total across Australia on an areal basis over the years 1997–2011 (Maier, 2016). Larger gains in constraining estimates of mercury release from biomass burning across the Australian continent can be made by focussing on tropical/subtropical grassland and savanna, and desert/xeric shrub ecoregions, which combined account for over 97% of burned area. In

addition to the large relative burned areas, total mercury concentrations within vegetation and soils in these regions are currently subject to large uncertainty. Packham et al. (2009) observed vegetation concentrations of 212 and $290 \mu\text{g kg}^{-1}$ for tropical grassland and shrubland ecoregion samples, respectively, and soil concentrations of $105 \mu\text{g kg}^{-1}$ for tropical grassland ecoregion samples. These results agree well with the $198 \mu\text{g kg}^{-1}$ mercury emission factor given by Friedli et al. (2009) for tropical regions. Howard et al. (2017) however observed vegetation and soil concentrations in a tropical grassland site of only $9 \mu\text{g kg}^{-1}$, stating that these samples were taken in an area that had undergone burning within the previous 12 months. Clearly further vegetation and soil sampling in these ecoregions can assist in constraining Australian biomass burning mercury emission estimates.

5. Conclusions

Mercury and greenhouse gas emissions from the burning of dry sclerophyll surface fuels were measured in the CSIRO Pyrotron combustion wind tunnel. This experimental setup provided a unique ability to observe changes in relative emissions due to fire progression throughout the burns. Heading and backing fires were considered both with and without the addition of coarse fuels. Due to the relatively low mercury concentrations in these fuels, increasing the coarse loading lead to an effective decrease in mercury concentration across the entire fuel bed. PBM represented less than 1% of emitted mercury, which we attributed to the consistent and relatively low fuel moistures used in this experiment. As this experiment was designed to simulate fire intensity conditions during prescribed burns (i.e. higher fuel moisture than during large wildfires), we hypothesise that wildfire burning events will likely emit similarly small percentages of PBM.

Volatilisation of mercury was found to occur predominantly during the early flaming combustion phase of the burns when flame temperatures are highest. Values of ER_{GEM/CO_2} significantly over-predicted mercury release during the early stages of the burn, whilst $ER_{GEM/CO}$ values in the early stages agreed well with mercury release predicted from mass balance techniques. As the onset of smouldering combustion occurred after this early volatile period, mercury emissions at this stage were low, with both ER_{GEM/CO_2} and $ER_{GEM/CO}$ significantly under-predicting mercury release. $ER_{GEM/CO}$ values observed during experimental burns spanned a range greater than those reported in the literature, however those obtained during the flaming stationary stage of the burns ($0.56 \pm 0.01 \times 10^{-7}$) were deemed to give the most realistic representations of mercury release from the fuels. Comparison with plume strike data collected from CGBAPS ($0.58 \pm 0.01 \times 10^{-7}$) confirmed this as the most appropriate value for estimating mercury release. These values are ~62% lower than the global average used previously in Australian biomass burning mercury release modelling.

Fuel mercury concentrations at the two eucalypt sites agreed well with each other and with other values for eucalypt vegetation and soils reported in the literature. Based on our observations, we offer a conservative mercury emission factor of $28.7 \pm 8.1 \mu\text{g kg}^{-1}$ for surface fuels, noting that inclusion of coarse fuels in our calculations leads to a decrease in this estimate. Our estimated range of mercury emission factors for eucalypt soils is between 4.4 and $32.5 \mu\text{g kg}^{-1}$. Both of these values are again considerably lower than previous emission factors used in modelling emission of mercury from biomass burning in Australia. This is an important result for mercury emission modelling efforts however we note that, in terms of total area burned, eucalypt forests represent a relatively minor source of biomass burning emissions across the Australian continent. Future investigations into Australian mercury biomass burning release should be focused on the tropical grassland and desert shrub ecoregions, as these are the regions that are burned most extensively and frequently, thus potentially being regions of high atmospheric mercury turnover.

Conflicts of interest

The authors declare that they have no competing interests, financial or otherwise.

Acknowledgements

This work was supported by the Victorian Department of Environment, Land, Water and Planning and the Australian Bureau of Meteorology/CSIRO Cape Grim Program. The authors thank Martin Cope of CSIRO Oceans and Atmosphere for leading the experimental burn project and Sam Cleland, Jeremy Ward, Nigel Somerville, Stuart Baly and Cindy Hood of the Bureau of Meteorology for their continued efforts in operating the Cape Grim Baseline Air Pollution Station.

References

- Aalde, H., van Amstel, A., Gonzalez, P., Gytarsky, M., Krug, T., Kurz, W.A., Lasco, R.D., Martino, D.L., McConkey, B.G., Ogle, S., Paustian, K., Raison, J., Ravindranath, N.H., Schoene, D., Smith, P., Somogyi, Z., Verchot, L., 2006. Generic methodologies applicable to multiple land-use categories. In: Eggleston, H.S., Buendia, L., Miwa, K., Ngara, T., Tanabe, K. (Eds.), '2006 IPCC Guidelines for National Greenhouse Gas Inventories', Institute for Global Environmental Strategies (IGES) for the Intergovernmental Panel on Climate Change (IPCC), Hayama, Japan, pp. 1–59.
- Abey, D., 2016. Call to Put Politics Aside in Fight for World Heritage Wilderness in Wake of Fire Threat. *Mercury* 31st Jan.
- Agnan, Y., Dantec, T.L., Moore, C.W., Edwards, G.C., Obrist, D., 2016. New constraints on terrestrial surface-atmosphere fluxes of gaseous elemental mercury using a global database. *Environ. Sci. Technol.* 50 (2), 507–524.
- Amos, H.M., Jacob, D.J., Streets, D.G., Sunderland, E.M., 2013. Legacy impacts of all-time anthropogenic emissions on the global mercury cycle. *Global Biogeochem. Cycles* 27 (2), 410–421.
- Andreae, M., Merlet, P., 2001. Emission of trace gases and aerosols from biomass burning. *Global Biogeochem. Cycles* 15 (4), 955–966.
- Australian Government Department of the Environment and Energy (DEE), 2016. *Australia's Native Vegetation Framework*. <http://www.environment.gov.au/land/publications/australias-native-vegetation-framework> Accessed: 2017-06-01.
- Bailey, R.G., 1995. In: Description of the Ecoregions of the United States, second ed. Misc. Pub No. 1391, Map scale 1:7,500,000. USDA Forest Service.
- Biswas, A., Blum, J.D., Klaue, B., Keeler, G.J., 2007. Release of mercury from Rocky Mountain forest fires. *Global Biogeochem. Cycles* 21 (1), 13.
- Blackwell, B.D., Driscoll, C.T., 2015. Deposition of mercury in forests along a montane elevation gradient. *Environ. Sci. Technol.* 49 (9), 5363–5370.
- Brunke, E.-G., Labuschagne, C., Slemr, F., 2001. Gaseous mercury emissions from a fire in the cape Peninsula, South Africa, during January 2000. *Geophys. Res. Lett.* 28 (8), 1483–1486.
- Byram, G.M., 1959. Combustion of forest fuels. In: Davis, K.P. (Ed.), *Forest Fire: Control and Use*. McGraw, New York, NY, United States, pp. 61–89.
- Chatto, K., Tolhurst, K.G., 1997. Development and Testing of the Wiltronics TH Fine Fuel Moisture Meter, Technical Report, Research Report 46. Department of Natural Resources and Environment, Fire Management Branch, Victoria, Australia.
- Cheney, N.P., Gould, J.S., Catchpole, W.R., 1993. The influence of fuel, weather and fire shape variables on fire-spread in grasslands. *Int. J. Wildland Fire* 3 (1), 31–44.
- Cobbett, F.D., Van Heyst, B.J., 2007. Measurements of GEM fluxes and atmospheric mercury concentrations (GEM, RGM and Hg₀) from an agricultural field amended with biosolids in Southern Ont., Canada (October 2004–November 2004). *Atmos. Environ.* 41 (11), 2270–2282.
- Cope, M.E., Hess, G.D., Lee, S., Tory, K., Azzi, M., Carras, J., Lilley, W., Manins, P.C., Nelson, P., Ng, L., Puria, K., Wong, N., Walsh, S., Young, M., 2009. The Australian air quality forecasting system. Part I: project description and early outcomes. *J. Appl. Meteorol.* 43 (5), 649–662.
- Desservettaz, M., Paton-Walsh, C., Griffith, D.W., Kettlewell, G., Keywood, M.D., van der Schoot, M.V., Ward, J., Mallet, M.D., Milic, A., Miljevic, B., Ristovski, Z.D., Howard, D., Edwards, G.C., Atkinson, B., 2017. Emission factors of trace gases and particles from tropical savanna fires in Australia. *J. Geophys. Res.: Atmosphere* 122 (11), 6059–6074.
- Draxler, R.R., 1999. HYSPLIT4 User's Guide, Technical Report ERL ARL-230. NOAA Air Resources Laboratory, Silver Spring, MD, United States.
- Draxler, R.R., Hess, G., 1998a. Description of the HYSPLIT 4 Modeling System, Technical Report ERL ARL-224. NOAA Air Resources Laboratory, Silver Spring, MD, United States.
- Draxler, R.R., Hess, G., 1998b. An overview of the HYSPLIT 4 modelling system for trajectories. *Aust. Meteorol. Mag.* 47, 295–308.
- Driscoll, C.T., Mason, R.P., Chan, H.M., Jacob, D.J., Pirrone, N., 2013. Mercury as a global pollutant: sources, pathways, and effects. *Environmental Science and Technology* 47 (10), 4967–4983.
- Ebinghaus, R., Slemr, F., Brenninkmeijer, C.A.M., van Velthoven, P., Zahn, A., Hermann, M., O'Sullivan, D.A., Oram, D.E., 2007. Emissions of gaseous mercury from biomass burning in South America in 2005 observed during CARIBIC flights. *Geophys. Res. Lett.* 34 (8), 5.
- Ericksen, J.A., Gustin, M.S., 2004. Foliar exchange of mercury as a function of soil and air mercury concentrations. *Sci. Total Environ.* 324 (1–3), 271–279.
- Ericksen, J.A., Gustin, M.S., Schorran, D.E., Johnson, D.W., Lindberg, S.E., Coleman, J.S., 2003. Accumulation of atmospheric mercury in forest foliage. *Atmos. Environ.* 37 (12), 1613–1622.
- Fitzgerald, W.F., Engstrom, D.R., Mason, R.P., Nater, E.A., 1998. The case for atmospheric mercury contamination in remote areas. *Environ. Sci. Tech.* 32 (1), 1–7.
- Friedli, H.R., Arellano, A.F., Cinnirella, S., Pirrone, N., 2009. Initial estimates of mercury emissions to the atmosphere from global biomass burning. *Environ. Sci. Tech.* 43 (10), 3507–3513.
- Friedli, H.R., Radke, L.F., Lu, J.Y., 2001. Mercury in smoke from biomass fires. *Geophys. Res. Lett.* 28 (17), 323–326.
- Friedli, H.R., Radke, L.F., Lu, J.Y., Banic, C.M., Leaitch, W.R., MacPherson, J.L., 2003. Mercury emissions from burning of biomass from temperate North American forests: laboratory and airborne measurements. *Atmos. Environ.* 37 (2), 253–267.
- Gill, A.M., 1981. Adaptive responses of Australian vascular plant species to fires. In: Gill, A.M., Groves, R.H., Noble, I.R. (Eds.), *Fire and the Australian Biota*. Australian Academy of Science, Canberra, Australia, pp. 101–127.
- Gill, A.M., Catling, P.C., 2002. Fire regimes and biodiversity of forested landscapes of southern Australia. In: Bradstock, R.A., Williams, J.E., Gill, A.M. (Eds.), *Flammable Australia: the Fire Regimes and Biodiversity of a Continent*. Cambridge University Press, Melbourne, Australia, pp. 353–363.
- Gramenz, E., 2016. Tasmanian Bushfires: Firefighters Gear up for at Least Four More Weeks Battling Blazes. Australian Broadcasting Corporation (ABC) News.
- Griffith, D.W.T., 1996. Synthetic calibration and quantitative analysis of gas-phase FT-IR spectra. *Appl. Spectrosc.* 50 (1), 59–70.
- Griffith, D.W.T., Deutscher, N.M., Caldwell, C., Kettlewell, G., Riggenbach, M., Hammer, S., 2012. A Fourier transform infrared trace gas and isotope analyser for atmospheric applications. *Atmos. Measur. Techn.* 5 (10), 2481.
- Hao, W.M., Ward, D.E., 1993. Methane production from global biomass burning. *J. Geophys. Res.: Atmosphere* 98 (D11), 20657–20661.
- Hartman, J.S., Weisberg, P.J., Pillai, R., Ericksen, J.A., Kuiken, T., Lindberg, S.E., Zhang, H., Rytuba, J.J., Gustin, M.S., 2009. Application of a rule-based model to estimate mercury exchange for three background biomes in the continental United States. *Environ. Sci. Technol.* 43 (13), 4989–4994.
- Hellings, J., Adeloju, S.B., Verheyen, T.V., 2013. Rapid determination of ultra-trace concentrations of mercury in plants and soils by cold vapour inductively coupled plasma-optical emission spectrometry. *Microchem. J.* 111, 62–66.
- Hintelmann, H., Harris, R., Heyes, A., Hurley, J.P., Kelly, C.A., Krabbenhoft, D.P., Lindberg, S., Rudd, J.W., Scott, K.J., St Louis, V.L., 2002. Reactivity and mobility of new and old mercury deposition in a boreal forest ecosystem during the first year of the METAALICUS study. *Environ. Sci. Technol.* 36 (23), 5034–5040.
- Holmes, C., Jacob, D., Corbitt, E., Mao, J., Yang, X., Talbot, R., Slemr, F., 2010. Global atmospheric model for mercury including oxidation by bromine atoms. *Atmos. Chem. Phys.* 10, 12037–12057.
- Horowitz, H.M., Jacob, D.J., Zhang, Y., Dibble, T.S., Slemr, F., Amos, H.M., Schmidt, J.A., Corbitt, E.S., Marais, E.A., Sunderland, E.M., 2017. A new mechanism for atmospheric mercury redox chemistry: implications for the global mercury budget. *Atmos. Chem. Phys.* 17, 6353–6371.
- Howard, D., Edwards, G.C., 2018. Mercury fluxes over an Australian alpine grassland and observation of nocturnal atmospheric mercury depletion events. *Atmos. Chem. Phys.* 18 (1), 129–142.
- Howard, D., Nelson, P.F., Edwards, G.C., Morrison, A.L., Fisher, J.A., Ward, J., Harnwell, J., van der Schoot, M., Atkinson, B., Chambers, S.D., Griffiths, A.D., Werczynski, S., Williams, A.G., 2017. Atmospheric mercury in the southern hemisphere tropics: seasonal and diurnal variations and influence of inter-hemispheric transport. *Atmos. Chem. Phys.* 17 (18), 11623–11636.
- Johnson, D.W., Lindberg, S.E., 1995. The biogeochemical cycling of Hg in forests: alternative methods for quantifying total deposition and soil emission. *Water Air Soil Pollut.* 80 (1–4), 1069–1077.
- Keeley, J.E., 2009. Fire intensity, fire severity and burn severity: a brief review and suggested usage. *J. Inter. Assoc. Wildland Fire* 18 (1), 116–126.
- Kessler, R., 2013. The Minamata Convention on Mercury: a first step toward protecting future generations. *Environ. Health Perspect.* 121 (10), 304–309.
- Krabbenhoft, D.P., Sunderland, E.M., 2013. Global change and mercury. *Science* 341, 1457–1458.
- Lawson, S.J., Selleck, P.W., Galbally, I.E., Keywood, M.D., Harvey, M.J., Lerot, C., Helmig, D., Ristovski, Z., 2015. Seasonal in situ observations of glyoxal and methylglyoxal over the temperate oceans of the Southern Hemisphere. *Atmos. Chem. Phys.* 15 (1), 223–240.
- Lindberg, S., Bullock, R., Ebinghaus, R., Engstrom, D., Fenh, X., Fitzgerald, W., Pirrone, N., Prestbo, E., Seigneur, C., 2007. A synthesis of progress and uncertainties in attributing the sources of mercury in deposition. *AMBIO A J. Hum. Environ.* 36 (1), 19–33.
- Maier, S.W., 2016. *Fire frequency - avhrr, Australian algorithm, Australia coverage*. <http://data.auscover.org.au/xwiki/bin/view/Product+pages/FireFreq+AVHRR#HReferences> Accessed: 2017-05-19.
- Mason, R.P., Choi, A.L., Fitzgerald, W.F., Hammerschmidt, C.R., Lamborg, C.H., Soerensen, A.L., Sunderland, E.M., 2012. Mercury biogeochemical cycling in the ocean and policy implications. *Environ. Res.* 119, 101–117.
- Mason, R.P., Reinfelder, J.R., Morel, F.M.M., 1995. Bioaccumulation of mercury and methylmercury. *Water Air Soil Pollut.* 80 (1–4), 915–921.
- Matthews, S., 2010. Effect of drying temperature on fuel moisture content measurements. *J. Inter. Assoc. Wildland Fire* 19 (6), 800–802.
- Melendez-Perez, J.J., Fostier, A.H., Carvalho Jr., J., Windmüller, C.C., Santos, J.C., Carpi, A., 2014. Soil and biomass mercury emissions during a prescribed fire in the

- Amazonian rain forest. *Atmos. Environ.* 96, 415–422.
- Meyer, C.P., Cook, G.D., Reisen, F., Smith, T.E.L., Tattaris, M., Russell-Smith, J., Maier, S.W., Yates, C.P., Wooster, M.J., 2012. Direct measurements of the seasonality of emission factors from savanna fires in northern Australia. *J. Geophys. Res.: Atmosphere* 117 (D20), 14.
- Montreal Process Implementation Group for Australia and National Forest Inventory Steering Committee, 2013. Australia's State of the Forests Report 2013, Technical Report CC BY 3.0. Australian Bureau of Agricultural and Resources Economics and Sciences (ABARES), Canberra, Australia.
- Nelson, P.F., Morrison, A.L., Malfroy, H.J., Cope, M., Lee, S., Hibberd, M.L., Meyer, C., McGregor, J., 2012. Atmospheric mercury emissions in Australia from anthropogenic, natural and recycled sources. *Atmos. Environ.* 62, 291–302.
- Nelson, P.F., Nguyen, N., Morrison, A.L., Malfroy, H., Cope, M.E., Hibberd, M.F., Lee, S., McGregor, J.L., Meyer, M., 2009. Mercury Sources, Transportation and Fate in Australia. Report. Department of Environment, Water, Heritage & the Arts.
- Obrist, D., Moosmüller, H., Schürmann, R., Antony Chen, L.-W., Kreidenweis, S.M., 2007. Particulate-phase and gaseous elemental mercury emissions during biomass combustion: controlling factors and correlation with particulate matter emissions. *Environ. Sci. Technol.* 42 (3), 721–727.
- Olson, D.M., Dinerstein, E., 2002. The global 200: Priority ecoregions for global conservation. Technical Report Annals of the Missouri Botanical Garden 89, 125–126. The Nature Conservancy, USDA Forest Service and U.S. Geological Survey).
- Packham, D., Tapper, N., Griepasma, D., Friedli, H., Hellings, J., Harris, S., 2009. Release of mercury in the Australian environment by burning: a preliminary investigation of biomass and soils. *Air Quality and Climate Change* 43 (1), 24–27.
- Paton-Walsh, C., Smith, T.E.L., Young, E.L., Griffith, D.W.T., Guérette, E.-A., 2014. New emission factors for Australian vegetation fires measured using open-path Fourier transform infrared spectroscopy – Part 1: methods and Australian temperate forest fires. *Atmos. Chem. Phys.* 14 (20), 11313–11333.
- Pirrone, N., Hedgecock, I., Cinnirella, S., Sprovieri, F., 2010. Overview of major processes and mechanisms affecting the mercury cycle on different spatial and temporal scales. In: EPJ Web of Conferences, vol. 9. EDP Sciences, pp. 3–33.
- Possell, M., Jenkins, M., Bell, T.L., Adams, M.A., 2015. Emissions from prescribed fires in temperate forest in south-east Australia: implications for carbon accounting. *Biogeosciences* 12 (1), 257–268.
- Rea, A.W., Lindberg, S.E., Keeler, G.J., 2001. Dry deposition and foliar leaching of mercury and selected trace elements in deciduous forest throughfall. *Atmos. Environ.* 35 (20), 3453–3462.
- Selin, N.E., 2009. Global biogeochemical cycling of mercury: a review. *Annu. Rev. Environ. Resour.* 34 (43–63).
- Sigler, J.M., Lee, X., Munger, W., 2003. Emission and long-range transport of gaseous mercury from a large-scale Canadian boreal forest fire. *Environ. Sci. Technol.* 37 (19), 4343–4347.
- Simone, F.D., Cinnirella, S., Gencarelli, C.N., Yang, X., Hedgecock, I.M., Pirrone, N., 2015. Model study of global mercury deposition from biomass burning. *Environ. Sci. Technol.* 49 (11), 6712–6721.
- Simone, F.D., Gencarelli, C.N., Hedgecock, I.M., Pirrone, N., 2016. A modeling comparison of mercury deposition from current anthropogenic mercury emission inventories. *Environ. Sci. Technol.* 50 (10), 5154–5162.
- Slemr, F., Angot, H., Dommergue, A., Magand, O., Barret, M., Weigelt, A., Ebinghaus, R., Brunke, E.-G., Pfaffhuber, K., Edwards, G., Howard, D., Powell, J., Keywood, M., Wang, F., 2015. Comparison of mercury concentrations measured at several sites in the Southern Hemisphere. *Atmos. Chem. Phys.* 15, 3125–3133.
- Smith-Downey, N.V., Sunderland, E.M., Jacob, D.J., 2010. Anthropogenic impacts on global storage and emissions of mercury from terrestrial soils: insights from a new global model. *J. Geophys. Res.: Biogeosciences* 115 (G3) 11 pp.
- Stamenkovic, J., Gustin, M.S., 2009. Nonstomatal versus stomatal uptake of atmospheric mercury. *Environ. Sci. Technol.* 43 (5), 1367–1372.
- Stein, A., Draxler, R., Rolph, G., Stunder, B., Cohen, M., F. N., 2015. NOAA's HYSPLIT atmospheric transport and dispersion modeling system. *Bull. Am. Meteorol. Soc.* 96, 2059–2077.
- Streets, D.G., Devane, M.K., Lu, Z., Bond, T.C., Sunderland, E.M., Jacob, D.J., 2011. All-time releases of mercury to the atmosphere from human activities. *Environ. Sci. Technol.* 45 (24), 10485–10491.
- Streets, D.G., Horowitz, H.M., Jacob, D.J., Lu, Z., Levin, I., Ter Schure, A.F.H., Sunderland, E.M., 2017. Total mercury released to the environment by human activities. *Environ. Sci. Technol.* 51 (11), 5696–5977.
- Sullivan, A.L., Knight, I.K., Hurley, R.J., Webber, C., 2013. A contractionless, low-turbulence wind tunnel for the study of free-burning fires. *Exp. Therm. Fluid Sci.* 44, 264–274.
- Sullivan, A., Surawski, N., Crawford, D., Hurley, R., Volkova, L., Weston, C., Meyer, C.P., 2018. Effect of woody debris on the rate of spread of surface fires in forest fuels in a combustion wind tunnel. *For. Ecol. Manag.* 424, 236–245.
- Surawski, N.C., Sullivan, A.L., Meyer, C.P., Roxburgh, S.H., Polglase, P.J., 2015. Greenhouse gas emissions from laboratory-scale fires in wildland fuels depend on fire spread mode and phase of combustion. *Atmos. Chem. Phys.* 15 (9), 5259–5273.
- Tolhurst, K.G., Cheney, N.P., 1999. Synopsis of the Knowledge Used in Prescribed Burning in Victoria.
- Volkova, L., Weston, C., 2013. Redistribution and emission of forest carbon by planned burning in *Eucalyptus obliqua* (L. hérit.) forest of south-eastern Australia. *For. Ecol. Manag.* 304 (15), 383–390.
- Walker, J., 1981. Fuel dynamics in Australian vegetation. In: Gill, A.M., Groves, R.H., Noble, I.R. (Eds.), *Fire and the Australian Biota*. Australian Academy of Science, Canberra, Australia, pp. 101–127.
- Ward, D.E., Radke, L.F., 1993. Emissions measurements from vegetation fires: a comparative evaluation of methods and results. In: Crutzen, P.J., Goldammer, J.G. (Eds.), *Fire in the Environment: the Ecological, Atmospheric and Climatic Importance of Vegetation Fires*. Report of the Dahlem Workshop, Berlin, 15–20 March, 1992'. Atmospheric Chemistry Department, Max Planck Institute for Chemistry, Mainz, Germany, pp. 53–76.
- Webster, J.P., Kane, T.J., Obrist, D., Ryan, J.N., Aiken, G.R., 2016. Estimating mercury emissions resulting from wildfire in forests of the Western United States. *Sci. Total Environ.* 568, 578–586.
- Weiss-Penzias, P., Jaffe, D., Swartzendruber, P., Hafner, W., Chand, D., Prestbo, E., 2007. Quantifying Asian and biomass burning sources of mercury using the Hg/CO ratio in pollution plumes observed at the Mount Bachelor observatory. *Atmos. Environ.* 41 (21), 4366–4379.
- Wright, L.P., Zhang, L., Marsik, F.J., 2016. Overview of mercury dry deposition, litterfall, and throughfall studies. *Atmos. Chem. Phys.* 16, 13399–13416.
- Yokelson, R.J., Griffith, D.W.T., Ward, D.E., 1996. Open-path fourier transform infrared studies of large-scale laboratory biomass fires. *J. Geophys. Res.* 101 (D15), 21067–21080.

CHAPTER 7

AUSTRALIA'S CONTRIBUTION TO THE GLOBAL MERCURY BIOGEOCHEMICAL CYCLE

7.1 Preface

Chapter 7 provides a comparison between Hg observations from the Oakdale field site and GEOS-Chem model simulations. Modelling is commonly used to gain a greater understanding of spatial and temporal variability in data that cannot be gained from stationary observations. GEOS-Chem is the most widely utilised chemical transport model by the broader Hg scientific community to understand global Hg trends and drivers. To date estimates of Australia's global Hg contributions are extrapolated from Northern Hemisphere understanding of Hg drivers and inventories. Lack of observations made in Australia has made it difficult to determine if these inferences align with what is occurring within the Australian environment. In order to address this significant gap and to provide a broader understanding of the findings from previous chapters, Chapter 7 aims to determine how well GEOS-Chem captures observed seasonal variability and the natural sources and sinks in Australia based on Oakdale's findings. The Chapter is layout to provide an overview of the whole of Australia's Hg sources and sinks,

compared with other attempts to quantify Australia's Hg budget. It then provides an in-depth comparison of GEOS-Chem's simulations with Oakdale's observations.

The purpose of this chapter is to put the main findings of this thesis into a broader global context by comparing observations with modelled outputs. Analysis was limited in its approach to default mercury simulations and the single site observations presented in chapters 3-5. The information presented in this chapter is not intended for publication beyond the thesis itself. As such Chapter 7 has been formatted in a traditional thesis style.

7.2 Introduction

The global cycling of atmospheric mercury (Hg) means that once it is emitted into the atmosphere from both anthropogenic and natural sources it can be found ubiquitously throughout the environment (Gustin et al., 2008; Obrist et al., 2018; Schroeder and Munthe, 1998). Understanding the global distribution of Hg requires comprehensive knowledge of the sources, sinks, transport and chemistry (Amos et al., 2015). Ambient measurements alone are not able to fully quantify the spatial extent of deposition and emission sources and are often limited in their temporal scales (longest running ground-based monitoring site established in the 1970s) (Sprovieri et al., 2016). Comprehensive global transport models have been developed over recent decades in an attempt to better understand the global attributes of atmospheric Hg. However, considerable uncertainties remain regarding fate and transport. Therefore, ambient measurements are also required to evaluate model accuracy.

Mercury enters the environment from both natural and anthropogenic sources. Natural geogenic sources account for approximately 5-13% of total emissions (Agnan et al., 2016;

Amos et al., 2013; Driscoll et al., 2013). Anthropogenic sources account for approximately 30% of annual global Hg emissions (Pirrone et al., 2010; Streets et al., 2017; UNEP, 2013b). Legacy Hg comprises of mercury previously deposited from both natural and anthropogenic sources and account for 60% of total atmospheric Hg (Amos et al., 2015).

Once Hg is released into the atmosphere, it continuously undergoes deposition and re-emission, creating a dynamic global cycle (Schroeder and Munthe, 1998). Within the atmosphere, Hg exists in three operationally defined states, gaseous elemental mercury (GEM), gaseous oxidised mercury (GOM), collectively referred to as Total Gaseous Mercury (TGM), and particulate bound mercury (PBM). Once deposited, oxidised Hg can then be reduced (photochemically and/or biochemically) to GEM and re-emitted to the atmosphere, or it can bind with organic carbon and be sequestered into soil pools (Corbitt et al., 2011). The bidirectional exchange of Hg between the atmosphere and Earth's surfaces occurs via evasion, wet deposition, and dry deposition. All atmospheric forms of Hg (GEM, GOM and PBM) can be deposited onto terrestrial surfaces, however the pathway depends upon the form of Hg, the surface type and environmental conditions (Gustin, 2012). Continuous re-emission and lack of global inventories means there are considerable uncertainties with the estimates of re-emission to the atmosphere (Wang et al., 2006).

Atmospheric measurements and monitoring of Hg is undertaken globally, employing a combination of ground-based short-term and long-term monitoring sites and aircraft and ship measurements aimed at providing a complete understanding of global Hg cycling and behaviour (Slemr et al., 2015; Sprovieri et al., 2016). However, spatial variation between measurement locations, measurement heavily skewed towards the Northern Hemisphere, and emission sources and deposition processes make it difficult to adequately capture the entirety and complexity of the Hg cycle (Han et al., 2004; Keeler et al., 2005). Numerous methods have

been developed to better estimate source attributed Hg characteristics on regional to global scales, such as isotopic measurements (Demers et al., 2013; Sherman et al., 2015), back trajectories and chemical mass balance (Keeler et al., 2005; Lamborg et al., 2002) or scaling up flux measurement data (Agnan et al., 2016; Lindberg et al., 1998). A number of numerical models at both the regional and global scales have been developed to simulate the biogeochemical cycle and the fate and transport of anthropogenically and naturally emitted Hg (Kikuchi et al., 2013; Selin et al., 2008; Smith-Downey et al., 2010). However, uncertainties regarding chemistry, sources and storage persist within these methods. Observational measurements are needed to verify these spatially expansive methods and therefore a combination of both observation and modelling has the potential for a greater and extensive understanding of the global nature of Hg (Obrist et al., 2018).

Chemical Transport Models (CTMs) are commonly employed to assess the biogeochemical cycle of Hg and determine exchange and storage between and with terrestrial and ocean reservoirs. CTMs simulate Hg cycling by employing up-to-date understanding of Hg emission, transport, atmospheric redox reactions, and deposition (Driscoll et al., 2013). However, not all CTMs utilise the same atmospheric depositions and land emission mechanisms, leading to inconsistencies between model output (Selin et al., 2008). Previously, CTMs either chose to neglect the complexity of natural emission, often incorporating it into global background emissions or over-simplifying the processes, leading to a limited understanding of natural Hg sources and sinks. Work by Selin et al. (2008) and Smith-Downey et al. (2010) attempted to better incorporate natural terrestrial Hg sources and sinks in GEOS-Chem chemical transport model which utilised mass balance and mechanistically-driven processes to simulate air-surface exchange. Smith-Downey et al. (2010) in their global terrestrial mercury model explored Hg's relationship for the carbon cycle to better estimate Hg cycling and long-term storage (Figure 1).

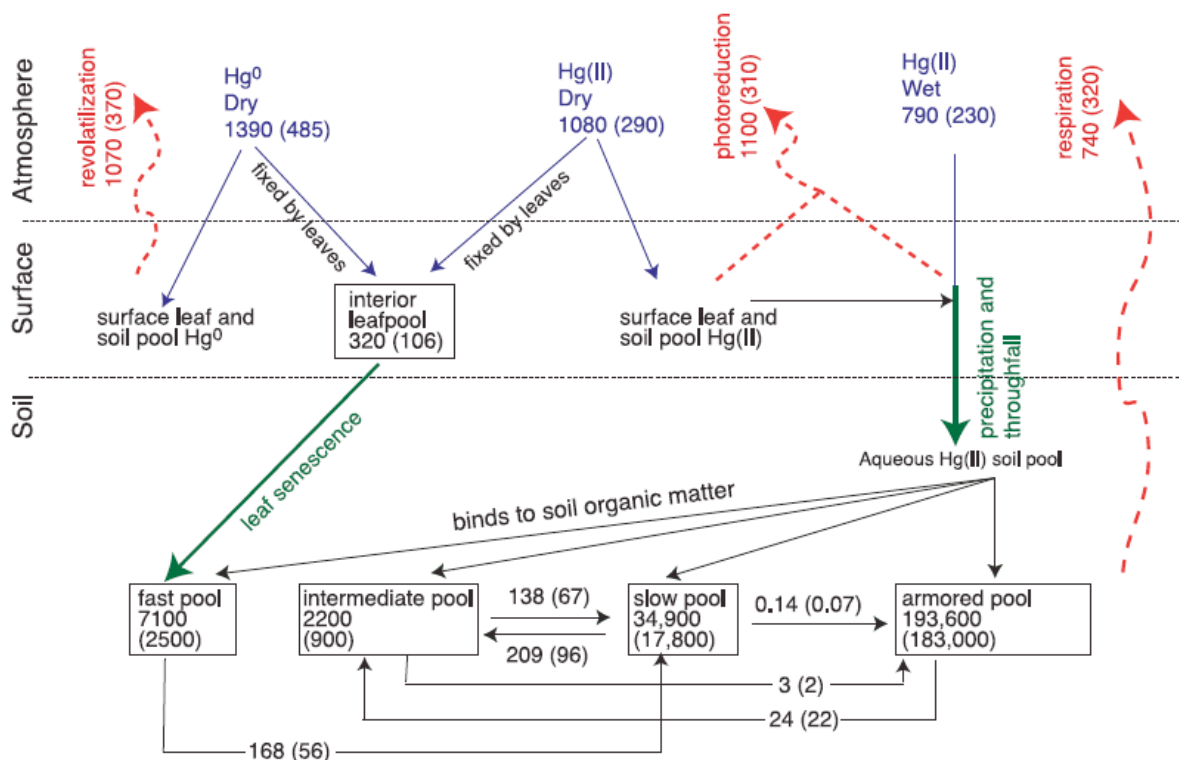


Figure 1. Schematic of the global terrestrial mercury model (GTMM). Boxes represent pools tied to carbon cycling in the model. Numbers in the boxes give the present-day storage of mercury (Mg), and other numbers give mercury fluxes in and out of pools (Mg yr⁻¹). Numbers in parenthesis are preindustrial values. Deposition of Hg⁰ and Hg²⁺ are taken from the GEOS-Chem mercury simulation [Selin et al., 2008]. Mercury enters organic soils by either leaf senescence or washoff and wet deposition of Hg²⁺ (green arrows). Soils emit mercury to the atmosphere via revolatilisation, photoreduction, and respiration (red arrows) (Smith-Downey et al., 2010).

GEOS-Chem is the most widely utilised CTM for the modelling of Hg biogeochemical cycling by the broader scientific community. The model represents the most up-to-date understanding of atmospheric Hg transport and fluxes. GEOS-Chem mercury simulation was developed to estimate biogeochemical cycling of Hg and determine the fate of anthropogenically emitted Hg within the environment on a global scale (Kikuchi et al., 2013). It utilises a seven box model comprised of fully coupled ocean (surface, sub-surface, and deep), terrestrial (fast, slow, and armoured soil pool) and atmosphere reservoir (Amos et al., 2013). Understanding of Hg air-surface exchange within terrestrial environments is one of the largest uncertainties that remain

in the GEOS-Chem model (Kwon and Selin, 2016). Bidirectional exchange of Hg is an extremely important component of the global Hg cycle. However, the highly coupled process of deposition and emission are treated as two separate processes within the model. Dry deposition is determined using the resistance-based approach and stomata and non-stomata uptake. However, this approach does not consider physiological processes of vegetation's response to varying environmental conditions within the ecosystem (Hicks et al., 2016; Wu et al., 2018). Surface emissions of Hg are treated as a function of substrate Hg concentration, solar radiation and temperature.

Extensive modelling has taken place across the Northern Hemisphere. However the Southern Hemisphere remains largely neglected. The large ratio of ocean to land and significantly less anthropogenic sources implies that Hg cycling in the region behaves differently than in the Northern Hemisphere (Zhu et al., 2016). Understanding of the Southern Hemisphere Hg cycling has primary been hampered by limited observation undertaken here (Soerensen et al., 2012). Australia is one of the largest landmasses in the Southern Hemisphere. Despite this little is known about Australia's sources and sinks (Edwards and Howard, 2013). Current emission inventories have found that 93% of Australia's total emissions come from natural sources, while only 7% is emitted from anthropogenic sources (Nelson et al., 2009; Nelson et al., 2012). Attempts to understand Australia's natural cycle in the past have been determined as part of global modelling studies and do not consider Australia's unique flora, fauna, soil type and diverse climate. Greater understanding of Australia's global contributions is needed if Australia wishes to meet the goals outlined by the global Minamata convention on mercury, of which Australia is a signatory, but still yet to ratify.

Despite significant advancement these models still do not adequately account for the mechanisms involved in enhancing and suppressing Hg flux from terrestrial environments.

Furthermore, lack of observation measurements undertaken in the Southern Hemisphere and specifically in Australia means that global contributions for these regions are largely estimated based on Northern Hemisphere emission and deposition drivers. This chapter aims to determine how well GEOS-Chem captures Australia's natural emission sources and its variability based on observational findings outlined in the previous chapters and previous attempts to model Australia's natural source emissions.

7.3 Methods

In order to assess how well the current understanding of Hg cycling in Australia aligns with observed measures of Hg cycling, GEOS-Chem biogeochemical Hg model outputs were compared with the 2017 observations made at Oakdale field site (presented in Chapters 3-5). Comparison is restricted to elemental mercury (Hg^0) to optimise compatibility with modelled output. Reactive mercury measurements made at Oakdale are not included in this chapter as the coarse time resolution and measurement gaps meant that observations were not sufficient to compare with modelled output.

7.3.1 GEOS-Chem model

GEOS-Chem chemical transport model was employed to simulate Australia's Hg cycle and for comparison with observations. Default simulations were run using GEOS-Chem V11-01 driven by assimilated meteorology from the NASA Goddard Earth Observing System Forward Processing (GEOS-FP) data product, at $2^\circ \times 2.5^\circ$ horizontal resolution and 47 vertical levels from the surface to 0.01 hPa. The model includes a 3D atmosphere coupled to a 2D ocean slab and terrestrial reservoir. The emissions inventories for global anthropogenic Hg emissions are taken from the United Nations Environment Programme (UNEP) for 2010 (AMAP/UNEP,

2013). Biomass burning Hg emissions are taken from the Global Fire Emissions Database and Fire Inventory from NCAR. The period January 2013 to December 2017 was simulated at monthly temporal resolution to provide an overview of Australia's total contributions. 2017 was also run at daily temporal resolution in order to compare modelled simulations with observation values. An initial 5-year spin-up was run for 2013 to achieve steady state concentration for the size of the Hg reservoir within GEOS-Chem. The spin-up repeated simulations for the year 2013 until the repeated simulation outputs were within 5% of each other.

The atmospheric redox chemistry in GEOS-Chem uses a two-step oxidation mechanism with Br, BrO, O₃ and OH available for the oxidation Hg⁰ to Hg²⁺. The reduction of Hg²⁺ to Hg⁰ occurs as photoreduction in the aqueous-phase and is scaled to NO₂ photolysis frequency, which is used as a proxy for the UV actinic flux (Song et al., 2016). GEOS-Chem uses a monthly mean value for Br concentrations (taken from the separate bromine simulation) that varies between each grid box (2° x 2.5°) in the model. This is designed to capture the spatial variability. The fast reaction rates in the atmosphere means that the monthly Br concentrations are limited in their ability to capture the temporal variability of Hg chemistry.

Biomass burning emission rates are determined using the Hg/CO emission ratios determined by (Friedli et al., 2009), from observational measurements. Within GEOS-Chem an emission ratio of 2.1×10^7 is applied to a monthly gridded climatological inventory of biomass burning CO emissions and all emissions is assumed to occur in the form of Hg⁰.

Global mean soil concentration of 50 ng g⁻¹ is applied uniformly across the terrestrial surfaces. A spatial scaling factor of 15% is applied globally to increase soil concentration following the present-day anthropogenic deposition pattern. GEM evasion included volatilization from soil and rapid recycling of newly deposited Hg. The former was estimated as a function of soil Hg

content and solar radiation. The latter was modelled by recycling a fraction of wet/dry deposited RM to the atmosphere as GEM immediately after deposition (60% for snow covered land and 20% for all other land surfaces) (Selin et al., 2008). Soil volatilization as a function of solar radiation is determined by the following Zhang et al., 2001 equation:

$$E = \beta C_s \exp(\alpha R_g)$$

Where E is soil emission, C_s is the soil mercury concentration (g g^{-1}), R_g is the solar radiation flux at the ground, and $\alpha = 1.1 \times 10^3 \text{ m}^2 \text{ W}^{-1}$. The scaling factor $\beta = 0.02 \text{ gm}^{-2} \text{ h}^{-1}$ is derived here from global mass balance in the preindustrial period, as described by Selin et al. (2008).

Dry deposition of Hg is based on the dry deposition velocities and resistance in series methods developed by (Wesely, 1989). Dry deposition can only be calculated over terrestrial surfaces and decoupled from surface emissions, and therefore bidirectional exchange cannot accurately be determined by GEOS-Chem simulations.

Dry deposition velocity is calculated by (Gustin et al., 2011):

$$F = V_d C$$

Where:

- F = flux;
- C = the concentration of the species of interest; and
- V_d = the dry deposition velocity.

And the resistance in series method (Wesely, 1989):

$$V_d = \frac{1}{(R_a R_b R_c)}$$

Where:

- R_a = the is the aerodynamic resistance;
- R_b = the near-surface boundary-layer resistance (or quasi-laminar subsurface resistance); and
- R_c = the surface resistance term that is applied for leaf and soil surfaces.

Mercury wet deposition in GEOS-Chem is simulated for rainout and washout during large-scale and convective precipitation using Henry's law constants (Selin et al., 2007). Henry's law determines the amount of gas that can be dissolved into a liquid at a given temperature and pressure (Lin and Pehkonen, 1999). Reactive Hg is highly soluble in water and therefore is readily scavenged from the atmosphere via wet deposition processes. GEM is relatively insoluble in water and as such is difficult to remove from the atmosphere in this way (Seigneur et al., 2001). Because of this, wet deposition was only modelled for reactive Hg as GEM's Henry law constant is too low to accurately calculate deposition (Selin et al., 2007). GEOS-Chem uses a Henry's law constant of $1.4 \times 10^6 \text{ M atm}^{-1}$ for reactive Hg to determine the rate at which it is deposited to the surface.

To determine the capability of GEOS-Chem to reproduce the observed Hg^0 concentrations, statistical analysis was undertaken to determine the mean difference (MD) as detailed in the equation below:

$$MD = \frac{1}{N} \sum 1, N \left(\frac{M - O}{O} \right)$$

where:

M = the predicted value from the model simulation;

O = the observed values from measurement; and

N = the sample size.

7.3.2 Observation methods

GEOS-Chem simulations for 2017 were compared to observation measurements made at Oakdale background site to assess and compare how well modelled values align with these observations. Gaseous Elemental Mercury (GEM) fluxes were measured using the micrometeorological aerodynamic flux gradient method described in detail by Edwards et al. (2005) and provided in Chapter 3. GEM gradients were constructed from samples taken at two heights and quantified using a Tekran 2537B (Tekran Instruments, Knoxville, TN, USA), with detection limit of 0.01 ng m^{-3} . Density corrections due to water vapour were undertaken according to Webb et al. (1980). Sample air was drawn from the sample inlets through a $0.2 \text{ }\mu\text{m}$ polytetrafluoroethylene (PTFE) filter by a PTFE pump drawing at 10 lpm. The 2537B subsampled from this flow through an additional $0.2 \text{ }\mu\text{m}$ PTFE filter. Switching of sampling between the intakes took place every 10 minutes ($2 \times 2537\text{B}$ samples). Ambient GEM concentrations were also quantified using the Tekran 2537B to provide 5-minute continuous samples. Automated calibration of the 2537B was obtained every 23 hours throughout the study using the internal mercury permeation source. Permeation sources were verified at the beginning and end of the study, as well as at the approximate half-way point of the study (September, 2017).

Standard quality assurance methods were applied to the micrometeorological data based on the constraints of Monin-Obukhov similarity theory. This included filtering for low wind speeds ($<0.5 \text{ m/s}$ for the sonic anemometer) and wind direction, to allow for sufficient fetch. Additionally, since the flux is determined from $1\frac{1}{2}$ hours of concentration data, data were also filtered for when stability assumptions were not met. Oakdale observation fluxes were also scaled up from $\text{ng m}^{-2} \text{ h}^{-1}$ to $\mu\text{g m}^{-2} \text{ d}^{-1}$ to be equivalent to GEOS-Chem's temporal resolution.

7.4 Results and Discussion

7.4.1 Australia's Hg Cycle

Figure 2 shows modelled average atmospheric Hg^0 concentration distribution and monthly source contributions for Australia. Overall, Hg concentrations show a slight latitudinal gradient over the ocean and lower terrestrial concentrations compared with oceanic concentrations. Three observation sites are also included (Cape Grim, Gunn Point and Oakdale [focus of this study]) to provide a comparison with modelled output. Gunn Point annual average concentration is 0.95 ng m^{-3} (Howard et al., 2017), similar to GEOS-Chem output, however, both Cape Grim (Howard, 2017) and Oakdale observations indicate lower Hg concentrations than the model output (0.88 ng m^{-3} and 0.68 ng m^{-3} respectively).

Figure 2 (right) shows the monthly source attributions for Australia. Source contribution was averaged over the same grid area shown in Figure 2 (left). Overall, Australia experiences net deposition to the surface. Terrestrial emissions in the region are primarily driven by soil evasion, followed by anthropogenic releases. Most emission sources are relatively constant, with the exception of biomass burning which increases in austral spring (September, October, November). Wet deposition appears to be the largest driver of the overall flux trends, showing strong seasonality, highest wet deposition occurring in during the warmer months (September to February). Figure 2 (right) also shows a significant proportion of Hg emissions coming from the ocean, which could be skewing the overall sources attributed to the region. The majority of Hg emitted from the ocean surface is deposited back to the ocean before reaching inland (Mason and Sheu, 2002).

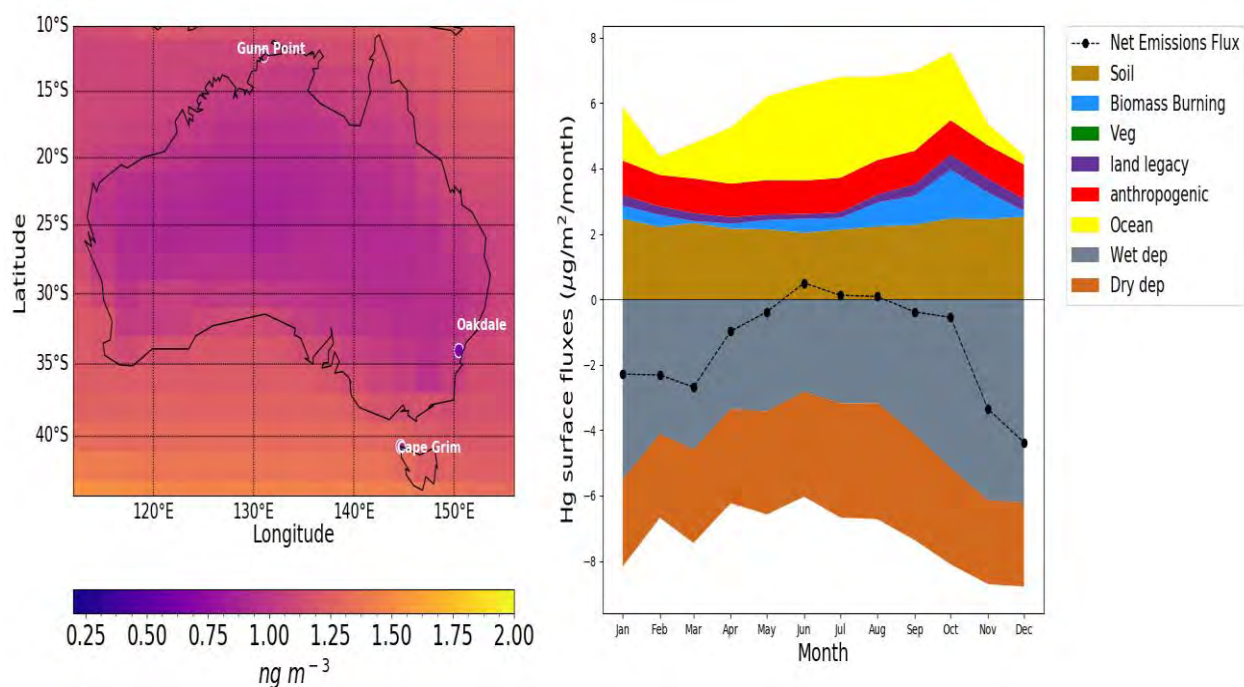


Figure 2 Australian atmospheric Hg^0 concentration distribution (left) and Australian surface fluxes (right) for latitudes 10° to 45° south and longitudes 110° to 155° east. Soil is soil Hg emissions, veg is vegetation Hg emissions, land legacy is Hg emissions from legacy sources, anthropogenic is anthropogenic Hg emission sources. Wet dep and dry dep is wet and dry Hg deposition, respectively. GEOS-Chem output averaged for 2013-2017.

Total loadings to the atmosphere, based on GEOS-Chem simulations, was 116.57 Mg a^{-1} . Soil and ocean emissions accounted for the greatest sources of Hg to the atmosphere 45.1 Mg a^{-1} and 35.40 Mg a^{-1} , respectively (Table 1), anthropogenic emissions accounted for 20.43 Mg a^{-1} . Nelson et al. (2012) estimated a total emission of 148 Mg a^{-1} from natural sources and 15 Mg a^{-1} from anthropogenic sources. Page (2017) estimated a total Hg budget of $110\text{-}144 \text{ Mg a}^{-1}$, which included ocean and anthropogenic evasion. Page (2017), estimates were determined from GEOS-Chem simulations, using inverse ocean simulations and updated chemistry as described by (Horowitz et al., 2017). Natural emissions accounted for 93 Mg a^{-1} , which is lower than simulated by Nelson et al. (2012). Differences between the different modelled values is likely due to the differences in how the rates of natural emissions are calculated. Nelson et al. (2012) estimated natural emissions based on activation energy within the substrate and

evapotranspiration. Whereas, GEOS-Chem uses a solar constant and air resistance to determine natural emissions.

Table 1. Comparisons of Hg Budget of Australia (rates are in Mg a⁻¹) determined using GEOS-Chem here and Hg budgets determined by Page (2017) and Nelson et al., (2012).

	This study Mg a⁻¹	Page (2017) Mg a⁻¹	Australia (Nelson et al. 2012)
Anthropogenic	20.43	18.3 - 20.1	10 - 20
Biomass	10.07	10.3 - 10.6	21 - 63
Soil	45.1	45.6 - 46.5	70 – 210
Geogenic	N/A	5.5 - 10.3	N/A
Land Legacy	5.57	5.4 - 5.7	N/A
Ocean (net)*	35.40	24.7 - 50.9	N/A
Total Sources	116.57	109.9 - 144.2	105 – 305
Deposition Dry	58.66	54.5 - 56.9	N/A
Deposition Wet	85.16	60.5 - 84.4	N/A
Total Sinks	143.82	115.1 - 141.3	N/A
Net Emissions Flux	-27.25	-5.1 - 2.9	N/A

* Ocean (net) is for ocean sources that fall within latitudes 10° to 45° south and longitudes 110° to 155° east around Australia's main land mass

7.4.2 Surface emissions

In order to explore how well Australian estimates match with observation, modelled results were compared to observations made at Oakdale. Figure 3 shows daily variability for the 2° x 2.5° grid square surrounding the Oakdale field site and is limited to GEM emissions. Net Emission Flux (NEF) is calculated by the addition of all sources, minus dry deposition. In order to be comparable with Oakdale observations only GEM and dry deposition are compared here

as reactive mercury and wet deposition were not directly measured at the site. Overall, GEOS-Chem NEF shows net emissions during austral summer (December, January, February) and autumn (March, April, May) and net deposition during winter and spring (Figure 3). The overall trend is a similar trend to Oakdale observations. However, observations exhibited greater variability. As with the whole of Australia, soil emissions (which is Hg stored in the substrate) are the dominant emission source for the region. Soil emissions follow the same seasonal trend as the observations, although emissions were still substantial throughout the year. Land legacy emissions are the second largest contributor to Hg emissions. Land legacy emissions are largely determined by the re-emission of previously deposited Hg from the surface. Highest land legacy re-emissions occurred during austral spring and summer. Limited land legacy emissions were experienced during winter.

Observation fluxes are higher than the NEF, showing a greater magnitude and variation, however the overall averages are still within range of the modelled values (Table 2). NEF was within range of the few flux studies that have taken place in Australia. Hg fluxes measured in the alpine region of Australia during austral summer had an average flux of $0.2 \text{ ng m}^{-2} \text{ h}^{-1}$, with an overnight average of $-1.5 \text{ ng m}^{-2} \text{ h}^{-1}$ and a daytime average of $1.8 \text{ ng m}^{-2} \text{ h}^{-1}$ (Howard and Edwards, 2017). Hg fluxes undertaken at a background site near central New South Wales presented with similar values, averaging $0.36 \text{ ng m}^{-2} \text{ h}^{-1}$ undertaken during austral winter (Edwards and Howard, 2013). Average observed Hg fluxes at Oakdale were lower, although still with range of these values ($0.002 \text{ ng m}^{-2} \text{ h}^{-1} \pm 14.23 \text{ ng m}^{-2} \text{ h}^{-1}$). Recent evaluation of GEOS-Chem's terrestrial cycling found that surface emissions did not capture the observed diel cycle. Modelled values still exhibited overnight emission despite most observation studies experiencing either zero emissions overnight or deposition (Khan et al., 2019). Page (2017) also noted that GEOS-Chem failed to capture the appropriate daily variability, despite reasonable overall agreement between modelled and observed values.

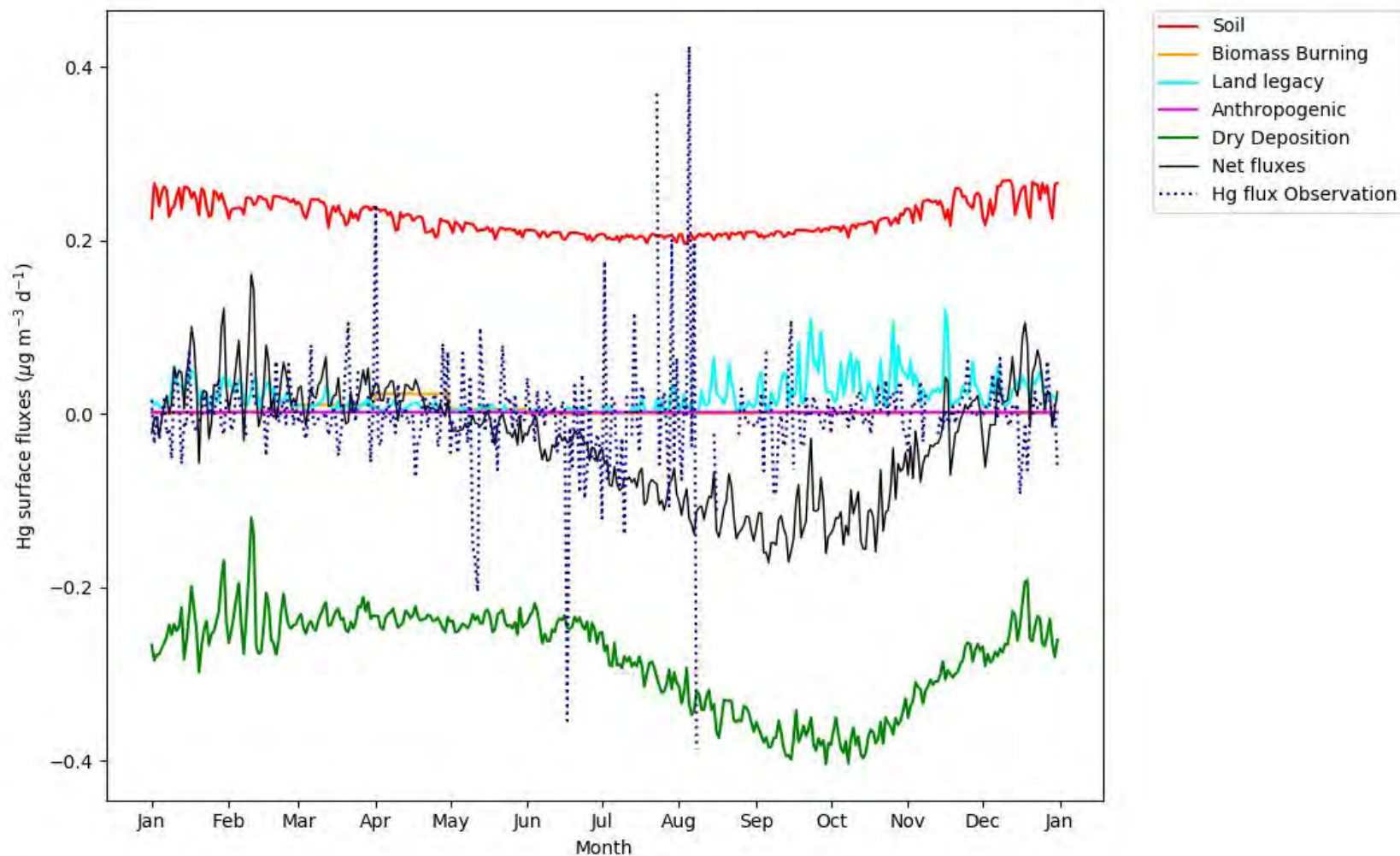


Figure 3. Daily simulated terrestrial surface Hg fluxes and Hg⁰ dry deposition for the 2° x 2.5° grid square surrounding Oakdale field site, along with observation Hg flux measurements made at Oakdale for 2017. Soil is soil Hg emissions, land legacy is Hg emissions from legacy sources, anthropogenic is anthropogenic Hg emission sources, Net fluxes are GEOS-Chem net emission sources + Hg dry deposition.

Despite overall similar seasonal trends GEOS-Chem Hg soil emissions alone are almost double observation values. This overestimation may be largely attributed to the nature of the observation site. Terrestrial surface emissions are significantly influenced by meteorology, substrate properties and dry deposition processes (Pirrone et al., 2010). Despite, Oakdale substrate concentrations (68 ng g^{-1}) being similar to the substrate concentrations used by GEOS-Chem to estimate soil emissions ($50\text{-}70 \text{ ng g}^{-1}$) (Selin et al., 2008). GEOS-Chem still overestimates the amount of Hg released from soils, indicating that more Hg may be trapped within the substrate than is assumed by the model. Background sites have been shown to be largely driven by atmospheric deposition driving the amount of Hg available for re-emission.

Previous studies have found that once Hg is bound in the substrate below depths of 7cm it is no longer available for emission (Demers et al., 2013; Obrist et al., 2014). Modelled attempts have also found the surface fast response pool to be the greatest driver of surface evasion, with little emitted from slow response or armoured pools (Amos et al., 2013). Therefore, release from soils is likely less than what is currently assumed for the model. Chapters 3 and 5 identified that solar radiation had a significant influence on the emission of Hg from the substrate and atmospheric Hg concentrations, particularly during the warmer months when solar radiation was highest. As the model uses solar radiation to parameterise Hg surface emissions, it is unsurprising that they follow a similar seasonal trend.

Land legacy Hg emission variation followed Oakdale observation emissions much more closely than GEOS-Chem soil emissions and NEF. This suggests that land legacy emissions may be the dominant source of Hg to the atmosphere rather than soil emissions alone, as suggested by the model output. The previous chapters also identified that the site relied on atmospheric deposition for the re-emission of GEM to the atmosphere. As land legacy emissions most closely follow observation variability it further confirms that the site is reliant

on atmospheric deposition to drive its air-surface exchange. Currently GEOS-Chem only uses 20% of deposited Hg for immediate re-emission which makes up the majority of land legacy re-emissions (Selin et al., 2008). However, Gustin et al. (2015) noted that under field conditions is it almost impossible to differentiate between Hg that is undergoing fast response re-volatilisation and Hg that is being released from longer-term soil storage. Therefore, it is plausible that the difference between land legacy emissions and the observed emissions is Hg being released from longer-term Hg stores.

Table 2. Seasonal Hg source average based on GEOS-Chem output for the 2° x 2.5° grid square surrounding Oakdale field site with observation measurements made at the Oakdale field site.

Units		Summer		Autumn		Winter		Spring		Annual	
		Mean	SD	Mean	SD	Mean	SD	Mean	SD	Mean	SD
Soil	$\mu\text{g m}^{-2} \text{ d}^{-1}$	0.25	0.01	0.22	0.01	0.21	0.00	0.22	0.02	0.27	0.02
Biomass Burning	$\mu\text{g m}^{-2} \text{ d}^{-1}$	0.00	0.00	0.01	0.01	0.00	0.00	0.00	0.00	0.00	0.01
Land Legacy	$\mu\text{g m}^{-2} \text{ d}^{-1}$	0.03	0.01	0.01	0.01	0.01	0.01	0.04	0.03	0.02	0.02
Wet deposition	$\mu\text{g m}^{-2} \text{ d}^{-1}$	0.30	0.56	0.12	0.30	0.09	0.26	0.24	0.49	0.19	0.28
Dry deposition	$\mu\text{g m}^{-2} \text{ d}^{-1}$	0.25	0.03	0.24	0.01	0.29	0.04	0.35	0.04	0.28	0.06
NEF	$\mu\text{g m}^{-2} \text{ d}^{-1}$	0.03	0.04	0.01	0.02	-0.08	0.04	-0.09	0.06	0.009	0.05
Observation flux	$\mu\text{g m}^{-2} \text{ d}^{-1}$	0.02	0.19	-0.01	0.17	-0.01	0.08	0.01	0.19	0.00	0.22
Observation dry deposition	$\mu\text{g m}^{-2} \text{ d}^{-1}$	0.14	0.14	0.20	0.14	0.16	0.09	0.12	0.08	0.17	0.12
Observation deposition velocity	cm s^{-1}	0.02	0.06	0.04	0.07	0.05	0.07	0.03	0.05	0.03	0.06
MD	%	70.60		-14.29		533.33		975.00		1800.00	

7.4.3 Terrestrial deposition

Beyond meteorology and substrate properties driving surface evasion, deposition also plays a key role, both by determining spatial distribution and influencing what is available for immediate reemission from the substrate. As a background site, Oakdale's surface concentrations are largely determined by deposition (Gustin et al., 2006). Figure 4 shows modelled deposition trends (both wet and dry deposition trends), and rainfall with observed dry deposition and deposition velocity. Modelled dry deposition shows slight seasonal variation, peaking mid-spring and decreasing in autumn and winter. Observed dry deposition exhibits the opposite trends, peaking in winter and decreasing during the warmer months. GEOS-Chem determines dry deposition based on dry deposition velocity (Gustin, 2012) and resistance-in-series methods (Wesely, 1989). As this approach is based on boundary layer properties it is plausible that this may be causing the seasonal differences between modelled and observation values.

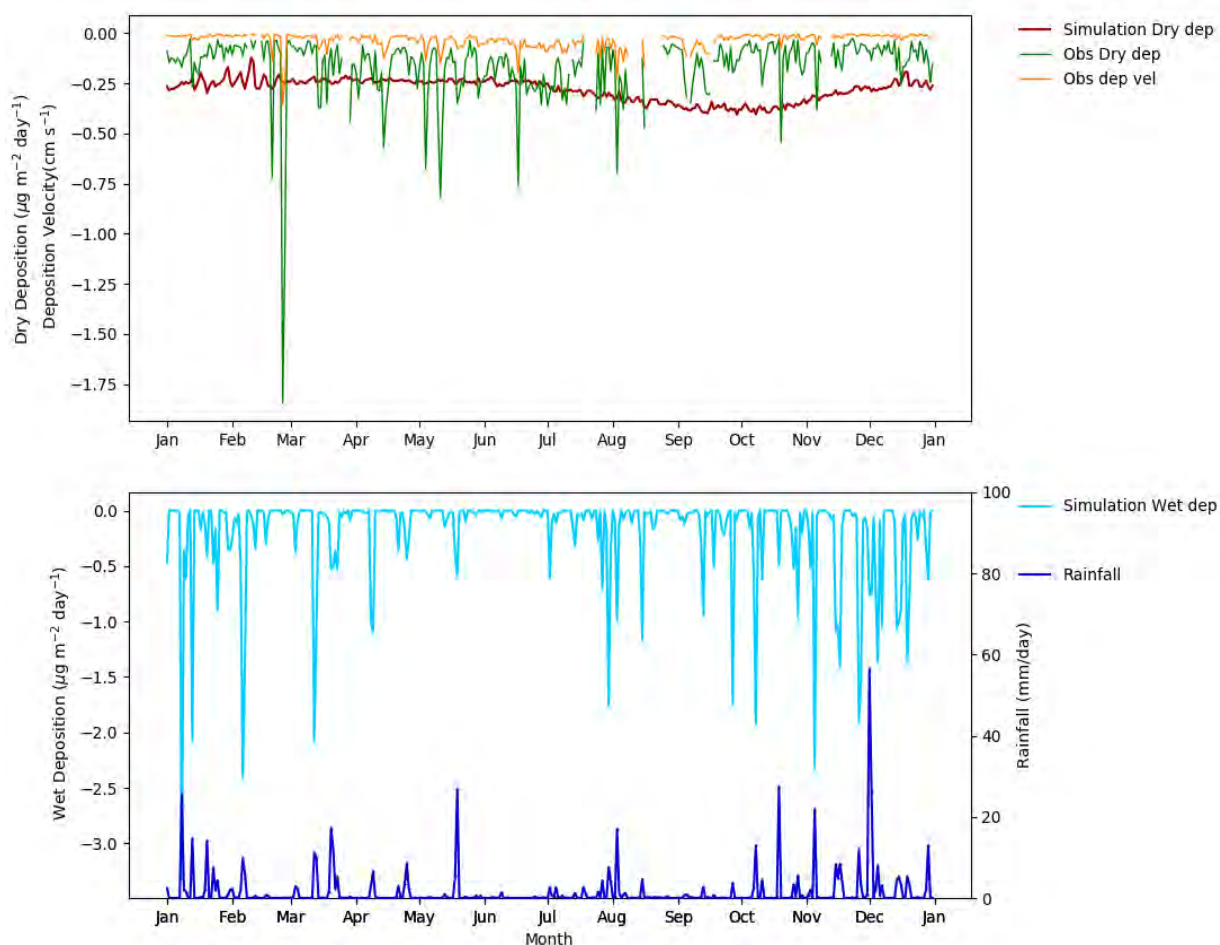


Figure 4. Daily simulated Hg^0 dry deposition, along with observed dry deposition and observed dry deposition velocity at Oakdale for 2017 (Top). Reactive Hg wet deposition and rainfall for the $2^\circ \times 2.5^\circ$ grid square surrounding Oakdale field site (Bottom).

Calculated average deposition velocity for the observed measurements was 0.034 cm s^{-1} (Table 2), which aligns with the current velocity used by GEOS-Chem when determining dry deposition (0.03 cm s^{-1}) (Selin et al., 2008). Deposition velocities are also similar to those recorded for typical background sites which generally have a deposition velocity less than 0.05 cm s^{-1} (Zhang et al., 2009), indicating the values presented here are not out of the normal for a background field site. Both the observed and modelled deposition velocities were higher than those previously observed in Australia. Deposition velocities calculated over bare soils during

winter averaged 0.004 cm s^{-1} , while summer alpine grass had a deposition velocity of 0.002 cm s^{-1} (Edwards and Howard, 2013; Howard and Edwards, 2017).

GEOS-Chem dry deposition values were higher than those observed at Oakdale, averaging $0.28 \mu\text{g m}^{-2} \text{ d}^{-1}$, while Oakdale experienced an average dry deposition of $0.17 \mu\text{g m}^{-2} \text{ d}^{-1}$. Oakdale also experienced significantly more diel variability than the GEOS-Chem simulations (Table 2). Observed annual GEM dry deposition values are similar to those seen at other background sites ($62.15 \mu\text{g m}^{-2} \text{ a}^{-1}$). A South-East Asian background site recorded a multi-year annual dry deposition of $66.1 \mu\text{g m}^{-2} \text{ a}^{-1}$ (Phu Nguyen et al., 2019). Nelson et al. (2009) estimated an annual dry deposition significantly less than the modelled GEOS-Chem values ($102.20 \mu\text{g m}^{-2} \text{ a}^{-1}$), averaging $21 \mu\text{g m}^{-2} \text{ a}^{-1}$. Vegetation type and coverage is spatially highly variable in the region of Oakdale and is therefore likely to vary within the model grid square. Vegetation at Oakdale was limited to surface grass and found to have little influence on Hg surface exchange. However, within the grid square is dense forest and sparse agricultural grazing fields which could be influencing the modelled deposition rate.

Dry deposition of Hg is assumed to increase during vegetation growing seasons as stomatal uptake increases (Hartman et al., 2009). This trend is seen in the modelled dry deposition, where deposition is greatest during spring when vegetation growth is greatest. However, this trend does not align with observation trends. As dry deposition is determined by resistance in series, which is in turn determined by leaf-area index, it is unsurprising that modelled trends follow an assumed growing season. However, using resistance-based calculations does not fully describe the physiological processes that may also influence dry deposition, such as vegetation stomatal responses to environmental conditions and lack of description of terrain complexity (Khan et al., 2019). While vegetation is a key determinant of dry deposition, the presence of vegetation at the Oakdale observation site was found to have little influence on Hg

exchange (Chapter 3, Paper 1). Dutt et al. (2009) found that total deposition fluxes at Glenville, New South Wales, were generally higher during the drier winter months, due to a combination of prevailing wind direction and lower mixing heights. Similar trends were seen at Oakdale where deposition rates were highest during autumn and winter, when it was also driest (Chapter 3, Paper 1).

Modelled Hg wet deposition was found to significantly influence variability of annual Hg trends. Overall though, wet deposition values were lower than dry deposition, averaging $0.19 \mu\text{g m}^{-2} \text{h}^{-1}$. However, as wet deposition measurements were not made at Oakdale field site it is not possible to compare modelled values with observed values. Modelled values here were slightly higher than other attempts to model wet deposition rates in Australia, with an annual value of $6.69 \mu\text{g m}^{-2} \text{a}^{-1}$, compared to Nelson et al. (2009) who estimated wet deposition to be $5 \mu\text{g m}^{-2} \text{a}^{-1}$. Both these values were significantly less than those observed by Dutt et al. (2009) who measured an annual average wet deposition of $29.13 \mu\text{g m}^{-2} \text{a}^{-1}$. However, these measurements were made in the vicinity of multiple coal-fired power plants which likely increased the amount of reactive Hg available for deposition. Modelled values however, do fall within the range of wet deposition observations for both the European monitoring station network and United States Mercury Deposition Network which reported ranges between $4\text{-}16 \mu\text{g m}^{-2} \text{a}^{-1}$ and $4\text{-}20 \mu\text{g m}^{-2} \text{a}^{-1}$, respectively (Travnikov et al., 2017).

7.5 Model verses observation evaluation

Comparisons between modelled and observed values was performed for modelled NEF with observed Hg flux and for modelled atmospheric GEM and observed atmospheric GEM (Figure 5). Correlations, in the form of linear least squares regression, between observed and simulated Hg fluxes were poor ($r = 0.02$), while model simulations and observed atmospheric GEM had

a strong and statistically significant correlation ($r = -0.69$, p -value < 0.05). Differences between Oakdale's observed atmospheric Hg and Hg fluxes suggest that GEOS-Chem is able to capture the overall atmospheric concentration but not the variability. This is likely because multiple interacting factors influence Hg exchange that also shift across temporal scales. Furthermore, the negative slope further indicates that GEOS-Chem is failing to accurately capture the seasonality seen in the observation measurements.

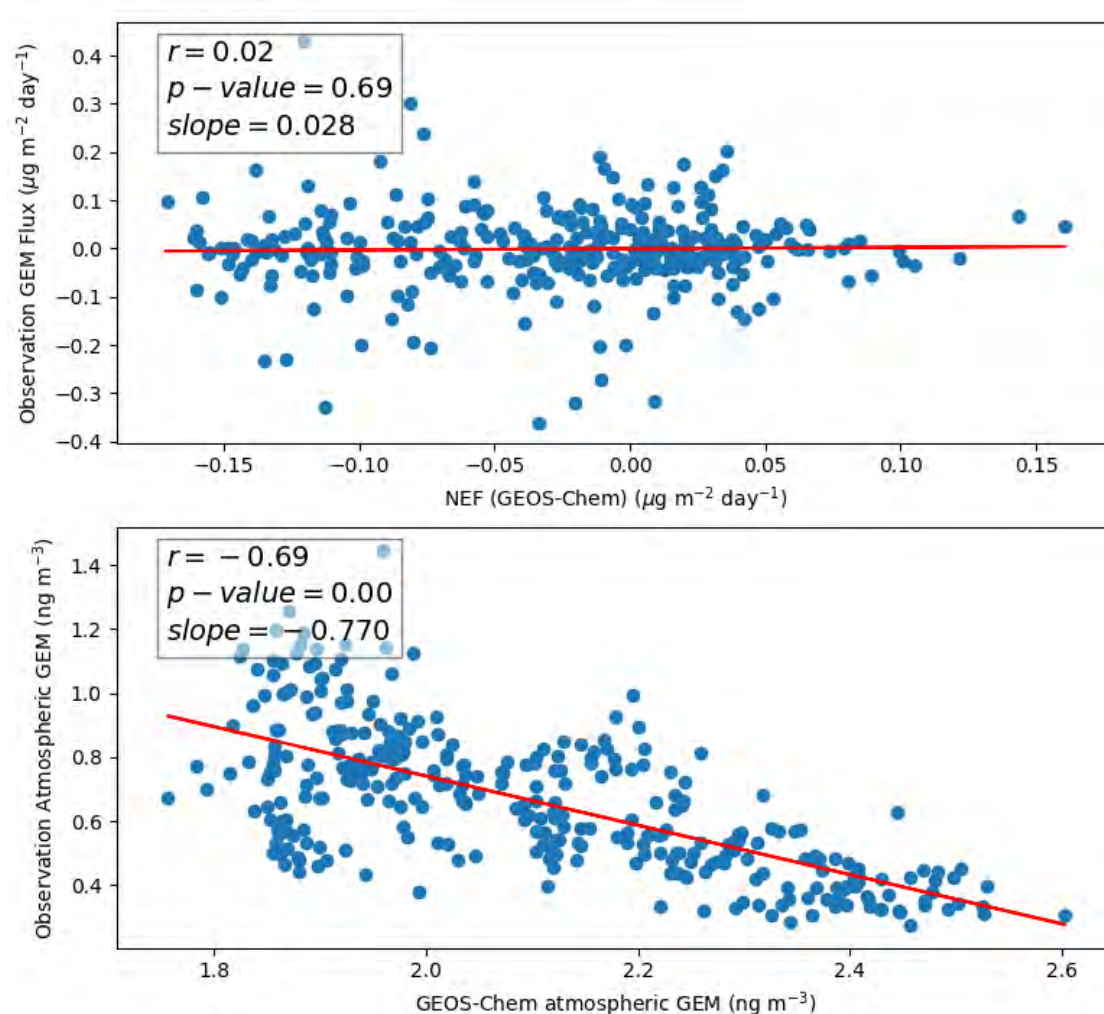


Figure 5. Linear least square regression for observation Hg flux with simulation NEF (GEOS-Chem) (top) and observation atmospheric Hg⁰ (ng m⁻³) with simulation atmospheric Hg⁰ GEOS-Chem (bottom).

Mean Difference (MD) values further indicate that GEOS-Chem fails to accurately predict Hg flux variability at Oakdale, overestimating annual emissions by 1800% (Table 2). Summer and autumn observations were the closest to modelled values, while winter and spring were dramatically overestimated. Page (2017) found that GEOS-Chem did not accurately simulate Hg characteristics found at an inland site in Glenville, New South Wales. The inability for GEOS-Chem to predict Hg characteristics at this site was attributed to the fact that Glenville was heavily influenced by local atmospheric conditions (Dutt et al., 2009) that could not be accurately captured when using a global transport model. Atmospheric GEM at Oakdale was also found to be influenced by variation in meso-scale atmospheric circulation across the year (Chapter 5, Paper 3). Spring's large overestimation is likely because the model assumes increased dry deposition during the growing season, leading to net deposition. However, Oakdale observations indicated increased emission caused by greater photo-reduction in the substrate. Autumn observations were the closest to modelled values (MD 14.11%), however, the model predicted net emission while the observations exhibited net deposition. The modelled emission value is most likely driven by the increased biomass burning emissions during this time. The close alignment between simulated values and observations during the warmer months is likely a reflection of natural surface emission within GEOS-Chem being a function of solar radiation and soil temperature which were also observed to be the dominant drivers of Hg surface emissions at the Oakdale field site.

7.6 Limitations and conclusions

The purpose of this chapter was to evaluate how well the understanding of natural Hg cycling in Australia developed here aligns with the current global understanding of Australia's Hg cycle. In order to achieve this, default GEOS-Chem simulation was run to simulate the sources

and sinks of Hg. This model was chosen as it represents the most scientifically up-to-date method for simulating the Hg cycle. Australia's Hg budget calculated here was 116.57 Mg a⁻¹ which was in range of previous attempts to quantify Australia's Hg budget. GEOS-Chem output did not accurately predict Hg exchange at Oakdale observation site, significantly overestimating net emission fluxes. This was largely driven by a significant over-estimation of dry deposition during spring and winter.

The comparison undertaken here only examines a single terrestrial site over a 12-month period. Comparison with a single site is likely too limited to accurately capture the Australia-wide contribution. Furthermore, the highly spatial and temporal variability of the Hg cycle is likely not fully represented by a single stationary site. However, GEOS-Chem results did agree with other multiple site studies. The daily and seasonal variability of the modelled simulations failed to accurately capture the high temporal variability seen in the observation data. Winter and spring concentrations tended to be over-estimated whereas autumn and summer agreed relatively well. Winter and autumn dry deposition trends were also underestimated. A combination of substrate properties and local air circulation is likely causing this difference. The use of a global model will not accurately simulate local atmospheric conditions which can heavily influence timing and magnitude of Hg air-surface exchange. Inclusion of more sites would help counteract this.

Better quantification of Hg storage in Australian substrate would better inform the life-time of Hg in the terrestrial environment. The observation study used for comparison was primarily driven by fast response re-emission at the surface. Mercury isotopes can be used to differentiate soil mercury between geogenic sources and atmospheric-derived mercury that has been incorporated into organic matter, thereby determining terrestrial storage (Demers et al., 2013). Analysis of this type has not been performed in Australia but would be useful for determining

how Hg is transferred to long-term storage and the amount of Hg currently stored there. As found in Chapters 3 and 5, Hg exchange at this site is largely driven by the atmosphere but it is unclear what is being transferred into the longer-term storage and what is undergoing immediate re-emission, and it is not possible to distinguish between the two using flux measurements alone.

Net Deposition was found to have a significant influence on the modelled values, however, observation values do not show the same trend. Dry deposition within GEOS-Chem is determined based on leaf area index influencing resistance terms. Variation in vegetation type and density with the Oakdale grid square is likely influencing modelled dry deposition rate causing them to be higher than observation values. Further, the influence of vegetation coverage on Hg deposition is largely unknown for Australia and as such comparison and understanding is limited. Further research is needed into the spatial variability of dry deposition in the Australian environment and how different vegetation types can influence these rates.

Overall, the Hg budget for Australia aligns with what has been previously modelled for Australia. However, daily variability is not captured well by the model, likely due to multiple interacting factors influencing Hg exchange on local scales. There is still a significant need to better quantify Australia's contributions across different vegetation types. There is also a need to update Australia's contribution and the global drivers of terrestrial Hg exchange. Deposition and emission processes are still treated separately despite being known to be a highly coupled process. Given the importance of atmospheric GEM as a source and sink to/from ecosystems and complex bi-directional exchange behaviour, an improved parameterisation of atmosphere-surface exchange of GEM on a global scale is needed to facilitate a better understanding of the principal mechanisms governing Hg dispersion and cycling in the atmosphere.

CHAPTER 8

KEY FINDINGS AND CONCLUSIONS

Mercury (Hg) biogeochemical cycling is a complicated and highly variable process, particularly in the terrestrial environment. The work presented here is one of the first long-term Hg air-surface exchange studies to take place in the Southern Hemisphere and clearly demonstrates the complexities of understanding the drivers and parameters affecting emission and deposition in the environment. Behaviour of Hg in the environment varies considerably across temporal and spatial scales due to variation in environmental conditions such as meteorological drivers, plant production, and atmospheric chemistry. The primary focus of this thesis was to determine key drivers of Hg's natural cycle within an Australian context. Understanding of the causes of variation across different and understudied ecosystems is vital for quantifying the global nature of Hg and better mitigating the environmental and health consequences.

Atmospheric GEM, RM and Hg⁰ flux concentrations were all low at the Oakdale field site, averaging 0.68 ng m⁻³ (±0.22 ng m⁻³), 2.41 pg m⁻³ (±1.68 pg m⁻³) and 0.002 ng m⁻² h⁻¹ (±14.23 ng m⁻² h⁻¹), respectively. Most notably atmospheric Hg was below the currently held background concentrations for the Southern Hemisphere. Temporal variations were driven by changes in chemical and physical drivers both in the atmosphere and at the surface. Winter exhibited the lowest atmospheric concentrations (0.43 ng m⁻³) and net deposition to the surface,

while summer experienced highest atmospheric concentrations (0.88 ng m^{-3}) and net surface evasion. RM 2-weekly concentrations also peaked in summer (3.43 pg m^{-3}) and were lowest in winter (1.93 pg m^{-3}). Removal from the atmosphere is facilitated by photochemical transformation of GEM to RM and subsequent wet and dry deposition. Relationships observed between ozone, specific humidity and Hg suggest both aqueous and gaseous phase oxidation appear to be playing a key role in the reduction of GEM to RM.

Hg fluxes overall experienced emissions during the day and deposition at night during the warmer months and net zero exchange or daytime deposition during the cooler months. Summertime evasion was driven by increased volatilisation and photoreduction of Hg. Higher temperatures and incoming radiation during the warmer months increased photoreduction in both the substrate and the atmosphere, increasing Hg evasion from the surface and producing higher concentrations within the atmosphere. Chapter 5's atmospheric trends follow a similar pattern, where higher summer atmospheric Hg concentrations were caused by increased surface evasion at the field site coupled with a change in atmospheric circulation patterns that transported urban polluted air masses to the field site. Spring photochemical oxidation heavily influenced atmospheric concentrations due to increased urban influences, while vegetation uptake and photoreduction influenced surface exchange.

Wintertime deposition appears to primarily be driven by a combination of vegetation uptake and reduced surface emission caused by lower incoming radiation and temperatures. Lower net radiation and temperatures observed during winter reduce the ability for volatilisation and reduction reactions to occur in the substrate, allowing vegetation uptake to drive Hg flux trends. Autumn Hg fluxes indicated little influence from environmental variables, with diel composite trends showing little variation. The lack of relationship was likely caused by decreases in photoreduction occurring in the substrate, reducing evasion, and senescence causing a reduction in deposition. This leads to an overall balance between emission and deposition in

the Hg fluxes. Circulation patterns during winter and autumn were also such that atmospheric Hg concentrations were driven by air masses transported from ocean sources or rural terrestrial surfaces leading to lower atmospheric concentrations.

Vegetation at Oakdale had with little influence over the net emissions. This is most likely because vegetation spatial coverage is not sufficient enough to be the dominant source or sink of Hg to the atmosphere, allowing soil emissions to drive Hg exchange. Spring diel Hg fluxes indicated emissions during the day and near zero exchange overnight, despite the strong negative CO₂ flux observed over the same time, indicating that the influence of temperature and solar radiation on the evasion of Hg from the substrate is greater than the rate of uptake by vegetation at this site. For grasslands/low vegetated sites to see significant vegetation uptake of Hg, the parameters that most influence Hg exchange, net radiation, and air and soil temperature, need to be simultaneously reduced.

Rainfall and soil moisture appear to have very little lasting influence on Hg fluxes at this field site, despite it commonly assumed to be key drivers of Hg surface evasion at background sites. Simultaneous spikes in both soil volumetric water content (VWC) and Hg emissions suggest that Hg was being forced from the substrate by the infiltrating water. As the water infiltrates the soil column Hg-containing air within the soil pores is displaced into the atmosphere, resulting in a spike in Hg emission. There is also little evidence to suggest the Hg fluxes are influenced by the change in VWC beyond this initial spike. Despite VWC averaging between 14.03% and 30.23% across the study duration, no enhancement in Hg fluxes was observed, contrary the literature stating otherwise. Further, when VWC reached above 30%, Hg flux suppression was also not observed contradictory to the findings of Briggs and Gustin (2013). As a background site, Oakdale's substrate Hg concentrations are largely driven by deposition processes which replenish the substrate Hg pool, it is possible the pool is easily depleted and not quickly replenished. Similar spikes in negative Hg fluxes demonstrate scavenging of Hg

from the atmosphere occurring alongside the spikes in emissions. This deposition is introducing Hg back to the substrate likely in the form of Hg^{2+} . However, the initial pulse in Hg emissions appears to be sufficient to deplete Hg stores within the substrate, while atmospheric deposition and Hg^{2+} reduction reactions in the substrate are insufficient to see any prolonged flux enhancement.

Release of Hg from soils and vegetation during fires is a significant source of Hg to the atmosphere, however, no efforts have been made to quantify actual rate of release within the Australian environment. Chapter 6 found that Hg release during biomass burning was less than previously assumed, largely due to low Hg concentrations in both vegetation and soils. Volatilisation of Hg was found to occur predominantly during the early flaming combustion phase of the burns when flame temperatures are highest. The majority of Hg stored within the biomass fuel was released during this initial stage. With the onset of smouldering combustion, Hg emissions were considerably lower. Emission ratios obtained during the flaming stationary stage of the experimental burns ($0.56 \pm 0.01 \times 10^{-7}$) were deemed to give the most realistic representations of Hg release from the fuels. Comparison with plume strike data collected from Cape Grim Baseline Air Pollution Station in Tasmania ($0.58 \pm 0.01 \times 10^{-7}$) confirmed this as the most appropriate value for estimating mercury release. These values are ~62% lower than the global average used previously to estimate Australian biomass burning mercury release. Hg emission rates obtained in this study resulted in a conservative Hg emission factor of $28.7 \pm 8.1 \mu\text{g kg}^{-1}$ for surface fuels, considerably lower than previous emission factors used in modelling emission of mercury from biomass burning in Australia.

The analysis undertaken here only represents a single site or in the case of Chapter 6 a single vegetation type. Further, the Hg flux concentrations presented here were low (close to method resolution) and highly variability. This therefore limits the ability to definitively state that the relationships and drivers of the Hg cycle identified here are indicative of the whole of Australia

or even South-Eastern Australia. More long-term flux studies need to be undertaken in Australia across the different climate and vegetation zones to better quantify how representative this site is of Australia's natural Hg cycle. Vegetation has been shown in the Northern Hemisphere to be a significant driver of Hg air-surface exchange, however, that was not found to be the case here. In order to gain a better understanding of the role of vegetation within the Australian environment, flux studies in regions with more substantial and variable vegetation cover are required. Australia experiences significant inter-annual variability in its rainfall. Therefore, multiyear studies are needed to determine if the lack of relationship observed between Hg flux and soil moisture persists when annual rainfall is higher or less than was observed in this study. As stated in Chapter 6, temperate eucalypt forests represent only a small and less regularly burned proportion of Australia's vegetation zone. Therefore, a greater understanding of Hg concentrations within different vegetation types, particularly savannah grasses, and release during both prescribed and wild fires is needed to better quantify Hg release from biomass burning. RM measurements made as part of this study were of coarse temporal resolution making it difficult to assess relationships with fast reacting photo-chemical oxidants. Therefore, finer resolution RM measurements are needed to better determine the nature of RM reactions and deposition patterns over terrestrial landscapes.

Understanding of Australia's contributions to the global mercury cycle is vital for ensuring Australia meets the requirements laid out in the Minamata convention. With limited anthropogenic sources across the whole of Australia, the natural component of the cycle is a primary contributor to Australia's Hg budget. As demonstrated throughout this thesis, Australia's climate has a significant impact on the rate and timing of terrestrial emissions and atmospheric transport to and from the continent. Measurements of Hg concentrations in ambient air support the conclusion that Hg deposited in remote areas may originate from

anthropogenic sources far away. Thus, Hg becomes a global problem not only affecting local areas that are heavily industrialised, but also areas that are remote from emitting sources.

REFERENCES

- Agnan, Y., Le Dantec, T., Moore, C. W., Edwards, G. C. & Obrist, D. 2016. New Constraints on Terrestrial Surface-Atmosphere Fluxes of Gaseous Elemental Mercury Using a Global Database. *Environ Sci Technol*, 50, 507-24.10.1021/acs.est.5b04013
- AMAP/UNEP, Arctic Monitoring and Assessment Programme/United Nations Environment Programme 2013. Technical background report for the global mercury assessment 2013.
- Amos, H. M., Sonke, J. E., Obrist, D., Robins, N., Hagan, N., Horowitz, H. M., Mason, R. P., Witt, M., Hedgecock, I. M., Corbitt, E. S. & Sunderland, E. M. 2015. Observational and modeling constraints on global anthropogenic enrichment of mercury. *Environ Sci Technol*, 49, 4036-47.10.1021/es5058665
- Amos, Helen M., Jacob, Daniel J., Streets, David G. & Sunderland, Elsie M. 2013. Legacy impacts of all-time anthropogenic emissions on the global mercury cycle. *Global Biogeochemical Cycles*, 27, 410-421.10.1002/gbc.20040
- Angot, H., Barret, M., Magand, O., Ramonet, M. & Dommergue, A. 2014. A 2-year record of atmospheric mercury species at a background Southern Hemisphere station on Amsterdam Island. *Atmospheric Chemistry and Physics*, 14, 11461-11473.10.5194/acp-14-11461-2014
- Angot, Hélène, Magand, Olivier, Helmig, Detlev, Ricaud, Philippe, Quennehen, Boris, Gallée, Hubert, Del Guasta, Massimo, Sprovieri, Francesca, Pirrone, Nicola, Savarino, Joël & Dommergue, Aurélien 2016. New insights into the atmospheric mercury cycling in central Antarctica and implications on a continental scale. *Atmospheric Chemistry and Physics*, 16, 8249-8264.10.5194/acp-16-8249-2016
- Ariya, P. A., Amyot, M., Dastoor, A., Deeds, D., Feinberg, A., Kos, G., Poulain, A., Ryjkov, A., Semeniuk, K., Subir, M. & Toyota, K. 2015. Mercury physicochemical and biogeochemical transformation in the atmosphere and at atmospheric interfaces: a review and future directions. *Chem Rev*, 115, 3760-802.10.1021/cr500667e
- Ariya, Parisa A. , Khalizov, Alexei & Gidas, Alexios 2002. Reactions of Gaseous Mercury with Atomic and Molecular Halogens: Kinetics, Product Studies, and Atmospheric Implications. *The Journal of Physical Chemistry A*, 106
- Bahlmann, E., Ebinghaus, R. & Ruck, W. 2006. Development and application of a laboratory flux measurement system (LFMS) for the investigation of the kinetics of mercury emissions from soils. *J Environ Manage*, 81, 114-25.10.1016/j.jenvman.2005.09.022
- Bash, Jesse O. 2010. Description and initial simulation of a dynamic bidirectional air-surface exchange model for mercury in Community Multiscale Air Quality (CMAQ) model. *Journal of Geophysical Research*, 115.10.1029/2009jd012834
- Bash, Jesse O. & Miller, David R. 2008. A Relaxed Eddy Accumulation System for Measuring Surface Fluxes of Total Gaseous Mercury. *Journal of Atmospheric and Oceanic Technology*, 25, 244-257.10.1175/2007jtecha908.1

- Baya, A. P. & Van Heyst, B. 2010. Assessing the trends and effects of environmental parameters on the behaviour of mercury in the lower atmosphere over cropped land over four seasons. *Atmospheric Chemistry and Physics*, 10, 8617-8628.10.5194/acp-10-8617-2010
- Biswas, A., Blum, J. D. & Keeler, G. J. 2008. Mercury storage in surface soils in a central Washington forest and estimated release during the 2001 Rex Creek Fire. *Sci Total Environ*, 404, 129-38.10.1016/j.scitotenv.2008.05.043
- Blackwell, Bradley D, Driscoll, Charles T, Maxwell, John A & Holsen, Thomas M 2014. Changing climate alters inputs and pathways of mercury deposition to forested ecosystems. *Biogeochemistry*, 119, 215-228
- Boening, Dean W 2000. Ecological effects, transport, and fate of mercury: a general review. *Chemosphere*, 40, 1335-1351
- Briggs, Christian & Gustin, Mae Sexauer 2013. Building upon the Conceptual Model for Soil Mercury Flux: Evidence of a Link Between Moisture Evaporation and Hg Evasion. *Water, Air, & Soil Pollution*, 224.10.1007/s11270-013-1744-5
- Brunke, Ernst- G., Labuschagne, Casper & Slemr, F. 2001. Gaseous mercury emissions from a fire in the Cape Peninsula, South Africa, during January 2000. *Geophysical Research Letters*, 28, 1483-1486.10.1029/2000gl012193
- Bureau of Meteorology. 2019. *Long-range weather and climate* [Online]. <http://www.bom.gov.au/climate/>. [Accessed 2/8/2019 2019].
- Businger, J.A., Wyngaard, J.C., Izumi, Y. & Bradley, E.F 1971. Flux-Profile Relationships in the Atmospheric Surface Layer. *Journal of Atmospheric Sciences*, 28, 181-189
- Campos, Isabel, Vale, Carlos, Abrantes, Nelson, Keizer, Jan Jacob & Pereira, Patrícia 2015. Effects of wildfire on mercury mobilisation in eucalypt and pine forests. *Catena*, 131, 149-159.10.1016/j.catena.2015.02.024
- Carpi, Anthony 1997. Mercury from combustion sources: a review of the chemical species emitted and their transport in the atmosphere. *Water, Air, and Soil Pollution*, 98, 241-254
- Carpi, Anthony & Lindberg, S. 1997. Sunlight-Mediated Emission of Elemental Mercury from Soil Amended with Municipal Sewage Sludge. *Environmental Science & Technology*, 31, 2085-2091
- Choi, H. D. & Holsen, T. M. 2009. Gaseous mercury emissions from unsterilized and sterilized soils: the effect of temperature and UV radiation. *Environ Pollut*, 157, 1673-8.10.1016/j.envpol.2008.12.014
- Choi, H. D., Huang, J., Mondal, S. & Holsen, T. M. 2013. Variation in concentrations of three mercury (Hg) forms at a rural and a suburban site in New York State. *Sci Total Environ*, 448, 96-106.10.1016/j.scitotenv.2012.08.052
- Choi, Hyun-Deok, Sharac, Timothy J. & Holsen, Thomas M. 2008. Mercury deposition in the Adirondacks: A comparison between precipitation and throughfall. *Atmospheric Environment*, 42, 1818-1827.10.1016/j.atmosenv.2007.11.036
- Ci, Zhijia, Zhang, Xiaoshan, Yin, Yongguang, Chen, Jinsheng & Wang, Shiwei 2016. Mercury redox chemistry in waters of the eastern Asian seas: from polluted coast to clean open ocean. *Environmental Science & Technology*, 50, 2371-2380

- Cole, Amanda, Steffen, Alexandra, Eckley, Chris, Narayan, Julie, Pilote, Martin, Tordon, Rob, Graydon, Jennifer, St. Louis, Vincent, Xu, Xiaohong & Branfireun, Brian 2014. A Survey of Mercury in Air and Precipitation across Canada: Patterns and Trends. *Atmosphere*, 5, 635-668.10.3390/atmos5030635
- Converse, A. D., Riscassi, A. L. & Scanlon, T. M. 2010. Seasonal variability in gaseous mercury fluxes measured in a high-elevation meadow. *Atmospheric Environment*, 44, 2176-2185.10.1016/j.atmosenv.2010.03.024
- Cook, Kellie. 2017. *Comparative Analysis of Reactive Mercury Measurement Methodology and Environmental Correlates in Australia*. Masters of Research Thesis, Macquarie University.
- Corbett-Hains, Hamish, Walters, Nicholas E & Van Heyst, Bill J 2012. Evaluating the effects of sub-zero temperature cycling on mercury flux from soils. *Atmospheric Environment*, 63, 102-108
- Corbitt, E. S., Jacob, D. J., Holmes, C. D., Streets, D. G. & Sunderland, E. M. 2011. Global source-receptor relationships for mercury deposition under present-day and 2050 emissions scenarios. *Environ Sci Technol*, 45, 10477-84.10.1021/es202496y
- De Simone, F., Cinnirella, S., Gencarelli, C. N., Yang, X., Hedgecock, I. M. & Pirrone, N. 2015. Model study of global mercury deposition from biomass burning. *Environ Sci Technol*, 49, 6712-21.10.1021/acs.est.5b00969
- De Simone, Francesco, Cinnirella, Sergio, Gencarelli, Christian N., Carbone, Francesco, Hedgecock, Ian M. & Pirrone, Nicola 2016. Particulate-Phase Mercury Emissions during Biomass Burning and Impact on Resulting Deposition: a Modelling Assessment. *Atmospheric Chemistry and Physics Discussions*, 1-22.10.5194/acp-2016-685
- Dedik, AN, Hoffmann, P & Ensling, J 1992. Chemical characterization of iron in atmospheric aerosols. *Atmospheric Environment. Part A. General Topics*, 26, 2545-2548
- Demers, Jason D., Blum, Joel D. & Zak, Donald R. 2013. Mercury isotopes in a forested ecosystem: Implications for air-surface exchange dynamics and the global mercury cycle. *Global Biogeochemical Cycles*, 27, 222-238.10.1002/gbc.20021
- Dibble, TS, Zelig, MJ & Mao, H 2012. Thermodynamics of reactions of ClHg and BrHg radicals with atmospherically abundant free radicals. *Atmospheric Chemistry and Physics*, 12, 10271-10279
- Dommergue, A, Sprovieri, F, Pirrone, N, Ebinghaus, R, Brooks, S, Courteaud, J & Ferrari, CP 2010. Overview of mercury measurements in the Antarctic troposphere. *Atmospheric Chemistry and Physics*, 10, 3309-3319
- Driscoll, C. T., Mason, R. P., Chan, H. M., Jacob, D. J. & Pirrone, N. 2013. Mercury as a global pollutant: sources, pathways, and effects. *Environ Sci Technol*, 47, 4967-83.10.1021/es305071v
- Dutt, Upma, Nelson, Peter F, Morrison, Anthony L & Strezov, Vladimir 2009. Mercury wet deposition and coal-fired power station contributions: an Australian study. *Fuel Processing Technology*, 90, 1354-1359
- Eckley, C. S., Gustin, M., Lin, C. J., Li, X. & Miller, M. B. 2010. The influence of dynamic chamber design and operating parameters on calculated surface-to-air mercury fluxes. *Atmospheric Environment*, 44, 194-203.10.1016/j.atmosenv.2009.10.013

- Eckley, C. S., Gustin, M., Marsik, F. & Miller, M. B. 2011. Measurement of surface mercury fluxes at active industrial gold mines in Nevada (USA). *Sci Total Environ*, 409, 514-22.10.1016/j.scitotenv.2010.10.024
- Edwards, G. C. & Howard, D. A. 2013. Air-surface exchange measurements of gaseous elemental mercury over naturally enriched and background terrestrial landscapes in Australia. *Atmospheric Chemistry and Physics*, 13, 5325-5336.10.5194/acp-13-5325-2013
- Edwards, G. C., Rasmussen, P. E. , Schroeder, W. H. , Wallace, D. M. , Halfpenny-Mitchell, L. , Dias, G. M. , Kemp, R. J. & Ausma, S. 2005. Development and evaluation of a sampling system to determine gaseous Mercury fluxes using an aerodynamic micrometeorological gradient method. *Journal of Geophysical Research*, 110.10.1029/2004jd005187
- Engle, Mark A, Gustin, Mae Sexauer & Zhang, Hong 2001. Quantifying natural source mercury emissions from the Ivanhoe Mining District, north-central Nevada, USA. *Atmospheric Environment*, 35, 3987-3997
- Engle, Mark A, Tate, Michael T, Krabbenhoft, David P, Schauer, James J, Kolker, Allan, Shanley, James B & Bothner, Michael H 2010. Comparison of atmospheric mercury speciation and deposition at nine sites across central and eastern North America. *Journal of Geophysical Research: Atmospheres*, 115
- Ericksen, J. A. & Gustin, M. S. 2004. Foliar exchange of mercury as a function of soil and air mercury concentrations. *Sci Total Environ*, 324, 271-9.10.1016/j.scitotenv.2003.10.034
- Ericksen, J. A., Gustin, M. S., Schorran, D. E., Johnson, D. W., Lindberg, S. E. & Coleman, J. S. 2003. Accumulation of atmospheric mercury in forest foliage. *Atmospheric Environment*, 37, 1613-1622.10.1016/s1352-2310(03)00008-6
- Ericksen, J. A., Gustin, M. S., Xin, M., Weisberg, P. J. & Fernandez, G. C. 2006. Air-soil exchange of mercury from background soils in the United States. *Sci Total Environ*, 366, 851-63.10.1016/j.scitotenv.2005.08.019
- Feng, Xinbin, Wang, Shaofeng, Qiu, Guangle, Hou, Yamin & Tang, Shunlin 2005. Total gaseous mercury emissions from soil in Guiyang, Guizhou, China. *Journal of Geophysical Research: Atmospheres*, 110, n/a-n/a.10.1029/2004jd005643
- Friedli, H. R., Radke, L. F., Prescott, R., Hobbs, P. V. & Sinha, P. 2003. Mercury emissions from the August 2001 wildfires in Washington State and an agricultural waste fire in Oregon and atmospheric mercury budget estimates. *Global Biogeochemical Cycles*, 17, n/a-n/a.10.1029/2002gb001972
- Friedli, H.R. , Arellano, A.F. , Cinnirella, S. & Pirrone, N. 2009. Initial Estimates of Mercury Emissions to the Atmosphere from Global Biomass Burning. *Environmental Science & Technology*, 43, 3507-3513
- Friedli, Hans R, Radke, Lawrence F & Lu, Julia Y 2001. Mercury in smoke from biomass fires. *Geophysical Research Letters*, 28, 3223-3226
- Fritsche, J., Obrist, D., Zeeman, M., Conen, F., Eugster, W. & Alewell, C. 2008. Elemental mercury fluxes over a sub-alpine grassland determined with two micrometeorological methods. *Atmospheric Environment*, 42, 2922-2933.10.1016/j.atmosenv.2007.12.055
- Fu, X. W., Zhang, H., Lin, C. J., Feng, X. B., Zhou, L. X. & Fang, S. X. 2015. Correlation slopes of GEM / CO, GEM / CO₂, and GEM / CH₄ and

- estimated mercury emissions in China, South Asia, the Indochinese Peninsula, and Central Asia derived from observations in northwestern and southwestern China. *Atmospheric Chemistry and Physics*, 15, 1013-1028.10.5194/acp-15-1013-2015
- Gabriel, Mark C., Williamson, Derek G. & Brooks, Steve 2011. Potential impact of rainfall on the air-surface exchange of total gaseous mercury from two common urban ground surfaces. *Atmospheric Environment*, 45, 1766-1774.10.1016/j.atmosenv.2010.11.035
- Gabriel, Mark C., Williamson, Derek G., Zhang, Hong, Brooks, Steve & Lindberg, Steve 2006. Diurnal and seasonal trends in total gaseous mercury flux from three urban ground surfaces. *Atmospheric Environment*, 40, 4269-4284.10.1016/j.atmosenv.2006.04.004
- Gaffney, Jeffrey S & Marley, Nancy 2014. In-depth review of atmospheric mercury: sources, transformations, and potential sinks. *Energy and Emission Control Technologies*, 2, 1-21
- Giang, Amanda, Stokes, Leah C, Streets, David G, Corbitt, Elizabeth S & Selin, Noelle E 2015. Impacts of the minamata convention on mercury emissions and global deposition from coal-fired power generation in Asia. *Environmental Science & Technology*, 49, 5326-5335
- Gillis, Alison A. & Miller, David R. 2000. Some local environmental effects on mercury emission and absorption at a soil surface. *The Science of the Total Environment*, 260, 191-200
- Goodsite, Michael Evan, Plane, JMC & Skov, H 2004. A theoretical study of the oxidation of Hg⁰ to HgBr₂ in the troposphere. *Environmental Science & Technology*, 38, 1772-1776
- Gratz, LE, Ambrose, JL, Jaffe, DA, Shah, V, Jaeglé, L, Stutz, J, Festa, J, Spolaor, M, Tsai, C & Selin, NE 2015. Oxidation of mercury by bromine in the subtropical Pacific free troposphere. *Geophysical Research Letters*, 42, 10,494-10,502
- Gratz, Lynne E, Keeler, Gerald J & Miller, Eric K 2009. Long-term relationships between mercury wet deposition and meteorology. *Atmospheric Environment*, 43, 6218-6229
- Gratz, Lynne E, Keeler, Gerald J, Morishita, Masako, Barres, James A & Dvonch, J Timothy 2013. Assessing the emission sources of atmospheric mercury in wet deposition across Illinois. *Science of The Total Environment*, 448, 120-131
- Graydon, Jennifer A, St. Louis, Vincent L, Lindberg, Steve E, Hintelmann, Holger & Krabbenhoft, David P 2006. Investigation of mercury exchange between forest canopy vegetation and the atmosphere using a new dynamic chamber. *Environmental Science & Technology*, 40, 4680-4688
- Gustin, M. S., Amos, H. M., Huang, J., Miller, M. B. & Heidecorn, K. 2015. Measuring and modeling mercury in the atmosphere: a critical review. *Atmospheric Chemistry and Physics*, 15, 5697-5713.10.5194/acp-15-5697-2015
- Gustin, Mae S, Lyman, Seth N, Kilner, P & Prestbo, E 2011. Development of a passive sampler for gaseous mercury. *Atmospheric Environment*, 45, 5805-5812
- Gustin, Mae Sexauer 2003. Are mercury emissions from geologic sources significant? A status report. *Science of The Total Environment*, 304, 153-167.10.1016/s0048-9697(02)00565-x
- Gustin, Mae Sexauer 2012. Exchange of mercury between the atmosphere and terrestrial ecosystems. *Environmental chemistry and toxicology of mercury*, 423-451

- Gustin, Mae Sexauer, Biester, Harald & Kim, Christopher S. 2002. Investigation of the light-enhanced emission of mercury from naturally enriched substrates. *Atmospheric Environment*, 36, 3241–3254.1352-2310/02/\$
- Gustin, Mae Sexauer, Engle, Mark, Ericksen, Jody, Lyman, Seth, Stamenkovic, Jelena & Xin, Mei 2006. Mercury exchange between the atmosphere and low mercury containing substrates. *Applied Geochemistry*, 21, 1913-1923.10.1016/j.apgeochem.2006.08.007
- Gustin, Mae Sexauer, Lindberg, Steven E. & Weisberg, Peter J. 2008. An update on the natural sources and sinks of atmospheric mercury. *Applied Geochemistry*, 23, 482-493.10.1016/j.apgeochem.2007.12.010
- Gustin, Mae Sexauer & Stamenkovic, Jelena 2005. Effect of Watering and Soil Moisture on Mercury Emissions from Soils. *Biogeochemistry*, 76, 215-232.10.1007/s10533-005-4566-8
- Gustin, Mae Sexauer, Taylor, George E. & Maxey, Rachel A. 1997. Effect of temperature and air movement on the flux of elemental mercury from substrate to the atmosphere. *Journal of Geophysical Research: Atmospheres*, 102, 3891-3898.10.1029/96jd02742
- Haikerwal, A., Reisen, F., Sim, M. R., Abramson, M. J., Meyer, C. P., Johnston, F. H. & Dennekamp, M. 2015. Impact of smoke from prescribed burning: Is it a public health concern? *J Air Waste Manag Assoc*, 65, 592-8.10.1080/10962247.2015.1032445
- Hamilton, Jacqueline F., Allen, Grant, Watson, Nicola M., Lee, James D., Saxton, Julie E., Lewis, Alastair C., Vaughan, Geraint, Bower, Keith N., Flynn, Michael J., Crosier, Jonathan, Carver, Glenn D., Harris, Neil R. P., Parker, Robert J., Remedios, John J. & Richards, Nigel A. D. 2008. Observations of an atmospheric chemical equator and its implications for the tropical warm pool region. *Journal of Geophysical Research*, 113.10.1029/2008jd009940
- Han, Young-Ji, Holsen, Thomas M., Lai, Soon-Onn, Hopke, Philip K., Yi, Seung-Muk, Liu, Wei, Pagano, James, Falanga, Lauren, Milligan, Michael & Andolina, Chris 2004. Atmospheric gaseous mercury concentrations in New York State: relationships with meteorological data and other pollutants. *Atmospheric Environment*, 38, 6431-6446.10.1016/j.atmosenv.2004.07.031
- Hanson, P. J., Lindberg, S.E., Tabberer, T.A., Owens, J.G. & Kim, K.-H. 1995. Foliar exchange of mercury vapor: Evidence for a compensation point. *Water Air Soil Pollution*, 80, 373-382
- Hararuk, O., Obrist, D. & Luo, Y. 2013. Modelling the sensitivity of soil mercury storage to climate-induced changes in soil carbon pools. *Biogeosciences*, 10, 2393-2407.10.5194/bg-10-2393-2013
- Hartman, Jelena S, Weisberg, Peter J, Pillai, Rekha, Ericksen, Jody A, Kuiken, Todd, Lindberg, Steve E, Zhang, Hong, Rytuba, James J & Gustin, Mae S 2009. Application of a rule-based model to estimate mercury exchange for three background biomes in the continental United States. *Environmental Science & Technology*, 43, 4989-4994
- Hicks, Bruce B, Saylor, Rick D & Baker, Barry D 2016. Dry deposition of particles to canopies—A look back and the road forward. *Journal of Geophysical Research: Atmospheres*, 121, 14,691-14,707
- Hintelmann, Holger, Harris, Reed, Heyes, Andrew, Hurley, James P, Kelly, Carol A, Krabbenhoft, David P, Lindberg, Steve, Rudd, John WM, Scott, Karen J & St. Louis, Vincent L 2002. Reactivity and mobility of new and old mercury deposition in a boreal

- forest ecosystem during the first year of the METAALICUS study. *Environmental Science & Technology*, 36, 5034-5040
- Hojdova, M., Rohovec, J., Chrastny, V., Penizek, V. & Navratil, T. 2015. The influence of sample drying procedures on mercury concentrations analyzed in soils. *Bull Environ Contam Toxicol*, 94, 570-6.10.1007/s00128-015-1521-9
- Holland, Frank, Hofzumahaus, Andreas, Schäfer, Jürgen, Kraus, Alexander & Pätz, Hans-Werner 2003. Measurements of OH and HO₂ radical concentrations and photolysis frequencies during BERLIOZ. *Journal of Geophysical Research: Atmospheres*, 108, PHO 2-1-PHO 2-23
- Holmes, C. D., Jacob, D. J., Corbitt, E. S., Mao, J., Yang, X., Talbot, R. & Slemr, F. 2010. Global atmospheric model for mercury including oxidation by bromine atoms. *Atmospheric Chemistry and Physics*, 10, 12037-12057.10.5194/acp-10-12037-2010
- Holmes, Christopher D, Jacob, Daniel J, Mason, Robert P & Jaffe, Dan A 2009. Sources and deposition of reactive gaseous mercury in the marine atmosphere. *Atmospheric Environment*, 43, 2278-2285
- Holmes, Christopher D, Jacob, Daniel J & Yang, Xin 2006. Global lifetime of elemental mercury against oxidation by atomic bromine in the free troposphere. *Geophysical Research Letters*, 33
- Horowitz, H. M., Jacob, D. J., Amos, H. M., Streets, D. G. & Sunderland, E. M. 2014. Historical Mercury releases from commercial products: global environmental implications. *Environ Sci Technol*, 48, 10242-50.10.1021/es501337j
- Horowitz, Hannah M., Jacob, Daniel J., Zhang, Yanxu, Dibble, Theodore S., Slemr, Franz, Amos, Helen M., Schmidt, Johan A., Corbitt, Elizabeth S., Marais, Eloïse A. & Sunderland, Elsie M. 2017. A new mechanism for atmospheric mercury redox chemistry: implications for the global mercury budget. *Atmospheric Chemistry and Physics*, 17, 6353-6371.10.5194/acp-17-6353-2017
- Howard, D. 2017. *Aspects of the Biogeochemical Cycling of Mercury in Australia and the Southern Hemisphere*. PhD, Macquaire University.
- Howard, Dean & Edwards, Grant C. 2017. Mercury fluxes over an Australian alpine grassland and observation of nocturnal atmospheric mercury depletion events. *Atmospheric Chemistry and Physics Discussions*, 1-24.10.5194/acp-2017-580
- Howard, Dean, Nelson, Peter F., Edwards, Grant C., Morrison, Anthony L., Fisher, Jenny A., Ward, Jason, Harnwell, James, van der Schoot, Marcel, Atkinson, Brad, Chambers, Scott D., Griffiths, Alan D., Werczynski, Sylvester & Williams, Alastair G. 2017. Atmospheric mercury in the southern hemisphere tropics: seasonal and diurnal variations and influence of inter-hemispheric transport. *Atmospheric Chemistry and Physics Discussions*, 1-20.10.5194/acp-2017-307
- Huang, J., Miller, M. B., Weiss-Penzias, P. & Gustin, M. S. 2013. Comparison of gaseous oxidized Hg measured by KCl-coated denuders, and nylon and cation exchange membranes. *Environ Sci Technol*, 47, 7307-16.10.1021/es4012349
- Jaffe, Dan & Strode, Sarah 2008. Sources, fate and transport of atmospheric mercury from Asia. *Environmental Chemistry*, 5, 121.10.1071/en08010
- Jardine, Timothy D & Bunn, Stuart E 2010. Northern Australia, whither the mercury? *Marine and Freshwater Research*, 61, 451-463

- Jiang, N., Betts, A. & Riley, M. 2016. Summarising climate and air quality (ozone) data on self-organising maps: a Sydney case study. *Environ Monit Assess*, 188, 103.10.1007/s10661-016-5113-x
- Jiang, Ningbo, Scorgie, Yvonne, Hart, Melissa, Riley, Matthew L., Crawford, Jagoda, Beggs, Paul J., Edwards, Grant C., Chang, Lisa, Salter, David & Virgilio, Giovanni Di 2017. Visualising the relationships between synoptic circulation type and air quality in Sydney, a subtropical coastal-basin environment. *International Journal of Climatology*, 37, 1211-1228.10.1002/joc.4770
- Jiao, Yuge & Dibble, Theodore S 2017. First kinetic study of the atmospherically important reactions $\text{BrHg}^+ \text{NO}_2$ and $\text{BrHg}^+ \text{HOO}$. *Physical Chemistry Chemical Physics*, 19, 1826-1838
- Jiskra, Martin, Sonke, Jeroen E., Obrist, Daniel, Bieser, Johannes, Ebinghaus, Ralf, Myhre, Cathrine Lund, Pfaffhuber, Katrine Aspmo, Wängberg, Ingvar, Kyllönen, Katriina, Worthy, Doug, Martin, Lynwill G., Labuschagne, Casper, Mkololo, Thumeka, Ramonet, Michel, Magand, Olivier & Dommergue, Aurélien 2018. A vegetation control on seasonal variations in global atmospheric mercury concentrations. *Nature Geoscience*, 11, 244-250.10.1038/s41561-018-0078-8
- Jones, Colleen P, Lyman, Seth, Jaffe, Daniel A, Allen, Tanner & O'Neil, Trevor L 2016. Detection and quantification of gas-phase oxidized mercury compounds by GC/MS. *Atmospheric Measurement Techniques*, 9
- Karthik, R., Paneerselvam, A., Ganguly, D., Hariharan, G., Srinivasalu, S., Purvaja, R. & Ramesh, R. 2017. Temporal variability of atmospheric Total Gaseous Mercury and its correlation with meteorological parameters at a high-altitude station of the South India. *Atmospheric Pollution Research*, 8, 164-173.10.1016/j.apr.2016.08.010
- Keeler, Gerald J, Gratz, Lynne E & Al-Wali, Khalid 2005. Long-term atmospheric mercury wet deposition at Underhill, Vermont. *Ecotoxicology*, 14, 71-83
- Khan, T. R., Obrist, D., Agnan, Y., Selin, N. E. & Perlinger, J. A. 2019. Atmosphere-terrestrial exchange of gaseous elemental mercury: parameterization improvement through direct comparison with measured ecosystem fluxes. *Environ Sci Process Impacts*, 21, 1699-1712.10.1039/c9em00341j
- Kikuchi, T., Ikemoto, H., Takahashi, K., Hasome, H. & Ueda, H. 2013. Parameterizing soil emission and atmospheric oxidation-reduction in a model of the global biogeochemical cycle of mercury. *Environ Sci Technol*, 47, 12266-74.10.1021/es401105h
- Kim, K. H., Yoon, H. O., Jung, M. C., Oh, J. M. & Brown, R. J. 2012. A simple approach for measuring emission patterns of vapor phase mercury under temperature-controlled conditions from soil. *ScientificWorldJournal*, 2012, 940413.10.1100/2012/940413
- Kim, Ki-Hyun , Lindberg, Steven E. & Meyer, C. P. 1995. Micrometeorological Measurements Of Mercury Vapor Fluxes Over Background Forest Soils In Eastern Tennessee. *Atmospheric Environment*, 29, 267-282
- Kwon, Sae Yun & Selin, Noelle E. 2016. Uncertainties in Atmospheric Mercury Modeling for Policy Evaluation. *Current Pollution Reports*, 2, 103-114.10.1007/s40726-016-0030-8
- Laacouri, A., Nater, E. A. & Kolka, R. K. 2013. Distribution and uptake dynamics of mercury in leaves of common deciduous tree species in Minnesota, U.S.A. *Environ Sci Technol*, 47, 10462-70.10.1021/es401357z

- Lamborg, Carl H, Fitzgerald, William F, O'Donnell, James & Torgersen, Thomas 2002. A non-steady-state compartmental model of global-scale mercury biogeochemistry with interhemispheric atmospheric gradients. *Geochimica et Cosmochimica Acta*, 66, 1105-1118
- Lan, X., Talbot, R., Castro, M., Perry, K. & Luke, W. 2012. Seasonal and diurnal variations of atmospheric mercury across the US determined from AMNet monitoring data. *Atmospheric Chemistry and Physics*, 12, 10569-10582.10.5194/acp-12-10569-2012
- Landis, Matthew S, Stevens, Robert K, Schaedlich, Frank & Prestbo, Eric M 2002. Development and characterization of an annular denuder methodology for the measurement of divalent inorganic reactive gaseous mercury in ambient air. *Environmental Science & Technology*, 36, 3000-3009
- Laurier, Fabien & Mason, Robert 2007. Mercury concentration and speciation in the coastal and open ocean boundary layer. *Journal of Geophysical Research*, 112.10.1029/2006jd007320
- Lee, Xuhui , Benoit, Gaboury & Hu, Xinzhang 2000. Total gaseous mercury concentration and flux over a coastal saltmarsh vegetation in Connecticut, USA. *Atmospheric Environment*, 34, 4205-4213
- Li, Zheng, Xia, Chonghuan, Wang, Xinming, Xiang, Yunrong & Xie, Zhouqing 2011. Total gaseous mercury in Pearl River Delta region, China during 2008 winter period. *Atmospheric Environment*, 45, 834-838
- Liang, P., Zhang, C., Yang, Y. & Wang, D. 2014. A simulation study of mercury release fluxes from soils in wet-dry rotation environment. *J Environ Sci (China)*, 26, 1445-52.10.1016/j.jes.2014.05.010
- Lin, Che-Jen, Gustin, Mae S, Singhasuk, Pattaraporn, Eckley, Chris & Miller, Matthieu 2010. Empirical models for estimating mercury flux from soils. *Environmental Science & Technology*, 44, 8522-8528
- Lin, Che-jen & Pehkonen, Simo O 1997. Aqueous free radical chemistry of mercury in the presence of iron oxides and ambient aerosol. *Atmospheric Environment*, 31, 4125-4137
- Lin, Che-Jen & Pehkonen, Simo O 1999. The chemistry of atmospheric mercury: a review. *Atmospheric Environment*, 33, 2067-2079
- Lin, Che-Jen, Pongprueksa, Pruek, Lindberg, Steve E, Pehkonen, Simo O, Byun, Daewon & Jang, Carey 2006. Scientific uncertainties in atmospheric mercury models I: Model science evaluation. *Atmospheric Environment*, 40, 2911-2928
- Lindberg, S. E., Zhang, H., Gustin, M., Vette, A., Marsik, F., Owens, J., Casimir, A., Ebinghaus, R., Edwards, G., Fitzgerald, C., Kemp, J., Kock, H. H., London, J., Majewski, M., Poissant, L., Pilote, M., Rasmussen, P., Schaedlich, F., Schneeberger, D., Sommar, J., Turner, R., Wallschläger, D. & Xiao, Z. 1999. Increases in mercury emissions from desert soils in response to rainfall and irrigation. *Journal of Geophysical Research: Atmospheres*, 104, 21879-21888.10.1029/1999jd900202
- Lindberg, SE and & Stratton, WJ 1998. Atmospheric mercury speciation: concentrations and behavior of reactive gaseous mercury in ambient air. *Environmental Science & Technology*, 32, 49-57

- Lindberg, SE, Hanson, PJ, Meyers, TP and & Kim, K-H 1998. Air/surface exchange of mercury vapor over forests—the need for a reassessment of continental biogenic emissions. *Atmospheric Environment*, 32, 895-908
- Lindberg, Steve, Bullock, Russell, Ebinghaus, Ralf, Engstrom, Daniel, Feng, Xinbin, Fitzgerald, William, Pirrone, Nicola, Prestbo, Eric & Seigneur, Christian 2007. A synthesis of progress and uncertainties in attributing the sources of mercury in deposition. *AMBIO: a Journal of the Human Environment*, 36, 19-34
- Liu, Fei, Cheng, Hangxin, Yang, Ke, Zhao, Chuandong, Liu, Yinghan, Peng, Min & Li, Kuo 2014. Characteristics and influencing factors of mercury exchange flux between soil and air in Guangzhou City. *Journal of Geochemical Exploration*, 139, 115-121.10.1016/j.gexplo.2013.09.005
- Liu, Yan, Xu, Zhenghe & Kuznicki, Steven M. 2010. Development of a Novel Mercury Cartridge for Mercury Analysis†. *Energy & Fuels*, 24, 10-17.10.1021/ef900501p
- Lyman, Seth N, Gustin, Mae Sexauer, Prestbo, Eric M & Marsik, Frank J 2007. Estimation of dry deposition of atmospheric mercury in Nevada by direct and indirect methods. *Environmental Science & Technology*, 41, 1970-1976
- Lyman, Seth N. & Gustin, Mae Sexauer 2008. Speciation of atmospheric mercury at two sites in northern Nevada, USA. *Atmospheric Environment*, 42, 927-939.10.1016/j.atmosenv.2007.10.012
- Lynam, Mary M & Keeler, Gerald J 2005. Artifacts associated with the measurement of particulate mercury in an urban environment: The influence of elevated ozone concentrations. *Atmospheric Environment*, 39, 3081-3088
- Malcolm, Elizabeth G., Keeler, Gerald J. & Landis, Matthew S. 2003. The effects of the coastal environment on the atmospheric mercury cycle. *Journal of Geophysical Research*, 108.10.1029/2002jd003084
- Mao, H, Talbot, RW, Sigler, JM, Sive, BC & Hegarty, JD 2008. Seasonal and diurnal variations of Hg over New England. *Atmospheric Chemistry and Physics*, 8, 1403-1421
- Mao, Huiting, Cheng, Irene & Zhang, Leiming 2016. Current understanding of the driving mechanisms for spatiotemporal variations of atmospheric speciated mercury: a review. *Atmospheric Chemistry and Physics*, 16, 12897-12924.10.5194/acp-16-12897-2016
- Mason, Robert P & Sheu, G-R 2002. Role of the ocean in the global mercury cycle. *Global Biogeochemical Cycles*, 16, 40-1-40-14
- Mason, Robert P., Hammerschmidt, Chad R., Lamborg, Carl H., Bowman, Katlin L., Swarr, Gretchen J. & Shelley, Rachel U. 2017. The air-sea exchange of mercury in the low latitude Pacific and Atlantic Oceans. *Deep Sea Research Part I: Oceanographic Research Papers*, 122, 17-28.10.1016/j.dsr.2017.01.015
- Mastromonaco, M Nerentorp, Gårdfeldt, K, Jourdain, Bruno, Abrahamsson, K, Granfors, A, Ahnoff, M, Dommergue, Aurélien, Méjean, Guillaume & Jacobi, H-W 2016. Antarctic winter mercury and ozone depletion events over sea ice. *Atmospheric Environment*, 129, 125-132
- McKenzie, RL, Bodeker, GE, Keep, DJ, Kotkamp, M & Evans, J 1996. UV radiation in New Zealand: north-to-south differences between two sites, and relationship to other latitudes. *Weather and Climate*, 17-26

- Melendez-Perez, Jose J., Fostier, Anne H., Carvalho, João A., Windmöller, Claudia C., Santos, José C. & Carpi, Anthony 2014. Soil and biomass mercury emissions during a prescribed fire in the Amazonian rain forest. *Atmospheric Environment*, 96, 415-422.10.1016/j.atmosenv.2014.06.032
- Miller, Eric K, Vanarsdale, Alan, Keeler, Gerald J, Chalmers, Ann, Poissant, Laurier, Kamman, Neil C & Brulotte, Raynald 2005. Estimation and mapping of wet and dry mercury deposition across northeastern North America. *Ecotoxicology*, 14, 53-70
- Miller, Matthieu B 2018. *Concentrations of atmospheric reactive mercury in Australia and emissions of reactive mercury from contaminated mine materials using cation exchange membranes*. PhD Thesis, Macquarie University.
- Moore, Chad & Carpi, Anthony 2005. Mechanisms of the emission of mercury from soil: Role of UV radiation. *Journal of Geophysical Research: Atmospheres*, 110
- Moore, Christopher W & Castro, Mark S 2012. Investigation of factors affecting gaseous mercury concentrations in soils. *Science of The Total Environment*, 419, 136-143
- Mudroch, Alena & Bourbonniere, Richard A 1994. Sediment preservation, processing, and storage. *Handbook of Techniques for Aquatic Sediments Sampling*, 131-169
- Nelson, Darrell W & Sommers, Lee E 1996. Total carbon, organic carbon, and organic matter. *Methods of soil analysis part 3—chemical methods*, 961-1010
- Nelson, Peter F, Nguyen, Hao, Morrison, Anthony L, Malfroy, Hugh, Cope, Martin E, Hibberd, Mark F, Lee, Sunhee, McGregor, John L & Meyer, M 2009. Mercury sources, transportation and fate in Australia. *Report, Department of Environment, Water, Heritage & the Arts*,
- Nelson, Peter F., Morrison, Anthony L., Malfroy, Hugh J., Cope, Martin, Lee, Sunhee, Hibberd, Mark L., Meyer, C. P. & McGregor, John 2012. Atmospheric mercury emissions in Australia from anthropogenic, natural and recycled sources. *Atmospheric Environment*, 62, 291-302.10.1016/j.atmosenv.2012.07.067
- Nelson, Peter F., Peterson, Christian & Morrison, Anthony 2004. Atmospheric Emissions of Mercury-Sources and Chemistry. *Clean Air and Environmental Quality*, 38, 48
- Nguyen, Duc Luong, Kim, Jin Young, Shim, Shang-Gyoo & Zhang, Xiao-Shan 2011. Ground and shipboard measurements of atmospheric gaseous elemental mercury over the Yellow Sea region during 2007–2008. *Atmospheric Environment*, 45, 253-260
- Nriagu, Jerome & Becker, Christian 2003. Volcanic emissions of mercury to the atmosphere: global and regional inventories. *Science of The Total Environment*, 304, 3-12
- Obrist, D, Johnson, DW & Lindberg, SE 2009. Mercury concentrations and pools in four Sierra Nevada forest sites, and relationships to organic carbon and nitrogen. *Biogeosciences*, 6, 765-777
- Obrist, D., Johnson, D. W., Lindberg, S. E., Luo, Y., Hararuk, O., Bracho, R., Battles, J. J., Dail, D. B., Edmonds, R. L., Monson, R. K., Ollinger, S. V., Pallardy, S. G., Pregitzer, K. S. & Todd, D. E. 2011. Mercury distribution across 14 U.S. Forests. Part I: spatial patterns of concentrations in biomass, litter, and soils. *Environ Sci Technol*, 45, 3974-81.10.1021/es104384m
- Obrist, D., Kirk, J. L., Zhang, Lei, Sunderland, E. M., Jiskra, Martin & Selin, N. 2018. A review of global environmental mercury processes in response to human and natural

- perturbations: Changes of emissions, climate, and land use. *Ambio*.10.1007/s13280-017-1004-9
- Obrist, D., Pearson, C., Webster, J., Kane, T., Lin, C. J., Aiken, G. R. & Alpers, C. N. 2016. A synthesis of terrestrial mercury in the western United States: Spatial distribution defined by land cover and plant productivity. *Sci Total Environ*, 568, 522-35.10.1016/j.scitotenv.2015.11.104
- Obrist, D., Pokharel, A. K. & Moore, C. 2014. Vertical profile measurements of soil air suggest immobilization of gaseous elemental mercury in mineral soil. *Environ Sci Technol*, 48, 2242-52.10.1021/es4048297
- Obrist, Daniel , Moosmüller, Hans , Schürmann, Roger , Chen, L.-W. Antony & Kreidenweis, Sonia M. 2008. Particulate-Phase and Gaseous Elemental Mercury Emissions During Biomass Combustion: Controlling Factors and Correlation with Particulate Matter Emissions. *Environmental Science & Technology*, 42, 721–727
- Obrist, Daniel, Gustin, Mae S., Arnone, John A., Johnson, Dale W., Schorran, David E. & Verburg, Paul S. J. 2005. Measurements of gaseous elemental mercury fluxes over intact tallgrass prairie monoliths during one full year. *Atmospheric Environment*, 39, 957-965.10.1016/j.atmosenv.2004.09.081
- Osterwalder, S., Bishop, K., Alewell, C., Fritsche, J., Laudon, H., Akerblom, S. & Nilsson, M. B. 2017. Mercury evasion from a boreal peatland shortens the timeline for recovery from legacy pollution. *Sci Rep*, 7, 16022.10.1038/s41598-017-16141-7
- Page, Niel. 2017. *Using observations and modelling to quantify mercury biogeochemical cycling in the Australian context*. Master of Research thesis, , University of Wollongong.
- Pannu, R., Siciliano, S. D. & O'Driscoll, N. J. 2014. Quantifying the effects of soil temperature, moisture and sterilization on elemental mercury formation in boreal soils. *Environ Pollut*, 193, 138-146.10.1016/j.envpol.2014.06.023
- Park, Sang-Young, Holsen, Thomas M., Kim, Pyung-Rea & Han, Young-Ji 2014. Laboratory investigation of factors affecting mercury emissions from soils. *Environmental Earth Sciences*, 72, 2711-2721.10.1007/s12665-014-3177-x
- Paton-Walsh, C., Smith, T. E. L., Young, E. L., Griffith, D. W. T. & Guérette, É A. 2014. New emission factors for Australian vegetation fires measured using open-path Fourier transform infrared spectroscopy – Part 1: Methods and Australian temperate forest fires. *Atmospheric Chemistry and Physics*, 14, 11313-11333.10.5194/acp-14-11313-2014
- Phu Nguyen, L. S., Zhang, L., Lin, D. W., Lin, N. H. & Sheu, G. R. 2019. Eight-year dry deposition of atmospheric mercury to a tropical high mountain background site downwind of the East Asian continent. *Environ Pollut*, 255, 113128.10.1016/j.envpol.2019.113128
- Pirrone, N., Cinnirella, S., Feng, X., Finkelman, R. B., Friedli, H. R., Leaner, J., Mason, R., Mukherjee, A. B., Stracher, G. B., Streets, D. G. & Telmer, K. 2010. Global mercury emissions to the atmosphere from anthropogenic and natural sources. *Atmospheric Chemistry and Physics*, 10, 5951-5964.10.5194/acp-10-5951-2010
- Poissant, Laurier, Pilote, Martin, Beauvais, Conrad, Philippe & Zhang, Hong H 2005. A year of continuous measurements of three atmospheric mercury species (GEM, RGM and Hgp) in southern Quebec, Canada. *Atmospheric Environment*, 39, 1275-1287

- Poissant, Laurier, Pilote, Martin, Yumvihoze, Emmanuel & Lean, David 2008. Mercury concentrations and foliage/atmosphere fluxes in a maple forest ecosystem in Québec, Canada. *Journal of Geophysical Research*, 113.10.1029/2007jd009510
- Raich, James W & Schlesinger, William H 1992. The global carbon dioxide flux in soil respiration and its relationship to vegetation and climate. *Tellus B*, 44, 81-99
- Rea, A. W. , Lindberg, S. E., Scherbatskoy, T. & Keeler, G. J. 2002. Mercury accumulation in foliage over time in two northern mixed-hardwood forests. *Water, Air, and Soil Pollution*, 133, 49–67
- Ren, Xinrong, Luke, Winston T., Kelley, Paul, Cohen, Mark D., Artz, Richard, Olson, Mark L., Schmeltz, David, Puchalski, Melissa, Goldberg, Daniel L., Ring, Allison, Mazzuca, Gina M., Cummings, Kristin A., Wojdan, Lisa, Preaux, Sandra & Stehr, Jeff W. 2016. Atmospheric mercury measurements at a suburban site in the Mid-Atlantic United States: Inter-annual, seasonal and diurnal variations and source-receptor relationships. *Atmospheric Environment*, 146, 141-152.10.1016/j.atmosenv.2016.08.028
- Rutter, A. P., Shakya, K. M., Lehr, R., Schauer, J. J. & Griffin, R. J. 2012. Oxidation of gaseous elemental mercury in the presence of secondary organic aerosols. *Atmospheric Environment*, 59, 86-92.10.1016/j.atmosenv.2012.05.009
- Schlüter, K 2000. evaporation of mercury from soils. An integration and synthesis of current knowledge. *Environmental Geology*, 39, 249-271
- Schroeder, W. & Munthe, J. 1998. Atmospheric Mercury - An Overview. *Atmospheric Environment*, 32, 809-822
- Schultz, Martin G., Jacob, Daniel J., Wang, Yuhang, Logan, Jennifer A., Atlas, Elliot L., Blake, Donald R., Blake, Nicola J., Bradshaw, John D., Browell, Edward V., Fenn, Marta A., Flocke, Frank, Gregory, Gerald L., Heikes, Brian G., Sachse, Glen W., Sandholm, Scott T., Shetter, Richard E., Singh, Hanwant B. & Talbot, Robert W. 1999. On the origin of tropospheric ozone and NO_x over the tropical South Pacific. *J. Geophys. Res.*, 104, 5829-5843.10.1029/98jd02309
- Seigneur, Christian, Karamchandani, Prakash, Lohman, Kristen, Vijayaraghavan, Krish & Shia, Run-Lie 2001. Multiscale modeling of the atmospheric fate and transport of mercury. *Journal of Geophysical Research: Atmospheres*, 106, 27795-27809
- Selin, Noelle E. 2009. Global Biogeochemical Cycling of Mercury: A Review. *Annual Review of Environment and Resources*, 34, 43-63.10.1146/annurev.environ.051308.084314
- Selin, Noelle E., Jacob, Daniel J., Park, Rokjin J., Yantosca, Robert M., Strode, Sarah, Jaeglé, Lyatt & Jaffe, Daniel 2007. Chemical cycling and deposition of atmospheric mercury: Global constraints from observations. *Journal of Geophysical Research*, 112.10.1029/2006jd007450
- Selin, Noelle E., Jacob, Daniel J., Yantosca, Robert M., Strode, Sarah, Jaeglé, Lyatt & Sunderland, Elsie M. 2008. Global 3-D land-ocean-atmosphere model for mercury: Present-day versus preindustrial cycles and anthropogenic enrichment factors for deposition. *Global Biogeochemical Cycles*, 22, n/a-n/a.10.1029/2007gb003040
- Semeniuk, Kirill & Dastoor, Ashu 2017. Development of a global ocean mercury model with a methylation cycle: Outstanding issues. *Global Biogeochemical Cycles*, 31, 400-433
- Shah, V, Jaeglé, L, Gratz, LE, Ambrose, JL, Jaffe, DA, Selin, NE, Song, S, Campos, TL, Flocke, FM & Reeves, M 2016. Origin of oxidized mercury in the summertime free

- troposphere over the southeastern US. *Atmospheric Chemistry and Physics*, 16, 1511-1530
- Sherman, Laura S, Blum, Joel D, Dvonch, J Timothy, Gratz, Lynne E & Landis, Matthew S 2015. The use of Pb, Sr, and Hg isotopes in Great Lakes precipitation as a tool for pollution source attribution. *Science of The Total Environment*, 502, 362-374
- Si, Lin & Ariya, Parisa 2018. Recent Advances in Atmospheric Chemistry of Mercury. *Atmosphere*, 9, 76.10.3390/atmos9020076
- Sigler, JM, Mao, H & Talbot, R 2009. Gaseous elemental and reactive mercury in Southern New Hampshire. *Atmospheric Chemistry and Physics*, 9, 1929-1942
- Slemr, F., Angot, H., Dommergue, A., Magand, O., Barret, M., Weigelt, A., Ebinghaus, R., Brunke, E. G., Pfaffhuber, K. A., Edwards, G., Howard, D., Powell, J., Keywood, M. & Wang, F. 2015. Comparison of mercury concentrations measured at several sites in the Southern Hemisphere. *Atmospheric Chemistry and Physics*, 15, 3125-3133.10.5194/acp-15-3125-2015
- Slemr, F., Weigelt, A., Ebinghaus, R., Kock, H. H., Bödewadt, J., Brenninkmeijer, C. A. M., Rauthe-Schöch, A., Weber, S., Hermann, M., Zahn, A. & Martinsson, B. 2016. Atmospheric mercury measurements onboard the CARIBIC passenger aircraft. *Atmospheric Measurement Techniques Discussions*, 1-25.10.5194/amt-2015-376
- Smith-Downey, Nicole V., Sunderland, Elsie M. & Jacob, Daniel J. 2010. Anthropogenic impacts on global storage and emissions of mercury from terrestrial soils: Insights from a new global model. *Journal of Geophysical Research*, 115.10.1029/2009jg001124
- Soerensen, Anne L, Skov, Henrik, Jacob, Daniel J, Soerensen, Britt T & Johnson, Matthew S 2010. Global concentrations of gaseous elemental mercury and reactive gaseous mercury in the marine boundary layer. *Environmental Science & Technology*, 44, 7425-7430
- Soerensen, Anne L., Jacob, Daniel J., Streets, David G., Witt, Melanie L. I., Ebinghaus, Ralf, Mason, Robert P., Andersson, Maria & Sunderland, Elsie M. 2012. Multi-decadal decline of mercury in the North Atlantic atmosphere explained by changing subsurface seawater concentrations. *Geophysical Research Letters*, 39, n/a-n/a.10.1029/2012gl053736
- Sommar, Jonas, Hallquist, Mattias, Ljungström, Evert & Lindqvist, Oliver 1997. On the gas phase reactions between volatile biogenic mercury species and the nitrate radical. *Journal of Atmospheric Chemistry*, 27, 233-247
- Sommar, Jonas, Zhu, Wei, Shang, Lihai, Lin, Che-Jen & Feng, Xinbin 2016. Seasonal variations in metallic mercury (Hg⁰) vapor exchange over biannual wheat–corn rotation cropland in the North China Plain. *Biogeosciences*, 13, 2029-2049.10.5194/bg-13-2029-2016
- Song, S., Selin, N. E., Soerensen, A. L., Angot, H., Artz, R., Brooks, S., Brunke, E. G., Conley, G., Dommergue, A., Ebinghaus, R., Holsen, T. M., Jaffe, D. A., Kang, S., Kelley, P., Luke, W. T., Magand, O., Marumoto, K., Pfaffhuber, K. A., Ren, X., Sheu, G. R., Slemr, F., Warneke, T., Weigelt, A., Weiss-Penzias, P., Wip, D. C. & Zhang, Q. 2015. Top-down constraints on atmospheric mercury emissions and implications for global biogeochemical cycling. *Atmospheric Chemistry and Physics*, 15, 7103-7125.10.5194/acp-15-7103-2015

- Song, Shaojie, Selin, Noelle E., Gratz, Lynne E., Ambrose, Jesse L., Jaffe, Daniel A., Shah, Viral, Jaeglé, Lyatt, Giang, Amanda, Yuan, Bin, Kaser, Lisa, Apel, Eric C., Hornbrook, Rebecca S., Blake, Nicola J., Weinheimer, Andrew J., Mauldin Iii, Roy L., Cantrell, Christopher A., Castro, Mark S., Conley, Gary, Holsen, Thomas M., Luke, Winston T. & Talbot, Robert 2016. Constraints from observations and modeling on atmosphere–surface exchange of mercury in eastern North America. *Elementa: Science of the Anthropocene*, 4, 000100.10.12952/journal.elementa.000100
- Song, X. & Van Heyst, B. 2005. Volatilization of mercury from soils in response to simulated precipitation. *Atmospheric Environment*, 39, 7494-7505.10.1016/j.atmosenv.2005.07.064
- Sprovieri, F, Pirrone, N, Ebinghaus, R, Kock, H & Dommergue, A 2010. A review of worldwide atmospheric mercury measurements. *Atmospheric Chemistry and Physics*, 10, 8245-8265
- Sprovieri, Francesca, Pirrone, Nicola, Bencardino, Mariantonia, amp, apos, Amore, Francesco, Angot, Helene, Barbante, Carlo, Brunke, Ernst-Günther, Arcega-Cabrera, Flor, Cairns, Warren, Comero, Sara, Diéguez, María del Carmen, Dommergue, Aurélien, Ebinghaus, Ralf, Feng, Xin Bin, Fu, Xuewu, Garcia, Patricia Elizabeth, Gawlik, Bernd Manfred, Hageström, Ulla, Hansson, Katarina, Horvat, Milena, Kotnik, Jože, Labuschagne, Casper, Magand, Olivier, Martin, Lynwill, Mashyanov, Nikolay, Mkololo, Thumeka, Munthe, John, Obolkin, Vladimir, Ramirez Islas, Martha, Sena, Fabrizio, Somerset, Vernon, Spandow, Pia, Vardè, Massimiliano, Walters, Chavon, Wängberg, Ingvar, Weigelt, Andreas, Yang, Xu & Zhang, Hui 2017. Five-year records of mercury wet deposition flux at GMOS sites in the Northern and Southern hemispheres. *Atmospheric Chemistry and Physics*, 17, 2689-2708.10.5194/acp-17-2689-2017
- Sprovieri, Francesca, Pirrone, Nicola, Bencardino, Mariantonia, amp, apos, Amore, Francesco, Carbone, Francesco, Cinnirella, Sergio, Mannarino, Valentino, Landis, Matthew, Ebinghaus, Ralf, Weigelt, Andreas, Brunke, Ernst-Günther, Labuschagne, Casper, Martin, Lynwill, Munthe, John, Wängberg, Ingvar, Artaxo, Paulo, Morais, Fernando, Barbosa, Henrique de Melo Jorge, Brito, Joel, Cairns, Warren, Barbante, Carlo, Diéguez, María del Carmen, Garcia, Patricia Elizabeth, Dommergue, Aurélien, Angot, Helene, Magand, Olivier, Skov, Henrik, Horvat, Milena, Kotnik, Jože, Read, Katie Alana, Neves, Luis Mendes, Gawlik, Bernd Manfred, Sena, Fabrizio, Mashyanov, Nikolay, Obolkin, Vladimir, Wip, Dennis, Feng, Xin Bin, Zhang, Hui, Fu, Xuewu, Ramachandran, Ramesh, Cossa, Daniel, Knoery, Joël, Maruszczak, Nicolas, Nerentorp, Michelle & Norstrom, Claus 2016. Atmospheric mercury concentrations observed at ground-based monitoring sites globally distributed in the framework of the GMOS network. *Atmospheric Chemistry and Physics*, 16, 11915-11935.10.5194/acp-16-11915-2016
- St. Louis, Vincent L, Rudd, John WM, Kelly, Carol A, Hall, Britt D, Rolffhus, Kristofer R, Scott, Karen J, Lindberg, Steve E & Dong, Weijin 2001. Importance of the forest canopy to fluxes of methyl mercury and total mercury to boreal ecosystems. *Environmental Science & Technology*, 35, 3089-3098
- Stamenkovic, J., Gustin, M. S., Arnone, J. A., 3rd, Johnson, D. W., Larsen, J. D. & Verburg, P. S. 2008. Atmospheric mercury exchange with a tallgrass prairie ecosystem housed in mesocosms. *Sci Total Environ*, 406, 227-38.10.1016/j.scitotenv.2008.07.047

- Streets, D. G., Devane, M. K., Lu, Z., Bond, T. C., Sunderland, E. M. & Jacob, D. J. 2011. All-time releases of mercury to the atmosphere from human activities. *Environ Sci Technol*, 45, 10485-91.10.1021/es202765m
- Streets, D. G., Horowitz, H. M., Jacob, D. J., Lu, Z., Levin, L., Ter Schure, A. F. H. & Sunderland, E. M. 2017. Total Mercury Released to the Environment by Human Activities. *Environ Sci Technol*, 51, 5969-5977.10.1021/acs.est.7b00451
- Strode, Sarah A., Jaeglé, Lyatt, Selin, Noelle E., Jacob, Daniel J., Park, Rokjin J., Yantosca, Robert M., Mason, Robert P. & Slemr, Franz 2007. Air-sea exchange in the global mercury cycle. *Global Biogeochemical Cycles*, 21, n/a-n/a.10.1029/2006gb002766
- Subir, Mahamud, Ariya, Parisa A & Dastoor, Ashu P 2012. A review of the sources of uncertainties in atmospheric mercury modeling II. Mercury surface and heterogeneous chemistry—A missing link. *Atmospheric Environment*, 46, 1-10
- Sun, Ruoyu, Streets, David G., Horowitz, Hannah M., Amos, Helen M., Liu, Guijian, Perrot, Vincent, Toutain, Jean-Paul, Hintelmann, Holger, Sunderland, Elsie M. & Sonke, Jeroen E. 2016. Historical (1850–2010) mercury stable isotope inventory from anthropogenic sources to the atmosphere. *Elementa: Science of the Anthropocene*, 4, 000091.10.12952/journal.elementa.000091
- Sundseth, K., Pacyna, J. M., Banel, A., Pacyna, E. G. & Rautio, A. 2015. Climate change impacts on environmental and human exposure to mercury in the arctic. *Int J Environ Res Public Health*, 12, 3579-99.10.3390/ijerph120403579
- Travnikov, Oleg, Angot, Hélène, Artaxo, Paulo, Bencardino, Mariantonia, Bieser, Johannes, amp, apos, Amore, Francesco, Dastoor, Ashu, De Simone, Francesco, Diéguez, María del Carmen, Dommergue, Aurélien, Ebinghaus, Ralf, Feng, Xin Bin, Gencarelli, Christian N., Hedgecock, Ian M., Magand, Olivier, Martin, Lynwill, Matthias, Volker, Mashyanov, Nikolay, Pirrone, Nicola, Ramachandran, Ramesh, Read, Katie Alana, Ryjkov, Andrei, Selin, Noelle E., Sena, Fabrizio, Song, Shaojie, Sprovieri, Francesca, Wip, Dennis, Wängberg, Ingvar & Yang, Xin 2017. Multi-model study of mercury dispersion in the atmosphere: atmospheric processes and model evaluation. *Atmospheric Chemistry and Physics*, 17, 5271-5295.10.5194/acp-17-5271-2017
- UNEP, (United Nations Environment Programme) 2013a. Minamata convention on mercury: Text and annexes, Technical report. Geneva, Switzerland: United Nations Environment Programme.
- UNEP, (United Nations Environment Programme). 2017. *The Minamata Convention has entered into force* [Online]. <http://www.mercuryconvention.org/>. [Accessed 13/5/2019 2019].
- UNEP, (United Nations Environment Programme) 2013b. Sources, emissions, releases and environmental transport. In: BRANCH, U. C. (ed.). Geneva, Switzerland United Nations Environment Programme.
- Valente, Ralph J, Shea, Catherine, Humes, K Lynn & Tanner, Roger L 2007. Atmospheric mercury in the Great Smoky Mountains compared to regional and global levels. *Atmospheric Environment*, 41, 1861-1873
- Wagner-Riddle, C. , Thurtell, G. W. , Kidd, G. K. , Beauchamp, E. G. & Sweetman, R. 1997. Estimates of nitrous oxide emissions from agricultural fields over 28 months. *Canadian Journal Of Soil Science*, 77, 135–144

- Wang, D., He, L., Shi, X., Wei, S. & Feng, X. 2006. Release flux of mercury from different environmental surfaces in Chongqing, China. *Chemosphere*, 64, 1845-54.10.1016/j.chemosphere.2006.01.054
- Wang, F., Saiz-Lopez, A., Mahajan, A. S., Gómez Martín, J. C., Armstrong, D., Lemes, M., Hay, T. & Prados-Roman, C. 2013. Enhanced production of oxidised mercury over the tropical Pacific Ocean: a key missing oxidation pathway. *Atmospheric Chemistry and Physics Discussions*, 13, 21541-21572.10.5194/acpd-13-21541-2013
- Wang, X., Lin, C. J. & Feng, X. 2014. Sensitivity analysis of an updated bidirectional air-surface exchange model for elemental mercury vapor. *Atmospheric Chemistry and Physics*, 14, 6273-6287.10.5194/acp-14-6273-2014
- Wang, Xun, Lin, Che-Jen, Yuan, Wei, Sommar, Jonas, Zhu, Wei & Feng, Xinbin 2016. Emission-dominated gas exchange of elemental mercury vapor over natural surfaces in China. *Atmospheric Chemistry and Physics*, 16, 11125-11143.10.5194/acp-16-11125-2016
- Webb, E. K., Pearman, G. I. & Leuning, R. 1980. Correction of flux measurements for density effects due to heat and water vapour transfer. *Journal of the Royal Meteorological Society*, 106, 85-100
- Weiss-Penzias, P., Amos, H. M., Selin, N. E., Gustin, M. S., Jaffe, D. A., Obrist, D., Sheu, G. R. & Giang, A. 2015. Use of a global model to understand speciated atmospheric mercury observations at five high-elevation sites. *Atmospheric Chemistry and Physics*, 15, 1161-1173.10.5194/acp-15-1161-2015
- Weiss-Penzias, P., Jaffe, D., Swartzendruber, P., Hafner, W., Chand, D. & Prestbo, E. 2007. Quantifying Asian and biomass burning sources of mercury using the Hg/CO ratio in pollution plumes observed at the Mount Bachelor observatory. *Atmospheric Environment*, 41, 4366-4379.10.1016/j.atmosenv.2007.01.058
- Weiss-Penzias, Peter, Gustin, Mae Sexauer & Lyman, Seth N 2009. Observations of speciated atmospheric mercury at three sites in Nevada: Evidence for a free tropospheric source of reactive gaseous mercury. *Journal of Geophysical Research: Atmospheres*, 114
- Wesely, ML 1989. Parameterization of surface resistances to gaseous dry deposition in regional-scale numerical models. *Atmospheric Environment (1967)*, 23, 1293-1304
- WHO, (World Health Organization). 2019. *Mercury* [Online]. https://www.who.int/ipcs/assessment/public_health/mercury/en/: World Health Organization. [Accessed 13/5/2019 2019].
- Wright, L. Paige & Zhang, Leiming 2015. An approach estimating bidirectional air-surface exchange for gaseous elemental mercury at AMNet sites. *Journal of Advances in Modeling Earth Systems*, 7, 35-49.10.1002/2014ms000367
- Wu, Zhiyong, Schwede, Donna B, Vet, Robert, Walker, John T, Shaw, Mike, Staebler, Ralf & Zhang, Leiming 2018. Evaluation and intercomparison of five North American dry deposition algorithms at a mixed forest site. *Journal of Advances in Modeling Earth Systems*, 10, 1571-1586
- Xin, Mei & Gustin, Mae Sexauer 2007. Gaseous elemental mercury exchange with low mercury containing soils: Investigation of controlling factors. *Applied Geochemistry*, 22, 1451-1466.10.1016/j.apgeochem.2007.02.006

- Xu, L., Chen, J., Yang, L., Niu, Z., Tong, L., Yin, L. & Chen, Y. 2015. Characteristics and sources of atmospheric mercury speciation in a coastal city, Xiamen, China. *Chemosphere*, 119, 530-539.10.1016/j.chemosphere.2014.07.024
- Ye, Zhuyun, Mao, Huiting, Lin, Che-Jen & Kim, Su Youn 2016. Investigation of processes controlling summertime gaseous elemental mercury oxidation at midlatitudinal marine, coastal, and inland sites. *Atmospheric Chemistry and Physics*, 16, 8461-8478.10.5194/acp-16-8461-2016
- Yu, Qian, Luo, Yao, Wang, Shuxiao, Wang, Zhiqi, Hao, Jiming & Duan, Lei 2018. Gaseous elemental mercury (GEM) fluxes over canopy of two typical subtropical forests in south China. *Atmospheric Chemistry and Physics*, 18, 495-509.10.5194/acp-18-495-2018
- Zárate-Valdez, José L, Zasoski, Robert J & Läuchli, André E 2006. Short-term effects of moisture content on soil solution pH and soil Eh. *Soil Science*, 171, 423-431
- Zhang, H., Holmes, C. D. & Wu, S. 2016. Impacts of changes in climate, land use and land cover on atmospheric mercury. *Atmospheric Environment*, 141, 230-244.10.1016/j.atmosenv.2016.06.056
- Zhang, H. & Lindberg, S. E. 1999. Processes influencing the emission of mercury from soils: A conceptual model. *Journal of Geophysical Research: Atmospheres*, 104, 21889-21896.10.1029/1999jd900194
- Zhang, H., Lindberg, S., Marsik, F. & Keeler, G. J. 2001. Mercury air/surface exchange kinetics of background soils of the tahquamenon river watershed in the michigan upper peninsula. *Water, Air, & Soil Pollution*, 126, 151-169
- Zhang, Hong & Lindberg, Steve E 2001. Sunlight and iron (III)-induced photochemical production of dissolved gaseous mercury in freshwater. *Environmental Science & Technology*, 35, 928-935
- Zhang, Lei, Wang, Long, Wang, Shuxiao, Dou, Hongying, Li, Jianfeng, Li, Shu & Hao, Jiming 2017. Characteristics and Sources of Speciated Atmospheric Mercury at a Coastal Site in the East China Sea Region. *Aerosol and Air Quality Research*, 17, 2913-2923.10.4209/aaqr.2016.09.0402
- Zhang, Leiming, Wright, L. Paige & Blanchard, Pierrette 2009. A review of current knowledge concerning dry deposition of atmospheric mercury. *Atmospheric Environment*, 43, 5853-5864.10.1016/j.atmosenv.2009.08.019
- Zhang, Wei, Wei, Wen, Hu, Dan, Zhu, Yan & Wang, Xuejun 2013. Emission of Speciated Mercury from Residential Biomass Fuel Combustion in China. *Energy & Fuels*, 27, 6792-6800.10.1021/ef401564r
- Zhou, J., Wang, Z., Sun, T., Zhang, H. & Zhang, X. 2016. Mercury in terrestrial forested systems with highly elevated mercury deposition in southwestern China: The risk to insects and potential release from wildfires. *Environ Pollut*, 212, 188-196.10.1016/j.envpol.2016.01.003
- Zhou, Jun, Wang, Zhangwei, Zhang, Xiaoshan & Sun, Ting 2017. Investigation of factors affecting mercury emission from subtropical forest soil: A field controlled study in southwestern China. *Journal of Geochemical Exploration*, 176, 128-135.10.1016/j.gexplo.2015.10.007
- Zhu, Wei, Lin, Che-Jen, Wang, Xun, Sommar, Jonas, Fu, Xuewu & Feng, Xinbin 2016. Global observations and modeling of atmosphere-surface exchange of elemental mercury: a

critical review. *Atmospheric Chemistry and Physics*, 16, 4451-4480.10.5194/acp-16-4451-2016

APPENDIX 1

Table 3. Student two-way t-tests for diel Hg flux composite day/night values at Oakdale, New South Wales, from 3 April 2017 to 21 June 2018

	p	t-score	SD	df	95% confidence	
Winter	0.02	-2.41	1.99	46	-2.62	-0.24
Spring	0.36	1.06	1.06	46	-0.34	0.93
Summer	0.67	-0.43	1.92	46	-1.39	0.90
Autumn	0.5	1.67	1.67	46	-0.65	1.34

APPENDIX 2

Table 1. Seasonal average and standard deviation (SD) for Hg fluxes (Hg flux), fluxes measured during no rainfall (no rain Hg flux) and Hg fluxes measured during recorded rainfall (Rain Hg flux) at Oakdale, NSW (3 April 2017 to 21 June 2018).

Year	Season	Hg flux (ng m ⁻² h ⁻¹)		No rain Hg flux (ng m ⁻² h ⁻¹)		Rain Hg flux (ng m ⁻² h ⁻¹)	
		Mean	SD	Mean	SD	Mean	SD
2017	Autumn	-0.32	17.66	0.33	9.36	-6.82	13.91
	Winter	-0.12	11.53	-0.62	10.12	3.76	39.06
	Spring	0.25	9.88	0.17	8.78	3.94	19.50
2017/2018	Summer	0.34	16.60	0.71	6.31	1.70	19.92
2018	Autumn	-0.20	14.70	-0.17	15.50	-1.23	14.70
	Winter	-0.40	16.66	0.03	16.69	-4.93	15.68
All		0.00	14.23	0.02	11.29	1.03	20.78

Table 2. Student T-test between Hg fluxes that occurred during rainfall and no rain period (Rainfall) and Hg fluxes that occurred when VWC increased 1 standard deviation above the mean VWC at 5cm (VWC change), separated seasonally. Including 95% confidence intervals (CI +, CI -), Standard deviation (SD) and t value.

	Rainfall				VWC change			
	Winter	Spring	Summer	Autumn	Winter	Spring	Summer	Autumn
p-value	0.19	0.001	0.14	0.73	0.01	0.75	0.07	0.16
CI -	-0.93	1.00	-0.58	-2.17	-2.70	-1.02	-0.08	-0.34
CI +	4.79	4.12	4.07	3.11	-0.40	0.73	2.59	2.07
SD	11.55	10.00	17.25	15.12	11.50	9.87	16.62	14.68
t	1.32	3.20	1.47	0.35	-2.64	-0.32	1.84	1.40

APPENDIX 3

Table 1. Student two-way t-tests for seasonal variability for both GEM and RM at Oakdale, New South Wales, from 3 April 2017 to 21 June 2018.

	p	t-score	SD	df	95% confidence	
Winter 2017 GEM	<0.01	6.80	0.08	2453	0.02	0.03
Spring 2017 GEM	<0.01	-59.44	0.16	5597	-0.29	-0.27
Summer 2017/2018 GEM	<0.01	-38.43	0.19	7640	-0.18	-0.16
Autumn 2018 GEM	0.00	57.20	0.18	7552	0.23	0.25
Spring 2017 RM	<0.01	-4.56	0.91	11	-3.41	-1.19
Summer 2017/2018 RM	0.66	0.45	1.50	12	-1.39	2.10
Autumn 2018 RM	0.30	1.09	2.05	12	-1.20	3.58

Table 2. Student two-way t-tests for diel GEM composite day/night values at Oakdale, New South Wales, from 3 April 2017 to 21 June 2018.

	p	t-score	SD	df	95% confidence	
Winter	0.21	1.27	0.01	46	-0.0	0.01
Spring	0.003	-3.18	0.02	46	-0.03	-0.01
Summer	0.005	-2.97	0.05	46	-0.07	-0.01
Autumn	0.002	-4.12	0.01	46	-0.03	-0.01

APPENDIX 4

The paper is included in the thesis as it represents a significant body of work undertaken during the PhD candidature. However, it was not included in the main body of the thesis as it does not fit with the key aims. The paper has been accepted for publication in the journal: *Exposure and Health* (DOI: 10.1007/s12403-019-00332-w) and was originally intended as a companion to the paper presented in chapter 6.

Pages 191-203 of this thesis have been removed as they contain published material. Please refer to the following citation for details of the article contained in these pages:

MacSween, K., Paton-Walsh, C., Roulston, C. *et al.* Cumulative Firefighter Exposure to Multiple Toxins Emitted During Prescribed Burns in Australia. *Expo Health* 12, 721–733 (2020). <https://doi.org/10.1007/s12403-019-00332-w>